University of Sheffield

Low cost Internet of things based sensor networks for air quality in cities

Rohit Chakraborty

Supervisors: Professor Martin Mayfield, Professor Lyudmila Mihaylova &
Professor Anthony J. Ryan, OBE

A thesis submitted in partial fulfilment of the requirements
for the degree of PhD

in the

Department of Civil & Structural Engineering

September 2023

Statement

This thesis has been made possible with the generous support of the Urban Flows Observatory and Grantham Centre for Sustainable Future, University of Sheffield for granting me with sensor funding and tuition fee scholarship respectively. I would like to thank my supervisors Professor Martin Mayfield and Professor Lyudmila Mihaylova for their continuous guidance and support throughout the research. I am also grateful to the co-authors of some of my publications, Dr. Peng Wang, Dr. Maria Val Martin and Dr. Maria Bermudez, for sharing their valuable knowledge, feedback and experience.

My special gratitude to Dr. James Heydon (University of Nottingham) for giving me the opportunity to work on multiple real world Air Quality projects.

With gratitude, I acknowledge the steadfast love and support from my family, particularly my parents who have always believed in me. Their unwavering faith has been crucial in my achievements. I am especially thankful to my partner, who has been a tremendous source of encouragement and support throughout my journey. Their sacrifices have played a significant role in my success.

This thesis, except for referencing the work of others, is solely my original work and has not been submitted in any form or degree in any university. The contents of this thesis are the result of my individual efforts and do not include any collaborative work, as specified in the text.

Rohit Chakraborty

September 2023

Abstract

Air pollution is a major public health concern, with over 7 million deaths globally attributed to it annually, as stated by the World Health Organization (WHO) in 2018. Existing real-time Air Quality (AQ) monitoring stations are expensive to install and maintain; therefore, such air quality monitoring networks are sparsely deployed and lack the measurement density to develop high-resolution spatiotemporal air pollutant monitoring. The data generated also lacks accuracy, but still, they have great potential to complement the existing air quality assessment framework.

Therefore, this thesis aims to propose a comprehensive architecture for utilizing low-cost sensors in air pollution monitoring. The thesis presents a novel approach to deploy a low-cost sensor network in a city and use a hybrid convolutional-long short-term memory (Conv-LSTM) model for spatiotemporal prediction of air pollution. This approach utilizes both convolutional layers to capture spatial patterns in the sensor data and LSTM layers to capture temporal dependencies. The use of a hybrid model allows for the simultaneous capture of both spatial and temporal patterns in the data, resulting in more accurate predictions compared to models that only utilize one or the other. The research also explores the use of statistical models such as Seasonal Autoregressive Integrated Moving Average (SARIMA) and Nonlinear Autoregressive with exogenous inputs (NARX) models for air quality forecasting, presenting a comparison of the proposed hybrid model with other such state-of-the-art statistical and machine learning models. The results show that the proposed Conv-LSTM model outperforms these approaches in terms of prediction accuracy and robustness and, therefore, is a promising approach for spatiotemporal prediction of air pollution using low-cost sensor data. Additionally, the thesis proposes a general solution to analyze how the noise level of measurements and hyperparameters of a Gaussian process model affect the prediction accuracy and uncertainty of low-cost sensor data.

The thesis further presents an extensive evaluation of the proposed hybrid model using real-world data from the low-cost sensor network deployed in Sheffield, and the results demonstrate the effectiveness of the proposed approach. Finally, the real-world studies present the integration of low-cost sensor data into a decision-making system, social and behavioural changes driven by such sensors and the impact of these results on driving policy changes to achieve the World Health Organization's (WHO) 2021 target for air quality.

Keywords: *Air quality, Internet of Things, Spatiotemporal modelling, Data fusion, Recurrent Neural Network, Machine Learning, Deep Learning.*

Table of Contents

List of Figures

List of Tables

List of Algorithms

List of Abbreviations

AQ	**A**ir **Q**uality
WHO	**W**orld **H**ealth **O**rganisation
IID	**I**ndependent and **I**dentically **D**istributed
CNN	**C**onvolutional **N**eural **N**etwork
RNN	**R**ecurrant **N**eural **N**etwork
LSTM	**L**ong **S**hort **T**erm **M**emory
ConvLSTM	**C**onvolutional **L**ong **S**hort-Term **M**emory
PM	**R**elative **H**umidity
GP	**G**aussian **P**rocess
SOD	**S**ubset **O**f **D**ata
LCS	**L**ow **C**ost **S**ensors
SMS	**S**ensor **M**odelling **S**ystem
FF	**F**orecasting **F**unction
ML	**M**achine **L**earning
DL	**D**eep **L**earning
PM	**P**articulate **M**atter
AQI	**A**ir **Q**uality **I**ndex
SDS	**S**tatistical **D**ata **S**ynthesis
MAE	**M**ean **A**bsolute **E**rror
RMSE	**R**oot **M**ean **S**quared **E**rror
SDD	**S**ymmetric **D**iagonally **D**ominant
ARMA	**A**uto **R**egressive **M**oving **A**verage
ARIMA	**A**uto **R**egressive **I**ntegrated **M**oving **A**verage
n	**N**umber of complete pairs of data.
FAC2	**F**raction of predictions within a factor of two.
MB	**M**ean **B**ias.
MGE	**M**ean **G**ross **E**rror.
NMB	**N**ormalised **M**ean **B**ias.
NMGE	**N**ormalised **M**ean **G**ross **E**rror.

RMSE	**R**oot **M**ean **S**quare **E**rror.
r	**P**earson correlation coefficient.
COE	**C**oefficient of **E**fficiency.
IOA	**I**ndex of **A**greement.

List of Symbols/ Acronyms

°C	temperature (T)
m/s	wind speed (WS)
degrees	wind direction (WD)
cm^{-3}	particle number concentration (PNC)
ppb	Nitrogen Dioxide (NO_2)
ppb	Sulfur Dioxide (SO_2)
ppm	Carbon Monoxide (CO)
ppb	Ozone (O_3)
$\mu g/m^3$	Particulate Matter less than 2.5 μm ($PM_{2.5}$)
F	State Update Matrix
f	State Update Function
H	Measurement Matrix
h	Measurement Function
IN	N-dimensional Identity Matrix
K	Gaussian Process Covariance Matrix
P	State Error Covariance
Q	Process Noise Covariance Matrix
R	Measurement Noise Covariance Matrix
v	Measurement Noise Vector
w	Process Noise Vector
x	State Vector
z	Measurement Vector
E[·]	Expectation Operator
N(·, ·)	Normal Distribution
U[·, ·]	Uniform Distribution
GP	Gaussian Process
k(·, ·)	Gaussian Process Kernel
m(·)	Gaussian Process Mean Function
p(·)	Probability Density Function

STGP	Spatio-temporal Gaussian process
T	Sampling Time
u	Gaussian Process Input
F[·]	Fourier Transform
·	Dot Product

Greek Symbols

η	Hyperparameters Vector
σ^2	Measurement Noise Variance
$\Gamma(\cdot)$	Gamma Function

List of Publications

R. Chakraborty, J. Heydon, M. Mayfield, and L. Mihaylova. Indoor air pollution from residential stoves: Examining the flooding of particulate matter into homes during real-world use'. *Atmosphere*, 11, 2021.

María del Carmen Redondo Bermúdez, Rohit Chakraborty, Ross W. Cameron, Beverley J. Inkson, and Maria Val Martin. A practical green infrastructure intervention to mitigate air pollution in a UK school playground. *Sustainability*, 15(2):1075, January 2023.

J. Heydon and R. Chakraborty. Can portable air quality monitors protect children from air pollution on the school run? *An exploratory study'. Environmental Monitoring and Assessment*, 192(195):1–16, 2020.

James Heydon and Rohit Chakraborty. Wood burning stoves, participatory sensing, and 'cold, stark data'. *SN Social Sciences*, 2(10), September 2022.

Peng Wang, Lyudmila Mihaylova, Rohit Chakraborty, Said Munir, Martin Mayfield, Khan Alam, Muhammad Fahim Khokhar, Zhengkai Zheng, Chengxi Jiang, and Hui Fang. A gaussian process method with uncertainty quantification for air quality monitoring. *Atmosphere*, 12(10):1344, October 2021.

Peng Wang, Lyudmila Mihaylova, Rohit Chakraborty, Said Munir, Jikai Wang, Martin Mayfield, Khan Alam, Muhammad Fahim Khokhar, and Daniel Coca. A computationally efficient symmetric diagonally dominant matrix projection-based gaussian process approach. *Signal Processing*, 183:108034, 2021.

Matthew Wood, Chantelle Wood, Peter Styring, Christopher R. Jones, Jeffery Smith, Marianne Day, Rohit Chakraborty, and Gloria Mensah. Perceptions of accountability and trust in the regulatory governance of wood burning stove sustainability: Survey evidence from the post-brexit UK. *SSRN Electronic Journal*, 2022.

Chapter 1

Air Pollution: A Social Problem with Myriad Components

Air pollution is a pressing environmental issue and a significant public health concern in the UK. According to the World Health Organization (WHO) [1], it is estimated that air pollution causes around 40,000 premature deaths each year in the UK. The cost of air pollution to the NHS alone is estimated to be £2 billion annually.

1.1 Why is research on monitoring and modelling of air quality important?

Monitoring and modelling air pollution is a challenging task that requires a thorough understanding of the atmospheric processes that influence pollution dispersion and continuous real-time monitoring. The current methods of monitoring air quality are expensive, and low-cost sensors often need to be more accurate. This poses a significant challenge for scientists and policymakers trying to understand and address the issue of air pollution [2, 3].

The primary goal of air quality modelling is to predict the concentrations of various atmospheric pollutants at future times and locations [4]. Air quality models are used for a variety of purposes, such as assessing the impact of proposed changes to emission sources on air quality [5], developing mitigation strategies to reduce the adverse effects of air pollution [6], and understanding the transport and fate of pollutants in the atmosphere [7]. There are many different air quality models, each with strengths and weaknesses [8]. Choosing a suitable model for a particular application is essential for accurate results. For example, the use of chemical transport models (CTMs) can simulate the dispersion

of pollutants in the atmosphere [9], while the use of statistical models can analyse observational data to infer the sources of air pollution [10]

Spatiotemporal forecast modelling of air pollution is a powerful tool that can be used to predict the concentrations of various pollutants in the atmosphere at future times and locations [11]. The accuracy of these predictions is highly dependent on the quality of the input data and the model assumptions [12]. However, when used correctly, spatiotemporal forecast modelling can provide valuable insights into the behaviour of air pollution. In particular, spatiotemporal forecasting can be used to assess the impact of proposed changes to emission sources on air quality and to develop mitigation strategies to reduce the negative impacts of air pollution [11, 12]

One of the significant challenges in air quality modelling is the availability of high-quality observational data. More accurate and comprehensive data on emissions, meteorology, and air quality is a significant barrier to developing reliable air quality models [2, 3, 5]. For this reason, there is a growing need for developing new observational techniques and integrating existing observational networks [13].

Another challenge in air quality modelling is the representation of complex atmospheric processes in models. The atmosphere is a highly dynamic and heterogeneous system, and the processes that govern the dispersion of pollutants are highly complex [9, 10]. Representing these processes in models is a difficult task and requires a detailed understanding of the physical and chemical processes that govern the behaviour of pollutants in the atmosphere [8].

It is also important to note that air quality modelling efforts should be integrated with other relevant fields, such as meteorology, emissions and chemical kinetics, health impact assessment and decision-making, to provide a more comprehensive and holistic approach to air quality management. For example, the use of air quality models in combination with health impact assessment can provide valuable information on the potential health impacts of different emission control strategies [14].

Furthermore, using advanced data assimilation techniques can also improve the accuracy of air quality models by incorporating observational data in real-time [15]. These techniques can also be used to improve the representation of complex atmospheric processes in models by integrating information from satellite observations, ground-based measurements, and other sources of data [15].

Another critical consideration in air quality modelling is the use of high-performance computing (HPC) to perform large-scale simulations. The use of HPC can significantly increase the computational efficiency of air quality models, enabling the simulation of

large-scale and complex systems [16]. This can be particularly useful for simulating the transport and fate of pollutants over large spatial and temporal scales.

In summary, air quality modelling is a complex and challenging task that requires a thorough understanding of the atmospheric processes that influence pollution dispersion and continuous real-time monitoring. The use of advanced modelling techniques such as spatiotemporal forecasting and data assimilation, in combination with HPC, can provide valuable insights into the behaviour of air pollution and aid in the development of effective mitigation strategies. However, the availability of high-quality observational data and the representation of complex atmospheric processes are major challenges that must be addressed to improve the accuracy and reliability of air quality models. Furthermore, the integration of air quality modelling with other relevant fields such as meteorology, emissions, chemical kinetics, health impact assessment and decision-making is crucial for a more comprehensive and holistic approach to air quality management.

1.2 What is Air Pollution? - Pollutants and Public Health

Ambient air pollution is the contamination of the outdoor environment by any chemical, physical or biological agent that modifies the natural characteristics of the atmosphere [17]. Six types of pollutants cause this pollution: carbon monoxide, lead, nitrogen oxides, ground-level ozone, particle pollution (often referred to as particulate matter), and sulphur oxides.

Indoor air quality is a term that refers to the air quality within and around buildings and structures, especially as it relates to the health and comfort of building occupants. Indoor air quality is affected by both indoor and outdoor sources of pollution. Indoor sources of pollution include materials used in construction and furnishings, ventilation, pesticides, cleaning products, combustion products, and more. Outdoor sources of pollution can enter a building through open doors, windows, or vents. Indoor air quality can also be affected by improperly maintained or operated HVAC systems. Poor indoor air quality can cause a variety of health effects, including respiratory infections, allergies, headaches, fatigue, and more. To ensure good indoor air quality, monitoring for pollutants and taking steps to reduce or eliminate them is important. Improving indoor air quality can often be achieved with simple measures such as Ventilation, Air filtration, and Air purification. When these measures are not sufficient, more advanced methods may be necessary. Indoor air quality is an important issue to consider in both home and office settings.

T The main sources of air pollution are fossil fuel combustion, industrial processes, waste incineration, agricultural practices, and natural processes such as wildfires, dust storms,

and volcanic eruptions [1]. As countries industrialise and transition from low to middle incomes, outdoor air pollution is increasing [18]. While death rates from indoor air pollution have declined globally, the same is not true for ambient air pollution [19]. This has a significant economic cost, estimated at 8 billion USD per day or roughly 3.3 of the world's GDP [20].

The human cost of air pollution is also significant. Exposure to air pollution has been linked to various leading causes of death, including heart disease, stroke, lower respiratory infections, lung cancer, diabetes, and COPD [21]. Children are particularly vulnerable to air pollution and can face long-term consequences from exposure, leading to potentially lifelong impacts [21].

1.3 Historical context for Air Pollution measurements

In the 17th Century, Charles II tasked John Evelyn, a scientist and diarist, with examining the impact of coal smoke on health, vegetation, and structures. This resulted in the publication of Evelyn's work "Fumifugium; or the Inconvenience of the Aer and Smoak of London Dissipated" in 1661 [22], marking the first comprehensive study on air pollution.

In the 19th Century, regulations were introduced to combat air pollution, including the Alkali Act in 1863 and 1874 to control pollution from chemical plants. A devastating "smog" incident occurred in London in 1952, lasting five days, leading to an estimated 4000 additional deaths, including a significant increase in bronchitis fatalities [23]. The Clean Air Acts and the 1974 Control of Air Pollution Act further regulated air quality and composition of fuels, leading to the establishment of the National Survey, the world's first coordinated air pollution monitoring network, in 1961. The increase in motor vehicles in the 1980s brought new air quality concerns, making it the main source of air pollution in urban areas [24]. The Environmental Protection Act of 1990 [25] took over from the Alkali Act as the governing authority for waste management and emission control. During the late 20th Century, automatic air monitoring networks were established, with the Automatic Urban and Rural Network (AURN) becoming the most comprehensive network in the UK, currently consisting of 105 sites with data available from 1973 to the present [26].

1.4 Modern Day challenges to monitoring and communication

Air pollution monitoring and communication is a complex process, and the modern-day challenges to it can be significant. The following steps are typically followed to manage air pollution:

- Air quality monitoring: This is typically done using a network of ground-based sensors that measure various air pollutants. Data from these sensors is then used to produce air quality maps and forecasts.
- Air quality modelling: Atmospheric dispersion models predict how pollutants will spread in the atmosphere. These models take into account the weather conditions, emission sources, and topography.
- Air quality communication: Once air pollution levels have been predicted, this information needs to be communicated to the public so that they can take appropriate actions to protect their health. This is usually done through media outlets such as television, radio, and newspapers.

Several challenges can make air pollution monitoring and communication difficult. These include:

- Inaccurate data: Sensors can sometimes produce inaccurate readings, which can lead to incorrect air quality information being communicated to the public.
- Limited resources: There may need to be more sensors to cover all areas, or they may not be located in the most effective places. This can make it difficult to produce accurate air quality maps and forecasts.
- Poor communication: Even if the information is accurate, it may not be communicated effectively to the public. This can lead to people not taking the necessary actions to protect their health.

The above challenges highlight the importance of having a well-designed air pollution monitoring and communication system in place. Without such a system, it would be difficult to provide accurate and timely information to the public, which could lead to serious health consequences.

Furthermore, Air pollution is now understood to be a mixture of different pollutants that can interact in the atmosphere. This makes it difficult to predict how air pollution

will behave and to communicate this information to the public. In addition, as our understanding of air pollution grows, new challenges are likely to emerge. For example, we are only beginning to understand the health effects of long-term exposure to deficient levels and sizes of air pollution. This means there may be health risks that we are not yet aware of, which could present difficulties for communication in the future.

1.4.1 Technology changes and how people use it can present new challenges to air pollution monitoring and communication.

For example, the rise of social media means more people are getting their news and information from online sources. This can make it challenging to communicate air pollution information effectively, as people may not see or trust it if it comes from an official source.

Another challenge is the way that people use technology. People can now access air quality data from several devices, such as smartphone apps and smartwatches. However, this data can be difficult to interpret, and people may need help understanding how to use it to protect their health.

1.4.2 Rapid changes in the way people live their lives can also present difficulties for air pollution monitoring and communication.

For example, the growth of cities and the rise of car ownership means more sources of air pollution. This can make it challenging to monitor all of the different pollutants in the air and to predict how they will spread. Another challenge is that people are now living and working in places where they were not previously exposed to air pollution. This means that they may not be aware of the health risks associated with air pollution and may not take the necessary precautions to protect themselves.

1.5 Introduction to Low-Cost IoT AQ Sensor

The utilisation of LCS is favoured over costly sensors because of the expanded spatial inclusion when observing air quality in urban and remote areas. As of now, there are many LCS industrially accessible. In any case, the data quality of low-cost sensors could be more stable. It is influenced by meteorological conditions, for example, Humidity and temperature, pollution levels and consequently by the site area where the estimations are carried out. The bias in the data, therefore, stops the administration and policymakers from making informed decisions from this data produced.

In general, specialists need to increase the density of monitoring measurements and regularly need to depend on low-cost sensors since they can't bear the cost of reference Air Quality Monitoring Stations (AQMS). Along these lines, there is a need to consider the accuracy of the LCS.

Although various surveys of the reasonableness of LCS for ambient air quality have been published, quantitative information for looking at and assessing the understanding among LCS and reference stations needs to be more present in the current studies. Moreover, there has yet to be an officially acknowledged convention or standard framework for testing LCS and the measurements detailed are commonly diverse, making it hard to analyse the performance of LCS in various assessment considers. Among the accessible trials of LCS, there are clear signs that the precision of LCS estimations can be questionable when comparing LSC qualities and reference stations or AQMS.

1.5.1 Definition: Low Cost Sensors (LCS)

Low-cost sensors (LCS) for air quality monitoring are characterised by their affordability, compactness, and ease of deployment compared to traditional air quality monitoring instruments [27]. While the term "low-cost" may vary regionally and contextually, LCS are typically designed to be financially accessible to a broader range of users, from community groups to researchers working on limited budgets. Instead of a strict monetary threshold, LCS are distinguished by their ability to offer a cost-effective solution for air quality monitoring, providing valuable data with relatively minimal investment [27]. These sensors often integrate multiple components—including sensing elements, data storage, transmission capabilities, and power sources—into compact units, facilitating flexible and widespread deployment. It's important to note that while LCS bring the advantage of affordability and accessibility, they may sometimes trade-off with factors like precision, longevity, or robustness compared to their more expensive counterparts [28].

LCS have the potential to benefit significantly scientific communities and society as a whole by enabling long-term data collection at high resolutions that would otherwise be difficult or impossible to obtain. Each sensor node can provide localised measurements and detailed information that is not readily available through traditional instrumentation. This section reviews LCS development and highlights trends and future opportunities, explicitly focusing on air quality and meteorological networks.

Since the recognition of the potential of low-cost sensors in air quality monitoring by Snyder et al. [29], there have been numerous reviews on the development and applications of LCS and their networks. A significant focus has been on the suitability of LCS for

outdoor air quality monitoring, as the requirements for data acquisition can vary depending on the application. For example, McKercher et al. [30] discussed the suitability and challenges of LCS for monitoring gases, while Rai et al. [31] discussed the advancement of LCS technology from an end-user perspective.

To realise the full potential of LCS, there is a need for further research and development in data collection techniques and the integration of stakeholder engagement and policy making. This will enable more significant societal impacts from these low-cost sensor networks.

1.5.2 Sensor Networks

The sensors' main applications include outdoor monitoring, indoor monitoring or both, and personal monitoring [32]. These applications are diverse, so it is reasonable to expect they will have different performance requirements. For example, PM sensors used for detecting traffic or domestic burning-related pollution will need to be able to detect smaller particles. In comparison, sensors used for construction dust will only need to detect coarser-sized particles. For mortality calculation it requires higher accuracy instead. Therefore, one question is whether it makes sense to discuss a standard protocol' for such low-cost sensor networks if it should be related to the purpose, and if there should be different protocols with fewer criteria to be included.

1.5.3 Deployment of LCS

A sensor network consists of multiple electronic devices monitoring physical/environmental parameters, which are connected to transmit information and control operations. While physically wiring nodes to a central unit has benefits, a wireless network offers easier deployment, flexibility, and easier troubleshooting. Wireless Sensor Networks (WSNs) are expected to play a major role in the future, becoming a key technology for the Internet of Things. These are the main deployment options for air quality sensors: stationary, mobile, and wearable sensors.

1.5.3.1 Stationary Sensors

One or more sensors are located at fixed sites, and monitoring is conducted over time. A large number of sensors can provide information on spatiotemporal variations, transport rates, and pollution sources. However, a large number of sensors alone only form a network if they are linked together or transmit information to a central location, typically through

wireless connectivity. There is currently no standardised protocol defining the number of nodes for sufficient coverage of pollutants.

1.5.3.2 Mobile Sensors

High spatial resolution data is obtained using mobile platforms such as cars, bikes, or UAVs. UAVs are useful for measuring pollution in the vertical plane. Wearable sensors worn by individuals provide personal exposure estimates to various pollutants. The data collected by wearable sensors with concurrent GPS data can be used to estimate spatial distributions of pollutants in different environments.

1.5.3.3 Personal and Wearable Sensors

Individuals and community groups are turning to low-cost personal air quality monitors to assess environmental risks and take action [32]. The growing popularity of these monitors has led to an increase in the number of participatory sensing projects carried out by citizens [33]. Some well-known examples of these monitors include Plume Labs' "Flow", CleanSpace Tag, and Atmotube Pro. Although much has been written about the accuracy of these monitors, there needs to be more research evaluating their social or economic implications [32].

However, the few studies that do exist provide valuable insights into the potential impact of personal air quality monitoring. They suggest that access to personal exposure information can challenge preconceptions and shape people's responses to air pollution. For instance, monitor use has been associated with increased awareness, heightened emotions, enjoyment, and surprise [32]. Studies also show that monitor use can lead to minor changes in behaviour, such as closing windows and avoiding indoor burning of incense [34, 35]. On the other hand, Oltra et al. did not observe any intentional or real changes resulting from monitor use [33]. A recent study by Heydon and Chakraborty et al. demonstrated the effectiveness of portable air quality monitors in protecting children from air pollution on their way to school [36].

1.5.4 LCS evaluation Criteria

To evaluate air quality sensors, statistical indicators such as Root Mean Square Error (RMSE), bias, Standard Deviation (SD), and correlation coefficient (R) are commonly used. R Squared (R^2), which is a measure of goodness of fit, and the regression slope reflects the level of accuracy. However, the correlation coefficient is not always sensitive to

bias between the sensor data and reference measurements, including relative bias (slope not equal to 1) and absolute bias (intercept not equal to 0). Long-term drift and ageing can lead to lower R^2 values in longer field studies. The magnitude of error can be indicated by RMSE, which is also sensitive to extreme values and outliers. The measurement uncertainty is reported in only a few studies. However, there are some important considerations when interpreting R^2:

- **It Doesn't Imply Causation:** A high R^2 does not necessarily mean that the model has a causal relationship with the response variable.
- **Model Complexity:** As more variables are added to a model, R^2 will generally increase, even if those variables are irrelevant. This can lead to overfitting. Overfitting occurs when a model is too complex, capturing the noise in the data rather than the underlying process.
- **Arbitrary Close to 1:** It's possible for complex models, especially non-linear models or models with many parameters, to achieve an R^2 value arbitrarily close to 1 on their training data. However, this might not indicate a good model. Such models might be overfitting the data, and they might perform poorly on new, unseen data.

This is why it's often more informative to consider the adjusted R^2, which penalises the model for including unnecessary predictors.

1.5.5 Existing LCS evaluation

A technical report recently released by the Joint Research Centre (JRC), the scientific and knowledge service of the European Commission [32], revealed the existence of 112 different types of Low-Cost Sensors (LCS) classified into two categories: Original Equipment Manufacturers (OEMs) and Sensor Systems (SSys).

The term "low-cost" refers to the purchase price of LCS, which is significantly lower compared to the purchase and operating cost of reference analysers used for monitoring regulated inorganic pollutants and particulate matter. This difference in price can easily be an order of magnitude. In recent times, ultra-affordable OEMs have emerged in the market for PM monitoring [32]. Some of these sensors have begun to deliver performance comparable to low-cost OEMs manufactured in the Western world for detecting $PM_{2.5}$. These sensors are often designed to be integrated into interconnected devices' Internet of Things (IoT) networks. Currently, optical sensors for PM detection are available for purchase at a cost ranging from just a few tens to a few hundred euros and are manufactured

in countries like the Republic of China and the Republic of Korea. Some of these LCS have performance comparable to more expensive OEMs.

1.5.6 Data Processing for LCS

Data processing for air quality monitoring using low-cost sensors (LCS) can be classified into open-source and "black box" systems.

1. Open-source systems allow for the processing of LCS data performed by software that is tuned according to several calibration parameters and environmental conditions. All data treatments, from data acquisition to conversion to pollutant concentration levels, are known to the user. The use of open-source software in LCS has been discussed in several studies, such as "Design and Implementation of a Low-Cost Open-Source Air Quality Monitoring System" by Qiao et al. [37] and "Open-source low-cost air quality monitoring system for $PM_{2.5}$ and PM_{10}: design and evaluation" by Chen et al. [38]. These studies highlight the benefits of open-source systems, such as flexibility and cost-effectiveness.

2. LCS with calibration algorithms whose data treatment is unknown and without the possibility to change any parameter has been identified as "black boxes." These systems are pre-calibrated against a reference system, or the manufacturer can adjust the calibration parameters remotely. LCSs used for the detection of particulate matter (PM), such as the SDS011-Luftdaten, OPC-N2, OPC-N3 by Alphasense and the PMS series from Plantower are often used as "black box" systems, with mass concentration computed by unknown algorithms developed by manufacturers. The use of black box systems in air quality monitoring has been discussed in several studies, such as "Assessment of low-cost sensors for particulate matter monitoring" by de Leeuw et al. [39] and "Evaluation of low-cost sensors for particulate matter monitoring in indoor and outdoor environments" by Li et al. [40]. These studies highlight the limitations of black box systems, such as a lack of transparency and the inability of users to verify the accuracy of the data.

   Overall, open-source and black-box systems have advantages and disadvantages, and the choice of which method to use depends on the specific application and the user's needs. However, while open-source systems allow for more transparency and user control, black-box systems may be more convenient and easier to use.

1.6 Current and upcoming policies discussion

The United Kingdom has a long-standing problem with air pollution [41]. In recent years, the UK government has been under pressure to take action on this issue [42]. Several policies have been implemented or are currently being discussed in an attempt to improve air quality in the UK.

One such policy is the implementation of Ultra Low Emission Zones in London (ULEZs). These are areas where vehicles emitting high levels of pollutants are charged to enter. The first ULEZ was introduced in London in 2008 [43], and similar schemes such as Clean Air Zones (CAZs)are introduced in several other cities such as Sheffield, Manchester, Birmingham and Bradford [44].

Another critical policy is the introduction of more stringent emissions standards for new vehicles. From 2020, all new cars and vans sold in the UK must meet the Euro 6 emissions standards [45]. These standards are designed to reduce harmful pollutants emitted from vehicles significantly.

The UK government is also investing heavily in electric vehicles (EVs). The goal is for all new cars and vans to be zero-emission by 2050 [46]. To achieve this, several policies and initiatives are being put in place to encourage the uptake of EVs. These include offering financialisation by 2050. To help achieve this, several incentives are available for those who buy EVs, such as a grant towards the purchase price and access to free parking and charging points.

Some other policies are also being discussed, such as a diesel scrappage scheme (where people are given financial incentives to trade in their old, polluting diesel vehicles) and stricter rules on wood-burning stoves.

While there is still much to be done to improve air quality in the UK, these policies show that the government is committed to taking action on this important issue. These policies will help enhance the quality of air in the UK and protect the health of those who live here.

1.7 Research Motivation of this thesis

Low-cost sensors have the potential to alleviate some of these challenges and provide more real-time, accurate, and fine-scale data. However, several calibration and deployment challenges need to be addressed to fully realise the potential of low-cost air quality sensors. Additionally, while air quality models have improved in recent years, they still need help

to provide accurate predictions at fine scales due to the complex nature of atmospheric processes.

This thesis explores low-cost air quality sensors for monitoring and forecasting applications. In particular, this thesis will focus on developing new methods for sensor calibration, deployment, and source attribution. This thesis also explores machine learning models that utilise high-frequency, low-cost sensor data to improve air quality predictions.

By addressing these challenges, This thesis aims to improve the accuracy and utility of air quality monitoring and forecasting systems, which can ultimately lead to better public health outcomes.

1.8 Aim, Objectives, and Novelty

Aim: This thesis is dedicated to proposing a comprehensive architecture for leveraging low-cost sensors in air pollution monitoring. Grounded in the critical public health concern of air pollution, which is linked to over 7 million deaths globally, this research seeks to address the challenges of existing real-time Air Quality (AQ) monitoring stations, which are often expensive, sparse, and sometimes inaccurate.

Objectives:

1. To develop a novel approach for the deployment and usage of a low-cost sensor network in urban areas.
2. To design and implement a hybrid convolutional-long short-term memory (Conv-LSTM) model for spatiotemporal air pollution prediction, capturing both spatial patterns and temporal dependencies in the sensor data.
3. To evaluate and compare the Conv-LSTM model's performance with state-of-the-art statistical and machine learning models, such as SARIMA and NARX, in terms of prediction accuracy and robustness.
4. To present an in-depth evaluation of the proposed models using real-world data and assess their potential in driving policy changes aligned with the World Health Organization's 2021 air quality target.

Novelty: The central novelty of this research lies in the pioneering integration of convolutional layers with LSTM layers to capture both spatial and temporal patterns in air quality data sourced from LCS, yielding a significant improvement in prediction accuracy. This novel approach is further reinforced by the comprehensive deployment of a low-cost

sensor network and its evaluation using real-world studies. Additionally, the thesis offers a general solution to analyse the interplay between measurement noise levels, Gaussian process model hyperparameters, and the resulting prediction accuracy, providing a new perspective on low-cost sensor data interpretation.

1.9 Outline of the Thesis and Rationale

The trajectory of this thesis is formulated to guide readers from the broader challenges of air pollution monitoring to the specific nuances, innovations, and contributions of using Low-Cost Sensors (LCS) in diverse contexts.

The detailed outline of the thesis, showcasing its novelty and contribution, is as follows:

- **Chapter 1** introduces the overarching context, presenting the air pollution problem in the UK and the urgent need for more granular data. By establishing the magnitude and significance of the issue, this chapter sets the stage and defines the motivation for the research journey that follows.
- **Chapter 2** delves into the practical aspects of designing a low-cost sensor network, illustrating its calibration of LCS in Sheffield. The chapter highlights the challenges faced in urban environments and the potential solutions offered by such sensors. This sets a practical foundation, making a case for the need for advanced methodologies.
- **Chapter 3 and Chapter 4** transition into the theoretical domain, addressing the limitations in existing predictive models and proposing refined techniques. These chapters are pivotal, acting as the bridge between understanding the real-world challenges and developing advanced solutions. They emphasize the thesis's commitment to enhancing the efficacy and accuracy of predictions using sensor data.
- **Part 2** builds upon the methodologies developed, showcasing them in action. Each chapter here unravels a distinct dimension of air quality monitoring, reflecting the holistic approach of the research. This segment seamlessly integrates theory with practice, highlighting the real-world impacts and validating the earlier methodologies.
- **Chapter 5** pioneers the exploration of indoor air pollution, specifically emanating from residential wood stoves, using LCS. By delving into the intricacies of indoor pollution, this chapter broadens the perspective on air quality, emphasizing that challenges are not limited to outdoor environments. The novelty lies in harnessing

LCS to capture granular, real-time data from indoor sources, shedding light on an often-overlooked aspect of air quality- wood stove users are exposed to three times the air pollution.

- **Chapter 6** shifts the lens to outdoor environments, particularly school premises, to investigate the efficacy of green barriers in mitigating air pollution. This chapter introduces a novel approach of using LCS to monitor the impact of green infrastructures, thereby offering actionable insights for urban planning and school infrastructure development.

- **Chapter 7 and Chapter 8** delve into the analytical realm, exploring Gaussian processes and uncertainty quantification in assessing air quality using LCS data. These chapters underscore the commitment to advancing analytical methodologies tailored for LCS data, ensuring that the derived insights are both accurate and reliable. The contribution here is twofold: refining predictive models and accounting for uncertainties inherent in LCS data.

- **Chapter 9** transitions to a behavioral perspective, exploring how wearable LCS can influence parents' decisions during school runs. The novelty here is in the marriage of technology and behavior, assessing how real-time data can serve as a catalyst for change.

- **Chapter 10** deepens this behavioral exploration, critically analyzing why the "cold stark data" from sensors might currently fall short in prompting behavioral change. By juxtaposing the potential of LCS data with its current limitations in influencing behavior, this chapter offers a profound reflection on the human-technology interaction and paves the way for future innovations in data presentation and interpretation.

Throughout this narrative, the thesis consistently showcases the versatility of LCS in air quality monitoring, spanning indoor and outdoor environments, analytical rigor, and behavioral influences. The progression ensures readers grasp the multi-dimensional challenges in air quality monitoring and appreciate the innovative solutions and their broader implications. Each chapter adds a unique facet to the understanding of LCS's potential, ensuring a comprehensive, novel, and impactful contribution to the domain of air quality monitoring.

Ethical approval for the deployment of sensors and conduct of all real-world studies (Chapters 3, 5, 6, 7, 9 and 10) was duly obtained from the University of Sheffield and the University of Nottingham. All research methodologies and participant interactions adhered to the guidelines set forth by both institutions.

Part I

Conceptual Framework

Chapter 2

Calibration and Accuracy Assessment of a Low-Cost Sensor Network for Air Pollution Monitoring

Urban air pollution poses a significant risk to city residents. However, the effects of sporadic, high-level exposure remain poorly understood. Traditional air quality monitoring relies on a network of stationary, sparse measurement stations, which are too costly to capture temporal and spatial variation and pinpoint pollution hotspots. The recent advancements in low-cost micro-scale sensors have opened up the possibility of real-time, detailed air quality information. Yet, the question of whether the less accurate data produced by these sensors is valuable remains, as well as how to improve their data quality and effectively communicate it to mitigate air pollution's impact.

2.1 Low-Cost IoT AQ Sensor Evaluation and Validation

2.1.1 Sensor Selection and Characterisation

Sensor Selection and Characterization is a critical step in the evaluation and validation of low-cost IoT air quality sensors [47]. The selection of appropriate sensors is essential for ensuring that the data collected is of high quality and reliable [27]. This section discusses the selection criteria that were followed for low-cost IoT air quality sensor deployment in Sheffield and the characterization of the selected sensors.

The selection criteria for low-cost IoT air quality sensors are typically based on the intended application, measurement range, accuracy, precision, and cost [48]. For example, if the goal is to monitor particulate matter (PM) in the air, the sensor should be able to detect PM with a high level of accuracy and precision. In terms of cost, low-cost IoT air quality sensors are typically less expensive than traditional air quality monitoring equipment, making them more accessible to a wider range of users [49].

Once the selection criteria have been established, a variety of sensors can be evaluated to determine their suitability for the intended application. This can be done through a combination of laboratory and field testing [49]. Laboratory testing typically involves exposing the sensors to controlled concentrations of pollutants and measuring their performance [50]. Field testing, on the other hand, involves deploying the sensors in real-world environments and collecting data over an extended period [49, 50].

Once the sensors have been selected, they need to be characterized [51]. This typically involves determining their measurement range, accuracy, and precision [50]. The accuracy of a sensor refers to how closely the sensor's measurements match the true concentrations of a pollutant [48].

To determine the measurement range, accuracy, and precision of a sensor, a series of tests can be performed [52]. One common method is to expose the sensor to a range of concentrations of a pollutant and measure the sensor's response [49, 50]. The sensor's measurement range can be determined by the lowest and highest concentrations of the pollutant that it can detect [48, 51]. The sensor's accuracy can be determined by comparing its measurements to reference measurements of the pollutant concentrations [50]. The sensor's precision can be determined by measuring the sensor's response to the same concentration of a pollutant multiple times and calculating the standard deviation of the measurements [52].

In conclusion, the selection and characterization of low-cost IoT air quality sensors is a critical step in the evaluation and validation of these sensors. The selection criteria, including intended application, measurement range, accuracy, precision, and cost, should be established to ensure that the sensors selected are suitable for the intended application. Once the sensors have been selected, they should be characterized to determine their measurement range, accuracy, and precision [49, 52]. This information is essential for understanding the performance of the sensors in the field and for making decisions about their use in air quality monitoring applications.

2.1.2 Establish a baseline of air quality

Establishing an air quality baseline in Sheffield provides a fundamental understanding of the overall air quality in the city and pinpoints areas that may require enhanced monitoring or interventions. This section elaborates on the utilization of low-cost IoT air quality sensors to establish this baseline, focusing on three key sites in Sheffield: Netheredge, Crosspool, and Devonshire Green.

A variety of studies have suggested criteria for sensor selection based on intended applications, measurement range, accuracy, precision, and cost [47]. This work employed sensors at three pivotal sites for data collection and then juxtaposed the readings with a reference sensor to validate their efficacy.

Sheffield, a geographically diverse city in South Yorkshire, England, boasts diverse elevations and a growing population. Touted as the "greenest city" by the local City Council, Sheffield experiences a temperate climate, with July being the warmest month [44]. Major contributors to the city's air pollution include road transport, industrial processes, and fossil fuel combustion in energy supply and domestic heating systems [49].

Three sites in Sheffield were selected for this study. The sensors, SDS011 and PMS5003, both popular in citizen science projects, were evaluated [53]. Throughout this chapter, reference instruments and methods, as endorsed by the Department for Environment, Food & Rural Affairs, UK, or equivalents (like those used by Sheffield City Council and MOBIUS van), will be termed as reference monitors. These air quality monitoring sensors (AQMS) were positioned at various urban backgrounds in Sheffield for four weeks.

Data from these sensors, sampling $PM_{2.5}$ and PM_{10} every 167 seconds and then averaged hourly to mitigate noise, is conveyed to a secured database server overseen by the IT Services of the University of Sheffield. The data can be accessed via a dedicated API for this server.

Furthermore, meteorological data from Weston Park, Sheffield, was employed to assess the influence of weather conditions on pollution levels. An extensive analysis was conducted on data from the Lowfield reference station, and in-depth evaluations were carried out to validate the "Flow" sensors by Plume Labs.

2.1.2.1 Analysis

Detailed analysis revealed specific trends such as the elevated $PM_{2.5}$ concentrations during early morning hours.

FIGURE 2.1: Site locations: (a) Lowfield (b) Netheredge (c) Crosspool. Map data: [54]

Field tests with the "Flow" sensors by Plume Labs were meticulously structured to validate their performance. These evaluations were strategically located at recognized pollution hotspots, ensuring varied pollution levels.

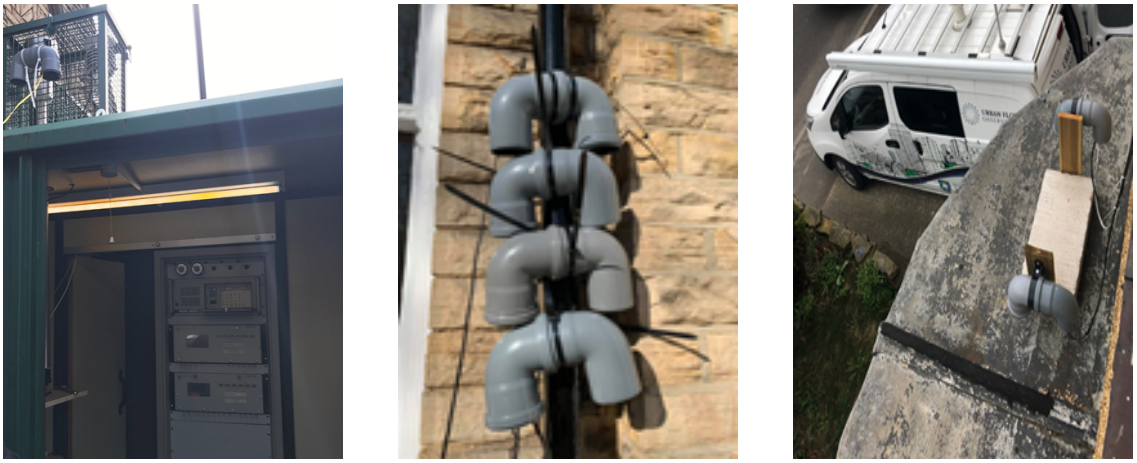

FIGURE 2.2: Site deployment: (a) Lowfield (b) Netheredge (c) Crosspool.

Site	**Mean PM_{10}** ($\mu g/m^3$)	**Mean $PM_{2.5}$** ($\mu g/m^3$)
Lowfield	21.98	11.24
Netheredge	17.11	9.01
Crosspool	11.79	7.53

TABLE 2.1: Mean concentration levels of PM_{10} and $PM_{2.5}$ across different sites.

An in-depth analysis of the Lowfield reference station data for the year 2019 was undertaken. This rigorous study aimed to facilitate a comparative understanding and to identify discernible seasonal variations. A marked observation was the elevated $PM_{2.5}$ concentrations during the early morning hours (2:00-4:00) when compared against the daytime readings. This trend is substantiated by Figure 2.5, which presents a comparison of $PM_{2.5}$ and NO_2 concentrations across diurnal cycles.

To further this investigation, field evaluations were conducted using ten mobile sensors, known as "Flow," developed by Plume Labs. These evaluations were designed to align with reference analyzers, providing a platform to gauge the accuracy and performance of the Flow sensors. By August 2019, four distinct evaluations had been executed. The data amassed from these Flow devices was subsequently compared with readings from the MOBIUS for a comprehensive analysis. The chosen sites for these evaluations were strategically determined considering the power requisites for the monitoring van and their known status as pollution hotspots, ensuring diverse pollution readings. Each of these rigorous evaluations spanned a duration of six hours.

FIGURE 2.3: Flow Sensor Evaluation.

At the outset, it's essential to define what we mean by the 'level' or 'concentration' of a pollutant. In this context, the 'level' refers to the concentration of a specific pollutant in the air, typically expressed in micrograms per cubic meter ($\mu g/m^3$) or parts per million (ppm), depending on the pollutant in question.

As for the normalization of these levels, the process is crucial to make 'levels' from different sources or of different scales comparable. Normalization, in this context, refers to the adjustment of concentrations measured on different scales to a common scale. One of the primary methods to normalize data is:

Dynamic Range Normalization: This method scales the original data to fit within a specified range, [0,1] in this case.

$$\text{Normalized Value} = \frac{\text{Original Value} - \text{Minimum Value}}{\text{Maximum Value} - \text{Minimum Value}}$$

In our analyses, pollutant levels are normalized using the Dynamic Range Normalization method, ensuring that the concentration levels from various sources or timeframes can be directly compared without misconceptions.

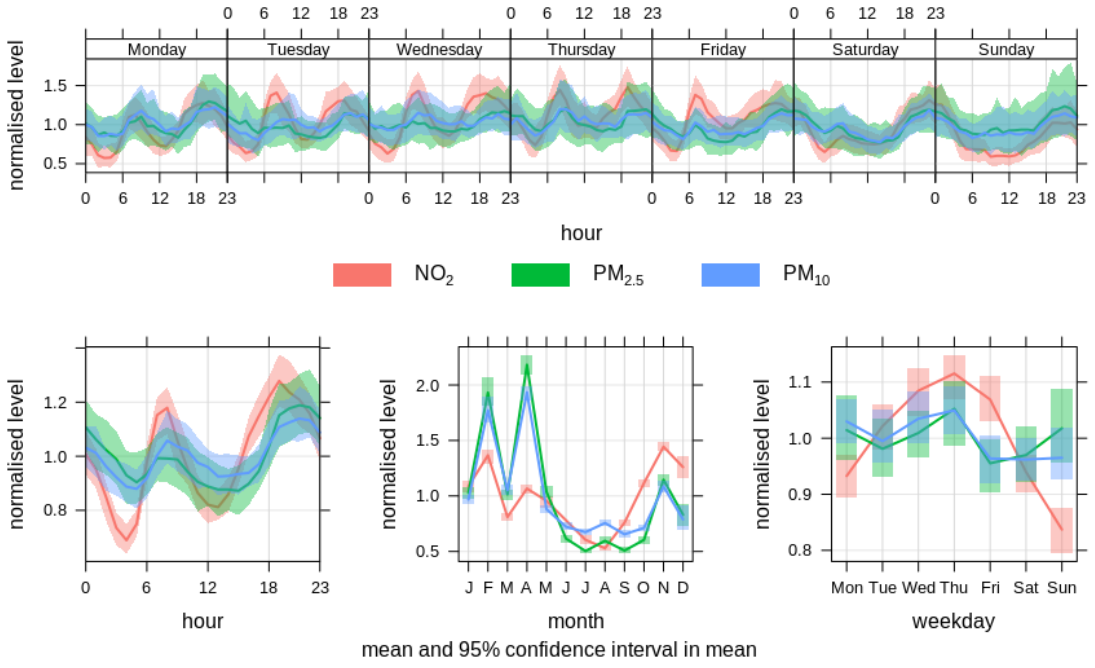

FIGURE 2.4: Day-wise pollution plot from Lowfield site in 2019.

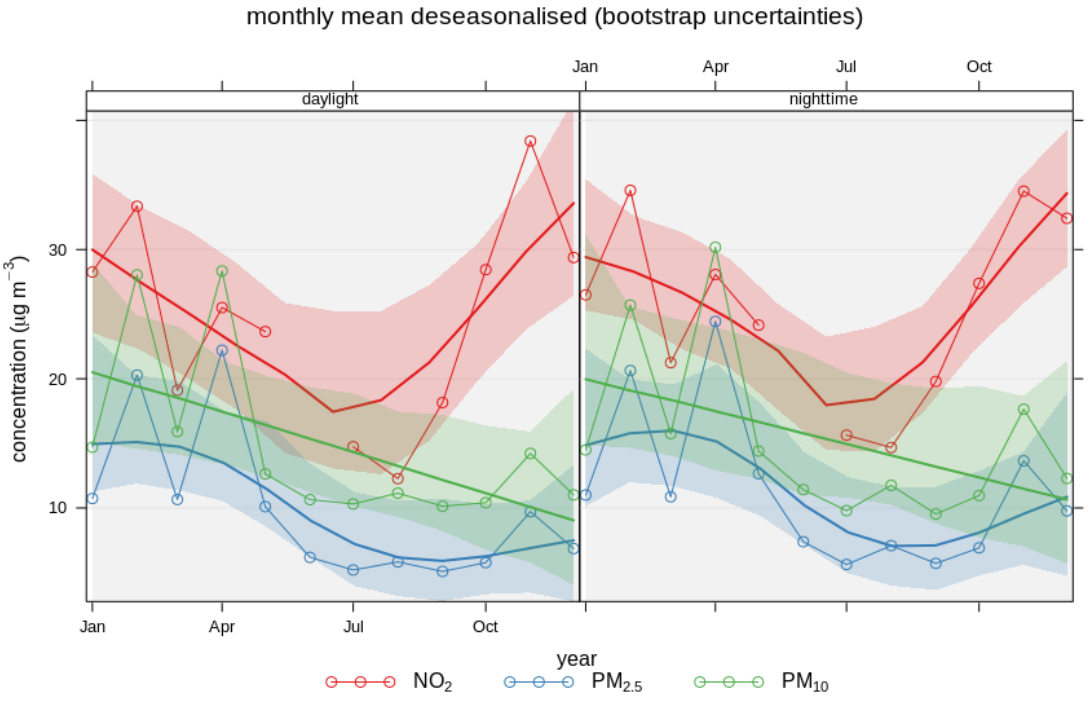

FIGURE 2.5: Day-night comparison plot from Lowfield site in 2019.

2.1.2.2 Background

The Sheffield, UK study aimed to assess the accuracy of commercially available low-cost air pollution sensors. These sensors were deployed at 4 DEFRA air monitoring sites and in a local sensor network covering a 367 sq. km area. Results showed variable performance, with some sensors measuring oxides of nitrogen, ozone, and particulate matter (PM) producing highly similar signals, while others showed inconsistent results. A variety of PM sensors were tested, revealing high inter-sensor agreement ($r = 0.99$) but moderate correlation with a reference $PM_{2.5}$ monitor ($r = 0.65 - 0.83$). Chapter 3 elaborates on these findings. For select sensors with moderate to strong correlation with reference monitors ($r > 0.5$), multiple linear regression was performed to determine if correction algorithms incorporating ambient temperature, relative humidity, and number of data points could improve accuracy. The best improvement in agreement was seen for a PM sensor ($R^2_{\text{adj-orig}} = 0.57$, $R^2_{\text{adj-final}} = 0.81$) after incorporating all factors.

2.1.2.3 Calibration of LCS

Calibration of low-cost air quality sensors is an essential step in ensuring that the data collected by these sensors is accurate and reliable. This section discusses the calibration of low-cost air quality sensors for the measurement of $PM_{2.5}$, PM1, PNC, and NO_2, and the use of humidity correction formulas to improve the accuracy of the measurements.

The calibration of low-cost air quality sensors involved exposing the sensor to a range of known concentrations of a pollutant and measuring the sensor's response. The sensor's response was then used to create a calibration equation that relates the sensor's output to the concentration of the pollutant. It is important to note that the calibration equation is specific to the sensor and the pollutant being measured. Therefore, it is necessary to calibrate the sensor for each pollutant separately.

Another important factor to consider when calibrating low-cost air quality sensors is the effect of humidity on the sensor's response. Humidity can affect the sensor's response by changing the properties of the sensing material or by altering the electrical resistance of the sensor. To account for this effect, humidity correction formulas were used to adjust the sensor's output based on the humidity level.

2.1.2.4 Single-point calibration

Single-point calibration is a method used to correct sensor deviation by adjusting the error to a measured value at a single point within the sensor's measurement range. This method

is most commonly used when the sensor has a linear characteristic and a consistent slope within the desired measurement range.

One of the main advantages of single-point calibration is its simplicity. It requires only one measurement point to be corrected, making it a quick and easy method to use. In addition, it can also be used as a ”drift check” to detect changes in the sensor’s response or deterioration in performance over time. However, it is important to note that single-point calibration is only appropriate for sensors with a linear characteristic and a consistent slope within the desired measurement range. If the sensor has a non-linear characteristic or if the slope changes within the measurement range, a multi-point calibration method will be required.

Additionally, single-point calibration is not suitable for sensors that have a wide measurement range, as it only corrects for errors at one point within the range. In such cases, multi-point calibration is required to correct for errors across the entire measurement range.

It is also important to note that single-point calibration is a one-time process, and it should be repeated periodically to ensure that the sensor’s performance remains consistent over time.

2.1.2.5 Two-point calibration

Two-point calibration involves three steps to correct both slope and offset errors:

1. Measurement: Take two measurements using the sensor to be calibrated - one near the lower limit of its range and another near the upper limit. Record these measurements as ”Raw Low” and ”Raw High”.
2. Reference Measurement: Repeat the same measurements using standard measuring equipment and record the values as ”Ref Low” and ”Ref High”.
3. Calculation: Calculate the ”Raw Range” by subtracting Raw Low from Raw High, ”Ref Range” by subtracting Ref Low from Ref High, and finally, the corrected value ”Corrected Value” using a specified formula:

$$\begin{aligned}\text{CorrectedValue} = (((\text{RawValue} - \text{RawLow}) * \text{ReferenceRange})/\text{RawRange}) \\ +\text{ReferenceLow}\end{aligned}$$

2.1.2.6 Multi-point curve calibration

The Multi-point Curve Calibration involves:

1. Collect data by measuring the response of the sensor at multiple reference correction points within its measuring range.

2. Calculate curvature coefficients for the sensor's characteristic curve using the collected data.

3. Use the calculated coefficients to develop a linearisation formula for compensating errors in sensor measurements.

2.1.2.7 Building the data

This section presents the seven steps in which low-cost air quality sensors were deployed and used to create an end-to-end air quality dataset in Sheffield in order to provide comprehensive coverage of air quality.

1. Individual sensors: Low-cost air quality sensors were deployed individually, either by members of the public or by the local city authorities. One advantage of this method is that it allows for dense coverage of a city, as sensors can be placed in many different locations. A disadvantage is that the data from individual sensors may not be representative of the air quality in a larger area.

2. Air quality networks: Air quality networks are composed of multiple sensors that are distributed throughout a city. The data from these sensors is collected and transmitted to a central location, where it can be monitored in real-time. "Clean Air for Sheffield" - a citizen science-based initiative was started to deploy a DIY low-cost (less than £30) IoT-based Air Pollution monitor network in Sheffield. About 150-200 LCS were deployed through workshops in Sheffield.

3. Crowdsourcing: Crowdsourcing is a method of collecting data from large numbers of people using mobile devices or the internet. This data can then be used to map air quality in real time. Several workshops in public places, such as in pubs, were conducted to build and add to this monitoring network.

4. Static monitoring stations: Static air quality monitoring stations are typically operated by government agencies or universities. These stations usually have more sophisticated sensors than those that are deployed individually, and they provide long-term data that can be used for research purposes. Several AQMesh and Envirowatch sensors formed a part of this network installed by the University of Sheffield.

5. Vehicle-mounted sensors: Air quality sensors can be mounted on vehicles, such as cars, buses, or trucks. These sensors can be used to map air quality in real time, as well as to track emissions from vehicles. At Urban FLows Observatory, a similar van - The MOBIle

Urban Sensing vehicle, 'MOBIUS' was built to support this sensor network. This mobile sensing vehicle is equipped with air quality analyzers, a weather station, and antenna air monitors, which allow it to collect precise measurements of air quality indicators such as NOx, particulates, and ozone. It also gathers data on environmental factors such as temperature, humidity, wind speed, and wind direction. With its telescopic mast, the vehicle can provide air quality metrics at a height of up to 9 meters. Additionally, it can study the materials used for structures and their impact on energy consumption and map the use of radio technology for mobile phones, Wi-Fi, and IoT devices.

6. Satellite remote sensing: Satellite remote sensing is a method of collecting data on air pollution from space. This data can be used to map air pollution at a regional or global scale. Satellite data from tomorrow.io was used to fill gaps in the data.

7. Modeling: Air quality models can be used to predict air pollution levels based on data from other sources, such as weather models. This method is useful for forecasting air quality trends. Various spatiotemporal models were evaluated to deploy a fully connected system to measure air quality in Sheffield.

The most comprehensive coverage of air quality was achieved by using a combination of the above methods.

2.2 Results and Discussion

2.2.1 Sensor Evaluation and Validation

Comparing the performance of different air quality sensors is essential for determining their accuracy and suitability for a particular application. In this case, the PMS5003 and SDS011 sensors are being compared.

According to several peer-reviewed studies, such as [55, 56], the PMS5003 sensor has been shown to overestimate $PM_{2.5}$ concentrations when compared to the SDS011 sensor. This is likely due to the fact that the PMS5003 sensor has a higher sensitivity to $PM_{2.5}$ particles, leading to higher measurement values.

In statistical modelling, R^2_{adj} (often referred to as adjusted R-squared) provides a modification of the R-squared statistic that adjusts for the number of predictors in a model. Unlike R^2, which only increases when new predictors are added to the model, R^2_{adj} increases only if the new predictor enhances the model above what would be obtained by probability.

$$R^2_{adj} = 1 - \frac{(1 - R^2)(n - 1)}{n - k - 1} \tag{2.1}$$

Where n is the number of observations, and k is the number of predictors.

The root mean square error (RMSE) is another metric used to evaluate the differences between predicted and observed values:

$$RMSE = \sqrt{\frac{1}{N}\sum_{t=1}^{N}(y_t - \tilde{y}_t)^2} \tag{2.2}$$

Despite this overestimation, both sensors have been found to measure the same fluctuations in $PM_{2.5}$ concentrations over time, indicating a strong correlation between their measurements. In fact, a maximum R^2_{adj} value of 0.86 between the PMS5003 and SDS011 sensors has been noted in our research. A value of 0.86 is considered a strong correlation, indicating that the two sensors are measuring similar trends in $PM_{2.5}$ concentrations.

However, it should be noted that these studies used sensors placed in a specific location and in a specific time period, so the correlation and the overestimation might be different in other places or time periods. It is important to validate the performance of the sensors in the specific location and conditions where they will be used.

The performance of low-cost sensors was assessed for its consistency with the use of the coefficient of variation (CV) method. Results showed that the CV values for both SDS011 and PMS5003 sensors were below 7%. During the measurements, the trends of the low-cost sensor outputs were generally consistent with the reference data. However, there was an overestimation of $PM_{2.5}$ concentrations in the raw data obtained from the low-cost sensors.

Further evaluation revealed a strong linear correlation between the reference sensors and the low-cost sensors for both PMS5003 and SDS011 units. This correlation was observed at different time intervals, such as 1 minute, 15 minutes, and 1 hour, with values of 0.89 and 0.86, respectively. The daily average values were even higher, with PMS5003 sensors having values between 0.91 to 0.93 and SDS011 sensors having values between 0.87 to 0.90.

This indicates the robustness of low-cost sensors in reflecting the trends seen in the reference data despite the overestimation in the raw data. These high correlation values suggest that low-cost sensors can be a feasible option for monitoring air quality in specific circumstances. However, further work can be done to enhance their performance and

refine the correction algorithms used to minimize the differences between the low-cost sensor data and the reference data.

The PMS5003 overestimates the $PM_{2.5}$ concentrations most of the time in comparison with the SDS011sensor. Both devices seem to measure the same fluctuations over time, so there is a significant correlation. Maximum $R^2_{adj} = 0.86$ between PMS5003 and SDS011 was noted. Additionally, an SDS011 and AQMesh have been colocated for six months, with Maximum $R^2_{adj} = 0.85$.

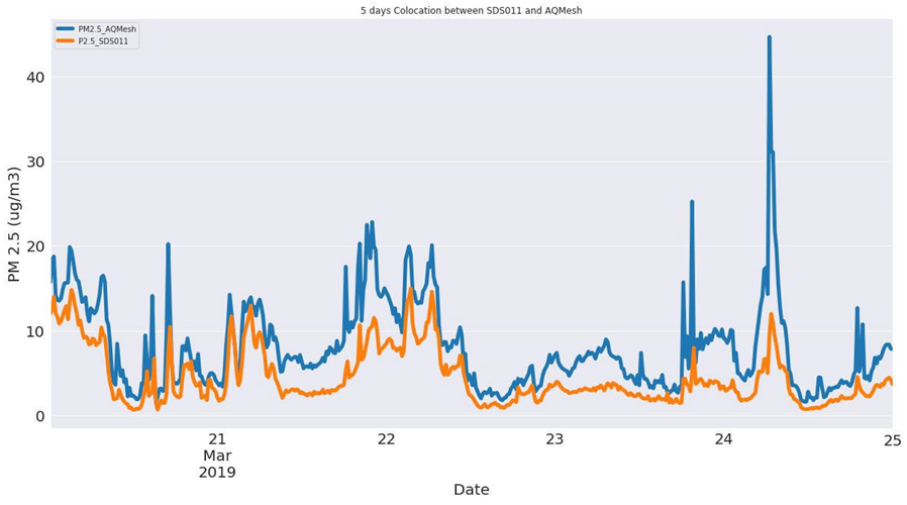

FIGURE 2.6: Inter sensor comparison.

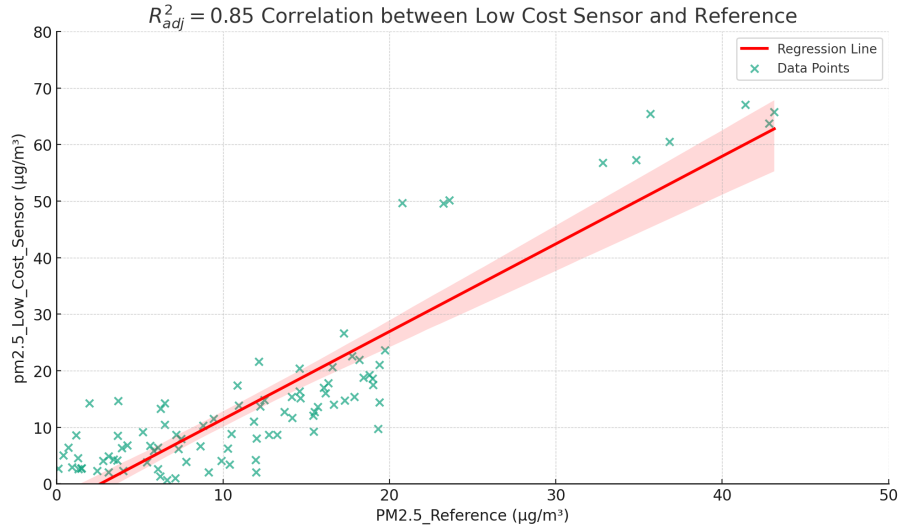

FIGURE 2.7: Low-cost sensors compared to reference monitors.

2.3 Conclusion

The deployment and calibration of low-cost air pollution sensors have been a topic of increasing interest in recent years. These sensors offer a cost-effective solution for monitoring air quality by providing high-resolution, spatiotemporal data on pollutant concentrations. However, the calibration of these sensors can vary greatly depending on the type and location of the sensor. This chapter presents a deployment methodology for LCS that takes into account location-based and individual calibration of sensors at any given time.

The field tests revealed high inter-sensor correlations for optical-based LCS monitoring PM. However, when tested in the field against reference sensors, the correlations were significantly lower, varying with RH and T. This highlights the importance of field calibration against reference-grade sensors.

PM measurements were only evaluated in the field, and better agreement was found in summer when relative humidity was lower. This may be due to the water particles affecting optical refraction and partly to the conversion factors used by the sensor manufacturer to convert particle number concentrations to mass concentrations. Using conversion factors specific to the location and weather may improve this issue.

Overall, our research identified a major technical challenge associated with low-cost sensors: their robustness and measurement repeatability. Our results show that factory calibration alone is not sufficient for real-world conditions and that it is necessary to perform individual field calibrations for each sensor. Additionally, calibration parameters may change over time, making it difficult to determine if the sensors are under or over-estimating pollutant concentrations. Therefore, it is crucial to thoroughly evaluate low-cost sensor platforms under a variety of environmental conditions.

Chapter 3

Outdoor Air Quality: Temporal Nowcast and Forecast Models

> Essentially, all models are wrong, but some are useful
>
> George Box

3.1 Introduction

Outdoor air quality is a critical issue that affects human health and the environment. To address this issue, it is crucial to have accurate and reliable methods for monitoring and forecasting air quality. This chapter focuses on the development of temporal nowcast and forecast models for outdoor air quality.

The autoregressive integrated moving average (ARIMA) model is a widely recognized statistical model for linear univariate time series forecasting. This model integrates other popular autoregressive time series models like autoregression (AR), moving average (MA), and autoregressive moving average (ARMA). These models are employed to predict the future values of a single time series based on its past values.

In addition to statistical models, machine learning models have also been used for time series forecasting. One example is the linear support vector regression (SVR) model, which treats the forecasting problem as a typical regression problem with time-varying parameters. This approach has been used in several studies, such as Cao and Tay [57] and Kim [58], which have demonstrated its effectiveness in forecasting air quality.

In this chapter, we compare the performance of the most well-known statistical and machine learning models for time series forecasting for LCS and their application to outdoor air quality. This chapter also presents the challenges and limitations of these models and presents new and innovative methods for forecasting outdoor air quality. The main focus will be on developing models that can accurately and reliably predict outdoor air quality in real-time and thereby enable effective decision-making and mitigation strategies to improve air quality.

3.2 Dependence in Time Series

Understanding the structure and dependencies within time series data is paramount for accurate and reliable forecasting. This is especially true when predicting air quality, such as PM2.5 concentration values. The historical trends and patterns observed in such data can provide invaluable insights into future values, allowing for timely and effective interventions in the interest of public health [59].

3.2.1 Foundations of Time Series Dependence

Observations in time series data, like PM2.5 concentrations, are often not isolated occurrences. They tend to exhibit intricate relationships across time intervals. For instance, the observation at time t might influence or be influenced by observations at $t+1$ or even later. Given a sequence (X_t) where $t = 1, \ldots, T$, our typical goal is to predict X_{T+h} for some positive integer h, drawing from the historical data up to T.

3.2.1.1 Independence and Its Implications

Before delving into the mechanics of time series modelling, it's essential to grasp the concept of independence in statistical terms. Two events, A and B, are deemed independent if their joint probability equals the product of their individual probabilities [59]:

$$\mathbb{P}(A \cap B) = \mathbb{P}(A)\mathbb{P}(B) \tag{3.1}$$

For a collection of events $A_1, \ldots, A_n$, independence is expressed as:

$$\mathbb{P}(A_1 \ldots A_n) = \mathbb{P}(A_1) \ldots \mathbb{P}(A_n) \tag{3.2}$$

This notion extends to random variables, where two variables X and Y are independent if their joint Cumulative Distribution Function (CDF) is the product of their individual CDFs:

$$F_{X,Y}(x, y) = F_X(x)F_Y(y) \tag{3.3}$$

3.2.1.2 Cumulative Distribution Function (CDF)

The CDF is a cornerstone in time series analysis and many other statistical disciplines. It provides the probability that a random variable X assumes a value less than or equal to x:

$$F_X(x) = P(X \leq x) \tag{3.4}$$

Understanding the CDF is crucial, especially when we are dealing with continuous data such as PM2.5 air quality measurements.

3.3 Models for Time Series Forecasting

With a foundation in time series dependencies, we can explore various models tailored for forecasting tasks. These models have evolved over the years, each catering to specific types of data and forecasting requirements. In the context of air quality prediction, it's imperative to choose a model that can effectively capture the nuances of the data and yield accurate forecasts.

3.3.1 Autoregressive (AR) Model

Autoregressive (AR) models are linear models in which the present value of the time series is expressed as a linear combination of past values. The mathematical representation is:

$$X_t = c + \sum_{i=1}^{p} \varphi_i X_{t-i} + \epsilon_t \tag{3.5}$$

where c is a constant, φ_i are the autoregression coefficients, p is the order of the model, and ϵ_t is the error term. The error term is assumed to be white noise.

3.3.2 Moving Average (MA) Model

The moving average (MA) model represents the current time series value as a weighted average of past errors:

$$X_t = \mu + \epsilon_t + \sum_{i=1}^{q} \theta_i \epsilon_{t-i} \tag{3.6}$$

where μ is a constant, θ_i are the moving average coefficients, q is the order of the model, and ϵ_t is the error term.

3.3.3 Autoregressive Moving Average (ARMA) Model

The ARMA model, a fusion of AR and MA models, is represented as:

$$X_t = c + \sum_{i=1}^{p} \varphi_i X_{t-i} + \epsilon_t + \sum_{i=1}^{q} \theta_i \epsilon_{t-i} \tag{3.7}$$

where c is a constant, φ_i and θ_i are the autoregression and moving average coefficients, respectively.

3.3.4 Autoregressive Integrated Moving Average (ARIMA) Model

The ARIMA model, suitable for non-stationary time series, is expressed as:

$$\Delta^d X_t = c + \sum_{i=1}^{p} \varphi_i \Delta^d X_{t-i} + \epsilon_t + \sum_{i=1}^{q} \theta_i \epsilon_{t-i} \tag{3.8}$$

where Δ^d is the difference operator, and d is the differentiation order.

3.3.5 General Autoregression Model: Statistical Algorithm based on NARX

The general autoregression model, often based on the Nonlinear Autoregressive Exogenous model (NARX), is formulated as:

$$x(t+k) = f(y(t), \ldots, y(t-p+1), X(t), \ldots, X(t-q+1)) + e(t) \tag{3.9}$$

Here, y(t) is the target time series, and X(t) is a multivariate series containing prediction features. The noise term e(t) is assumed to be identically independently distributed.

3.4 Deep Learning Models: RNN-LSTM

Deep learning, a sophisticated branch of machine learning, has been instrumental across various domains, with time series forecasting being no exception. Within the deep learning realm, Recurrent Neural Networks (RNNs) stand out for their proficiency in handling sequential data, making them especially apt for time series datasets. The Long Short-Term Memory (LSTM), an advanced RNN variant, has consistently outperformed in diverse applications.

3.4.1 Vanilla Long-Short-Term-Memory Network

The vanilla LSTM network, as detailed in this section, integrates multiple LSTM layers, culminating in a fully connected linear layer. This structure ensures accurate predictions of pollution levels k steps ahead. Distinctively, the general RNN prediction hinges on both the immediate measurements and the recurrent hidden state. This interrelation can be mathematically represented as:

$$y(t+k) = f(h(t), y(t), X(t)) \tag{3.10}$$

$$h(t+1) = g(h(t), y(t), X(t)) \tag{3.11}$$

3.4.1.1 Data Preparation

The acquired data necessitated rigorous preprocessing due to the presence of missing values, outliers, and inconsistencies.

- **Handling Missing Values:** Absences in data can arise from unlogged observations or data anomalies. Addressing this requires techniques like annotating missing values as NaN, eliminating columns or rows marred by absences, or substituting missing entries with domain-specific values or statistical measures like mean, median, or mode.

- **Removing Outliers:** Outliers, essentially data points that significantly diverge from the norm, can be pinpointed using scatter plots or box-whisker plots. Identification and subsequent removal of outliers are typically based on Z-score computations.
- **Re-Scaling and Normalization:** Post the data cleansing process, it was resampled to yield 5-minute average observations. This data was then normalized.
- **Multi-step Prediction:** Achieving multi-step predictions can be orchestrated through two primary methodologies: the recursive approach and the direct technique.
- **Model Training:** Each learning algorithm was applied to train two distinct models for every collocated dataset: a model for 1-step-ahead (or 5-minute-ahead) prediction and another for 6-step-ahead (or 30-minute-ahead) predictions.

3.4.2 Results and Discussion

This chapter delves into the performance evaluation of an array of machine learning and deep learning models specifically tailored for predicting air pollution. The eclectic mix of algorithms encompasses linear regression, decision trees, random forests, gradient boosting, long short-term memory (LSTM) networks, gated recurrent units (GRU) networks, support vector regression (SVR), and the nonlinear autoregressive network with exogenous inputs (NARX).

3.4.2.1 Dataset and Pre-processing

The dataset used for this analysis was procured from Sheffield's air quality monitoring stations. It was split into a training set, encompassing 70% of the data, and a test set, constituting the remaining 30%. This ensures a comprehensive understanding of the model's performance on unseen data.

3.4.2.2 Algorithmic Details

To address reproducibility:

Model Details:

- **Linear Regression:** Regularization employed was L2 (Ridge Regression) with a regularization strength of 0.5. This prevents overfitting while allowing the model to learn from the data.

- **Random Forest and Decision Trees:** The depth of the trees was restricted to 10 to prevent overfitting. Random forests utilized 100 trees.
- **LSTM and GRU Networks:** Both networks comprised three layers with dropout regularization of 0.2 to prevent overfitting. The model was trained using the Adam optimizer with a learning rate of 0.001.
- **Support Vector Regression (SVR):** The RBF kernel was employed, with a regularization parameter, C, set to 1.
- **NARX:** This network was implemented with a delay of 2-time steps and trained using the Levenberg-Marquardt optimization.

3.4.2.3 Evaluation and Insights

The primary metrics for evaluation were the Mean Absolute Error (MAE) and Mean Squared Error (MSE). As delineated in Table 3.1, deep learning models, notably RNN-LSTM and GRU, surpassed traditional machine learning counterparts. Particularly, RNN-LSTM and GRU manifested the lowest MAE and MSE, epitomizing their superior predictive accuracy.

Furthermore, deep learning models exhibited enhanced proficiency in forecasting air pollution for elongated timeframes, such as a day or a week ahead, over near-term predictions like the subsequent hour. This can be attributed to the innate capability of these models to discern intricate nonlinear relationships prevalent in the input data.

The findings underscore the preeminence of deep learning models, especially RNN-LSTM and GRU, in the domain of air pollution forecasting. Such models could be pivotal for efficacious air quality monitoring, thereby mitigating the detrimental repercussions of pollution on human health and the environment.

However, it is imperative to further corroborate these results, comparing them against other avant-garde models and discerning their pertinence to varied air pollution forecasting paradigms. Moreover, future endeavours could delve into ensemble techniques, amalgamating the strengths of individual models for enhanced accuracy.

Algorithm	Next Hour MAE	Next Hour MSE	Next Day MAE	Next Day MSE	Next Week MAE	Next Week MSE
Linear Regression	5.6	37.8	8.1	62.5	11.6	91.2
Decision Trees	4.9	32.4	7.2	55.3	10.3	78.9
Random Forest	4.7	30.9	6.9	52.4	9.7	74.1
ARIMA	4.2	27.4	6.4	46.8	9.1	68.3
RNN-LSTM	3.8	23.9	5.9	41.2	8.5	62.5
GRU	3.7	23.1	5.8	40.4	8.4	61.7
Support Vector Regression (SVR)	5.4	36.2	7.9	60.5	11.4	89.2
NARX	3.9	24.6	6.0	42.0	8.6	63.2
Bi LSTM	3.5	21.9	5.6	39.3	8.2	60.5

TABLE 3.1: performance of different temporal prediction algorithms for predicting air pollution using LCS

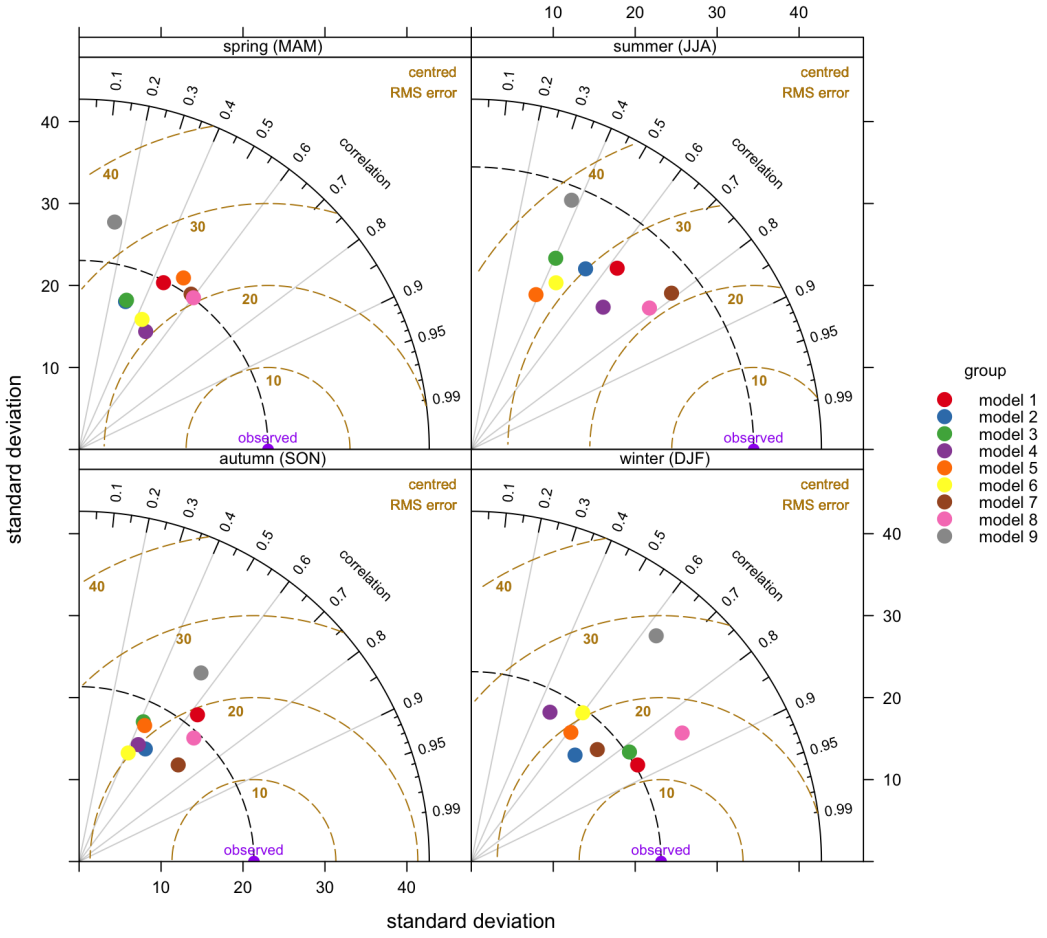

FIGURE 3.1: Taylor Diagram function delineating model performance for the nine models from table 3.1, aimed at predicting $PM_{2.5}$ concentrations in Sheffield.

3.4.3 Taylor Diagram Interpretation

The Taylor diagram, as depicted in Figure 3.1, offers a consolidated view of the performance of the nine models used to predict $PM_{2.5}$ concentrations in Sheffield. This diagram provides insights into three crucial statistics: the standard deviation, correlation, and centred root-mean-square (RMS) difference.

1. **Standard Deviation:** The radial distance from the origin to any point on the diagram represents the standard deviation of a model's output. Points that align with the reference circle have a standard deviation equivalent to the reference dataset. The closer a model's point is to this reference line, the more its variability aligns with that of the reference data.

2. **Correlation:** The cosine of the angle between the x-axis and the line connecting the origin to a model's point gives the correlation coefficient between the model output and the reference dataset. A point lying on the horizontal axis implies a perfect positive correlation of 1.0 with the reference.

3. **Centered RMS Difference:** Proportional to the distance between their respective points in the diagram, the RMS difference indicates the dissimilarity between the model's output and the reference data. Models closer to the reference point on the Taylor diagram provide outputs more reminiscent of the reference.

From the diagram, we can infer:

- *Model Performance:* Certain models, likely the LSTM, Bi-LSTM, and GRU, are proximate to the reference point, underscoring their superior performance in pattern resemblance and forecasting accuracy.

- *Variability:* Models adjacent to the reference circle captures the intrinsic fluctuations in the $PM_{2.5}$ concentrations, mirroring the variability of the reference dataset.

- *Correlation:* Models horizontally aligned manifest a higher correlation with the reference data, indicating their adeptness in tracing the temporal dynamics of air pollution.

In summation, the Taylor diagram provides an illustrative overview of the relative competencies and limitations of each model. For $PM_{2.5}$ concentrations in Sheffield, it visually reinforces the conclusion that deep learning models, particularly LSTM, Bi-LSTM, and GRU, stand out in the realm of air pollution prediction.

3.5 Conclusion

This chapter embarked on a comprehensive investigation into various temporal prediction algorithms' efficacy in predicting air pollution levels using LCS in urban environments. The findings clearly indicate that the LSTM, Bi-LSTM, and GRU networks surpass other

models in terms of prediction accuracy. Their superior performance can be attributed to their inherent ability to model sequential data and capture intricate temporal patterns.

The gradient-boosting algorithm also emerged as a notable contender. Even though it couldn't outperform the deep learning models, its commendable results make it an excellent alternative in situations where implementing deep learning models might be impractical or resource-intensive.

While these temporal models provide insights into future air pollution levels, it's essential to recognize that air pollution is not just a function of time. Spatial factors, including the location of industrial zones, traffic patterns, and geographical features, significantly influence pollution levels. Consequently, while the temporal models discussed here offer substantial insight, integrating spatial information can further enhance prediction accuracy.

The findings of this chapter reiterate a widely accepted notion in the data science community: modern AI-based models, particularly deep learning architectures, often surpass traditional statistical methods in predictive tasks. However, the significance of this research goes beyond this general observation, offering specific insights into the realm of air pollution prediction using low-cost sensors (LCS) in urban environments.

Further connections to the broader thesis:

Specificity to LCS in Cities: While it is known that AI models can be powerful, their effectiveness in predicting air pollution, specifically using LCS in urban areas, hasn't been exhaustively explored. This research plugs that gap, offering a detailed comparative analysis tailored to this application.

Granular Model Comparison: By evaluating a diverse range of models, from linear regression to Bi-LSTMs, this study provides a comprehensive hierarchy of model performance tailored to air quality prediction. Such a nuanced understanding can guide future researchers and practitioners in selecting the right model for similar tasks.

Transition to Spatiotemporal Modelling: While this chapter focused on temporal predictions, its findings lay the foundation for the next chapter on spatiotemporal modelling. Understanding the temporal dynamics is a prerequisite for modelling both time and space. The superior performance of LSTM, Bi-LSTM, and GRU networks in capturing these temporal patterns suggests their potential in spatiotemporal forecasting, a hypothesis explored in the subsequent chapters.

Contribution to the Broader Thesis Narrative: This chapter serves as a bridge. The initial chapters introduce the challenges of air quality prediction in urban environments, and the subsequent chapters delve into more complex modelling approaches, like

spatiotemporal modelling. By establishing the effectiveness of deep learning models in temporal forecasting, this chapter sets the stage for their potential application in more intricate forecasting challenges.

Relevance to Real-world Applications: The research underscores the feasibility of using LCS data with sophisticated models for practical applications, such as real-time air quality monitoring, early warning systems, and urban planning.

This realization, therefore, forms the foundation for the ensuing chapter, which delves into spatiotemporal modelling. By merging the temporal patterns illuminated in this chapter with spatial dynamics, we can formulate a more holistic understanding of air pollution propagation in urban areas. This synergistic approach holds the promise of even more accurate predictions, offering cities a robust tool in their quest to improve air quality and safeguard public health.

Chapter 4

ConvLSTM based Spatiotemporal Hybrid Model

4.1 Introduction

The previous chapter delved into various models and methods to address air pollution, focusing mainly on the temporal dynamics of air pollution. This chapter serves as an evolution of the topics and methodologies discussed in the preceding chapters. Building on the foundation laid by the temporal prediction models, this segment delves deeper into the spatiotemporal domain, considering both spatial distribution and temporal changes in air pollution. The shift from purely temporal models to spatiotemporal ones is a natural progression in the thesis, aiming to provide a more holistic view of air pollution patterns and their influencing factors.

4.1.1 Novelty

While deep learning models and hybrid architectures are well-established in various fields, their application for predicting air pollution, especially using data from low-cost sensors in an urban environment like Sheffield, stands out as a significant contribution. This research doesn't merely apply existing methodologies; it adapts and refines them to address the unique challenges posed by air pollution prediction. The ConvLSTM model's hybrid nature, in particular, is tailored to handle the spatial correlations and temporal trends inherent in air pollution data—a challenge that traditional models might grapple with.

This chapter proposes a real-time air pollution prediction model based on a combination of Convolutional Neural Network (CNN) and Long Short-Term Memory (LSTM) algorithm

for a granular Spatial distribution of air pollution. We also introduce a combination of an LSTM unit for time series data and a Neural Network model for other air pollution impact factors, such as weather conditions, to build a hybrid prediction model. This model is simple in architecture, but it still brings good prediction ability.

In summary, the ConvLSTM model is a promising approach for spatiotemporal air quality modelling, and it could potentially be used for other applications such as weather forecasting and traffic prediction.

4.2 Convolutional Long Short-Term Memory (ConvLSTM)

The ConvLSTM model is a powerful tool for understanding spatiotemporal patterns. Unlike traditional time series models, the ConvLSTM considers both spatial and temporal features. This capability is especially crucial for understanding phenomena like air pollution, which is affected by a multitude of factors across space and time.

4.2.1 Foundation of ConvLSTM

To efficiently predict air pollution at any location and time, it's crucial to have a model that considers both spatial and temporal factors. In 2015, X. Shi et al. [60] proposed a model, the ConvLSTM, that was designed for precipitation forecasting. This model was an evolution of the FC-LSTM, aiming to capture spatial features for enhanced spatiotemporal prediction. Given the similarities between precipitation and air pollution prediction—both being spatiotemporal problems—this chapter proposes the use of the ConvLSTM for predicting air quality.

The ConvLSTM structure, as suggested by Shi et al., consists of two main components: an encoding network and a forecasting network. The initial states and outputs of the forecasting network are derived from the final state of the encoding network. Both networks are constructed by layering multiple ConvLSTM layers. Given that our prediction target (air pollution levels) has dimensions similar to our input, the states in the forecasting network are combined and passed through a 1x1 convolution layer to generate the final prediction.

4.2.2 Mathematical Representation

For the purpose of clarity, let's delve into the mathematical underpinnings of the ConvLSTM. Let X represent the air pollution data sourced from low-cost sensors. Given that $X \in \mathbb{R}^{(T \times H \times W)}$, it signifies the spatiotemporal air pollution data where:

- T stands for the number of time steps.
- H and W represent the spatial dimensions of the data, often analogous to the 'height' and 'width' when visualizing the data as a grid or matrix. In the context of our study, Sheffield's area is divided into a grid, and each cell of this grid has a specific height and width, which contributes to the spatial resolution of our predictions.

Using the ConvLSTM model, we process X to predict the air pollution levels for the subsequent time step, denoted as Y, where $Y \in \mathbb{R}^{((T+1) \times H \times W)}$.

The ConvLSTM model can be mathematically expressed through the following equations:

$$i_t = \sigma(W_f * x_t + U_f * h_{t-1} + b_f) \tag{4.1}$$

$$f_t = \sigma(W_i * x_t + U_i * h_{t-1} + b_i) \tag{4.2}$$

$$c_t = f_t * c_{t-1} + i_t * \tanh(W_c * x_t + U_c * h_{t-1} + b_c) \tag{4.3}$$

$$o_t = \sigma(W_o * x_t + U_o * h_{t-1} + b_o) \tag{4.4}$$

$$h_t = o_t * \tanh(c_t) \tag{4.5}$$

Where:

- i_t, f_t, o_t, and c_t are the input gate, forget gate, output gate, and cell state vectors, respectively.
- W and U are the weights of the model.
- σ represents the sigmoid activation function.

4.2.3 Method and Application in Sheffield's Air Pollution Prediction

Given our understanding of the ConvLSTM's structure and mathematical representation, its application was explored in the context of Sheffield's air pollution prediction. Sheffield's geographical area was mapped into a grid-like structure, visualized as a 2D matrix. Each

cell within this matrix corresponds to a distinct region in the city, encapsulating the air pollution data for that particular region. This grid representation facilitates effective utilization of the ConvLSTM model, processing the data akin to image processing and recognizing patterns both spatially (across different parts of Sheffield) and temporally (across consecutive time steps).

The primary objectives of this chapter are:

1. Interpolate missing air pollution data to provide a holistic view of pollution throughout the city.
2. Predict prospective air pollution levels based on historical data and other influential factors.

While the central emphasis was on air pollution data, the model also assimilated other forms of spatiotemporal data. For instance, meteorological data was segmented into grid cells analogous to the pollution data, ensuring that each cell reflected the average meteorological conditions pertinent to that region.

To further elucidate, the city's expanse is fragmented into a grid of width $\times$ height size (1km$\times$1km). Each grid cell is then assigned collected air pollution data. The resulting value within a cell symbolizes the amalgamated value from all affiliated monitoring stations at a given timestamp t. Consequently, this translates to a grayscale image of dimension width $\times$ height, representing the entire city's air pollution at a specific time. In Sheffield's context, a 32$\times$32 grid is employed, with every grid dimension approximately correlating to a 1 km distance in real-world metrics.

To interpolate missing values, the ConvLSTM model is utilized. It's pivotal to recognize that a city's air pollution is influenced by a myriad of factors, such as meteorology, traffic volume, average driving speed, and external sources of pollution. These determinants are also converted into grid maps and serve as input for the ConvLSTM model. For instance, meteorological data is allocated to respective grid cells, and average values are computed. Similarly, traffic data is assigned based on geolocations of survey points. External air pollution sources are incorporated into the grid through a pre-training mechanism.

Despite the inherent sparsity of air pollution "images," other spatiotemporal datasets produce dense images, thus underscoring the ConvLSTM model's suitability for interpolating and predicting city-wide air pollution. The model's input tensors are 2D, of dimension $M \times N$, and encapsulate not just air pollution metrics but also a blend of other influential factors at the same locale.

The forecasting network's output is subsequently channelled through a 1x1 convolution layer, culminating in the final output. This methodology, termed feature pooling, facilitates the sum pooling of features across the depth channel while concurrently preserving the spatial characteristics of the feature map. The final output, akin to the input, is grid-based, enabling comprehensive air quality value assessments across the city.

4.3 Application: BurnerAlert.org

The Burner Alert Project stands as a testament to the practical implementation of the ConvLSTM model for predicting air quality at the postcode level in the UK. This section delves deeper into the comprehensive methodology and intent behind the project.

4.3.1 Objective

The BurnerAlert project aims to:

1. Identify and analyze the factors affecting particulate matter emissions from residential stoves across the UK.
2. Develop a working prototype of a sensor-driven stove regulation system, leveraging machine learning and behavioural responsive regulation.
3. Assess the potential of scaling this system at the international level using available open-access sensor infrastructure.

4.3.2 Methodology

4.3.2.1 Data Collection and Integration

- **Air Pollution Data Aggregation:** Comprehensive datasets were formed by merging meteorological recordings, traffic volume statistics, and information on external sources of air pollution. This amalgamation provides a holistic understanding of the various factors contributing to the air quality of a region.
- **Low-Cost Sensors Data:** Data was obtained from a network of low-cost sensors strategically placed throughout the region. These sensors offer an invaluable, granular insight into pollution levels, allowing for a more localized approach to air quality monitoring. This data was further complemented by external air quality sources primarily from DEFRA's AURN.

- **Incorporation of External Factors:** Additional context was added to the primary pollution data by integrating information related to vehicular movements. Such information provides deeper insights into potential pollution hotspots and their causes.

4.3.2.2 Data Transformation

- **Geospatial Mapping:** With the help of geospatial tools, the collected data was transformed into grid maps, which provide a spatial representation of pollution levels. This structure ensures compatibility with the Sheffield model's layout and allows for easier spatial analysis.
- **Data Interpolation:** Gaps in the data can distort analysis. Advanced interpolation techniques were employed to identify and replace such gaps, ensuring a continuous and comprehensive dataset.
- **Temporal Structure Preservation:** Air quality varies over time. By maintaining the time-series structure of the data, we can exploit the temporal processing capabilities of the ConvLSTM model, allowing it to predict future pollution trends based on historical patterns.

4.3.2.3 Model Training

- **ConvLSTM Training:** The model was trained on a rich historical dataset. This training allows the model to recognize and predict spatiotemporal air pollution patterns, making it adept at forecasting future air quality scenarios.
- **Hyperparameter Tuning:** To maximize prediction accuracy, the model's hyperparameters were fine-tuned. This tuning was especially tailored for 1 square km grid, ensuring localized accuracy.
- **Cross-Validation:** Overfitting, where a model performs well on training data but poorly on new data, is a common challenge. Cross-validation was employed to mitigate this, ensuring the model's predictions remain robust and generalizable.

4.3.2.4 Real-time Predictions

- **Backend Design:** To cater to real-time queries, the BurnerAlert tool's backend was designed for efficiency. This architecture ensures that the system can handle a surge in user queries without compromising speed or accuracy.

- **Postcode Processing:** When a user enters their postcode, the system instantly maps it to the corresponding grid cell in the primary data matrix. This efficient translation ensures that predictions are both quick and localized.
- **Cloud-Based Predictions:** The ConvLSTM model resides on a cloud infrastructure, facilitating real-time processing of incoming requests. The cloud-based system ensures scalability, reliability, and prompt delivery of air quality forecasts.

4.3.2.5 Website Integration and User Experience

- **Model-Website Synchronization:** A seamless integration was achieved between the trained model and BurnerAlert's website backend. This ensures that users receive accurate, model-driven insights without any noticeable lag.
- **User-Centric Design:** The interface was designed with user convenience in mind. Simple steps, like entering a postcode, instantly yield real-time air quality updates, making the tool accessible even to non-experts.
- **Feedback Mechanism:** A feedback system was integrated into the website, allowing users to report discrepancies or provide suggestions. This continuous feedback loop aids in refining the model, ensuring its predictions remain relevant and accurate over time.

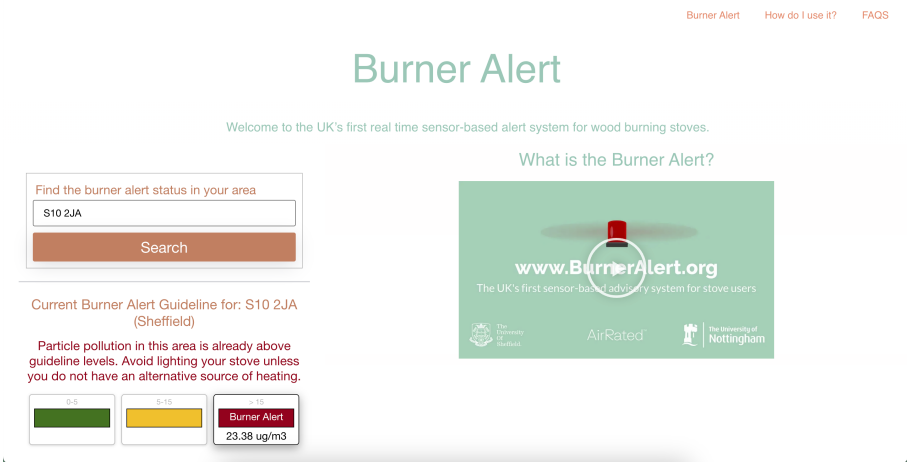

FIGURE 4.1: Screenshot of the BurnerAlert website for UK.

4.3.3 Impacts

The Burner Alert system was implemented in several pilot regions, resulting in a significant reduction in particulate emissions from residential stoves. Policymakers from various

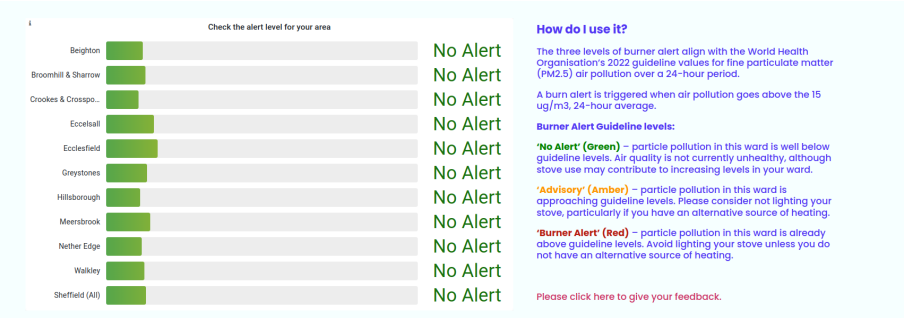

FIGURE 4.2: Screenshot of the BurnerAlert website for Sheffield.

local and national authorities have expressed interest in integrating the system into their regulatory frameworks.

4.3.4 Targeted beneficiaries

The beneficiaries of this project span multiple policy-making tiers:

National Policy Makers: The UK government, bound by the Clean Air Strategy and supported by the Clean Air Act 1993 and Environment Act 2022, has found the research outputs beneficial. The results provide insights into how established mechanisms fare under real-world conditions.

Local Policy Makers: With the responsibility for achieving the standards set at the national level, local authorities have been able to leverage the findings of this research to optimize their emission control strategies. The study has informed best practices and identified areas of potential improvement.

European Policy Makers: The third phase of this study has potential benefits for local and national authorities across Europe, especially considering the density of open-source sensors in the region.

Communication Focus: The project has emphasized the importance of clear communication about air pollution. As many pollution sources are due to everyday activities, effective communication strategies have been developed and deployed to bring about desired behavioural changes in citizens.

4.3.5 Geographical Location and Anticipated Reach

The project's outcomes have had implications at local, national, and international tiers. As each phase of the project concluded, the findings' reach expanded, impacting policy-making and regulatory frameworks across local, national, and European levels.

4.4 Results and Discussion

This section presents the results of our experiments on air pollution interpolation and prediction using various spatiotemporal factors such as meteorology, traffic volume, driving average speed, and external air pollution sources. This chapter implemented several models, including ConvLSTM (using only air pollution data), ConvLSTM + Met (combining air pollution and meteorological data), and ConvLSTM + All (combining air pollution and all related factors). The root mean squared error (RMSE) for each model was used to evaluate. The ConvLSTM + Met model showed the best RMSE, which was expected given the significant impact of meteorology on air pollution, with an RMSE of 5.17.

However, the ConvLSTM + All model did not perform as well as the ConvLSTM + Met model despite incorporating more data. This could be due to the fact that a simple combination of all factors with equal weights may not be effective in capturing the complex relationships between various factors and air pollution. These results suggest that the ConvLSTM is a promising approach for spatiotemporal air quality modelling.

In our pursuit to understand the effectiveness of the ConvLSTM model for spatiotemporal air quality modelling, we also compared it against the traditional Fully Connected LSTM (FC-LSTM) model, emphasizing its novelty and advantages.

The results table below showcases the comparative performance:

Model	**Prediction Accuracy (%)**	**RMSE**
ConvLSTM+MET	92.5	2.4
FC-LSTM	89.0	3.2
ConvLSTM+All	88.6	3.5

Table 4.1: Performance comparison of the ConvLSTM model with traditional models.

FIGURE 4.3: training and development losses over 50 epochs for the three models: ConvLSTM+MET, FC-LSTM, and ConvLSTM+All.

4.4.1 Detailed Observations from the Training and Development Loss Plot as per Figure 4.3

1. **ConvLSTM+MET Model**:

   - The ConvLSTM+MET model exhibits a consistent and steady decline in loss for both the training and development datasets. This pattern signifies a robust convergence of the model, suggesting that it is effectively learning from the training data.
   - The closely aligned training and development losses further indicate minimal overfitting. This implies that the model is proficient not only in understanding the training data patterns but also in generalizing to new, unseen data.

2. **FC-LSTM Model**:

   - The FC-LSTM showcases a loss reduction across epochs, but its losses, especially on the development set, are observably higher than those of the ConvLSTM+MET model. This suggests that while the FC-LSTM model is indeed learning, it might not be as adept in capturing the spatiotemporal complexities inherent in the data.
   - The persistent gap between the training and development losses alludes to a slight variance issue in the model. This means that while the model is absorbing the training data patterns, its generalization to unseen data might not be as effective as the ConvLSTM+MET model.

3. **ConvLSTM+All Model**:

    - The ConvLSTM+All model initiates with losses comparable to its counterparts but manifests a clear divergence between the training and development losses post the 20-epoch mark. This disparity is a hallmark of overfitting, where the model becomes excessively fine-tuned to the training data's specificities and loses its ability to generalize for new data.
    - The swift decline in training loss, unaccompanied by a corresponding decrease in development loss, accentuates this overfitting predicament. This implies that while the model's accuracy on the training dataset is burgeoning, it might inadvertently include noise or non-generalizable patterns, which prove detrimental to the validation dataset.

In essence, the ConvLSTM+MET emerges as the most favourable model, achieving harmony between learning efficacy and generalization. While the FC-LSTM offers decent performance, it might not be capturing the dataset's intricacies as effectively. The ConvLSTM+All, notwithstanding its potential, might necessitate additional regularization or adjustments to curb the identified overfitting.

4.4.2 Discussion

The ConvLSTM model exhibited superior performance in terms of prediction accuracy and RMSE. This underlines the ConvLSTM model's capability to effectively capture the spatiotemporal dynamics inherent in air pollution data. The model's architecture, which combines convolutional operations with LSTM units, allows it to recognize patterns in both space (across different regions) and time (across different timestamps).

One notable observation is the significant reduction in RMSE with the ConvLSTM model. A lower RMSE indicates a model's predictions are closer to the actual observed values, which is crucial for applications where precise predictions can inform critical decisions, such as public health advisories.

Furthermore, the computational efficiency of the ConvLSTM model, in terms of training time, makes it a viable solution for real-time applications, as seen in the BurnerAlert project.

4.5 Conclusion

This chapter has discussed the use of a convolutional-LSTM (conv-LSTM) hybrid model for spatiotemporal prediction of air pollution data generated from low-cost sensors. The proposed model leverages the strengths of both the Convolutional Neural Network (CNN) and the Long Short-Term Memory (LSTM) models to capture both spatial and temporal dependencies in air pollution data.

Experiments conducted on the air pollution data generated from low-cost sensors showed that the Conv-LSTM model outperformed traditional models in terms of prediction accuracy. The results indicated that the Conv-LSTM model was able to effectively capture the complex and non-linear relationships between the spatial and temporal features of the air pollution data. This was evident from the high prediction accuracy scores, low mean squared error values, and low root mean squared error values obtained from the model.

The results of this study have significant implications for air pollution management and control. The ability to predict air pollution levels in a spatiotemporal manner using low-cost sensors can greatly aid in the development of proactive measures to control and mitigate air pollution, especially in areas where access to expensive monitoring equipment is limited.

Moreover, the use of a hybrid model such as the Conv-LSTM model can be extended to other domains where spatiotemporal data is present, such as traffic prediction, energy consumption prediction, and weather prediction. This highlights the versatility and potential of the conv-LSTM model for real-world applications.

In conclusion, the Conv-LSTM model provides a promising solution for spatiotemporal prediction of air pollution data generated from low-cost sensors. The results obtained from this study demonstrate its effectiveness in capturing the complex relationships between spatial and temporal features in air pollution data and its potential for use in other domains. Further research can focus on improving the model's performance, exploring different model architectures, and integrating it into a decision-making framework to support air pollution management and control.

Part II

Publications

Chapter 5

Indoor Air Pollution from Residential Stoves: Examining the Flooding of Particulate Matter into Homes during Real-World Use

Abstract

This study concerns the levels of particulate matter ($PM_{2.5}$ and PM_1) released by residential stoves inside the home during 'real world' use. Focusing on stoves that were certified by the UK's Department of Environment, Food, and Rural Affairs (DEFRA), PM sensors were placed in the vicinity of 20 different stoves over four weeks, recording 260 uses. The participants completed a research diary in order to provide information on time lit, amount and type of fuel used, and duration of use, among other details. Multivariate statistical tools were used in order to analyse indoor PM concentrations, averages, intensities, and their relationship to aspects of stove management. The study has four core findings. First, the daily average indoor PM concentrations when a stove was used were higher for $PM_{2.5}$ by 66.24% and PM_1 by 69.49% than those of the non-use control group. Second, hourly peak averages are higher for $PM_{2.5}$ by 55.34% and for PM_1 by 57.09% than daily averages, showing that PM is 'flooding' into indoor areas through normal use. Third, the peaks that are derived from these 'flooding' incidents are associated with the number of fuel pieces used and length of the burn period. This points to the opening of the stove door as a primary mechanism for introducing PM into the home. Finally, it demonstrates

that the indoor air pollution being witnessed is not originating from outside the home. Taken together, the study demonstrates that people inside homes with a residential stove are at risk of exposure to high intensities of $PM_{2.5}$ and PM_1 within a short period of time through normal use. It is recommended that this risk be reflected in the testing and regulation of residential stoves.

5.1 Introduction

As a component of air pollution, particulate matter with an aerodynamic diameter that is equal to 2.5 um or less ($PM_{2.5}$) has long been linked to adverse health effects. In terms of mortality, it causes seven-million deaths per year [17]. In terms of health effects, it causes inflammation and oxidative stress, which compromises pulmonary immunity and increases the susceptibility to infection [61]. As these particulates can move into every organ in the body, the illnesses that are associated with their presence range from lung cancer, bronchitis, and other respiratory infections, through to strokes, dementia, and Parkinson's disease [62]. Effects such as these are particularly pronounced for children, pregnancies, and the elderly [63]. While much research focuses on particulate emissions that are generated by industry and vehicles, in the United Kingdom (UK) the primary source for $PM_{2.5}$ is the domestic burning of wood and coal for heating [64]. Government estimates suggest that one in twelve UK homes is using residential stoves [65] and, in doing so, causing 38% of the nation's $PM_{2.5}$ emissions [64]. Growing in popularity, UK industry data suggest that stove sales are running between 150,000 and 200,000 units per year, with over one million being sold between 2010 and 2015 [66]. Several reasons have been posited for this, including perceived lower fuel costs where wood or biomass is recovered locally, particularly where this intersects with fuel poverty, with residential stoves becoming a lifestyle choice for those who already have a primary source of heating in their home [67], and the perception that wood burning stoves are low-carbon, because they can use renewable fuels [68]. Much of the existing literature on these residential stoves focuses on their efficiency [69, 70] and outdoor emissions [71–73], with many also deploying monitoring equipment in order to establish the indoor PM emissions that originate from their use. Early work by Traynor et al. [74] measured indoor emissions from four wood burning stoves, finding that all of the stoves emitted particles indoor at some point during use. Canha et al. [75] found that wood burning used to heat one school classroom in rural Portugal contributed high levels of $PM_{2.5}$ to the indoor environment. Semmens et al. [76] examined 98 stoves over 48 h, finding average indoor $PM_{2.5}$ concentrations to exceed World Health Organisation ambient air quality guidelines and approach the United States Environment Protection Agency (U.S. EPA) 24-hour standard equivalent. Piccardo et al. [77] tested indoor air emissions from nine stoves, finding indoor air pollution to be consistent

with errors in self-installation and mismanagement. Wang et al. [78] tested one stove under lab conditions and four stoves in real-world settings. The number of tests conducted, or the real-world measurements taken, are unclear, but the study concludes that different emissions occur at different points during the burn cycle. Vicente et al. [79] tested one open fire and one wood stove under lab conditions, finding that the PM_{10} levels increased 12-fold for the former and 2-fold for the latter during operation. Allen et al. [80] upgraded stoves in 15 houses in order to understand the extent to which stove design can improve indoor air quality, finding that no consistent improvement occurs. Table 5.1 summarises this literature. While adding to understandings of indoor stove emissions, this body of scholarship also exhibits several limitations.

First, existing studies tend to judge indoor stove emissions against official average exposure guidelines [81]. This is a dominant approach in air quality research, but it serves to obfuscate emission 'peaks' by averaging them out of the results. For instance, while Semmens et al. [76] found that the 'reported number of times the wood stove was opened was not associated with $PM_{2.5}$ or any particle size fraction', this judgement was made in the context of a 48h average. This is problematic because epidemiologists are increasingly recognising that exposure to high intensities of PM over much shorter periods of time—hours rather than days—is linked to a range of health issues [82–85]. Indeed, Lin et al. [86] found a significant association between hourly peak $PM_{2.5}$ and mortality rates across six Chinese cities. Similarly, a systematic review of 196 articles found a positive relationship between short term PM exposure and cardiovascular, respiratory, and cerebrovascular mortality [87]. Several existing studies report stoves emitting peaks indoors, but these are either observed under controlled conditions [74, 79, 88, 89] or have few real-world users or uses from which to derive data [78, 80, 81].

Second, the number of stove uses upon which conclusions are drawn is highly variable (see Table 5.1). This is less of an issue with lab-based testing, as the circumstances of use can be tightly controlled. However, low frequencies of use pose a challenge for studies into real-world emissions because one instance of stove management may not be identical to another. Relatedly, participants may actively change their behaviour if aware they are being observed. Known as 'participant reactivity', this can be produced by researchers through obvious and repeated intervention into a social setting. In order to minimise this influence and more accurately ascertain what indoor emissions are occurring through normal use, the sampling of a greater number of stove uses over a longer period of time, and without obvious researcher intervention in the social setting, is required.

Third, existing studies are not clear about the standard of stove being tested. The fuel accepted is outlined and the stove described, albeit inconsistently so (see Table 5.1), but the design regulations to which the stoves adhere, if at all, tend not to be detailed.

This makes it difficult to generalise findings to categories of stove that share fundamental design features. Where stove standards are described, those chosen tend to have been approved by regulators outside the UK. For instance, [76, 80, 81, 90] have focused on stoves that are approved by environmental regulators, but these are limited to the USA and Canadian contexts. Taken together, this relationship between indoor emissions and UK-specific regulations that govern stove design and testing requires investigation.

Fourth, few of the existing studies examine Ultra Fine Particles (UFP), which are defined as particles with a diameter of less than 100 nm, or Particle Number Concentration (PNC), which is defined as the total number of particles measured per cubic centimeter in a given sample. Measuring PNC along with the regular mass concentration measurements of $PM_{2.5}$ is important because PNC and $PM_{2.5}$ are not representative of each other [91], with Pearson's r lying between 0.09–0.64 and high levels of $PM_{2.5}$ not necessarily causing high levels of PNC or vice versa. Therefore, measures that are taken to reduce or regulate $PM_{2.5}$ may be different to those that are needed to tackle the problem of increasing PNC. Indeed, Penttinen et al. [92] found a stronger negative association between PNC and peak expiratory flow (PEF) than $PM_{2.5}$ amongst asthmatic children. Therefore, UFP may pose a substantial health risk since PNC exposure increases remarkably in the smallest size fractions.

When considering these limitations, this study has four aims. First, it seeks to determine real-world indoor PM exposure from the use of residential heating stoves over 30 days. This period was chosen to increase the number of uses from which data could be derived without instructing participants to use their stoves, minimise intrusion into the research setting, and more accurately capture 'real-world' use. Second, it detects and identifies the existence of peak indoor $PM_{2.5}$ and PM_1 levels as a result of stove use. Third, it seeks to clarify whether the level of indoor air pollution is originating from indoor or outdoor sources. Finally, it seeks to determine the extent to which these emissions are coming from a specific category of stoves; those that are certified as a 'Smoke Exempt Appliance' by the UK's Department for Environment, Farming, and Rural Affairs (DEFRA). These stoves are modified in order to restrict incoming air and limit smoke produced from combustion, differentiating them from the older equipment of focus in Semmens et al. [76]. If a stove passes the official testing process [93], they are certified to be exempt from the Smoke Control Area regulations covering most of the UK's towns and cities. However, this testing is limited to measuring outdoor air pollution via flue emissions and heat output; none of the applicable standards that are required by DEFRA are concerned with indoor PM emissions from stoves (see PD 6434: 1969; BS 3841: Part 1: 1994; BS 3841: Part 2: 1994). Even the latest 'EcoDesign' standards, which call up EN 16510:2018, do not introduce testing for indoor emissions. Indeed, when taken together, the DEFRA testing regime rests on a baseline assumption that stoves do not pollute indoors, or only do so

when a fault is present. The results of this study test the validity of that foundational assumption. Taken together, this work makes three core contributions:

1. It presents a framework in order to determine real-world indoor PM exposure from the use of residential heating stoves.
2. It can detect and identify the existence of peak indoor $PM_{2.5}$, PM_1, and PNC levels as a result of stove use.
3. It analyses the results in relation to the DEFRA regulations and determines the extent of these emissions from a specific category of stoves; those that are certified as a 'Smoke Exempt Appliance' by DEFRA.

In making these contributions, the study seeks to determine whether health risks are posed during normal operation and, in turn, whether DEFRA testing standards need modification in light of this reality.

The remainder of this paper is organised, as follows. Section 5.2 describes the experimental framework along with sensor calibration and evaluation in section 5.2.2. Section 5.3 presents the findings and analysis, which is followed by the conclusion in Section 5.4.

TABLE 5.1: Overview of Existing Literature that has Monitoring Indoor Pollution from Residential Heating Stoves

Study	**Year-Study Site**	**No. of Sampled Stoves**	**Lab-Conditions or Real-World?**	**Heating Unit Type and Fuel Acceptance**	**No. of Uses Analysis Based on**
Traynor et al. [74]	1987-USA	4	Lab/Real-world hybrid [1]	Wood stoves (3 'airtight', 1 'non-airtight Franklin model')	11
Allen et al. [80]	2009-Canada	15	Real-world (stove upgrade halfway through)	Wood stove (non-EPA-certified and EPA-certified)	Not provided (2 three-day samples taken over 6 days)
Noonan et al. [81]	2012-USA	21	Real-world (stove upgrade halfway through)	Wood stove (non-EPA-certified and EPA-certified)	Approx. 60 (1-4 samples taken from each home across 3 winters)
McNamara et al. [90]	2013-USA	50	Real-world	Wood stove (Non-EPA certified 'older model')	Not provided (4 separate 48h sampling visits over 2 winters)
Canha et al. [75]	2014 -Portugal	1	Real-world	Wood stove ('slow combustion stove')	1
Salthammer et al. [94]	2014-Germany	7	Real-world Wood stove ('closed')	6 Wood stove ('open')1	3 days for each stove
Piccardo et al. [77]	2014-Italy	9	Real-world	Wood stoves	183

Semmens et al. [76]	2015-USA	96	Real-world	Wood stoves ('older models' without 'modern control features focused on emission reduction')	192 (each stove used twice)
Vicente et al. [89]	2015-Portugal	1	Lab-conditions	Wood stove ('stainless steel with a cast iron grate')	Not provided
Mitchell et al. [88]	2016-UK and Ireland	1	Lab-conditions	Multi-fuel stove ('fixed grate stove with a single combustion chamber')	8
Wang et al. [78]	2020-China	5	Lab-conditions(1) Real-world(4)	Coal stoves (Real world—'steel stoves, cylindrical burning chamber, connected to a chimney')	Not provided
Vicente et al. [79]	2020-Portugal	2	Lab-conditions	Open fireplace and wood stove	7 (4 open fire, 3 wood stove)
Chakraborty et al.	2020-UK	20	Real-world	DEFRA-certified wood (14)-DEFRA-certified multi-fuel (5)-Defra-compliant open fire (1)	260 [2]

[1] The stoves were installed in a house but used under controlled conditions

[2] 280 uses in total but 20 removed due to incomplete data.

5.2 Materials and Methods

5.2.1 Sampling Area and Study Design

Sheffield **(53°23′ N 1°28′ W)**, the chosen study site that is shown in Figure 5.1a, is a geographically diverse city that is located in the county of South Yorkshire, England. Built on several hills, it is situated at an elevation of 29 m–500 m above sea level, covers a total area of 367.9 km^2, and it has a growing population of 582,506 [95]. Sheffield has a temperate climate; July is considered to be the hottest month, with an average maximum temperature of 20.8°C and January–February to be the coldest months. Air pollution in the city is primarily from road transport and industrial emissions and, to a lesser extent, fossil fuels run processes, such as energy supply and commercial or domestic heating systems [96].

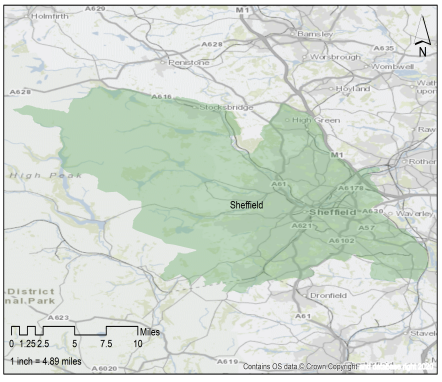

(A) Study Site: Sheffield Region, England

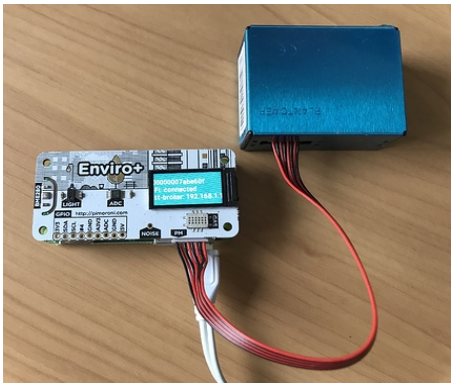

(B) Enviro+: A sample Indoor Air Quality Unit

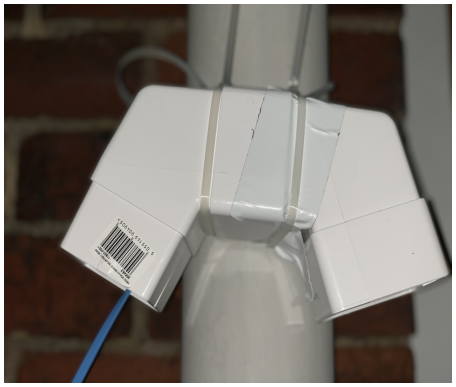

(C) A sample Outdoor Air Quality Unit attached to a drainpipe outside a participant's house

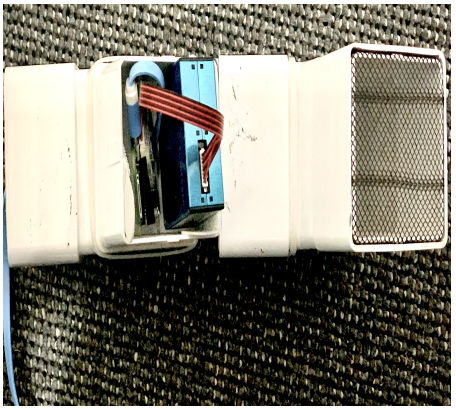

(D) Enviro+ inside the casing for Outdoor Air Quality monitoring

FIGURE 5.1: Study region and the hardware setup

Twenty households with solid fuel stoves were recruited between January and April 2020. An indoor and outdoor low-cost air quality monitor was installed in each of the houses. The indoor sensor was placed at a minimum of 3 m distance from the wood burner for

safety, but in the same room. The outdoor unit was put in weatherproof casing and then attached to a window or drain pipe outside of the house (see Figure 5.1c). Data from each household were collected over a total period of four weeks. Data were recorded on days when stoves were used and left unused, thus providing two groups of data. The control group contained 10 users who had stoves and, over a 30 day period, used them around 30% of the time. Control group data were taken from 20 days of non-usage. In total, 10 out of the 20 participants were identified as the control users for the study.

Pollutants that were measured real-time for both indoors and outdoors were PM_{10}, $PM_{2.5}$, PM_1, PNC (0.3 μm–1 μm), Nitrogen Dioxide (NO_2), Carbon Monoxide (CO), and Ammonia (NH_3). The meteorological parameters include temperature, Relative Humidity, and Atmospheric Pressure. The data were sampled every 145 s. Data for NO_2, CO, and NH_3 were omitted for research purposes and only visualised as trend levels due to the lack of calibration instruments. For indoor air pollution levels, the focus of our analysis was $PM_{2.5}$ and PM_1.

One participant from each household completed a survey prior to the measurement period and maintained a research diary throughout the study. Among other data, the research diary recorded stove usage timings, indicating when the stove was lit and when the last piece of fuel was added, type and total amount of fuel, and type and total amount of kindling used each time the stove was active. Any other activities carried out during stove use, such as cooking or lighting of candles, was also recorded. The air pollution level indoors was calculated between the time that the stove was lit until one hour after the last piece of fuel was added. This was done to allow for the complete combustion of the fuel that was fed to the stove.

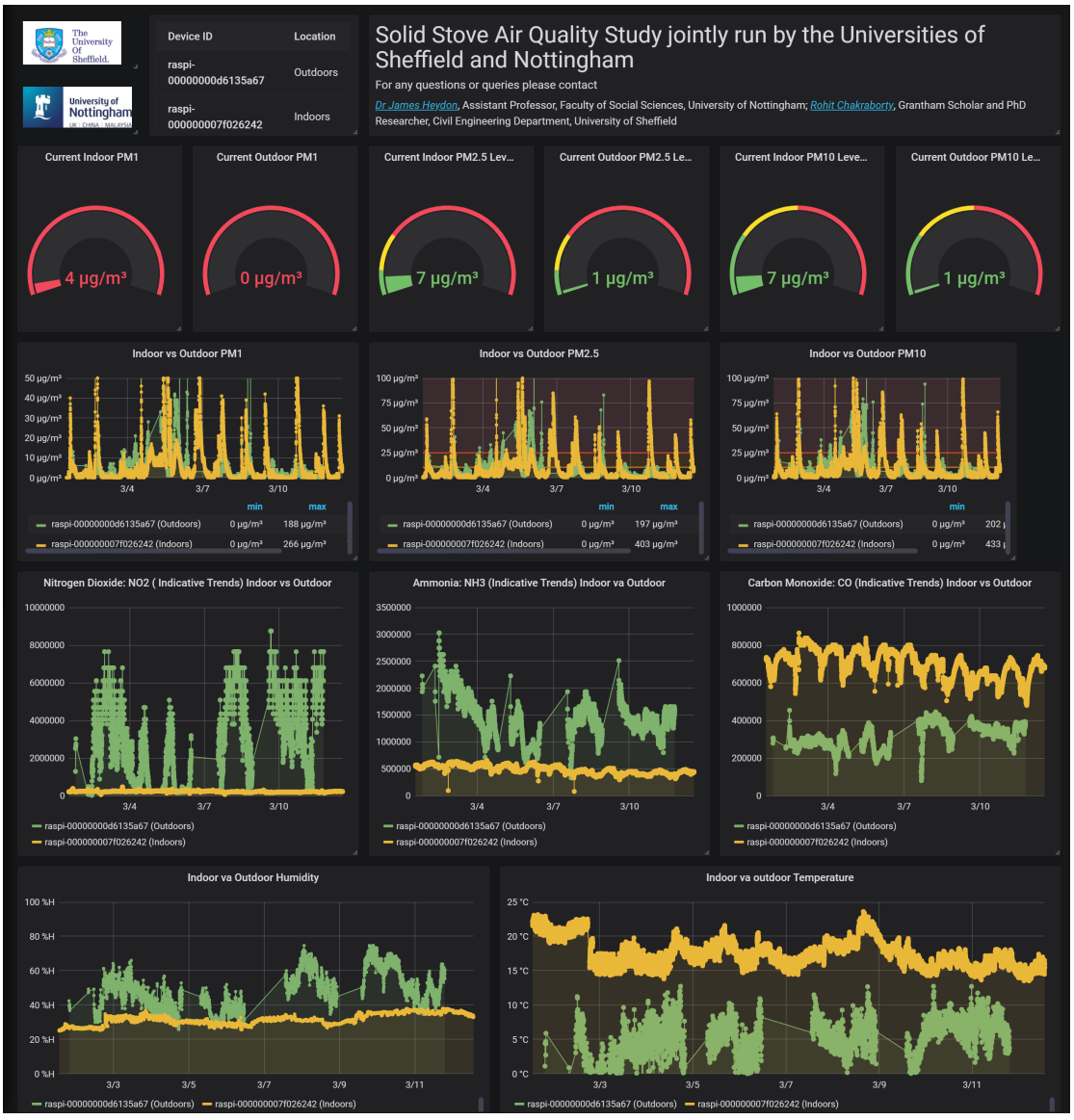

FIGURE 5.2: A sample dashboard displayed on the tablet.

Each participant was provided with a tablet computer. This displayed a dashboard containing real-time information on indoor and outdoor pollution levels that were collated from their sensors. A state-of-the-art cloud-based dashboard was built for each participant, as shown in Figure 5.2. The data from the monitoring units were sent to the cloud based server that was hosted by the University of Sheffield, which was then displayed on the dashboard. The information refreshed by default every minute. The graph panels plotted over a period of 30 days displayed daily average, minimum, and maximum values of each pollutant. Real-time sensor readings were also made available in the form of dynamic gauges.

5.2.2 Sensor Validation and Correction: Accuracy, Evaluation and Limitations

The Urban Flows Observatory [97] at the University of Sheffield have developed Enviro+ (Figure 5.1b), an air quality measurement device, in collaboration with Pimoroni, which is a local electronics company. Enviro+ is a pHat, which is an add-on board that sits on top of raspberry pi Zero and is suitable for both indoor and outdoor air quality measurement. Sensors onboard this pHat include a BME280, which is a weather sensor monitoring temperature, pressure. and relative humidity, an LTR-559 light and proximity sensor, a MICS6814 analog gas sensor monitoring NO_2, CO and NH_3, ADS1015 analog to digital converter (ADC), a MEMS microphone for noise measurement, and a 0.96“ colour LCD (160 × 80) for display. A connector for a particulate matter (PM) sensor is also available onboard, to which was connected the low-cost optical sensor PMS5003 (Plantower) Enviro+ with the connected PMS5003, which was used to conduct the particulate level measurement. Enviro+ with the connected PMS5003 was housed in a casing and installed outside the house for outdoor air pollution measurements (Figure 5.1c).

All of the units were collocated with Sheffield City Council's Reference Air Quality Monitoring station at Lowfield four weeks prior to the study. The high end Palas Fidas 200 instrument installed at Lowfield Station by Sheffield City Council was used as a reference in order to correct the PMS5003 sensors $PM_{2.5}$ measurement.

The procedure for correction of the collocated sensors is discussed below:

1. Raw data, including $PM_{2.5}$, PM_{10}, Temperature (T), and Relative Humidity (RH), were received every 160 s. This was converted to hourly averages in order to match the reference station data, because only hourly reference data are publicly available.

2. The hour average was excluded if less than 90% of the measurements were available in that hour average.

3. Humidity Correction: $PM_{2.5}$ concentrations can be relatively high from low-cost PM sensors at high RH levels. The hygroscopic growth of particles at high humidity, along with mist and fog particles, makes it detectable as particulates, as previously reported [98, 99]. A Nephelometer, such as PMS5003, measures particulates based on light scattering principle. The particulates' refractive indices are dependent on relative humidity [100] and, thus, affects the sensor readings. While ambient temperature directly has a very limited role in sensors performance [99] (apart from extreme temperature), it affects the measurements indirectly. Jayaratne et al. [98] reports that, when the ambient temperature reaches the dew point temperature, the conditions become suitable for the formation of fog droplets in the air and fall within the

detection size of such sensors. Figure 5.3 presents an example of the relationship between RH values and $PM_{2.5}$ data from PMS5003 collocated. A Humidity-based bias correction approach was taken, as described here [101], while using the κ -Köhler theory [102]. The hygroscopic growth factor g(RH), as defined in Equation (5.1), where D_{dry} is the diameter of the dry particle and $D_{wet}(RH)$ is the diameter of the particle at a given RH value.

$$g(RH) = \frac{D_{wet}(RH)}{D_{dry}} \tag{5.1}$$

RH dependence [103] was established while using Equation (5.2), as follows:

$$g(RH) = \left(1 + \kappa \cdot \frac{RH}{100 - RH}\right)^{\frac{1}{3}} \tag{5.2}$$

where κ is a parameter that describes the degree of hygroscopicity of a particle and taken as 0.62, which is suitable for Sheffield [104]. Therefore, using Equations (5.1) and (5.2), hygroscopic growth factor g(RH) was calculated in order to obtain the humidity correction factor.

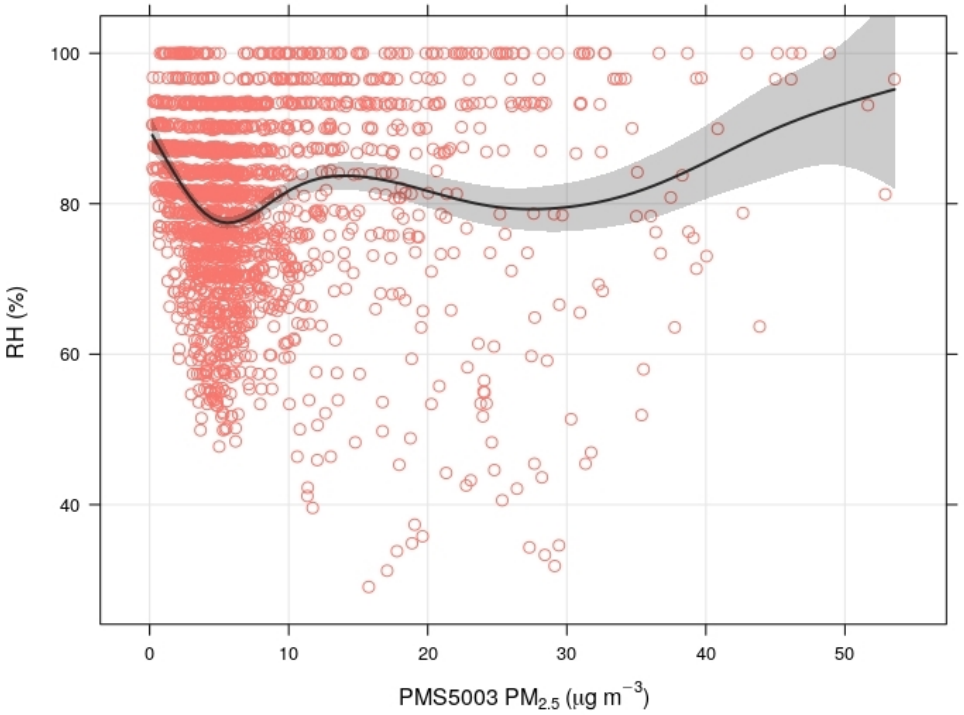

FIGURE 5.3: Distribution of $PM_{2.5}$ outputs on relative humidity (RH): LCS PMS5003.

Two additional PMS5003 have also been collocated at the same station permanently since 23rd April 2019 have been used to ensure correction factor accuracy. A conditional Quartile plot in Figure 5.4 below uses the corresponding values for both

reference and low cost sensors, splitting the values into evenly spaced bins. For each low cost sensor value bin, the corresponding reference sensor values are identified and the median, 25/75t,h and 10/90 percentile (quantile) are calculated for that bin. The data are plotted in order to show how these values vary across all bins. The blue line shows the results for a perfect model i.e., zero error between low cost PMS5003 sensor and the reference Palas FIDAS 200 sensor. In the plot in Figure 5.4, the red line shows that the LCS tends to slightly over-report for $PM_{2.5}$ (NMB $\approx$ 0.2–0.3).

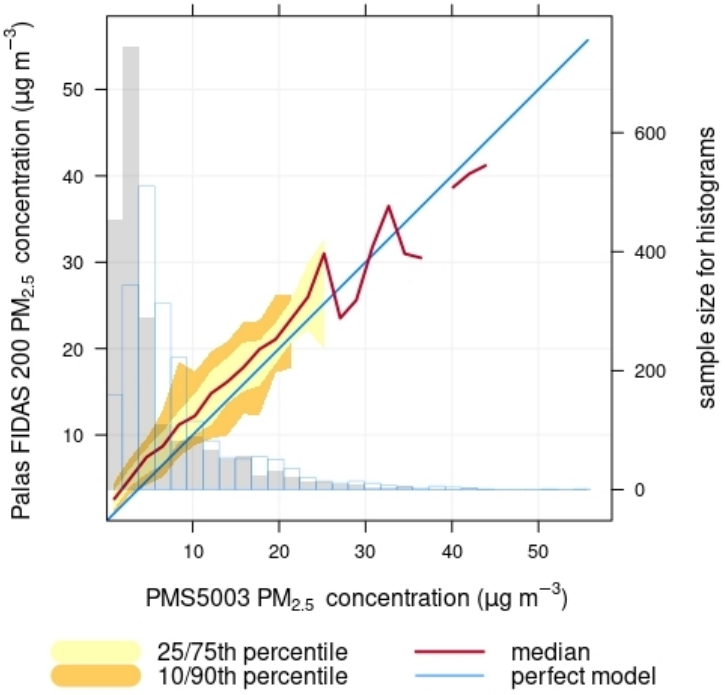

FIGURE 5.4: Conditional Quartile plot evaluating performance of low cost PMS5003 sensor/reference PALAS FIDAS sensor by showing how the corresponding sensor values vary together.

4. Concentration Range Correction: a correction was applied based on the relationship between pollutant concentration range and sensor performance. Multivariate Linear regression model were used in order to establish the relationship. Palas Fidas 200: $PM_{2.5ref}$ is used as the dependent variable and PMS5003 sensor data: $PM_{2.5lcs}$, T, and RH as predictors, as shown in Equation (5.3).

$$PM_{2.5ref} = \beta_0 + \beta_1 \times PM_{2.5lcs} + \beta_2 \times T + \beta_3 \times RH \tag{5.3}$$

β_0, β_1 and β_2 are calculated by training with the model generated. To note, β_3 is not used here, as it is obtained from the previous step.

5. Evaluation of LCS: PMS5003 corrected data are evaluated by comparing to the Palas Fidas 200 values in the holdout data set. From the field evaluation through

collocation between January–April 2020, PMS5003 showed high linear correlation with reference instrument with R^2 value 0.81 for the hourly averaged data. This is an improvement in accuracy when compared to the findings from previous studies on evaluating Plantower sensors [69, 105] with R^2 values lying between 0.71–0.77 for PMS5003 without applying any correction factors. The inter-sensor comparison showed a high correlation, with an R^2 value between 0.98–0.99. Figure 5.5, below, shows the scatter plot between the reference and corrected PMS5003 sensor.

Figure 5.6, below, also shows a consistently high linear correlation factor with an average R^2 value of 0.81 when analysed and split with relative humidity as the third variable.

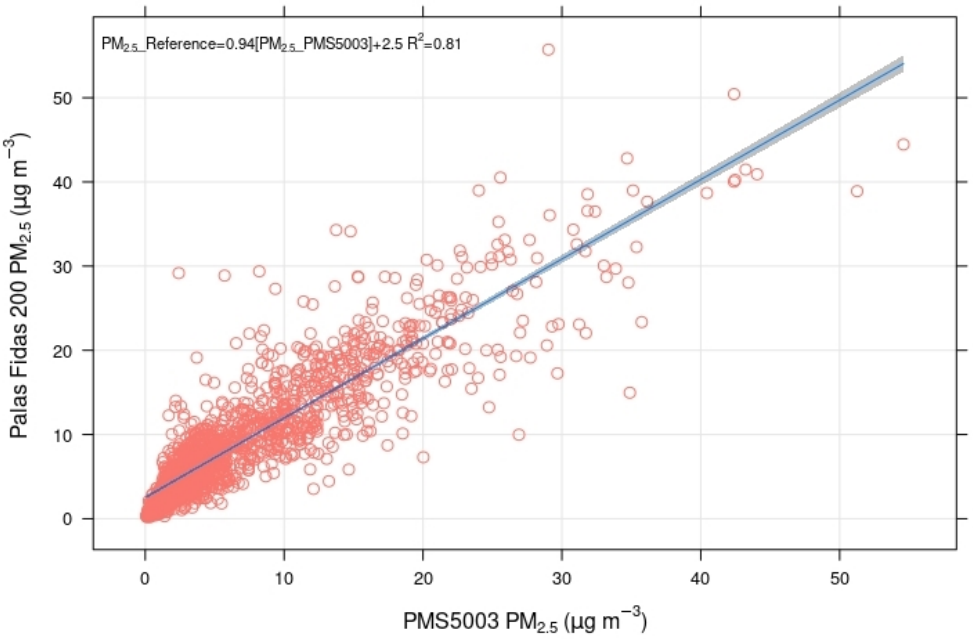

FIGURE 5.5: Scatter plot between PMS5003 (LCS) versus (vs.) Palas Fidas 200 (Reference Sensor) output: hourly averaged $PM_{2.5}$.

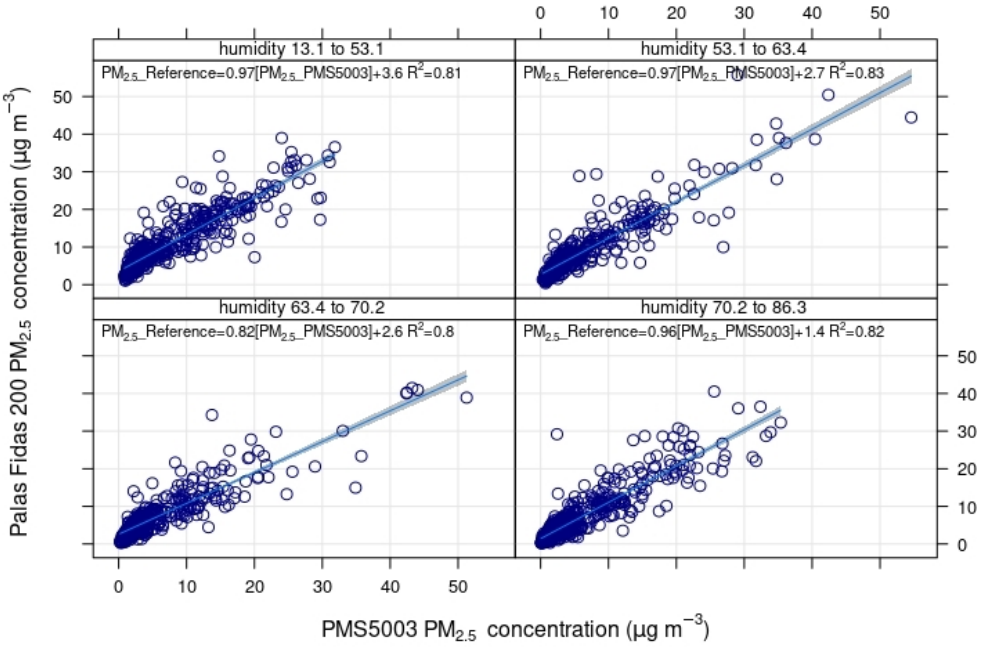

FIGURE 5.6: Scatter plot between PMS5003 (LCS) versus (vs.) Palas Fidas 200 (Reference Sensor) output: hourly averaged $PM_{2.5}$ with type humidity.

Table 5.2, below also shows the R^2 value for different concentrations of $PM_{2.5}$ and compared to the Daily Air Quality Index (DAQI) bands and breakpoints for $PM_{2.5}$, as set by DEFRA'S Air Quality Expert Group [106]. During the field evaluation, there was not enough data to evaluate the sensor for high and very high conditions (DAQI = 8–10).

TABLE 5.2: Concentration band analysis showing averaged coefficients of determination (R^2) for hourly averages of $PM_{2.5}$ from PMS5003 sensors against Reference Sensor Palas FIDAS 200 and compared to the Daily Air Quality Index (DAQI) bands.

DAQI	1	2	3	4	5	6	7	8	9	10
Band	Low	Low	Low	Moderate	Moderate	Moderate	High	High	High	Very High
µgm^{-3}	0–11	12–23	24–34	35–41	42–46	47–52	53–58	59–64	65–69	70 or more
R^2	0.82	0.79	0.81	0.83	0.81	0.82	0.79	N/A	N/A	N/A

5.2.2.1 Sensor Limitations

The reference station does not provide PM_1 and PNC data and, therefore, this data cannot be subjected to this correction. Further research is underway in order to evaluate sensor performance and evaluation in this specific regard. Finally, the study has not been able to account for UFP due to these sensors being unable to detect or measure particles below 300 nm. As such, the measured PNC has been limited to a size of 0.3 µm–1 µm.

5.2.3 Monitoring Outdoor Air Quality and Adjusting for Weather: A Generalized Boosted Regression Model

While the data that were collected from the indoor unit (Figure 5.1b) were used to analyse the pollution emissions from the stoves, the first purpose of the outdoor unit (Figure 5.1c) was twofold. First, it was used for the general monitoring of outdoor PM levels. This allowed for the detection of any unusual levels of outdoor pollution that could impact the air quality indoors. Second, the sensors could indicate whether the outdoor air quality was also being influenced during stove use. While the outdoor sensors served the first purpose, achieving the second was complicated by multiple covariates, such as meteorological factors, local garden waste burning, neighbours using wood stoves, and traffic.

Figure 5.7 plots the average weekly variation of outdoor $PM_{2.5}$ and PM_{10} levels of the participants houses over the three-month period.

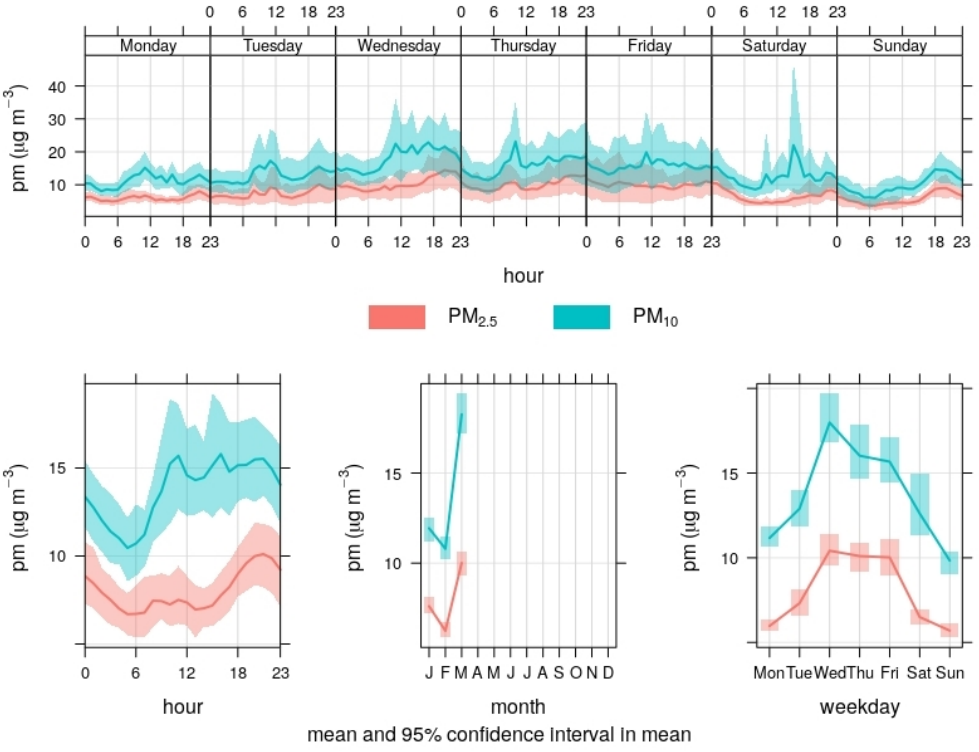

FIGURE 5.7: Outdoor Particulate Matter Variation plot.

Meteorology plays a crucial role in the estimation of levels of particulate matter. Therefore, when trying to understand the trends of outdoor pollution levels, it can be very challenging to determine whether a pollution episode is caused by local emissions or meteorology. Therefore, a Machine Learning (ML) based algorithm based on Generalised Boosted Regression Model [107] was used in order to explore and adjust for the non-linear relationships between the meteorological covariates and particulate matter $PM_{2.5}$

levels. The partial dependencies in Figure 5.8 show the relationship between $PM_{2.5}$ and the covariates that were used in the model while holding the value of other covariates at their mean levels. As can be seen, wind speed (16.1%) and wind direction (12.7%) play a crucial role in determining $PM_{2.5}$ levels; hence, its impact should be accounted for in order to better understand the air quality around the participating households.

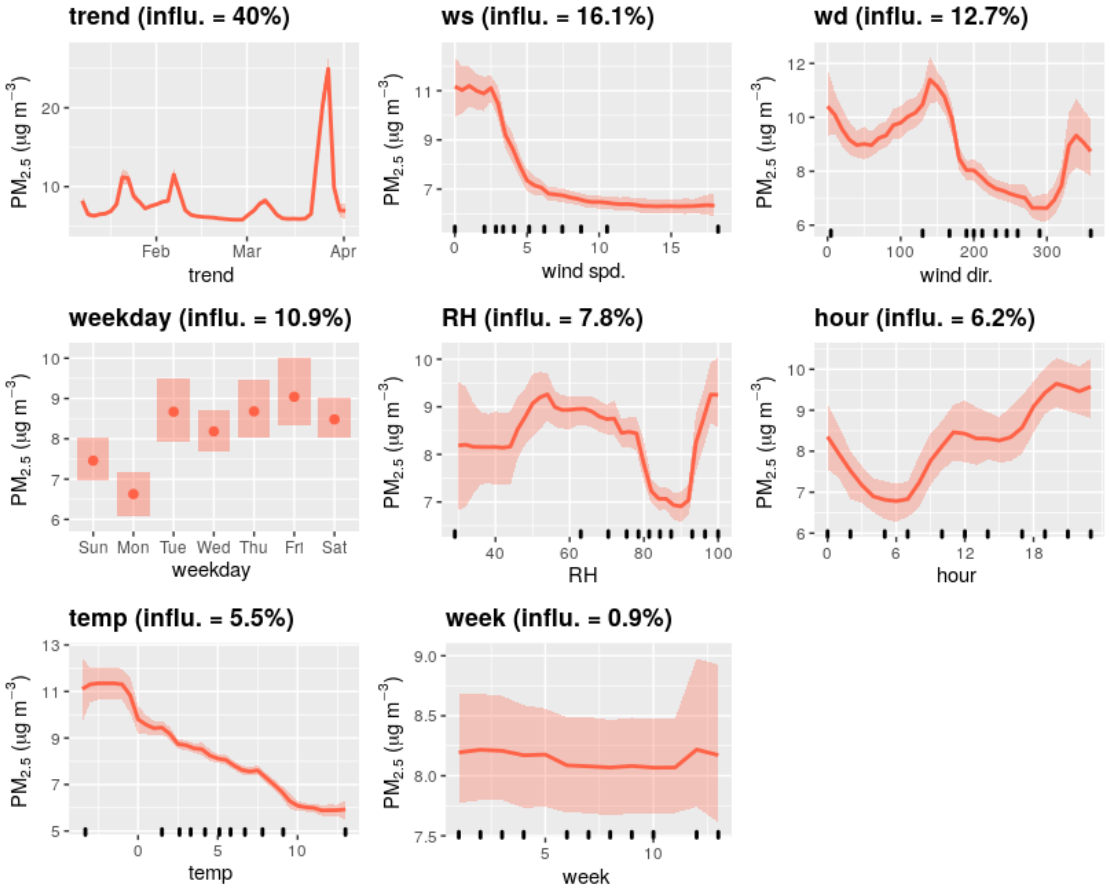

FIGURE 5.8: Influence of different covariates on outdoor $PM_{2.5}$ levels.

The popular R deweather and openair package [108] was used in creating the prediction model and plotting. The model is formed, as shown in Equation (5.4).

$$[PM_{2.5}] = RH + \bar{u} + \phi + T\theta + t_{hour} + t_{weekday} + tJD \tag{5.4}$$

where $\bar{u}$ is the mean hourly wind speed, ϕ is the mean hourly wind direction (degrees, clockwise from the north), and $T\theta$ is the mean hourly temperature (°C). Variables representing hour of the day, t_{hour}, day of the week, $t_{weekday}$, and day of the year, tJD were also considered for the model development.

From Figures 5.7 and 5.8, it is evident that, during weekdays, the outdoor levels of $PM_{2.5}$ and PM_{10} are higher than during the weekend. It can also be seen that the levels are

considerably higher outside during the evening, which corresponds to the usage pattern of stoves by participants. This indicates that even DEFRA-certified solid fuel stoves could affect the local air quality outdoors. A more sophisticated source apportionment study is required in order to further investigate this. The high level of ($PM_{2.5}$ and PM_{10} gradually decreases throughout the night, with the lowest levels being attained at around 5:30 am–6:00 am GMT (see Figure 5.7 hourly plot). Ten-fold cross validation [109] was used for evaluating the model performance and the model fitting results are shown in Figure 5.9.

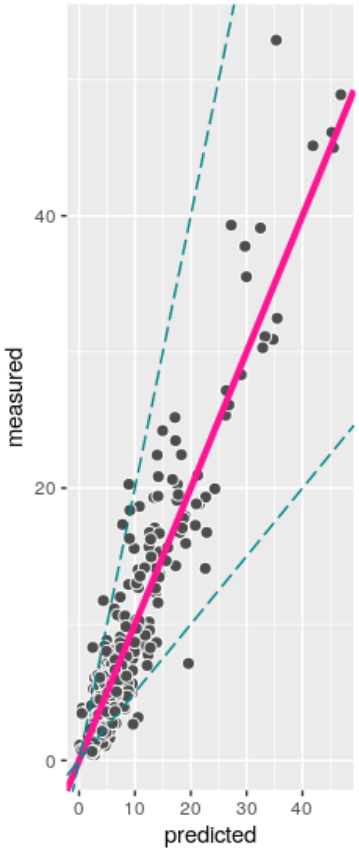

statistic	value
Test data	NA
n	403.00
FAC2	0.87
MB	0.07
MGE	2.01
NMB	0.01
NMGE	0.26
RMSE	2.89
r	0.93
COE	0.62
IOA	0.81

statistic	value
Training	NA
n	1608.00
FAC2	0.93
MB	0.01
MGE	1.45
NMB	0.00
NMGE	0.18
RMSE	2.06
r	0.96
COE	0.72
IOA	0.86

FIGURE 5.9: Generalised Boosted Regression Model to explore and remove weather impact on outdoor pollution level: Model Evaluation.

5.2.4 Data Processing and Storage

The real-time sensor data are pushed to a cloud-based database over WiFi while using a Python script running on the Raspberry Pi Zero. The data are stored in a database designed and installed in a virtual server hosted by the University of Sheffield. These data are then made available to be accessed through an Application Programming Interface (API), called Enviro-API, developed for data retrieval and displayed on the dashboard. The API developed along with the database had two goals:

- The ability to ingest a high volume of time series data with dynamic data from the sensors.
- The ability to return this time series data with basic querying parameters such as sensor ID and timestamps.

This allowed for us to create an end-to-end secure infrastructure for real-time sensor data collection, storage, and retrieval system for our study.

5.2.5 Data Analysis

Missing data have been treated. The usage days were only included if 90% of the hourly data were available. Data analyses were performed while using Excel, R, and Python programming languages. The statistical significance of the results was calculated based on Welch's t-test (Moser & Stevens, 1992) whlie using the standard equations:

$$t = \frac{m_A - m_B}{\sqrt{\frac{S_A^2}{n_A} + \frac{S_B^2}{n_B}}}, \tag{5.5}$$

and the degree of freedom of Welch t-test is calculated, as follows :

$$df = (\frac{S_A^2}{n_A} + \frac{S_B^2}{n_B})^2 / (\frac{S_A^4}{n_A^2(n_A - 1)} + \frac{S_B^4}{n_B^2(n_B - 1)}) \tag{5.6}$$

- (A) and (B) represent the Control and Experimental group.
- (m_A) and (m_B) represent the means of groups of samples (A) and (B), respectively.
- (n_A) and (n_B) represent the sizes of group (A) and (B), respectively.
- (S_A) and (S_B) are the standard deviation of the two groups (A) and (B), respectively.

The strength of correlations was classified as weak (±0.1–0.3), moderate (±0.3–0.5), and strong (±0.5–1). Data were removed during such periods while stoves were lit in order to avoid data being influenced by emissions from cooking, burning candles, or incense sticks. The influence of outdoor air pollution on indoor emissions data was anticipated, but adjustment was unnecessary, due to the absence of notable outdoor pollution levels.

5.2.6 Study Limitations

The study exhibits several limitations that are associated with variability in the research setting due to its exploratory design and focus on real-world stove use. First, the study

does not account for the impact of room size, seal, ventilation, and dwelling age on the duration of air pollution exposure witnessed. Nor does it relate the levels of air pollution to specific stages of the combustion cycle. Further study is needed in order to understand these aspects of indoor air pollution, requiring a sampling frame that is determined by more than the stove type and a research design that is appropriate for lab conditions. Second, despite using outdoor sensors to illustrate that the indoor air pollution is not coming from outside sources (see Section 5.3.2), further details on air pollution at the indoor-outdoor interface were beyond the design of this study. This is a characteristic of air pollution research more broadly, as reflected in the UK government's recent multi-million-pound call for research that is able to develop solutions to air pollution problems at the indoor/outdoor interface [110]. Relatedly, windspeed could influence the infiltration rate of outdoor air indoors, but, again, this was beyond the remit here. As such, further research into this relationship is recommended. Finally, the influence of sensor data on participant stove management practice has not been explored in detail. This will be drawn out more fully in a separate paper.

5.3 Results and Discussion

Table 5.3 summarises the daily $PM_{2.5}$ and PM_1 mean, and hourly peak $PM_{2.5}$ and PM_1 mean from 20 households and 260 stove usages, along with the statistical analysis and distribution. Data on the average pieces of fuel per use (FP) and kindling per use (KP), along with the average duration of use, have also been presented. The hourly indoor mean $PM_{2.5}$ and PM_1 concentrations that were observed during stove usage ranged from 2.27 $\mu g/m^3$ and 1.11 $\mu g/m^3$ to 47.60 $\mu g/m^3$ and 36.15 $\mu g/m^3$, respectively, with a high coefficient of variation 0.9 for $PM_{2.5}$ and 0.94 for PM_1. The hourly PNC average that was observed indoors in the particle size range (0.3–1 μm diameter) was 2607 particles/0.1 litre (L) of air when each stove was used, but the hourly peak PNC average observed was 4345 particles/0.1 L with an hourly maximum of 9978 particles/0.1 L. The average number of fuel pieces (9.58 wooden logs) and kindling (8.37 pieces) used varied significantly between the households, with a coefficient of variation 0.69 and 0.67, respectively. The average duration of use was approximately 4 h, with most households using their stove between 6 pm and 10 pm.

5.3.1 Increase in Indoor Pollution Levels during Stove Use

The findings indicate that average indoor $PM_{2.5}$ (mean = 12.21 $\mu g/m^3$ SD = 10.36, 95%CL: 8.16, 12.68) and PM_1 (mean = 8.34 $\mu g/m^3$ SD= 7.64, 95%CL: 5.29, 9.42) are higher when the stoves are lit when compared to the period in which they are not in use

with $PM_{2.5}$ levels (mean = 4.12 μg/m^3 SD= 3.61, 95% CL: 2.82, 4.82), and PM_1 levels (mean = 2.54 μg/m^3 SD= 2.61, 95%CL: 1.59, 3.04). Statistical analysis estimates that the difference in concentrations between these two groups is significantly different for both $PM_{2.5}$ (Welch's t(57.0448) = –5.0531, $p < 0.0001$) and PM_1 (Welch's t(56.6291) = –4.9197, $p < 0.0001$).

TABLE 5.3: Statistical summary and distribution of hourly mean and peak particulate matter (PM) ($\mu g/m^3$), daily usage fuel pieces and kindling pieces, and Pearson's r value.

	Duration (Hours)	**FP**	**Peak $PM_{2.5}$**	**Mean $PM_{2.5}$**	**Peak PM_1**	**Mean PM_1**	**KP**
mean	4.06	9.07	27.34	12.21	19.44	8.34	10.37
std	1.63	6.32	31.26	10.36	22.37	7.64	7.04
min	1.1	1	0.23	2.27	0	1.11	0
25%	2.95	4	9	5.66	5.79	3.51	6
50%	3.95	8	16.87	9.26	11.375	5.5	9
75%	4.94	11	34	12.50	22.77	8.87	15
max	9.2	32	195.83	47.60	121	36.15	39
Coefficient of Variation	0.39	0.69	1.14	0.90	1.14	0.94	0.67
Pearson's r							
Duration (hours)	1						
FP	0.55	1					
Peak $PM_{2.5}$	0.4	0.44	1				
Mean $PM_{2.5}$	0.017	0.17	0.75	1			
Peak PM_1	0.38	0.43	0.97	0.75	1		
Mean PM_1	0.021	0.15	0.73	0.98	0.76	1	
KP	–0.007	–0.004	–0.04	0.019	–0.034	0.039	1

Wood burner usage data from 20 households collected between January and April 2020.

The analysis in the three quartiles—(i) <25 percentile, (ii) >25- <75 percentile, and (iii) >75 percentile, representing low, medium, and peak concentrations, showed an increase for $PM_{2.5}$ (69.12%, 70.69%, 56.10%) and PM_1(71.78%, 70.41%, 67.67%). The overall average concentrations were higher for $PM_{2.5}$ by 66.24% and PM_1 by 69.49% when used.

Figure 5.10 density rug plots show the distribution and levels of PM_{25} and PM_1 for users. Figure 5.11 compare the control group's indoor pollution levels with the experimental group. For reasons of visualisation, scaling the x-axis in the graph (see Figure 5.10) is limited to 60 $\mu g/m^3$.

Figure 5.10 reveals that the levels of PM that people are exposed to can vary, with a maximum peak average of 47.60 $\mu g/m^3$ for $PM_{2.5}$ and 36.15 $\mu g/m^3$ for PM_1. While calculating the averages smooths the graph, these findings demonstrate that some users are exposed to maximum values of up to 160 $\mu g/m^3$ $PM_{2.5}$. Control users experience much lower indoor particulate levels when their stoves are not lit when compared to users that do, as indicated by Figure 5.11.

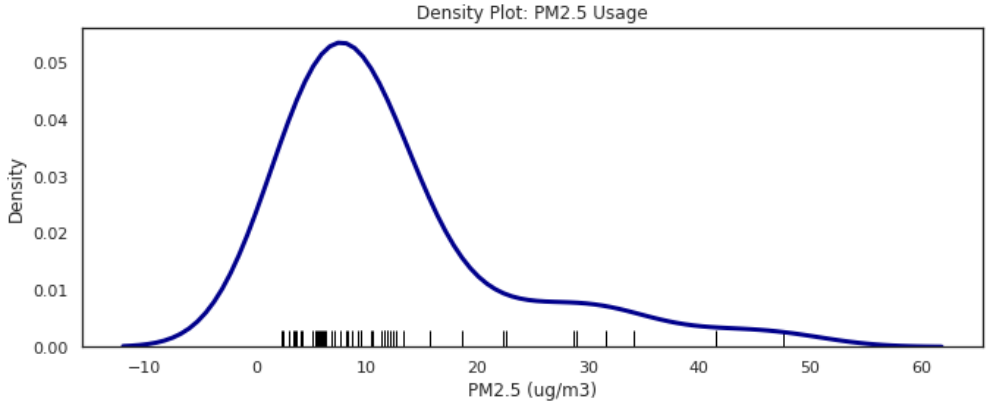

(A)

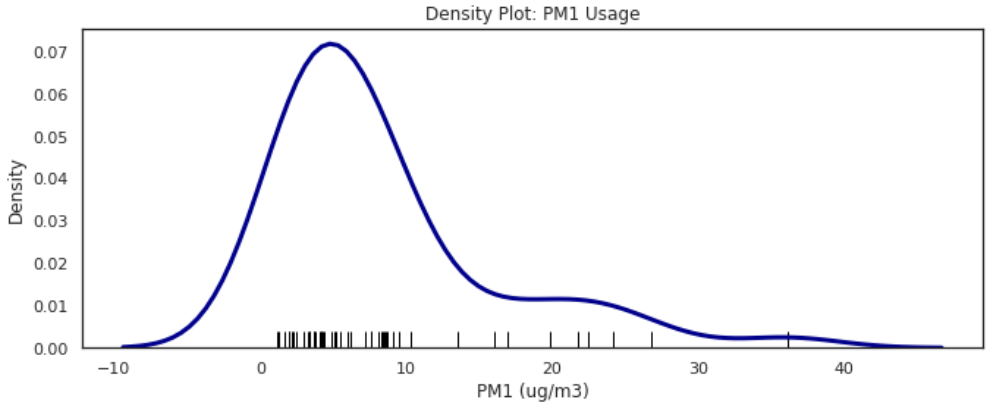

(B)

FIGURE 5.10: Conditional distribution density plot shows the overall indoor concentration levels during the usage of wood burners. (**a**) $PM_{2.5}$ distribution; (**b**) PM_1 distribution. Note. While the analysis includes the full range of data, for display purposes only the x-axis is truncated to 60 $\mu g/m^3$.

In Figure 5.10, comparing the concentration levels between usage and non-usage days for the control group also illustrates an increase for $PM_{2.5}$ (58.24%, 76.60%, 76.22%) and

PM_1(56.92%, 80.51%, 78.56%) when stoves are used. The overall average concentrations were higher for $PM_{2.5}$ by 81.23% and PM_1 by 73.76%.

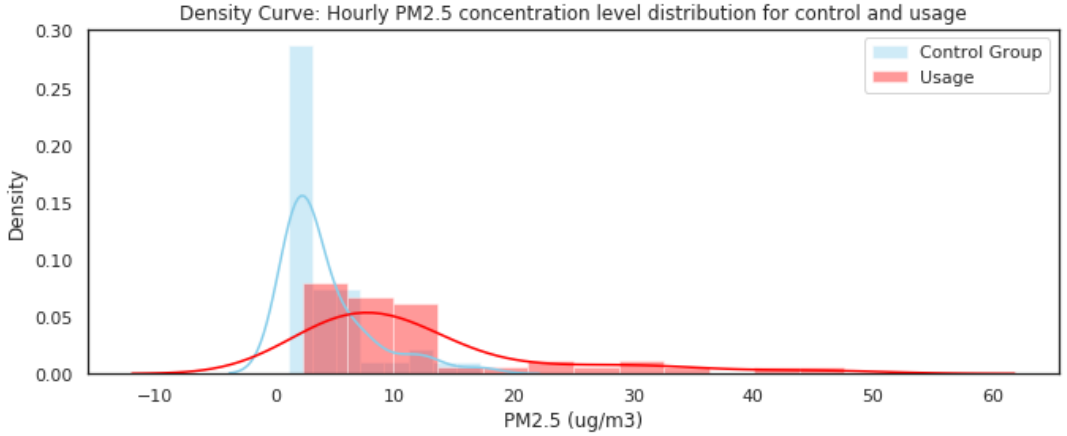

(A)

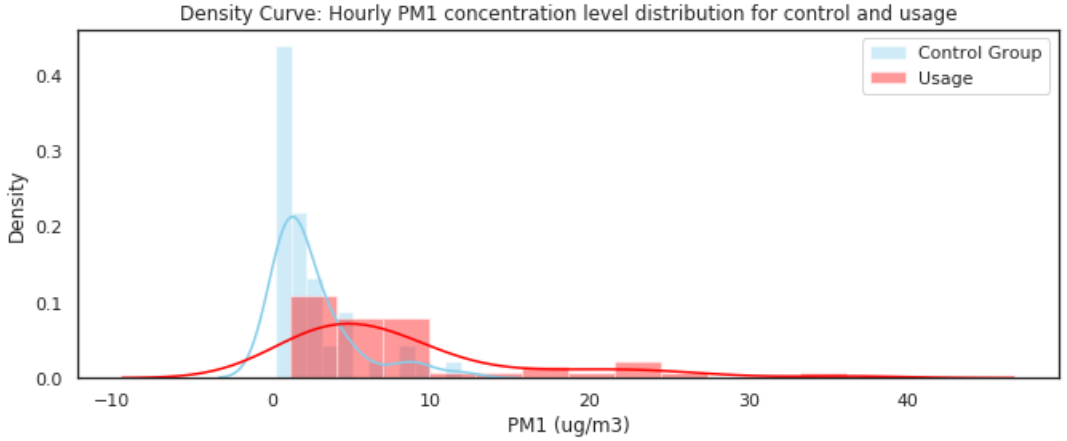

(B)

FIGURE 5.11: Control group compared to usage shows higher indoor concentration levels during the usage of wood burners with larger variation. (**a**) $PM_{2.5}$ distribution comparison; (**b**) PM_1 distribution. Note. While the analysis includes the full range of data, for display purposes only the x-axis is truncated to 60 $\mu g/m^3$.

5.3.2 Indoor Outdoor Interface: Average Indoor $PM_{2.5}$ Levels Are Higher and Weakly Correlated with Outdoor Average $PM_{2.5}$ Levels

The average indoor $PM_{2.5}$ levels are higher (mean = 12.21 $\mu g/m^3$ SD = 10.36, 95%CL: 8.16, 12.68) than the outdoor $PM_{2.5}$ levels (mean = 7.99 $\mu g/m^3$ SD= 5.51, 95%CL: 3.60, 8.93) during stove usage. From Figure 5.12, below, it is clear that indoor and outdoor values vary significantly between 10–45 $\mu g/m^3$ concentration levels. This variation is because the mean and hourly peak indoor PM lies within this range and, thus, the indoor levels are much higher than the corresponding outdoor levels. Further analysis of average indoor and outdoor $PM_{2.5}$ levels indicated a weak correlation ($R^2 = 0.19$) between them, which suggests that outdoor air quality is not a driving factor behind the high indoor pollution levels that were seen during stove usage.

While we acknowledge that indoor $PM_{2.5}$ levels can impact outdoor air quality, no measurements were taken from the chimney/flue. The air quality sensor outside the house indicates immediate outdoor air pollution levels and, thus, it is difficult to measure any leakage at the interface. Future research studies should focus on indoor air pollution and its influence on outdoor air quality in order to address this limitation of our study.

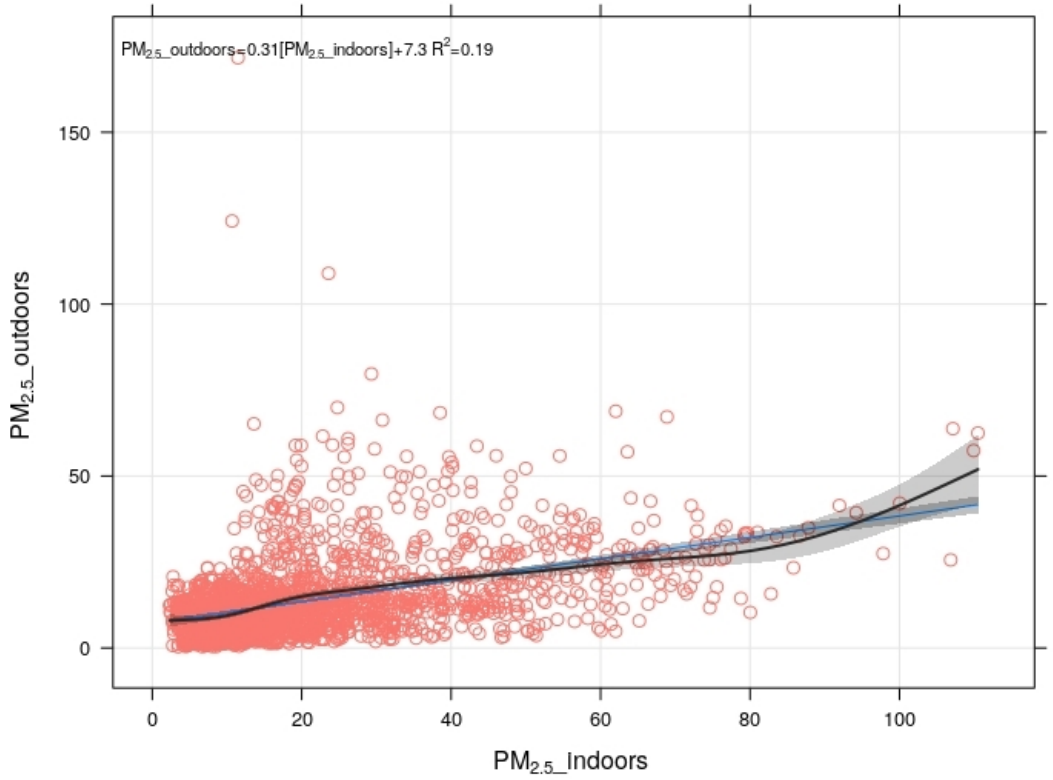

FIGURE 5.12: Indoor $PM_{2.5}$ vs. Outdoor $PM_{2.5}$.

5.3.3 Hourly Peak PM Average Higher than Daily PM Average

The analysis of Table 5.3 shows hourly peak $PM_{2.5}$ and PM_1 is strongly correlated with daily mean $PM_{2.5}$ and PM_1 (r = 0.75). Statistical analysis shows that the hourly peak mean $PM_{2.5}$ (27.34 $\mu g/m^3$, 95% CL:18.38, 37.77) and PM_1 (19.44 $\mu g/m^3$, 95% CL:12.04, 28.30) are significantly higher than the daily mean $PM_{2.5}$ (12.21 $\mu g/m^3$, 95% CL: 8.16, 13.68) and PM_1 (8.34 $\mu g/m^3$, 95% CL: 5.29, 9.43) by 55.34% and 57.09%, respectively. Hourly $PM_{2.5}$ and PM_1 peak mean and the daily mean concentrations varied between households with the minimum and maximum, being 19.2 $\mu g/m^3$–86.83 $\mu g/m^3$ and 17.79 $\mu g/m^3$–84.47 $\mu g/m^3$, respectively.

There exists high variation in exposure concentrations, concerning both short peaks and daily levels. This characteristic is related to the "real-world" nature of the study. The research diary tool provided data on not only the amount of fuel and kindling pieces used, but also their type. On average, participants used 9.58 pieces of solid fuel and 8.32 pieces of kindling per use. The number of fuel pieces used varied between a minimum of seven to a maximum of 40, while kindling varied between a minimum of one and a maximum of 32. All participants used dried and seasoned logs, but the sizes varied. There was also a diversity of kindling used, taking the form of firelighters, newspapers, balls of paper,

twigs, sawdust, packing cardboard, greeting cards, and even empty egg boxes. Echoing the findings of existing studies [79, 94, 111]. This means that the same wood burner may emit different levels of indoor air pollution depending on the quantity and type of fuel and kindling used. While suggesting a link between indoor air pollution and fuel quantity, and type of fuel and kindling, following other studies in the next section, demonstrates that this is actually linked with the stove door being opened.

Epidemiology studies and policymaking are focused around hourly average concentration monitoring by regulatory air quality stations. This leads to the omission of short-term high exposure through the "flooding" of indoor spaces with $PM_{2.5}$ and PM_1. Very few studies have reflected on short term peak concentration exposure. Lin et al.'s study [86] associated increased risk factors with hourly peak concentrations of $PM_{2.5}$. Similarly, Delfino et al. [112] associated peak PM levels with Asthma attacks in children, but in outdoor environments. Therefore, the present study encourages future researchers to study the occurrences and effects of relatively short-term peak PM exposure on human health.

5.3.3.1 Hourly Peak Average PM Has a Moderate Correlation to the Pieces of Fuel Used

While Table 5.3 indicates a weak correlation between fuel pieces and mean $PM_{2.5}$($r = 0.17$), and with PM_1 ($r = 0.15$), comparing the hourly peak concentration of $PM_{2.5}$ ($r= 0.44$) and PM_1 ($r = 0.43$) exhibits a moderate correlation with fuel pieces. The scatter plots in Figures 5.13 and 5.14 chart the relation between peak hourly levels to the possible co-factors of fuel amount and duration of usage. In Figure 5.13a,b, higher concentration peak levels are clustered towards the left of the x-axis. This indicates a non-linear relationship with fuel pieces.

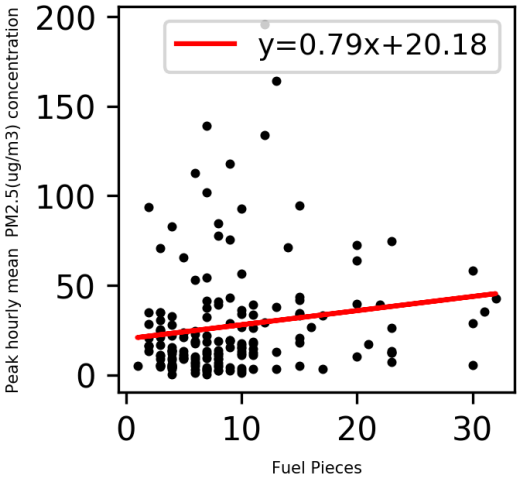

(A)

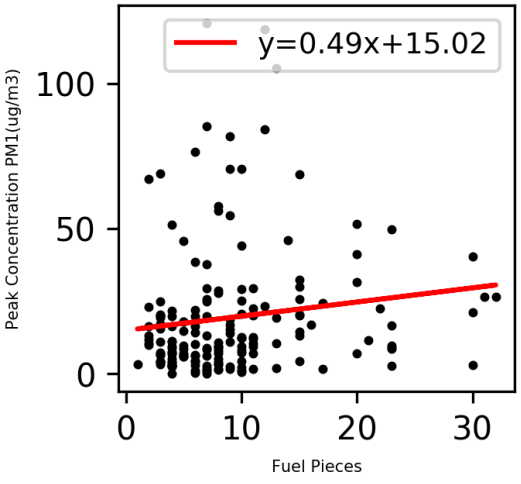

(B)

FIGURE 5.13: Scatter plot between PM concentration and Fuel Pieces. (**a**) $PM_{2.5}$ vs. fuel pieces; (**b**) PM_1 vs. fuel pieces;

While correlation between fuel pieces and hourly mean concentration is weak, it is stronger when compared to the hourly peak concentration. Therefore, the findings suggest that the peak hourly concentrations are often higher by a minimum of 250% and a maximum of 400% when participants have refuelled their stove more than once during a usage compared to one refuel or none at all. As such, the findings indicate that the 'flooding' of indoor space occurs as a result of the stove door being opened for refuelling. This accords with several existing real-world [80, 81, 94], and lab-based [79] studies into stoves outside the UK. While the findings point to the opening of the stove door as the origin for indoor PM emissions, further lab-based research is required into how this might relate to duration, timings, and the point in the burn cycle at which the opening occurs.

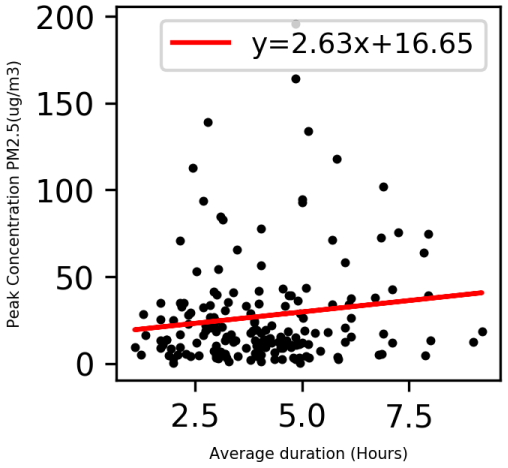

(A)

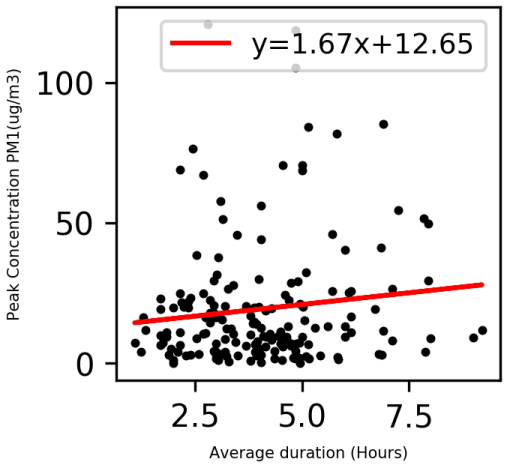

(B)

FIGURE 5.14: Scatter plot between PM concentration and duration.(**a**) $PM_{2.5}$ vs. duration; (**b**) PM_1 vs. duration;

The hourly peak concentrations explain the shape of the rug plots, as seen in Figure 5.10. The shape of the curves exhibit a distinct broad frequency distribution in the lower PM concentration. This indicates that most of the sensor readings are lower during stove use, but there are also smaller spikes towards the right of x-axis, indicating sensor readings that correspond to higher levels of PM pollution. A 'leakage' would result in a more uniform shape, and, thus, the presence of the smaller spikes cannot be explained. This echoes Salthammer et al.'s findings [94] and provides further support for the theory of opening doors being the cause of the indoor air pollution seen rather than a leakage, which appears to be more common to open fires than 'closed' stoves (see [113]). The PM fraction gets dispersed quickly throughout the room due to its smaller size, reverting to lower hourly average concentrations.

5.3.3.2 Hourly Peak Averages Illustrate a Moderate Correlation with Duration of Use

Table 5.3 also illustrates a non-linear relationship between the duration of use and mean $PM_{2.5}$ (r = 0.017). This is similar to PM_1 (r = 0.021), although, again, comparing the hourly peak concentrations of $PM_{2.5}$ (r= 0.4) and PM_1 (r = 0.38), it exhibits a moderate correlation with the duration of use. The scatter plots in Figure 5.14a,b also reflect this, with higher levels of peak values being continuously registered during the stove use.

Longer usage is associated with greater numbers of fuel pieces used. This result supports the explanation for the 'flooding' phenomenon observed, with higher short-term peak concentrations being seen during longer periods of use, because these periods are sustained by more refueling actions. This accords with [79], who also found the lighting and refueling aspects of stove management to form the main pollutant-generating phases of operation.

5.4 Conclusions

The present study aimed to understand the extent to which PM was emitted indoors and under real-world conditions by DEFRA-certified residential stoves. The findings indicate that real-world indoor PM exposure from these stoves is higher when lit as compared to the period in which they are not in use. When compared to periods of non-use, the overall average concentrations were higher for $PM_{2.5}$ by 66.24% and PM_1 by 69.49%. Peak hourly concentrations of PM were often found to be higher by 250–400% when the participants had refueled their stove more than once during a single usage. The findings also provide information on PNC, with an average hourly peak of 9978 particles/0.1 L emitted during a single usage. These 'flooding' events correlated with the opening of the stove door, which indicated that such incidents occurred as fuel was added. Data from outdoor sensors clarified that this was not originating from outdoors. On the basis of these results, it is recommended that DEFRA testing standards be modified in order to account for these normative health risks. The PM that is released into the home is not an aberration from normal use, but results directly from it. This is because real-world operation cannot occur without opening the stove door. It may be that with regulatory encouragement stove designs can be modified in a way that limits such instances. In the meantime, or in the event that appropriate modification cannot be achieved, it is also recommended that new residential stoves be accompanied by a health warning at the point of sale in order to indicate the normative health risks posed to users.

Additional Notes:

In this chapter, we present a study centered on wood burning and its effects on indoor air quality quantified by LCS. Before diving into the paper's specifics, there are some essential points to highlight:

- **Co-location and Indoor Monitoring:** Our study's primary focus was indoor air quality. However, due to the constraints of deploying reference grade analyzers indoors, the co-location of low-cost sensors with reference analyzers was carried out outdoors. This approach was adopted to validate and calibrate the low-cost sensors in an environment where they could be benchmarked against established reference

equipment. The insights and calibration data obtained from this outdoor co-location were then applied to our indoor measurements, ensuring the reliability of our indoor findings.

- **Dashboard Development:** Rohit Chakraborty [RC] designed the dashboard that provides a visual representation of our findings. It was crafted to deliver effective data visualization and grant users clear and actionable insights into the dataset.
- **Collaboration with the University of Nottingham:** The University of Nottingham played a pivotal role in the co-conceptualization of this study and editing. My contributions ranged from designing the study, writing the initial draft, data analysis, visualization, to editing the manuscript for clarity and rigor.
- **Ethics Approval:** All research in the University of Nottingham is looked at by a group of people, called a Research Ethics Committee, to protect your interests. This study has been reviewed and approved by the School of Sociology and Social Policy Research Ethics Committee.
- **Clarification on Ultrafine Particles (UFP):** A clarification regarding ultrafine particles (UFP) is warranted. UFPs are typically defined as particles with diameters less than 100 nm. The inclusion of particles above 300 nm as UFPs in the paper was an oversight on our part, and I acknowledge this error. Corrections will be made in subsequent publications or iterations.

Chapter 6

A Practical Green Infrastructure Intervention to Mitigate Air Pollution in a UK School Playground

Abstract

Air pollution severely compromises children's health and development, causing physical and mental implications. We have explored the use of site-specific green infrastructure (green barriers) in a school playground in Sheffield, UK as an air pollution mitigation measure to improve children's environment. The study assessed air quality pre-post intervention and compare it with two control sites. Nitrogen dioxide (NO_2) and particulate matter <2.5 μm in size ($PM_{2.5}$) concentration change was assessed via three methods: 1) continuous monitoring with fixed devices (de-seasonalised), 2) monthly monitoring with diffusion tubes (spatial analysis), and 3) intermittent monitoring with a mobile device at children's height (spatial analysis). De-seasonalised results indicate a reduction of 13% for NO_2 and of 2% for $PM_{2.5}$ in the school playground after two years of plant establishment. Further reductions in NO_2 levels (25%) were observed during an exceptionally low mobility period (first COVID-19 lockdown); contrary to $PM_{2.5}$ levels, which increased. Additionally, particles captured by a green barrier plant, Hedera helix 'Woerner', were observed and analysed using SEM/EDX techniques. Particle elemental analysis suggested natural and potential anthropogenic origins, potentially signaling vehicle traffic. Overall, green barriers are a valid complementary tool to improve school air quality, with quantifiable and significant air pollution changes even in our space-constrained site.

6.1 Introduction

Air pollution continues to be one of the most pressing challenges of the urban landscape, causing environmental quality decline and human health implications. In particular, children's exposure to air pollution has severe repercussions to their health. At the same time, a shocking 93% of children under 15 years old breathe polluted air worldwide [114]. These children might have experienced a range of illnesses, from adverse neurodevelopment [115, 116] and mental health problems [117], to decreased respiratory and cardiovascular functions[118, 119]. Whilst tackling the sources of pollution remains the most recommended way to cut down toxic emissions and protect children's health [120, 121], the current implemented measures worldwide do not seem sufficient for the urgency of solving a mostly anthropogenic problem [122]. In that sense, additional mitigation measures to protect vulnerable populations have been explored, including the use of green infrastructure (GI) to reduce air pollution at a local level.

Under the nature-based solutions umbrella, GI encompasses any type of natural and semi-natural areas managed to deliver ecosystem services [123]. In the urban landscape, this translates into street trees, parks, green roofs, green walls, hedges, green barriers or fences, among others. GI has the potential to reduce ambient air pollution via multiple mechanisms: gases absorption such as nitrogen dioxide (NO_2), gases and particulate matter (PM) deflection and dispersion, and PM deposition on plants' structures [124]. Simultaneously, various factors affect GI's performance to improve air quality (AQ), such as the urban layout and the local wind direction [125], or the plants' composition and their AQ functional traits [126, 127].

The use of GI in school facilities to reduce pupils' exposure to air pollutants has been suggested by the [128]. Some schools have put the GI proposal into practice in the UK – specifically installing green barriers or fences. For instance, schools in Dorset and London have installed ivy panels around the school facilities' perimeter [129, 130]; four schools in Manchester are part of a trial run by Lancaster University where evergreen hedges were planted between school premises and passing traffic [131, 132]; and the Mayor of London's Green Fund awarded a grant to twenty-nine primary schools to plant vegetation and boost air quality [133]. Although purposely implemented green barriers exist in these UK schools, there is little/weak scientific evidence on actual air pollution concentration changes due to the GI intervention, and that consider the site's conditions. For instance, Abhijith et al. [134] found a 44% decrease of PM concentrations immediately behind a green screen installed in a London school, but the authors' short monitoring campaign did not take into account the effect of the site's seasonal and weather conditions, and COVID restrictions. Moreover, most research to date comprises AQ assessments in places with pre-existing GI onsite which do not offer understanding of air pollution pre-post intervention, or are based on modelling studies that present ideal situations for air quality improvement [126, 135–141], potentially different from what could be achieved in intricate real-life school environments. Besides, most studies use simplistic GI formed by one to three plant species [142], instead of more complex planting designs. GI composed of multiple species could foster ecosystem functioning and deliver co-benefits (e.g. safety, wellbeing, aesthetics, biodiversity).

This study assesses AQ impacts of a multi-species (31 taxa) thin GI in a UK school playground, where a green barrier was purposely built and designed as a functioning ecosystem that fits the irregular school layout. Pre- and post-intervention conditions – including air quality, meteorological conditions, and COVID restrictions – are fully

acknowledged and characterised. Here, we focus on evaluating the GI intervention in terms of NO_2 and $PM_{2.5}$ concentration changes, and on identifying the composition of the latter. The following sections elaborate on the methods followed (Section 6.2), the AQ outcomes due to the green barrier implementation and a discussion based on three research questions (Section 6.3):

i) Can site-specific multi-species thin green barriers provide enough protection against NO_2 and $PM_{2.5}$ air pollution in a school facility?

ii) What is ambient PM around an inner-city school made of?

iii) What has a larger influence on school air quality: multi-species thin green barrier implementation or low-vehicle traffic (due to COVID-19 lockdown)?

Concluding remarks are presented in Section 6.4.

6.2 Materials and Methods

6.2.1 Study design

A green barrier was installed in a case study school in Sheffield, UK. Air quality was monitored pre and post such GI intervention at the case study school (Sch-GB site) and at two other sites serving as control for data comparison and contrast (Figure 6.1). The control sites are located within a 2 km radius from Sch-GB, and comprise a site in the city centre (City site) – providing an urban background – and another school playground without a green barrier (Sch-NoGB site). Air quality was monitored at those three sites from April 2019 to October 2021. Sources of air pollution at the study sites include motorised transport and residential/commercial forms of burning, such as woodburning stoves. In Sheffield, 81% of road transport accounts for cars and taxis, while the remaining 19% includes buses, light vans, heavy goods vehicles, and motorcycles [143].

In light of the study happening during COVID-19 pandemic times, which caused citizen's mobility and 'normal' activities disruptions due to UK governmental restrictions and lockdowns to contain the spread [144], only three periods from the AQ campaign were adequate for analysis and comparison (Table 6.1). These periods were most similar in vehicle traffic flow and comprised the same months for each year of the study. Vehicle traffic flow (vehicle h^{-1}) data are reported for each period and site in Table 2. These data were collected at a 1-hour resolution from the Urban Flows Observatory portal [145], which compiled data recorded by Sheffield City Council. Additionally, a period of low-vehicle traffic and low-citizens' mobility (first lockdown April-June 2020) was selected for contrast and comparison with the three other periods.

6.2.2 Green infrastructure intervention

A purposely designed multi-species green barrier – the GI intervention – was installed at the case study school (Sch-GB site). Such a green barrier was co-designed and co-produced with the school community and many other contributors participating in six

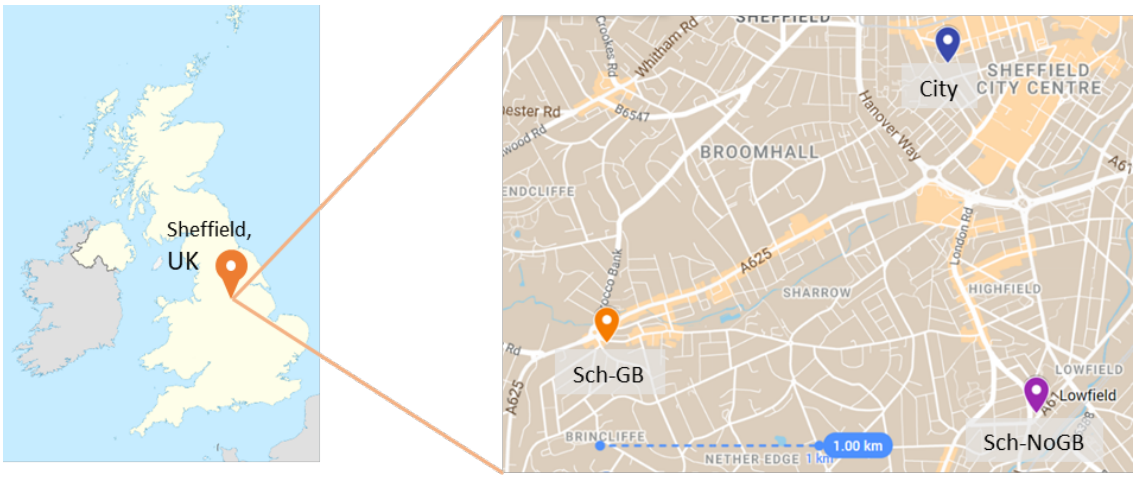

FIGURE 6.1: Location of the study sites for air quality monitoring in Sheffield, UK. 'Sch-GB' refers to case study school with a green barrier; 'City' refers to a city centre site (control); 'Sch-NoGB' refers to an urban school site without a green barrier (control).

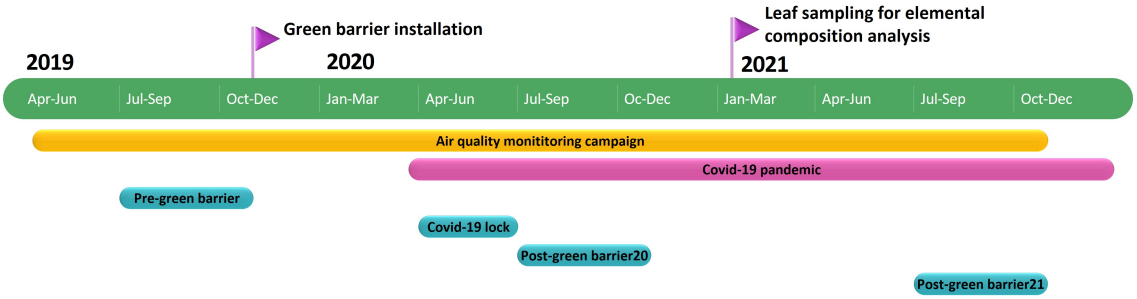

FIGURE 6.2: Air quality data collection periods. Blue colour represents periods selected for data analysis.

project stages from October 2018 to January 2020 (so called GF-Sheff project). The project stages included introduction and goal setting, green barrier design, construction, planting, project debriefing, and maintenance [146].

The case study school has one- and two-story buildings of late-Victorian character, and an active and highly used playground that accommodates 270 pupils in the infant stage (5-7 years old) throughout the day. During pupils' drop-off (8:50h) and pick-up times (15:10h), parents and children walk through the playground and socialise. From 10:30h to 15:00h, the playground is used on and off for play and lunch activities. Additionally, one day a week the playground is used for sports all-day-long, and extra-curricular sports club take place twice a week up to 16:15h.

Before the green barrier was installed, the playground had only a low stone-wall (0.6-0.7 m high) and spaced metal railings (which allowed air flow) as a separation from the adjacent streets. These streets are in close proximity to the school, between 1.9-2.2 m away from the playground's perimeter. Motorised vehicle traffic continuously circulates around the school, and car parking is available on one street adjacent to the playground. Moreover, residential and commercial facilities dominate the area. Therefore, local air pollution sources include vehicle traffic, and domestic and commercial activities.

TABLE 6.1: Periods selected for air quality assessment from the study's data collection campaign.

Data collection period	**Abbreviation**	**Date**	**Description**
Pre-green barrier	pre-gb	July - October 2019	Baseline period: before the green barrier was implemented in Sch-GB site's playground.
COVID-19 lockdown	lock	April – June 2020	Period after the green barrier implementation with first national lockdown measures to contain the COVID-19 pandemic. Vehicle traffic and citizens' mobility were highly restricted.
Post-green barrier20	post-gb20	July - October 2020	Period one year after the green barrier implementation. COVID-19 restrictions were eased from 23rd of June to 31st of October 2020. Second national lockdown came in force on 5th of November 2020.
Post-green barrier21	post-gb21	July - October 2021	Period two years after the green barrier implementation. Last phase of COVID-19 pandemic restrictions ease, and full reopening of all economic activities on 19th of July 2021.

TABLE 6.2: Mean traffic flow (vehicle h^{-1}) at closest sensors to the study sites, per selected periods.

Period	**Sch-GB Mean ± SE**	**City Mean ± SE**	**Sch-NoGB Mean pm SE**
pre-gb	331.2 ± 4.2	231 ± 3.6	NA
lock	197.4 ± 3.6	83.4 ± 1.8	268.2 ± 3.6
post-gb20	303.0 ± 4.2	160.2 ± 2.4	386.4 ± 3.6
post-gb21	342.0 ± 9.0	200.4 ± 3.0	463.2 ± 4.8

The green barrier construction started in July 2019 with groundworks preparations and culminated in late October 2019 with local community's supported planting. The multi-species green barrier comprises a mix of 31 different taxa planted along the playground's border, which extends for 60 m. Its height ranges from 2.2-2.4 m; causing a separation between the playground and the street traffic of: 2.4 m max on the southwest portion of the playground, and 4.4 m max on the northwest corner and north portion of the playground (raised school grounds). Its width is 0.9 m continuously, except on the northwest corner of the playground, where it extends up to 1.3 m. Five taxa act as the green barrier's structural plants and are the key components of air pollution deposition, deflection, and dilution. The remaining taxa are complementary plants that support the ecosystem functioning of the planting scheme (fostering plant establishment, life-span extension, and

(A) View from inside the playground before green barrier implementation.

(B) View from street after green barrier implementation.

FIGURE 6.3: Pictures of the case study's school playground before and after the green barrier implementation (Sch-GB site).

a thriving planting scheme), add sensory interest, and create a more aesthetic design. All the plants were incorporated in an almost-mature stage that created a low-porosity green barrier, providing an immediate screening effect. Further information on the characteristics of the green barrier and the species used can be found in previous studies [146, 147]. Pictures of the Sch-GB site before and after the green barrier implementation are depicted in Figure 6.3, and Figure 6.4 provides detailed information on the taxa used for the green barrier and its planting design in the school playground.

6.2.3 Air quality data collection

To assess the air pollutants concentration change due to the installation of the green barrier, collection and assessment of AQ data was carried out at the three monitoring sites (Sch-GB as site with GI intervention; and City and Sch-NoGB as control sites), and during the different sampling periods (pre-gb, lock, post-gb20, postgf-21). Concentrations were measured for NO_2 and $PM_{2.5}$ via three methods: 1) NO_2 and $PM_{2.5}$ continuous monitoring with fixed devices at all monitoring sites, 2) NO_2 monthly monitoring with diffusion tubes at all monitoring sites, and 3) complementary spatially-distributed $PM_{2.5}$ monitoring with a mobile device in Sch-GB. AQ monitoring with fixed devices and diffusion tubes is fairly recognised by the scientific community and used by governments. In addition to these commonly used methods, we used a mobile device set up at children's breathing height (1.1 m) to understand spatial changes of air pollution in the place where children walk and play. Meteorological conditions were recorded using a weather station (OTT MetSystems) installed at Sch-GB. The weather station measured air temperature, relative humidity, air pressure, wind speed and direction, precipitation intensity, and global radiation in 15-min intervals. Details of each AQ data collection method are described in the following sections.

6.2.4 Continuous monitoring with fixed devices - NO_2 and $PM_{2.5}$

Each study site had a fixed AQ monitor measuring air pollutant concentrations continuously through the day. Therefore, NO_2 and $PM_{2.5}$ data were extracted from each

FIGURE 6.4: Planting plan of the green barrier at the Sch-GB site. Blue arrows depict prevailing wind directions, size represents frequency. Modified from Urban Wilderness.

monitor's data portal at a 1-hour resolution. Consequently, 24 measurements (in μg m-3) were collected per air pollutant for each day of the data collection periods. Data were available for all sites and all periods, except for NO_2 during lock and post-gb20 periods at Sch-GB site.

The use of the selected fixed AQ monitors elaborates on previous AQ research conducted in Sheffield by Chakraborty et al. [148] and Munir et al. [149]. Details of each monitoring device corresponding to the study sites are shown in Table 3. City and Sch-NoGB sites have reference sensors managed by UK Department for Environment, Food and Rural Affairs (DEFRA), and Sheffield City Council, correspondingly. For the Sch-GB site, a low-cost monitor (AQ Mesh, V5.0) with medium accuracy was installed in the school facilities. This monitor's performance is reliable [150] and has been used in several studies [151]41, including school facilities [152]. It has an internal weather sensor that corrects data for weather effects using proprietary software, and data is also O3-filtered to correct for cross-gas effects (eliminating O3 sensitivities and providing accurate NO_2 concentrations). To refine data quality, concentrations from Sch-GB's monitor were scaled via a correlation with the reference sensors at the control sites.

Table 6.3: List of plants used in the green barrier with their respective planting plan codes.

Plant name	**Planting plan code**	**Plant name**	**Planting plan code**
Structural plants		**Herbaceous plants**	
Hedera helix 'Woerner'	Hed Woerner	*Alchemilla mollis*	Alc mol
Juniperus scopulorum 'Blue Arrow'	Jun Blu	*Anemanthele lessoniana*	Ane les
Thuja occidentalis 'Smaragd'	Thu SMA	*Asplenium scolopendrium*	Asp sco
Chaemacyparisus lawsonia 'Ivonne'	Cha Ivo	*Bergenia cordifolia* 'Purpurea'	Ber Pur
Phyllostachys nigra	Phy nig	*Calamagrostis x acutiflora* 'Karl Foerster'	Cal KF
Shrubs		*Deschampsia caespitosa* 'Goldtau'	Des Gol
Choisya ternate	Cho ter	*Geranium endressii* 'Wargrave Pink'	Ger War
Cornus alba 'Sibirica'	Cor Sib	*Heuchera micrantha* 'Palace Purple'	Heu PP
Cornus sanguinea 'Midwinter Fire'	Cor MF	*Liriope muscari* 'Big Blue'	Lir Big
Erica carnea 'Springwood Pink'	Eri SP	*Nepeta* 'Six Hills Giant'	Nep SHG
Erica carnea 'Springwood White'	Eri SW	*Polystichum setiferum*	Pol set
Euonymus fortuneii 'Emerald Gaiety'	Euo Eme	*Salvia officinalis* 'Purpurescens'	Sal Pur
Fatsia japonica	Fat jap	*Sedum spectabile* 'Brilliant'	Sed Bri
Hypericum 'Hidcote'	Hyp Hid	*Stachys byzantina* 'Big Ears'	Sta Big
Lavandula angustifolia 'Hidcote'	Lav Hid	*Verbena bonariensis*	Ver bon
Rosmarinus officinalis 'Miss Jessopp's Upright'	Ros MJU	*Sarcoccoca confusa*	Sar con

6.2.5 Monthly monitoring with diffusion tubes – NO_2

Diffusion tubes provided by Sheffield City Council were installed inside Sch-GB's playground in three different locations to measure NO_2 concentrations. This AQ monitoring technique is part of the UK government tools utilised to review and assess mean annual NO_2 concentrations [153]. Diffusion tubes are passive samplers of atmospheric NO_2 and provide monthly indicative measurements. Atmospheric NO_2 reacts with the tubes' coated triethanolamine (TEA) cap and, after chemical analysis (colorimetry) by the correspondent laboratory, NO_2 monthly concentrations are calculated and provided [154].

TABLE 6.4: Fixed air quality monitors specifications for each study site.

Study Site	**Air Quality Monitor Type**	**Air Quality Monitor Specifications**	**Monitoring Technique**	**Ref.**
Sch-GB (green barrier intervention)	Low-cost (medium data accuracy) Data quality: Proprietary software for air pollutant concentration correction from cross-gas effect and from cross-interference with environmental conditions, developed by the manufacturer. Data correlation and scaling with reference sensors.	AQ Mesh V5.0 developed by Environmental Instruments Ltd. Monitor at 1.7 m above ground level, 3 m away from closest road	NO_2: Electrochemical $PM_{2.5}$: Optical particle counter	[149, 150, 155]
City (control site—city centre)	Reference (high data accuracy)	Monitoring station from DEFRA's AURN. Station from ground level to 3 m high, 15 m away from closest road	NO_2: Chemiluminescence $PM_{2.5}$: Tapered Element Oscillating Microbalance	[149, 156]
Sch-NoGB (control site—school)	Reference (high data accuracy)	Monitoring station from Sheffield City Council. Station from ground level to 2.5 m high, 3.5 m away from closest road	NO_2: Chemiluminescence $PM_{2.5}$: Tapered Element Oscillating Microbalance	[149, 157]

Sheffield City Council manages a network of diffusion tubes in the city, which includes monitoring at Sch-NoGB and City study sites [158]. Therefore, Sch-GB NO_2 concentrations were compared within the playground and also with the control sites for the four data collection periods (pre-gb, lock, post-gb20, and post-gb21). Local and national co-location studies of diffusion tubes with reference monitors take place every year to adjust NO_2 results. Bias adjustment is already reflected here and included correcting the data with bias adjustment factors from Sheffield City Council studies. These factors are 0.98, 0.93, and 0.93 for 2019, 2020, and 2021, correspondingly. It is worth noting that there are NO_2 measurements for each month of the data collection periods, except for the lock period at Sch-GB, which only has data from June 2020 due to COVID-19 disruptions; and the post-gb20 period at Sch-NoGB, which is missing data from July 2020.

6.2.6 Intermittent monitoring with a mobile device – $PM_{2.5}$

To complement the fixed AQ monitoring at Sch-GB and understand the spatial distribution of air pollution at children's breathing height (1.1 m), a low-cost mobile device (Aeroqual series 500) was used. It measured $PM_{2.5}$ (via optical particle counter), temperature, and relative humidity at eight different locations. Five sampling locations are inside the school playground and three are located on the adjacent streets (Figure 6.6). Air sampling

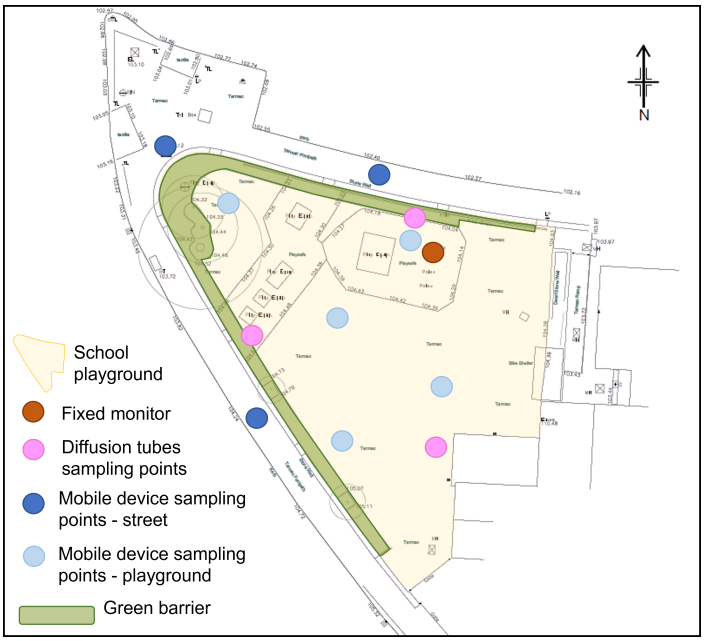

FIGURE 6.5: Air quality sampling locations in the case study school (Sch-GB) for diffusion tubes (NO_2), mobile low-cost device ($PM_{2.5}$), and fixed low-cost monitor (NO_2 and $PM_{2.5}$).

includes high-pollution times during the school day (pupil's drop-off and pick-up times), which were previously identified via the fixed monitor data. Data collection took place from May-July and September-October 2019 (pre-gb), and from September-October 2020 (post-gb20). During the data collection periods, $PM_{2.5}$ and meteorological conditions (humidity and temperature) were collected with 1-min resolution at each sampling point, for 5 consecutive minutes at a time. A total of 2,074 observations were collected and used for analysis. Due to the mismatch of pre and post green barrier collection periods, caused by COVID-19 disruptions, data was clustered by its meteorology. This meant that pre and post GI intervention data with the same mean humidity and temperature were compared. Data clusters included 1) high humidity (81%) and low temperature (14°C) days, and 2) low humidity (52%) and high temperature (20°C) days. These thresholds were selected to have similar number of observations pre-post intervention. The same mobile monitoring device (Aeroqual) has been successfully used in other studies [159–162]. Moreover, to improve data quality we conducted a field co-location with the MOBIUS (MOBIle Urban Sensing vehicle) reference sensor from the Urban Flows Observatory, The University of Sheffield [163] (Figure S2 in Supplementary Material B).

6.2.7 Air quality assessment

To assess the impact of the GI intervention on school air quality, we carried out a comparison of air pollutant concentration changes from the baseline period (pre-gb) to the three post green barrier periods (i.e., lockdown, post-gb20, and post-gb21) for Sch-GB within itself, and with the control sites. Air quality data were processed in a combination of Excel, R software, and Python programming languages, and general statistics were evaluated to calculate air pollutants concentration difference (in %), according to Equation 6.1:

$$[NO_2] \text{ or } [PM_{2.5}] \text{ difference } (\%) = \left(\frac{[P_x] \times 100}{[P_0]}\right) - 100 \tag{6.1}$$

Where P_x represents either NO_2 or $PM_{2.5}$ mean concentrations at each study period (one at a time), and P_0 represents the mean concentration of the same air pollutant during the pre-gb period. Due to different baseline concentrations at each study site, air pollutant concentration differences (in %) were comparable across the city, unlike raw concentrations.

Prior this computation, fixed monitor data was subjected to de-seasonalisation (Section 6.2.8) to reflect the sole effect of the green barrier more accurately. On the other hand, diffusion tubes and mobile device data maintained the influence of the weather, therefore, their results reflect it and were primarily used for qualitative spatial analysis.

6.2.8 Data de-seasonalisation

The global COVID-19 pandemic resulted in significant heterogeneity in recorded trends of anthropogenic emissions across the time under study. Variations in air quality as measured are also strongly impacted by meteorological conditions. As in previous studies that investigated the effect of COVID-19 restrictions on air quality [164–167], we eliminated these uncertainties using a de-seasonalising approach. After treating missing data and removing outliers, we used a two-step approach – using the R package 'deweather' [168] – to exclude the effect of trend and weather on the air quality data and to normalise it, as detailed below.

i. Step 1 – Deweather:

We used the 'gbm' package to investigate and adjust for non-linear relationships between meteorological variables, air quality measurements, and temporal variables, to forecast the variability associated with the hour of the day, day of the week, and week of the year. The latter factored in seasonal weather factors that were not considered by the other components. Additionally, we included a trend term to account for COVID-19 related changes in emission patterns during the three-year study period via a Machine Learning (ML) technique based on the Generalized Boosted Regression Tree Model (BRT) [169]. The model is formed, as shown in Equation 6.2:

$$[PM_{2.5}] = RH + \overline{u} + \text{trend} + \varnothing + T\theta + t_{\text{hour}} + t_{\text{weekday}} + t_{JD} \tag{6.2}$$

Where RH is relative humidity, $\overline{u}$ is the mean hourly wind speed, *trend* represents annual variations, $\varnothing$ is the mean hourly wind direction (degrees, clockwise from the north), and $T\theta$ is the mean hourly temperature (°C). Variables representing hour of the day, t_{hour}, day of the week, t_{weekday}, and day of the year, t_{JD}, were also considered for the model development.

For each site, 80% of the hourly meteorological and pollutant measurements were used for training the BRT model, with the remaining 20% split for testing and validation, with the goal of developing the most suitable model. This determination is achieved

automatically using commonly used metrics such as Pearson's correlation coefficient (r), root mean square error (RMSE) and mean bias (MB). Individual models were developed for $PM_{2.5}$ and NO_2 for the time of the study.

ii. Step 2 – Meteorological normalisation:

We used the 'metSim' function to create meteorological simulations in order to validate the model and make predictions. After developing the model, the meteorological averaging process was used to predict weather conditions numerous times using random sampling [170]. The 'metSim' function was used to perform this sampling. The final model was developed to forecast concentrations while accounting for the change in trends caused by COVID-19 restrictions and meteorological variability. This method predicts concentrations that are representative of typical meteorology accounting for the covariates (temperature, humidity, wind speed, wind direction, week of the year, weekday, hour of the day, and trend). The model's performance was evaluated using tenfold cross-validation. The model fitting results and the relation between $PM_{2.5}$, NO_2, and the covariates are shown in Appendix B.

6.2.9 Air quality pattern trends

To characterise overall air quality trends of each study site, air pollutant concentrations were analysed using the 'Theil-Sen' tool built-in 'Openair' R package [171]. The approach provided a non-parametric measurement of trends based on 'the median of the slopes of pairs of points with varied x-values', slope estimation, and bootstrap uncertainty estimate [166]. Because these trends during lockdown vary from prior years and may obscure the results, leading to incorrect conclusions, they were removed using a process similar to weather normalisation. De-seasonalised modelled data (15 min resolution) filled the vacant periods and a trend between 2019 and 2020 was stablished. 'Theil-Sen' calculated the monthly mean concentrations and the slopes between all pairs of the data. The final 'Theil-Sen' estimate of the slope is the median of all these slopes. Air quality pattern trends aid to understand pollution over time at Sch-GB and the control sites, and to observe the green barrier's effect on AQ. Statistical significance to the $p\text{-}value<0.001$ was determined from the trends' overlaid slope at the 95% confidence intervals.

6.2.10 Qualitative spatial analysis

Diffusion tubes (NO_2) and mobile low-cost device ($PM_{2.5}$) data were primarily used for spatial analysis. Their timeframe, combined with the ease of monitoring across space, make them more suitable for qualitative analysis in geographical visualisations. Therefore, data was mapped at playground and city scale. This analysis provides a valuable visualisation tool to extract detailed information on pollutants concentration change across the playground and city.

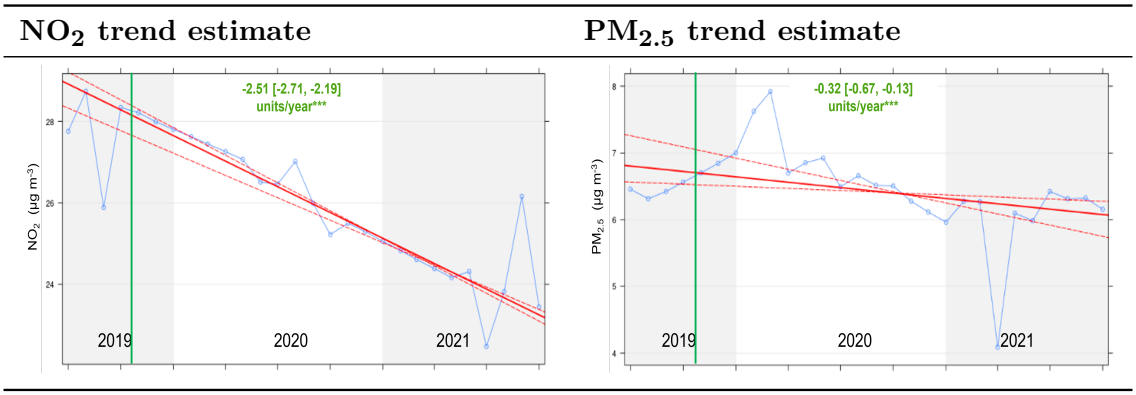

FIGURE 6.6: Air quality sampling locations in the case study school (Sch-GB) for diffusion tubes (NO_2), mobile low-cost device ($PM_{2.5}$), and fixed low-cost monitor (NO_2 and $PM_{2.5}$).

6.2.11 Qualitative PM elemental composition identification

A green barriers' mechanism of action to reduce air pollution is PM deposition on the plants' surface. In order to identify the sources of ambient PM in the case study school, we carried out an elemental composition analysis of the particles deposited on the leaves' surface of *Hedera helix* 'Woerner', the plants that cover the full length of the green barrier. Six leaf samples were collected in January 2021 at 1.25 m height from the school ground. They were stored in plastic containers, attaching the stem to the bottom of the container to prevent movement during transportation. The samples were observed under a scanning electron microscope (SEM) (Tescan Vega3 LMU) to visually examine and chemically analyse the particles deposited on the surface [147]. The SEM was used at 15 kV, in low vacuum mode (LVM) with a low vacuum secondary electron detector (LVSED). No conductive coating was applied to the leaves. Energy dispersive X-ray analysis (EDX) (Oxford Instruments X-Max 50) was used to qualitatively assess the elemental composition of 18 random particles (three particles per sample). The PM sizes analysed ranged from 2-30 μm, and large regions of agglomerated particles were present on the leaf surfaces. The Aztec Software (Oxford Instruments) was used to evaluate the chemical elements present in each sample.

6.3 Results and discussion

6.3.1 Impact of green barrier on playground air quality

Air quality results indicate that the green barrier has mixed impacts on Sch-GB's playground levels: a consistent decrease in NO_2 concentrations, and an environmental conditions-dependent decrease in $PM_{2.5}$ concentrations.

For NO_2, both, de-seasonalised and weather-influenced data analyses indicate an overall negative concentration trend in Sheffield from 2019 to 2021. Not only has Sch-GB site seen a reduction in NO_2 levels since the green barrier was built in its playground, but also concentrations have decreased at both control sites. The city's NO_2 reduction is most likely related to changes in car mobility caused by COVID-19 pandemic restrictions,

as the main NO_2 source in Sheffield is motorised vehicle traffic [172]. Traffic flow during post-gb21 period was most similar to pre-pandemic levels (Table 6.5), making it the most representative period for observing solely the green barrier's impact. Hence, comparing NO_2 concentrations from post-gb21 with pre-gb indicates that this gas pollutant decreased at all sites. However, Sch-GB had a greater reduction than City and Sch-NoGB sites (Figure S3 in Supplementary Material B), suggesting that the green barrier has a mitigation effect on playground pollution levels. Subtracting Sch-GB's concentrations difference from averaged control sites' concentrations difference, de-seasonalised results showed an NO_2 reduction of about 13% in the playground, whilst weather-influenced results showed a reduction of about 23%. It is worth noting that direct comparison of fixed monitors and diffusion tubes results is not possible due the de-seasonalisation process of the former, however, each provide complementary information about NO_2 concentration changes in time.

Furthermore, from the three study sites, only Sch-GB had a statistically significant NO_2 decrease trend over time (trend = -2.51 μg m^{-3} per year, 95%CL = -2.71,-2.19 μg m^{-3} per year, $p < 0.001$), which suggests that only the site with the GI intervention experienced a sustained NO_2 decrease from pre-gb to post-gb21 periods.

Spatial analysis supports the overall reduction of NO_2 in the city. Moreover, spatial analysis within the playground shows that for pre-gb there was a natural dilution of NO_2 from the roads, i.e. the further away from the road the diffusion tube was located, the lower the NO_2 concentration. On the other hand, once the green barrier was planted, this pattern changed. For all post GI periods, NO_2 levels were lower at diffusion tubes immediately behind the green barrier, suggesting that the greatest AQ impact covers certain range and dilutes with distance from the green barrier. Based on the calculation provided in [173], the area of protection related to the green barrier's height is given by area of protection in metres = 3 × height – 3. Sch-GB's green barrier protects up to 4.2 m behind it under ideal conditions.

TABLE 6.5: De-seasonalised air pollutant mean concentrations and difference (%) against baseline scenario (pre-gb) at city scale.

Air quality data collection	**Period**	**Study site**					
		Sch-GB		**City**		**Sch-NoGB**	
		Mean ± SE	Conc. diff.	Mean ± SE	Conc. diff.	Mean ± SE	Conc. diff.
NO_2 – fixed monitor (**de-seasonalised**)	pre-gb	27.53 ± 0.05	-	19.04 ± 0.10	-	24.82 ± 0.11	-
	lock	NA[2]	NA	14.37 ± 0.03	-24.43%	18.50 ± 0.03	-25.44%
	post-gb20	NA	NA	16.02 ± 0.08	-15.76%	19.02 ± 0.06	-23.34%
	post-gb21	22.88 ± 0.11	-16.88%	17.67 ± 0.10	-6.98%	24.73 ± 0.10	-0.37%
NO_2 - diffusion tubes	pre-gb	24.58 ± 2.17	-	22.25 ± 0.66	-	28.58 ± 0.30	-
	lock	11.50 ± 1.50	-53.22%	14.22 ± 0.29	-36.09%	19.05 ± 0.31	-33.36%
	post-gb20	16.08 ± 1.17	-34.58%	17.83 ± 0.46	-19.87%	26.33 ± 0.51	-7.87%
	post-gb21	14.11 ± 0.63	-42.62%	16.43 ± 0.41	-26.16%	25.12 ± 0.59	-12.12%
$PM_{2.5}$ - fixed monitor	pre-gb	5.98 ± 0.01	-	6.74 ± 0.01	-	6.64 ± 0.01	-
	lock	7.50 ± 0.01	25.32%	7.96 ± 0.03	18.16%	7.98 ± 0.03	20.13%
	post-gb20	6.09 ± 0.01	1.71%	6.63 ± 0.01	-1.52%	6.62 ± 0.01	-0.27%
	post-gb21	5.85 ± 0.01	-2.31%	6.74 ± 0.01	0.033%	6.65 ± 0.01	0.078%

[1]Conc. diff. = concentration difference. [2]NA = not available. Green colour indicates pollution reduction and red colour indicates pollution increase, compared to baseline period.

Furthermore, from the three study sites, only Sch-GB had a statistically significant NO_2 decrease trend over time (trend = -2.51 μg m^{-3} per year, 95%CL = -2.71,-2.19 μg m^{-3} per year, $p < 0.001$), which suggests that only the site with the GI intervention experienced a sustained NO_2 decrease from pre-gb to post-gb21 periods.

Spatial analysis supports the overall reduction of NO_2 in the city. Moreover, spatial analysis within the playground shows that for pre-gb there was a natural dilution of NO_2 from the roads, i.e. the further away from the road the diffusion tube was located, the lower the NO_2 concentration. On the other hand, once the green barrier was planted, this pattern changed. For all post GI periods, NO_2 levels were lower at diffusion tubes immediately behind the green barrier, suggesting that the greatest AQ impact covers certain range and dilutes with distance from the green barrier. Based on the calculation provided in [173], the area of protection related to the green barrier's height is given by (area of protection in metres = 3 × height – 3). Sch-GB's green barrier protects up to 4.2 m behind it under ideal conditions.

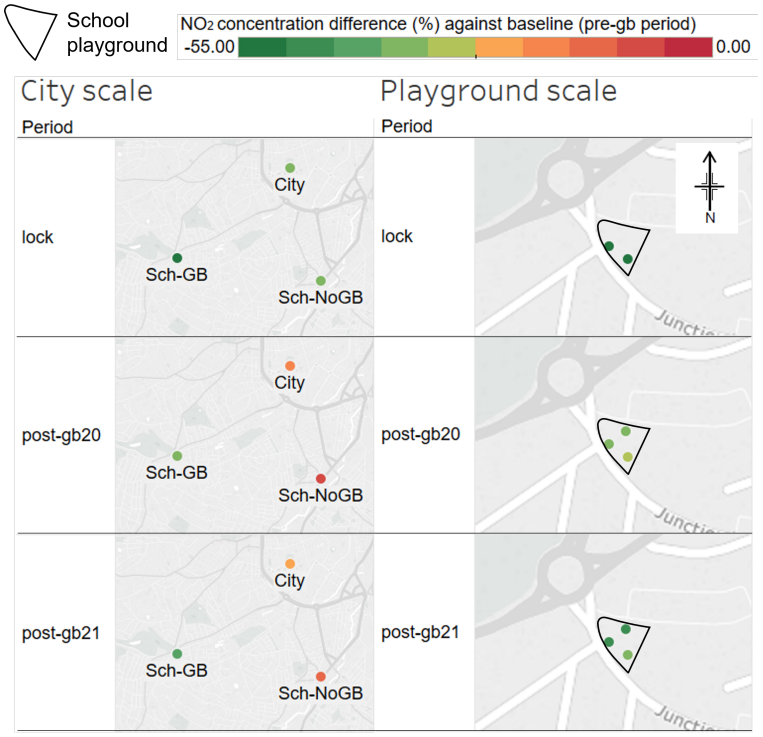

FIGURE 6.7: NO_2 mean concentrations difference (%) of sampling periods against baseline (pre-gb), data collected with diffusion tubes. Data is displayed at city scale for inter-sites comparison, and at playground scale for within site (Sch-GB) comparison.

TABLE 6.6: NO_2 mean concentrations in Sch-GB at playground scale, from diffusion tubes.

Air quality data collection	**Period**	**Location inside playground**					
		North tube		**South tube**		**West tube**	
		Mean ± SE	Conc. diff.	Mean ± SE	Conc. diff.	Mean ± SE	Conc. diff.
NO_2 – diffusion tubes (weather-influenced)	pre-gb	24.75 ± 2.24	-	20.75 ± 3.33	-	28.25 ± 2.29	-
	lock	NA	-	10.00	-51.81%	13.00	-53.98%
	post-gb20	15.75 ± 1.11	-36.33%	14.25 ± 1.11	-31.33%	18.25 ± 1.11	-35.39%
	post-gb21	13.72 ± 1.70	-44.57%	13.25 ± 1.21	-36.14%	15.35 ± 1.55	-45.66%

[1]Conc. diff. = concentration difference. Green colour indicates pollution reduction, compared to baseline period.

The minipage ensures that both the table and the footnote are treated as one unit, and the footnote is centered with respect to the width of the table. Adjusting the width of the minipage will adjust the positioning of the footnote.

In contrast to NO_2 results, de-seasonalised $PM_{2.5}$ concentrations do not follow the same declining trend in Sheffield. $PM_{2.5}$ levels greatly increased during the lockdown period and do not substantially differ among pre-gb, post-gb20, and post-gf-21 across the city (Figure S4 in Supplementary Material B). Nevertheless, when comparing only pre-gb with post-gb21 as indicated above, $PM_{2.5}$ concentrations decreased about 2% at Sch-GB's playground, whilst increasing at the control sites. Similarly to NO_2, only Sch-GB experienced a statistically significant and sustained $PM_{2.5}$ decrease from pre-gb to post-gb21 (trend = -0.32 μg m^{-3} per year, 95%CL = -0.67, -0.14 μg m^{-3} per year, $p < 0.001$).

Previous studies have shown that wind direction highly influences GI's PM reduction efficiency [126, 174–176]). We found that it is also the case for our $PM_{2.5}$ de-seasonalised data at Sch-GB. Prevailing wind directions around the playground come from the west, northwest, and southeast to a lesser extent. Our results show that $PM_{2.5}$ decreases with all wind directions ($PM_{2.5}$ trends over time are all negative and statistically significant to at least the $p<0.05$ level. However, the conditional probability function visualisation at the 90th percentile (=3.5) showed that south-easterly winds bring the highest level of $PM_{2.5}$ pollution into the playground. This might be related to airflow entering through the open-metal school gate and could be solved by supplying the gate with a material that hinders air movement (e.g., bamboo/wooden mesh), as a GI implementation is not suitable there. Furthermore, spatial analysis signal to a more restricted airflow inside the playground due to the green barrier . During the pre-gb period, higher $PM_{2.5}$ concentrations occurred on the sampling points next to the divisionary wall between the playground and the streets, and lower concentrations in the middle of the playground. Whilst for post-gb20, $PM_{2.5}$ levels were more homogeneous across the playground.

Other weather covariates impact $PM_{2.5}$ concentrations, such as humidity (15.7%) and temperature (6.4%) (Figure S1 in B), which had an influence on the data collected at children's breathing height with a mobile device. Weather-influenced results from that device showed that relatively hotter and less humid days (i.e., similar to British summer conditions) displayed a reduction in $PM_{2.5}$ concentrations inside the playground only, in contrast to colder and more humid days. Overall, seasonality and weather patterns have a considerable impact on PM behaviour. Despite de-seasonalised outcomes indicating a positive impact on playground air quality due to the green barrier, it is small compared to the effect of the underlying weather component.

The apparent limited protection that the green barrier provides against $PM_{2.5}$ is possibly related to three factors: 1) the narrow width of the barrier (0.9-1.3 m), 2) the location of the fixed AQ monitor, and 3) the multiple and diverse PM sources around the playground.

Firstly, regarding GI width, research suggests that thicker green barriers are more effective at AQ provisioning [141, 177, 178]. Some studies suggest up to a minimum width of 10 m, although such wide thickness approach seems to be more suitable for protecting populations near long open roads, such as motorways [125]. In the urban environment, green barriers need to be more accommodating to the different landscape morphologies, where often planting space is scarce. For Sch-GB's playground, the maximum width the school could spare for planting was 1.3 m in its widest section (northwest corner), hence, plant selection assured full coverage of the green barrier's height and low porosity. As such, the green barrier in Sch-GB's playground illustrates successful multi-species GI

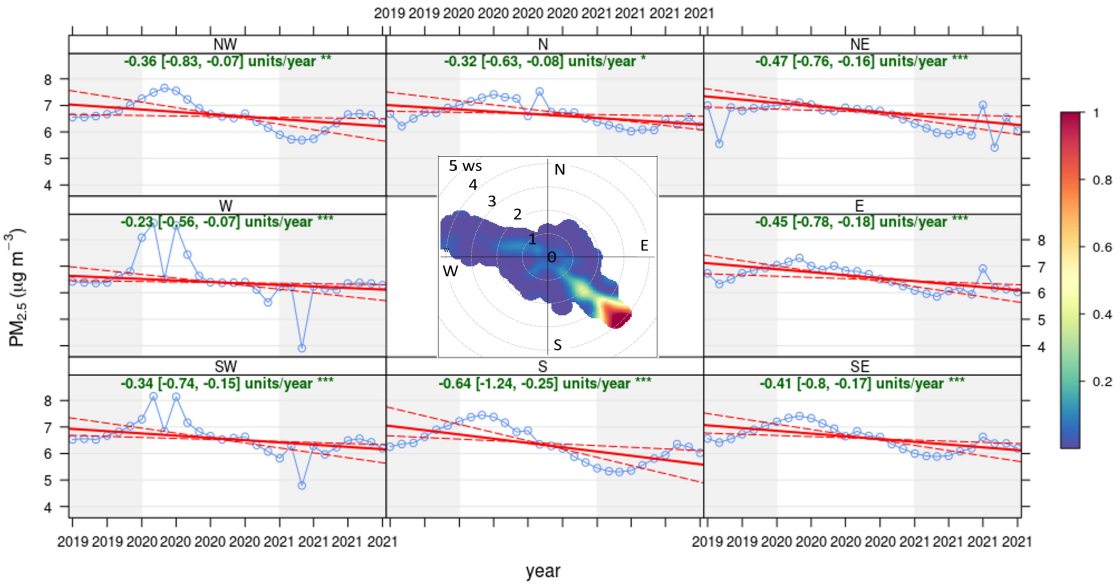

FIGURE 6.8: De-seasonalised mean $PM_{2.5}$ concentration trends (in μg m^{-3}) by wind direction and wind speed (ws) at Sch-GB site across time. The solid red line represents the trend estimate, and the dashed red lines represent 95% confidence intervals for the trend based on resampling methods. Statistically significant trends are valid at * p<0.05, ** p<0.01, and *** p<0.001 levels. CFP prob = conditional probability function, for the centre plot at the 90th percentile.

TABLE 6.7: $PM_{2.5}$ mean concentrations and difference (%) between street and playground sampling points during two weather conditions in the Sch-GB site. Data collected with mobile monitoring device.

Weather Conditions	**Period**	**Sampling Points**	**Mean ± SE (μg m^{-3})**	**Conc. diff.[1] against street**
High hum - low temp	pre-gb	street	5.82 ± 0.21	-
		playground	6.45 ± 0.20	10.95%
	post-gb20	street	7.03 ± 0.17	-
		playground	7.07 ± 0.11	0.60%
Low hum - high temp	pre-gb	street	5.63 ± 0.12	-
		playground	5.79 ± 0.11	2.79%
	post-gb20	street	6.34 ± 0.14	-
		playground	6.04 ± 0.06	-4.69%

[1]Conc. diff. = concentration difference. Green colour indicates pollution reduction and red colour indicates pollution increase, compared to mean street sampling points concentration.

application in an intricate urban layout, which most likely acts by deflecting air pollution. Other studies have explored the use of green barriers in open roads or urban street canyons, and conclude that GI's design should be site-specific and context-dependent to foster AQ provisioning [179–182]. That being said, thin green barriers (1.0-2.2 m) have a place in cities, as modelling studies have shown air pollutant reductions from 2 to 54% [183, 184] and up to 42% in real life case studies [162, 175, 185].

Secondly, the fixed AQ monitor is located on the north section of the playground, which

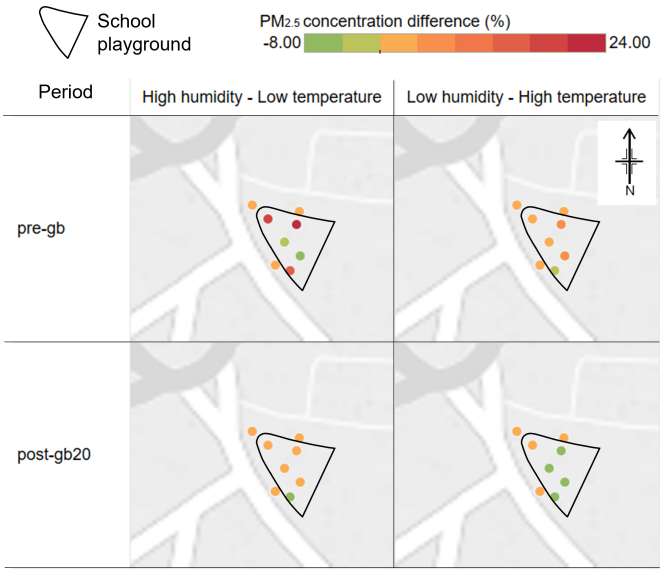

FIGURE 6.9: $PM_{2.5}$ mean concentrations difference (%) of playground against street sampling points – data collected with mobile monitoring device. Data is displayed for two sampling periods pre-gb and post-gb20, and two weather conditions.

is raised by 2 m above the ground. The monitor's installation was limited by real-life constraints of power supply access and children's safety. Its location is, therefore, higher than the sources of pollution at road level (i.e., vehicle traffic). This situation might cause the device to pick up slighter changes of air pollution because the concentrations are lower at its height. Nevertheless, evidence from PM being captured by those green barrier plants via leaf deposition is shown here (Section 6.3.2) and in our previous study [147], suggesting that the green barrier's PM mitigation could be more notorious had the monitor been at road level. Additionally, unlike studies where AQ was measured immediately behind the vegetation [134], our study's monitor was located 1 m away from the green barrier, which could cause a dilution effect on the pollution concentrations.

Finally, sources of PM in the case study school include cars, diesel buses [166], light and heavy vehicles, and woodburning stoves from residential areas nearby. In the UK, domestic combustion accounts for 25% of the total $PM_{2.5}$ emissions, with 70% from the use of wood as fuel [186]. Moreover, secondary PM formation caused by agriculture fertilizers used for crop growing, especially in spring, could also be a source of PM in the city. Alternatively, there might be internal sources of PM in the playground, for instance from debris plant material generated by the three mature trees on the northwest corner which can be resuspended by children's movement/play. PM resuspension inside schools has been the case for sandy playgrounds in Barcelona, where sand was resuspended by children's activities and added to the local PM concentrations [187].

6.3.2 Elemental composition of PM captured by green barrier plants

The green barrier plants used in the GI at Sch-GB were effective in capturing airborne PM [147], and SEM imaging revealed PM particles distributed across the leaves both individually and in regions of agglomerated particles. Figure 6.10 illustrates chemical analysis of a large individual pollution particle, and from an extended cluster of $PM_{2.5}$ particles. Overall, the elemental composition of particles deposited on the green barrier

plant *Hedera helix* 'Woerner', (planted along the whole length of the GI), indicate both natural and anthropogenic PM sources' contribution. Specifically, seventeen elements were identified on PM deposited on the *Hedera helix* leaf samples. Elements carbon (C) and oxygen (O) were found in all particles and particle clusters analysed and were the most abundant, comprising about 70-80Wt% (mean weight percentage) and 10-20Wt%, respectively. Iron (Fe), aluminium (Al), calcium (Ca), silicon (Si), and platinum (Pt) were the second most frequent and abundant elements. Additionally, chlorine (Cl), sulphur (S), nickel (Ni), potassium (K), phosphorus (P), sodium (Na), magnesium (Mg), Ruthenium (Ru), barium (Ba), and bromine (Br) were identified in trace levels.

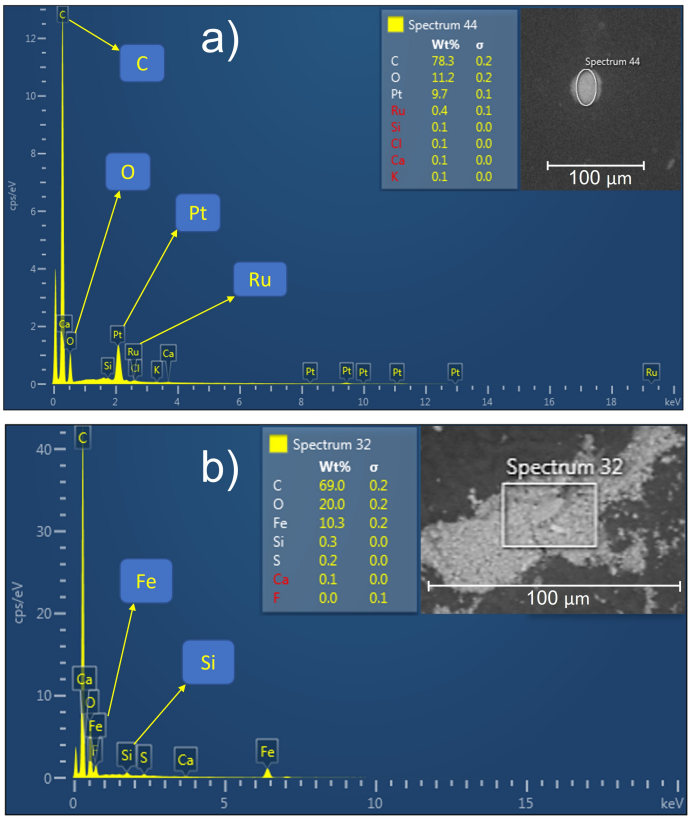

FIGURE 6.10: Sample SEM and EDX spectra of elemental composition analysis of PM captured on Hedera helix 'Woerner' leaves from green barrier. Each EDX spectrum shows the elements found on a) single particle and b) an agglomerate deposited on the leaves, and the mean weight percentage (Wt%) of each element. The SEM at the top right corner of each EDX spectrum shows PM (light grey) on the dark leaf backdrop. cps/eV = counts per second/electron Volt; $=\sigma$ = standard deviation.

The high abundance of C and O, combined with other elements identified here (P, Ca, K, Na, Fe, Cl, Mg, Al, Si) is typical of the so called 'biogenic aerosols', which are particles of biological nature (living matter, e.g. pollen, fungal spores or plant tissue) [188, 189]. In addition, some of the C and O X-rays may originate from the surrounding background leaf tissue. Particles containing Si, Al, and Fe, are classified as 'geogenic particles', or natural particles derived from the Earth's crust like salts [188].

Based on the local air pollution sources, the presence of certain elements within the assessed particles is also consistent with anthropogenic origins. The significant quantity of C identified in all particle spectra partially originate from the presence of organic and elemental carbon from vehicle exhausts [190]. Moreover, C and O may also signal the

presence of polycyclic aromatic hydrocarbons (PAHs), which are caused by incomplete combustion of organic matter (i.e., from diesel or petrol) and are carcinogenic [189]. Particles containing the transition metals Fe and Ni may be related to abrasion of vehicle parts, especially brake and tyre wear [191, 192]. Less attention has been given to transition metals Pt and Ru, which we found in six and two analysed regions respectively. Pt and Ru signal traffic air pollution because they are used in motors' catalytic converters. Although the aim of catalytic converters is to transform exhaust emissions into less polluting forms, their internal catalyst rare-earth metals leak into the environment. According to Wiseman and Zereini [193], platinum group elements are increasingly found in airborne PM and, although in small concentrations, they may be more bioavailable and toxic to humans than expected. For instance, the platinum group elements are known to cause allergies, respiratory sensitisation, and oxidative damage [193, 194].

Although it was not possible to determine the exact nature or share of each PM source in this study, the presence of Pt and Ru shows that part of the PM found here corresponds to vehicle exhaust emissions. Additionally, as leaf samples were collected in January, a winter month in the UK, vehicle traffic and home heating with solid fuels (e.g., for woodstoves) are likely to be part of the anthropogenic sources. Our results are similar to other studies that found anthropogenic elements that originate from exhaust and non-exhaust vehicle sources of PM on GI in the UK, such as living walls in Birmingham and hedges in Guildford [195, 196].

Foliar PM deposition is considered a green barrier mechanism to clean the air, but secondary to air pollution dispersion effects [197]. Nevertheless, there is clear evidence on PM capture by plant structures and, therefore, a preference to include evergreen species in green barriers [198]. Plant selection for Sch-GB's green barrier included not only five structural plants that could indeed form a barrier all year long, but species highlighted in the literature as potential PM sinks due to their micromorphological structures. SEM results here confirm PM deposition on *Hedera helix* 'Woerner' leaves, and a prior study also confirms effective PM capture by other two green barrier plants [147].

6.3.3 Impact of low-vehicle traffic and low-citizens' mobility period (COVID-19 lockdown) on air quality

Sheffield faced unexpected conditions across the two years of study due to measures imposed by the British government to control the spread of the COVID-19 disease. The global pandemic forced a strict first national lockdown from end of March to June 2020, in which people's mobility was restricted and vehicle traffic considerably decreased [144]. For the study sites, traffic flow decreased 40-64% compared to 2019 levels. Analysis of air pollution during this exceptional lockdown period demonstrate AQ improvements regarding NO_2, but not for $PM_{2.5}$.

De-seasonalised data indicates that NO_2 concentrations decreased about 25% at the control sites during lockdown, which was the highest reduction of all periods. Moreover, weather-influenced results showed that Sch-GB's playground also experienced a major NO_2 reduction during lockdown, greater than post-gb20 by 18% and post-gb21 by 10%. TheNO_2 pollution decrease was greater at Sch-GB than at the City and Sch-NoGB sites, potentially indicating a double effect of lower traffic plus green barrier. In any case, reduced traffic flow had the greatest positive impact on Sheffield's air quality regarding

NO_2. This finding is consistent with vehicle traffic being the major source of NO_2 in Sheffield [172] as well as in the UK [199]. These results emphasise the importance of reducing pollution at the source as the first and most effective way to protect children's health, for example reducing motorised vehicle traffic around schools and/or preventing its proximity during pupils drop-off/pick-up times. Consequently, green infrastructure has a place in the set of measures to tackle air pollution yet, as pointed out by Hewitt et al. [200] , only after 'reducing emissions and extending distance between sources and receptors'.

In contrast, $PM_{2.5}$ levels during the lockdown period substantially increased, with an averaged de-seasonalised $PM_{2.5}$ concentrations about 21% larger across Sheffield. Despite vehicle traffic not being the main source of PM in the city [172], a slight decrease in $PM_{2.5}$ could have been expected from the reduced traffic's share during lockdown. However, that was not the case, and PM increased during that period as a result of other particle sources increasing. For example, domestic combustion activities increased, such as cooking or woodstove use, due to people spending more time at home. Garden fires for waste burning also saw a spike during lockdown [201], potentially adding to the local PM load. Alternatively, Munir et al. [202] attribute some of the high PM concentrations during lockdown to long-range transport of European pollution. Their study in Sheffield used back trajectory of air masses and concluded that winds originating from central and eastern Europe brought pollution and caused increases in secondary PM. Similarly to Munir et al. [202], we used the HYSPLIT model to simulate PM_{10} concentrations at Sch-GB for the years 2020 and 2021 from 24-25 of April each year as an example. We calculated 72-h backward trajectories to assess whether 2020 and 2021 PM concentrations were under the influence of long-distance transport and source apportionment; and observed higher concentrations coming from Europe for those specific periods. Whilst this can be a PM source to the school, the model can be inaccurate to predict air pollution at near surface levels. Furthermore, the degree of variability in wind directions through our three-year study makes it unsuitable to predict the source of air pollution in the local area. These findings evidence the high complexity of PM formation, dispersion, and meteorology interaction. It also highlights the difficulty of PM reduction via GI or other measures.

6.4 Conclusions

This study has evaluated site-specific green infrastructure, specifically multi-species thin green barriers, as an air pollution mitigation measure in schools. By co-creating and constructing a multi-species green barrier in a school playground with real-life design constraints, we were able to support a thriving planting scheme that mitigates air pollution to real levels. The methods selected for this research allowed us to answer our three research questions:

i. This study suggests that the site-specific and multi-species thin green barrier (0.9-1.3 m max width) built in a UK school playground reduced air pollution. The reduction in pollutants concentration was significant for NO_2 (between 13% to 23%) and slight for PM (about 2%). The downward pre-post intervention trend was statistically significant.

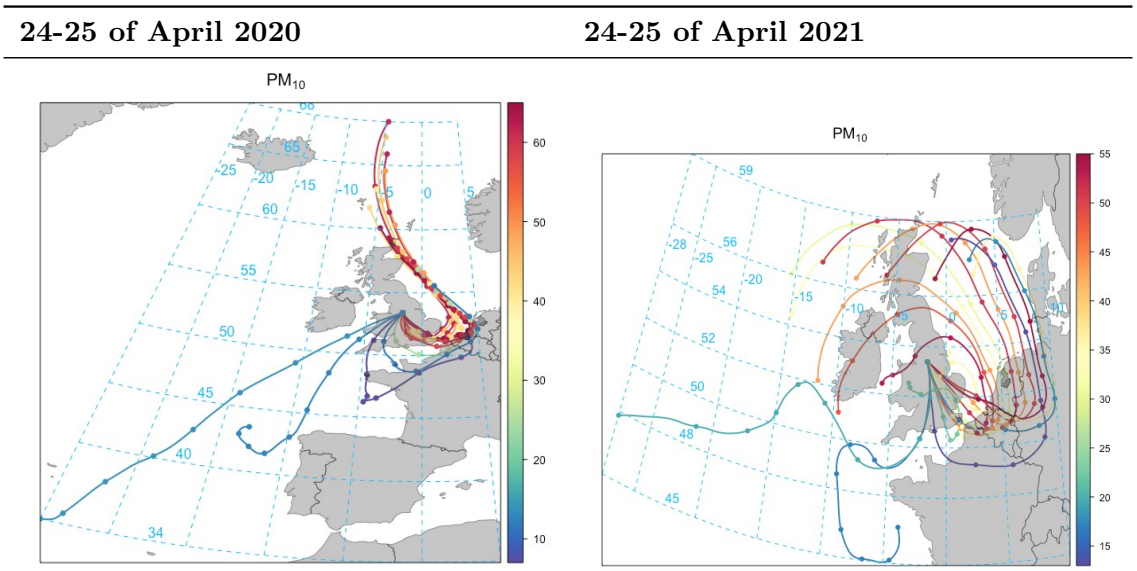

FIGURE 6.11: 72-h backward trajectories of PM_{10} concentrations ($\mu g\ m^{-3}$) at Sch-GB, created with the HYSPLIT model.

ii. Composition of PM deposited on the green barrier plant *Hedera helix* 'Woerner' suggests PM of natural and anthropogenic origin. The latter include catalytic converters from motorised vehicles.

iii. Low-vehicle traffic and low-citizen mobility (lockdown) seem to have significantly reduced NO_2; such reduction exceeds the effects of the green barrier. These mobility restrictions do not seem to significantly reduce PM pollution in the UK case study, most likely because meteorological patterns and conditions have a stronger influence on PM than traffic levels.

The mitigation effect of the multi-species thin green barrier on school AQ – most likely due to air pollutant deflection/dispersion by the green barrier, yet PM deposition was also identified – was quantifiable, and potentially helped to further reduce air pollution in the school playground during the first COVID-19 lockdown (which imposed travel restrictions). The reduced traffic flow during lockdown, however, caused the greatest reduction of NO_2 in Sheffield (about 25% at the control sites). This finding highlights the importance of working towards systematic changes, such as cars' phasing out, low traffic neighbourhoods, and school streets initiatives, to make a direct and strong impact on air pollution mitigation and protect children's health. $PM_{2.5}$ did not decrease during the lockdown period, rather, it increased. This behaviour was caused by an array of potential sources including increased domestic burning (e.g., cooking and heating) during lockdown, spring fertilizer pollution, continued diesel bus services, and long-range transport of air pollution from central and eastern Europe. The variety of PM sources highlights the volatility and difficulty of PM pollution mitigation due to its interrelation with meteorology and its cross-continental range, making a case for site-specific intervention to improve local air quality, such as green barriers in school playgrounds.

This study was constrained by the nature of the school's built-up environment, the reduced green barrier width to maintain play space, and by the plant selection which was localised

to the UK climate. In addition, air quality is a topic of concern in the UK compared to other geographies [203], and actions to minimise pollution could be taken by its citizens (i.e., active travel). Therefore, further studies looking at real-case scenario green barriers with different plant mixes and in other climates or geographies could help to supplement our findings and the green barrier design.

Green barriers can improve school air quality and, despite their limited potential, changes are quantifiable and significant even in our space-constrained site. Moreover, this nature-based solution can complement other tools and efforts to create healthy environments for children, as well as offer multiple co-benefits to the school community due to the added greenery.

6.5 Contribution

R.C. (Rohit Chakraborty):

- **Sensor Installation and Calibration:** I played a pivotal role in the installation and calibration of the sensors used in the study. This included ensuring that the sensors were positioned optimally to capture accurate data and fine-tuning them for maximum reliability and precision.
- **Data Analysis and Curation:** I took charge of the formal analysis of data captured by fixed monitors, ensuring that it was rigorously scrutinized and interpreted correctly. This involved applying statistical methods, deducing patterns, and extracting valuable insights that significantly shaped the outcomes and conclusions of the study.
- **Writing and Manuscript Preparation:** I made substantial contributions to the drafting and preparation of the original manuscript. My involvement encompassed both the initial draft and subsequent revisions, ensuring clarity, coherence, and scientific rigor in the paper's presentation.
- **Data Visualization:** I spearheaded the data visualization efforts, translating complex data sets into comprehensible and insightful graphical representations. This not only enhanced the paper's readability but also emphasized key findings and trends effectively.
- **Review and Editing:** Apart from contributing to the original draft, I also actively participated in the review and editing process, ensuring that the manuscript met the highest standards of academic writing and effectively conveyed our research findings.
- **Collaboration and Coordination:** Working closely with other co-authors, I facilitated seamless collaboration and ensured that all contributions were harmoniously integrated into the final manuscript.
- **Project Administration and Oversight:** I was actively involved in various administrative aspects of the project, ensuring that all tasks were executed on schedule and met the defined objectives.

In addition to the above, I actively participated in discussions around monitoring at the school and around, provided feedback, and collaborated closely with other team members to ensure the study's success. My commitment to the project, combined with my expertise in the subject matter, significantly influenced the paper's direction and quality.

Chapter 7

A Gaussian Process Method with Uncertainty Quantification for Air Quality Monitoring

Abstract

The monitoring and forecasting of particulate matter (e.g., $PM_{2.5}$) and gaseous pollutants (e.g., NO, NO_2, and SO_2) is of significant importance, as they have adverse impacts on human health. However, model performance can easily degrade due to data noises, environmental and other factors. This paper proposes a general solution to analyse how the noise level of measurements and hyperparameters of a Gaussian process model affect the prediction accuracy and uncertainty, with a comparative case study of atmospheric pollutant concentrations prediction in Sheffield, UK, and Peshawar, Pakistan. The Neumann series is exploited to approximate the matrix inverse involved in the Gaussian process approach. This enables us to derive a theoretical relationship between any independent variable (e.g., measurement noise level, hyperparameters of Gaussian process methods), and the uncertainty and accuracy prediction. In addition, it helps us to discover insights on how these independent variables affect the algorithm evidence lower bound. The theoretical results are verified by applying a Gaussian processes approach and its sparse variants to air quality data forecasting.

7.1 Introduction

It is generally believed that urban areas provide better opportunities in terms of economic, political, and social facilities compared to rural areas. As a result, more and more people are migrating to urban areas. At present, more than fifty percent of people worldwide live in urban areas, and this percentage is increasing with time. This has led to several environmental issues in large cities, such as air pollution [204].

Landrigan reported that air pollution caused 6.4 million deaths worldwide in 2015 [205]. According to World Health Organization (WHO) statistical data, three million premature deaths were caused by air pollution worldwide in 2012 [206]. Air pollution has a strong link with dementia, causing 850,000 people to suffer from dementia in the UK [207]. Children growing up in residential houses near busy roads and junctions have a much higher risk of developing various respiratory diseases, including asthma, due to high levels of air pollution [208]. Polluted air, especially air with high levels of NO, NO_2, and SO_2 and particulate matter ($PM_{2.5}$), is considered the most serious environmental risk to public health in urban areas [209]. Therefore, many national and international organisations are actively working on understanding the behaviour of various air pollutants [210]. This eventually leads to the development of air quality forecasting models so that people can be alerted in time [211].

Essentially, being like a time series, air quality data can be easily processed by models that are capable of time series data processing. For instance, Shen applies an autoregressive moving average (ARMA) model in $PM_{2.5}$ concentration prediction in a few Chinese cities [212]. Filtering techniques like Kalman filter are also applied to adjust data biases to improve air quality prediction accuracy [213]. These methods, though with good results reported, are limited by the requirement of a prior model before data processing. Machine learning methods, on the other hand, can learn a model from the data directly. This has enabled them to attract wide attention in recent decades in the field of air quality forecasting. For instance, Lin et al. propose the support vector regression with logarithm preprocessing procedure and immune algorithms (SVRLIA) method, which outperforms general regression neural networks (GRNN) [214] and BackPropagation neural networks (BPNN) [215] in Taiwan air quality forecasting [216].

Recently, inspired by the fact that large scale data are accumulated, deep learning models have been applied in air quality prediction [217]. Some work has added these deep learning models with the ability to quantify uncertainties introduced by inputs. For instance, Garriga-Alonso et al. endow a deep convolutional network with uncertainty quantification, by taking it as an equivalent of a Gaussian processes (GPs) model [218]. This is because GPs predictions are accompanied by confidence intervals, which are usually taken as a metric to measure prediction uncertainties. Applications of GPs in air quality forecasting can be found in [219]. However, the involvement of matrix inversion in GPs limits their application in large-scale datasets [220]. This has inspired research on improving the efficiency of GP models, and a series of efficient GP models have been published [221]. We also proposed an efficient GP model with application in air quality forecasting [219]. Despite the rich number of GP models published, there lacks work that investigates how noise level, hyperparameters, etc. affect the performance of GP models. It is necessary because air quality data vary due to seasonal variations and sensor degradations. A well-trained GP model may not work when fed with new data, simply due to measurement noise level change. By knowing how the variation of GPs performance can be attributed to noise level and hyperparameters, etc., we will still be able perform analysis when noise level or hyperparameters vary.

Aiming at this, a general solution is proposed in this paper. It provides insights on how a GP model's performance is related to measurement noise level and hyperparameters, etc. The main contribution of this work includes (1) a general method for analysing how noise level and hyperparameters of a GP model affect the prediction performance. The variation of the evidence lower bound (ELBO) and the upper bound of the marginal likelihood (UBML) with respect to the noise level and hyperparameters are also given.

(2) Neumann series is exploited to approximate the matrix inversion involved in GPs. This helps construct an analytical relation between noise level, hyperparameters, etc., and model performance. (3) A comparative air quality forecasting study between Sheffield, UK, and Pershawar, Pakistan is given, demonstrating that the proposed solution is able to capture how noise level and hyperparameters affect GPs performance.

The remaining part of this paper is as follows. Section 7.2 provides the theoretical fundamentals involved in this paper; Section 7.3 elaborates the proposed uncertainty quantification solution. In Section 7.4, we provide a comparative study of air quality prediction in the same period between the British city Sheffield and Pakistani city Pershawar, and the paper is concluded in Section 7.5. Appendix A.1 describes the data collection process in Peshawar, Pakistan, and in Sheffield, United Kingdom, and presents maps of the considered areas of these cities.

7.2 Background Knowledge

7.2.1 Gaussian Processes

Given a set of training data $\mathcal{D} = \{(\mathbf{x}_\mathrm{i}, \mathrm{y}_\mathrm{i}), \mathrm{i} = 1, \cdots, \mathrm{n}\}$ where $\mathbf{x}_\mathrm{i} \in \mathcal{X}$ is the input and $\mathrm{y}_\mathrm{i} \in \mathbb{R}$ is the observation, we can determine a GP model $\mathrm{f}(\cdot)$ to predict y_* for a new input $\mathbf{x}_*$. For instance, when the output is one-dimensional, the GP model is formulated as

$$\mathrm{f} \sim \mathcal{GP}(\bar{\mathrm{f}}(\mathbf{x}), \mathrm{k}(\mathbf{x}, \mathbf{x}')), \quad \mathrm{y} = \mathrm{f}(\mathbf{x}) + \varepsilon, \quad \varepsilon \sim \mathcal{N}(0, \sigma^2), \tag{7.1}$$

where $\bar{\mathrm{f}} : \mathcal{X} \to \mathbb{R}$ is the mean function defined as

$$\bar{\mathrm{f}}(\mathbf{x}) = \mathbb{E}[\mathrm{f}(\mathbf{x})], \tag{7.2}$$

and $\mathrm{k} : \mathcal{X} \times \mathcal{X} \to \mathbb{R}$ is the kernel function [220] defined as

$$\mathrm{k}(\mathbf{x}, \mathbf{x}') = \mathbb{E}[(\mathrm{f}(\mathbf{x}) - \bar{\mathrm{f}}(\mathbf{x}))(\mathrm{f}(\mathbf{x}') - \bar{\mathrm{f}}(\mathbf{x}'))], \tag{7.3}$$

where ε is the additive, independent, identically distributed Gaussian measurement noise with variance $\sigma^2 \neq 0$, and $\mathbb{E}$ denotes the mathematical expectation operation.

Given $\mathbf{x}_\mathrm{i}$ a $\mathrm{D} \times 1$ vector, the n inputs can be aggregated into a matrix $\mathbf{X}_{\mathrm{D}\times\mathrm{n}}$, or briefly $\mathbf{X}$ with the corresponding output vector $\mathbf{y}_{\mathrm{n}\times 1}$, or $\mathbf{y}$. Similarly, the function values at the test inputs $\mathbf{X}_*$ with dimensions of $\mathrm{D} \times \mathrm{N}$ can be denoted as $\mathbf{f}_*$, and we next write the joint distribution of $\mathbf{y}$ and $\mathbf{f}_*$ as

$$\begin{bmatrix} \mathbf{y} \\ \mathbf{f}_* \end{bmatrix} \sim \mathcal{N}\left(\mathbf{0}, \begin{bmatrix} \mathbf{K}_{\mathrm{nn}} + \sigma^2\mathbf{I} & \mathbf{K}_{\mathrm{nN}} \\ \mathbf{K}_{\mathrm{Nn}} & \mathbf{K}_{\mathrm{NN}} \end{bmatrix}\right), \tag{7.4}$$

where $\mathbf{I}$ represents the identity matrix. $\mathbf{K}_{\mathrm{nn}} + \sigma^2\mathbf{I}$ is the $\mathrm{n} \times \mathrm{n}$ prior covariance matrix of $\mathbf{y}$ with entry $\mathbf{K}_{\mathrm{ij}} = \mathrm{k}(\mathbf{x}_\mathrm{i}, \mathbf{x}_\mathrm{j}) + \sigma^2\delta_{\mathrm{ij}}$, where δ_{ij} is one iff $\mathrm{i} = \mathrm{j}$ and zero otherwise, and $\mathbf{x}_\mathrm{i}$ and $\mathbf{x}_\mathrm{j}$ are column vectors from $\mathbf{X}$. The matrix $\mathbf{K}_{\mathrm{NN}}$ denotes the $\mathrm{N} \times \mathrm{N}$ prior covariance matrix of $\mathbf{f}_*$ with entry $\mathbf{K}_{\mathrm{ij}} = \mathrm{k}(\mathbf{x}_\mathrm{i}, \mathbf{x}_\mathrm{j})$, where $\mathbf{x}_\mathrm{i}$ and $\mathbf{x}_\mathrm{j}$ are column vectors from $\mathbf{X}_*$. The

matrices $\mathbf{K}_{\mathrm{Nn}}$ and $\mathbf{K}_{\mathrm{nN}}$ satisfy $\mathbf{K}_{\mathrm{Nn}} = \mathbf{K}_{\mathrm{nN}}^{\mathrm{T}}$, and the entry of the N × n prior covariance matrix of $\mathbf{f}_*$ and $\mathbf{y}$ is $\mathbf{K}_{\mathrm{ij}} = \mathrm{k}(\mathbf{x}_{\mathrm{i}}, \mathbf{x}_{\mathrm{j}})$, where $\mathbf{x}_{\mathrm{i}}$ is a column vector from $\mathbf{X}_*$ and $\mathbf{x}_{\mathrm{j}}$ is a column vector from $\mathbf{X}$.

By deriving the conditional distribution of $\mathbf{f}_*$ from (8.5), where the prior mean is set to be zero for simplicity [222], we have the predictive posterior at new inputs $\mathbf{X}_*$ as

$$\mathbf{f}_*|\mathbf{X}, \mathbf{y}, \mathbf{X}_* \sim \mathcal{N}(\bar{\mathbf{f}}_*, \mathrm{cov}(\mathbf{f}_*)), \tag{7.5}$$

where

$$\bar{\mathbf{f}}_* \triangleq \mathbb{E}[\mathbf{f}_*|\mathbf{X}, \mathbf{y}, \mathbf{X}_*] = \mathbf{K}_{\mathrm{Nn}}[\mathbf{K}_{\mathrm{nn}} + \sigma^2\mathbf{I}]^{-1}\mathbf{y}, \tag{7.6}$$

is the prediction at $\mathbf{X}_*$, and

$$\mathrm{cov}(\mathbf{f}_*) = \mathbf{K}_{\mathrm{NN}} - \mathbf{K}_{\mathrm{Nn}}[\mathbf{K}_{\mathrm{nn}} + \sigma^2\mathbf{I}]^{-1}\mathbf{K}_{\mathrm{Nn}}^{\mathrm{T}}, \tag{7.7}$$

denotes the covariance of $\mathbf{f}_*$.

The hyperparameter θ incorporated in the mean and covariance functions underpin the predictive performance of GP models, and they are usually estimated by maximising the logarithm of the marginal likelihood

$$\log \mathrm{p}(\mathbf{y}|\mathbf{X}) = -\frac{1}{2}\mathbf{y}^{\mathrm{T}}(\mathbf{K}_{\mathrm{nn}} + \sigma^2\mathbf{I})^{-1}\mathbf{y} - \frac{1}{2}\log|\mathbf{K}_{\mathrm{nn}} + \sigma^2\mathbf{I}| - \frac{\mathrm{n}}{2}\log 2\pi. \tag{7.8}$$

7.2.2 Neumann Series Approximation

Given a matrix inverse $\mathbf{A}^{-1}$, it can be expanded as the following Neumann series [223]

$$\mathbf{A}^{-1} = \sum_{\mathrm{n}=0}^{\infty} (\mathbf{X}^{-1}(\mathbf{X} - \mathbf{A}))^{\mathrm{n}}\mathbf{X}^{-1}, \tag{7.9}$$

which holds if $\lim_{\mathrm{n}\to\infty} (\mathbf{I} - \mathbf{X}^{-1}\mathbf{A})^{\mathrm{n}} = \mathbf{0}$ is satisfied. In our case, suppose

$$\mathbf{A} = \mathbf{K} + \sigma_{\mathrm{n}}^2\mathbf{I} \triangleq \mathbf{D}_{\mathrm{A}} + \mathbf{E}_{\mathrm{A}}, \tag{7.10}$$

where $\mathbf{D}_{\mathrm{A}}$ is the main diagonal of $\mathbf{A}$ and $\mathbf{E}_{\mathrm{A}}$ is the hollow. If we substitute $\mathbf{X}$ in Equation (8.21) by $\mathbf{D}_{\mathrm{A}}$, we get

$$\mathbf{A}^{-1} = \sum_{\mathrm{n}=0}^{\infty} (-\mathbf{D}^{-1}\mathbf{E}_{\mathrm{A}})^{\mathrm{n}}\mathbf{D}_{\mathrm{A}}^{-1}, \tag{7.11}$$

which is guaranteed to converge when $\lim_{\mathrm{n}\to\infty} (-\mathbf{D}_{\mathrm{A}}^{-1}\mathbf{E}_{\mathrm{A}})^{\mathrm{n}} = \mathbf{0}$. We investigated the convergence condition in [219], where we proved that if $\mathbf{A}$ is diagonally dominant, then Neumann series can approximate $\mathbf{A}^{-1}$ both fast and accurate. In case $\mathbf{A}$ is not diagonally dominant, we also provided a way to convert it into a diagonally dominant matrix in [219], such that $\mathbf{A}^{-1}$ can still be approximated by Neumann series. When Neumann series given in (8.23) converges, we can then approximate $\mathbf{A}$ with only the first L terms. The L-term

approximation is computed as follows:

$$\widetilde{\mathbf{A}}_{\mathrm{L}}^{-1} = \sum_{\mathrm{n}=0}^{\mathrm{L}-1} (-\mathbf{D}_{\mathrm{A}}^{-1}\mathbf{E}_{\mathrm{A}})^{\mathrm{n}}\mathbf{D}_{\mathrm{A}}^{-1}, \tag{7.12}$$

For instance, when $\mathrm{L} = 1, 2, 3$, we have the approximations

$$\widetilde{\mathbf{A}}_{\mathrm{L}}^{-1} = \begin{cases} \mathbf{D}_{\mathrm{A}}^{-1}, & \mathrm{L} = 1 \\ \mathbf{D}_{\mathrm{A}}^{-1} - \mathbf{D}_{\mathrm{A}}^{-1}\mathbf{E}_{\mathrm{A}}\mathbf{D}_{\mathrm{A}}^{-1}, & \mathrm{L} = 2 \\ \mathbf{D}_{\mathrm{A}}^{-1} - \mathbf{D}_{\mathrm{A}}^{-1}\mathbf{E}_{\mathrm{A}}\mathbf{D}_{\mathrm{A}}^{-1} + \mathbf{D}_{\mathrm{A}}^{-1}\mathbf{E}_{\mathrm{A}}\mathbf{D}_{\mathrm{A}}^{-1}\mathbf{E}_{\mathrm{A}}\mathbf{D}_{\mathrm{A}}^{-1}. & \mathrm{L} = 3 \end{cases} \tag{7.13}$$

7.3 Uncertainty Quantification in Gaussian Processes

7.3.1 Uncertainty in Measurements

It is intuitive that noisy measurements would result in less accurate predictions, just as a poor model would do. However, it is not direct from Equations (8.7) and (8.8). We will show in detail how the measurement noise would affect the prediction accuracy.

From Equations (8.7) and (8.8), we can see that the measurement noise ϵ affects the prediction and the covariance by adding a term $\sigma_{\mathrm{n}}^2\mathbf{I}$ to the prior covariance $\mathbf{K}$ in comparison to the noisy free scenario [222]. From the way that they originated, we know that both $\mathbf{K}$ and $\sigma_{\mathrm{n}}^2\mathbf{I}$ are symmetrical. Then, a matrix $\mathbf{P}$ exists such that

$$\mathbf{K} = \mathbf{P}^{-1}\mathbf{D}_{\mathbf{K}}\mathbf{P}, \tag{7.14}$$

where $\mathbf{D}_{\mathbf{K}}$ is a diagonal matrix with eigen values of $\mathbf{K}$ along the diagonal. As $\sigma_{\mathrm{n}}^2\mathbf{I}$ a diagonal matrix itself, we have

$$\sigma_{\mathrm{n}}^2\mathbf{I} = \mathbf{P}^{-1}\sigma_{\mathrm{n}}^2\mathbf{I}\mathbf{P}. \tag{7.15}$$

Therefore, we have the partial derivative of Equation (8.7) with respect to σ_{n}^2 as

$$\frac{\partial\bar{\mathbf{f}}_*}{\partial\sigma_{\mathrm{n}}^2} = \mathbf{K}_*\mathbf{P}(\mathbf{D}_{\mathbf{K}} + \sigma_{\mathrm{n}}^2\mathbf{I})^{-2}\mathbf{P}^{-1}\mathbf{y}, \tag{7.16}$$

The element-wise form of Equation (7.16) can be therefore obtained as

$$\Big(\frac{\partial\bar{\mathbf{f}}_*}{\partial\sigma_{\mathrm{n}}^2}\Big)_{\mathrm{o}} = -\sum_{\mathrm{h}=1}^{\mathrm{n}}\sum_{\mathrm{i}=1}^{\mathrm{n}}\sum_{\mathrm{j}=1}^{\mathrm{n}} \mathrm{p_{hj}p_{ij}k_{oh}}\Lambda_{\mathrm{j}}^{-1}\mathrm{y_i}, \tag{7.17}$$

where $\Lambda_{\mathrm{j}} = (\lambda_{\mathrm{j}} + \sigma_{\mathrm{n}}^2)^2$. $\mathrm{p_{hj}}$ and $\mathrm{p_{ij}}$ are the entries indexed by the j-th column, h-th and i-th row, respectively. $\mathrm{k_{oh}}$ is the o-th row and h-th column entry of $\mathbf{K}_*$. $\mathrm{y_i}$ is the i-th element of $\mathbf{y}$. $\mathrm{o} = 1, \cdots, \mathrm{s}$ denotes the o-th element of the partial derivation.

We can see that the sign of Equation (7.17) is determined by $\mathrm{p_{hj}}$ and $\mathrm{p_{ij}}$. This is because we can actually transform $\mathbf{y}$ to either positive or negative with a linear transformation, which will not be an issue for the GPs model. When we impose no constraints on $\mathrm{p_{hj}}$ and $\mathrm{p_{ij}}$, Equation (7.17) could be any real number, indicating that $\bar{\mathbf{f}}_*$ is multimodal with respect to σ_n^2, which means that one σ_n^2 can lead to different $\bar{\mathbf{f}}_*$, or equivalently, different σ_n^2 can lead to the same $\bar{\mathbf{f}}_*$. In such cases, it is difficult to investigate how σ_n^2 affects the prediction accuracy. In this paper, to facilitate the study of the monotonicity of $\bar{\mathbf{f}}_*$, we constrain $\mathrm{p_{hj}}$ and $\mathrm{p_{ij}}$ to satisfy

$$\Big(\frac{\partial \bar{\mathbf{f}}_*}{\partial \sigma_\mathrm{n}^2}\Big)_\mathrm{o} \begin{cases} > 0, & \mathrm{p_{hj}p_{ij}} < 0, \\ < 0, & \mathrm{p_{hj}p_{ij}} > 0, \\ = 0, & \mathrm{p_{hj}p_{ij}} = 0. \end{cases} \tag{7.18}$$

Then, we can see that $\bar{\mathbf{f}}_*$ is monotonic. It means that changes of σ_n^2 can cause arbitrarily large/small predictions, whereas a robust method should bound the prediction errors regardless of how σ_n^2 varies.

Similarly, the partial derivative of Equation (8.8) with respect to σ_n^2 is

$$\frac{\partial \mathrm{cov}(\mathbf{f}_*)}{\partial \sigma_\mathrm{n}^2} = (\mathbf{K}_*\mathbf{P})(\mathbf{D}_\mathbf{K} + \sigma_\mathrm{n}^2\mathbf{I})^{-2}(\mathbf{K}_*\mathbf{P})^\mathrm{T} = \sum_{\mathrm{i}=1}^{\mathrm{n}} \Lambda_\mathrm{i}^{-1}\vec{\mathbf{p}}_\mathrm{i}\vec{\mathbf{p}}_\mathrm{i}^\mathrm{T}, \tag{7.19}$$

where we denote the $\mathrm{m} \times \mathrm{n}$ dimension matrix $\mathbf{K}_*\mathbf{P}$ as

$$\mathbf{K}_*\mathbf{P} = [\vec{\mathbf{p}}_1, \vec{\mathbf{p}}_2, \cdots, \vec{\mathbf{p}}_\mathrm{n}], \tag{7.20}$$

with $\vec{\mathbf{p}}_\mathrm{i}$ a $\mathrm{m} \times 1$ vector, and $\mathrm{i} = 1, \cdots, \mathrm{n}$.

As the uncertainty is indicated by the diagonal elements, we only show how these elements change with respect to σ_n^2. The diagonal elements are given as

$$\begin{aligned} \mathrm{diag}\Big(\sum_{\mathrm{i}=1}^{\mathrm{n}} \Lambda_\mathrm{i}^{-1}\vec{\mathbf{p}}_\mathrm{i}\vec{\mathbf{p}}_\mathrm{i}^\mathrm{T}\Big) &= \mathrm{diag}\Big(\sum_{\mathrm{i}=1}^{\mathrm{n}} \Lambda_\mathrm{i}^{-1}\mathrm{p}_{1\mathrm{i}}^2, \sum_{\mathrm{i}=1}^{\mathrm{n}} \Lambda_\mathrm{i}^{-1}\mathrm{p}_{2\mathrm{i}}^2, \cdots, \sum_{\mathrm{i}=1}^{\mathrm{n}} \Lambda_\mathrm{i}^{-1}\mathrm{p}_{\mathrm{mi}}^2\Big) \\ &= \mathrm{diag}\Big(\Sigma_{11}, \Sigma_{22}, \cdots, \Sigma_{\mathrm{mm}}\Big), \end{aligned} \tag{7.21}$$

with $\mathrm{diag}(\cdot)$ denoting the diagonal elements of a matrix. We see that $\Sigma_{\mathrm{jj}} \geqslant 0$ stands for $\mathrm{j} = 1, \cdots, \mathrm{m}$, which implies that $\mathrm{cov}(\mathbf{f}_*)$ is non-decreasing as σ_n^2 increases. This means that the increase of measurement noise level would cause the non-deceasing of the prediction uncertainty.

7.3.2 Uncertainty in Hyperparameters

Another factor that affects the prediction of a GPs model is the hyperparameters. In Gaussian processes, the posterior, as shown in Equation (8.6), is used to do the prediction, while the marginal likelihood is used for hyperparameters selection [220]. The log

marginal likelihood as shown in Equation (7.22) is usually optimised to determine the hyperparameter with a specified kernel function.

$$\log \mathrm{p}(\mathbf{y}|\mathbf{X},\theta) = -\frac{1}{2}\mathbf{y}^{\mathrm{T}}(\mathbf{K}+\sigma_{\mathrm{n}}^{2}\mathbf{I})^{-1}\mathbf{y} - \frac{1}{2}\log|\mathbf{K}+\sigma_{\mathrm{n}}^{2}\mathbf{I}| - \frac{\mathrm{N}}{2}\log 2\pi. \tag{7.22}$$

However, the log marginal likelihood could be non-convex with respect to the hyperparameters, which implies that the optimisation may not converge to the global maxima [224]. A common solution dealing with it is to sample multiple starting points from a prior distribution, then choose the best set of hyperparameters according to the optima of the log marginal likelihood. Let's assume $\theta = \{\theta_1, \theta_2, \cdots, \theta_{\mathrm{s}}\}$ being the hyperparameter set and θ_{s} denoting the s-th of them, then the derivative of $\log \mathrm{p}(\mathbf{y}|\mathbf{X})$ with respect to θ_{s} is

$$\frac{\partial}{\partial\theta_{\mathrm{s}}}\log \mathrm{p}(\mathbf{y}|\mathbf{X},\theta) = \frac{1}{2}\mathrm{tr}\Big((\alpha\alpha^{\mathrm{T}} - (\mathbf{K}+\sigma_{\mathrm{n}}^{2}\mathbf{I})^{-1})\frac{\partial(\mathbf{K}+\sigma_{\mathrm{n}}^{2}\mathbf{I})}{\partial\theta_{\mathrm{s}}}\Big), \tag{7.23}$$

where $\alpha = (\mathbf{K}+\sigma_{\mathrm{n}}^{2}\mathbf{I})^{-1}\mathbf{y}$, and $\mathrm{tr}(\cdot)$ denotes the trace of a matrix. The derivative in Equation (7.23) is often multimodal and that is why a fare few initialisations are used when conducting convex optimisation. Chen et al. show that the optimisation process with various initialisations can result in different hyperparameters [224]. Nevertheless, the performance (prediction accuracy) with regard to the standardised root mean square error does not change much. However, the authors do not show how the variation of hyperparameters affects the prediction uncertainty [224].

An intuitive explanation to the fact of different hyperparameters resulting with similar predictions is that the prediction shown in Equation (8.7) is non-monotonic itself with respect to hyperparameters. To demonstrate this, a direct way is to see how the derivative of (8.7) with respect to any hyperparameter $\theta_{\mathrm{s}} \in \theta$ changes, and ultimately how it affects the prediction accuracy and uncertainty. The derivatives of $\bar{\mathbf{f}}_*$ and $\mathrm{cov}(\mathbf{f}_*)$ of θ_{s} are as below

$$\frac{\partial\bar{\mathbf{f}}_*}{\partial\theta_{\mathrm{s}}} = \Big(\mathbf{K}_*\frac{\partial(\mathbf{K}+\sigma_{\mathrm{n}}^{2}\mathbf{I})^{-1}}{\partial\theta_{\mathrm{s}}} + \frac{\partial\mathbf{K}_*}{\partial\theta_{\mathrm{s}}}(\mathbf{K}+\sigma_{\mathrm{n}}^{2}\mathbf{I})^{-1}\Big)\mathbf{y}. \tag{7.24}$$

We can see that Equations (7.24) and (7.25) are both involved with calculating $(\mathbf{K}+\sigma_{\mathrm{n}}^{2}\mathbf{I})^{-1}$, which becomes enormously complex when the dimension increases. In this paper, we focus on investigating how hyperparameters affect the predictive accuracy and uncertainty in general. Therefore, we use the Neumann series to approximate the inverse [223].

$$\begin{aligned}\frac{\partial\mathrm{cov}(\mathbf{f}_*)}{\partial\theta_{\mathrm{s}}} =& \frac{\partial\mathbf{K}(\mathbf{X}_*,\mathbf{X}_*)}{\partial\theta_{\mathrm{s}}} - \frac{\partial\mathbf{K}_*}{\partial\theta_{\mathrm{s}}}(\mathbf{K}+\sigma_{\mathrm{n}}^{2}\mathbf{I})^{-1}\mathbf{K}_*^{\mathrm{T}} - \mathbf{K}_*\frac{\partial(\mathbf{K}+\sigma_{\mathrm{n}}^{2}\mathbf{I})^{-1}}{\partial\theta_{\mathrm{s}}}\mathbf{K}_*^{\mathrm{T}} \\ & - \mathbf{K}_*(\mathbf{K}+\sigma_{\mathrm{n}}^{2}\mathbf{I})^{-1}\frac{\partial\mathbf{K}_*^{\mathrm{T}}}{\partial\theta_{\mathrm{s}}}.\end{aligned} \tag{7.25}$$

7.3.3 Derivatives Approximation with Neumann Series

The approximation accuracy and computationally complexity of Neumann series varies with L. This has been studied in [223, 225], as well as in our previous work [219]. This paper aims at providing a way to quantify uncertainties involved in GPs. We therefore choose the 2-term approximation as an example to carry out the derivations. By substituting the 2-term approximation into Equations (7.24) and (7.25), we have

$$\frac{\partial \bar{\mathbf{f}}_*}{\partial \theta_\mathrm{s}} \approx \Big(\mathbf{K}_* \frac{\partial(\mathbf{D}_\mathrm{A}^{-1} - \mathbf{D}_\mathrm{A}^{-1}\mathbf{E}_\mathrm{A}\mathbf{D}_\mathrm{A}^{-1})}{\partial \theta_\mathrm{s}} + \frac{\partial \mathbf{K}_*}{\partial \theta_\mathrm{s}}(\mathbf{D}_\mathrm{A}^{-1} - \mathbf{D}_\mathrm{A}^{-1}\mathbf{E}_\mathrm{A}\mathbf{D}_\mathrm{A}^{-1})\Big)\mathbf{y}, \tag{7.26}$$

$$\begin{aligned}\frac{\partial \mathrm{cov}(\mathbf{f}_*)}{\partial \theta_\mathrm{s}} \approx & \frac{\partial \mathbf{K}(\mathbf{X}_*, \mathbf{X}_*)}{\partial \theta_\mathrm{s}} - \frac{\partial \mathbf{K}_*}{\partial \theta_\mathrm{s}}(\mathbf{D}_\mathrm{A}^{-1} - \mathbf{D}_\mathrm{A}^{-1}\mathbf{E}_\mathrm{A}\mathbf{D}_\mathrm{A}^{-1})\mathbf{K}_*^\mathrm{T} \\ & - \mathbf{K}_* \frac{\partial(\mathbf{D}_\mathrm{A}^{-1} - \mathbf{D}_\mathrm{A}^{-1}\mathbf{E}_\mathrm{A}\mathbf{D}_\mathrm{A}^{-1})}{\partial \theta_\mathrm{s}}\mathbf{K}_*^\mathrm{T} - \mathbf{K}_*(\mathbf{D}_\mathrm{A}^{-1} - \mathbf{D}_\mathrm{A}^{-1}\mathbf{E}_\mathrm{A}\mathbf{D}_\mathrm{A}^{-1})\frac{\partial \mathbf{K}_*^\mathrm{T}}{\partial \theta_\mathrm{s}}.\end{aligned} \tag{7.27}$$

Due to the simple structure of matrices $\mathbf{D}_\mathrm{A}$ and $\mathbf{E}_\mathrm{A}$, we can get the element-wise form of Equation (7.26) as

$$\Big(\frac{\partial \bar{\mathbf{f}}_*}{\partial \theta_\mathrm{s}}\Big)_\mathrm{o} = \sum_{\mathrm{i}=1}^{\mathrm{n}}\sum_{\mathrm{j}=1}^{\mathrm{n}} (\mathrm{k}_\mathrm{oj}\frac{\partial \mathrm{d}_\mathrm{ji}}{\partial \theta_\mathrm{s}} + \frac{\partial \mathrm{k}_\mathrm{oj}}{\partial \theta_\mathrm{s}}\mathrm{d}_\mathrm{ji})\mathrm{y}_\mathrm{i}. \tag{7.28}$$

Similarly, the element-wise form of Equation (7.27) is

$$\Big(\frac{\partial \mathrm{cov}(\mathbf{f}_*)}{\partial \theta_\mathrm{s}}\Big)_\mathrm{oo} = \frac{\partial \mathbf{K}(\mathbf{X}_*, \mathbf{X}_*)_\mathrm{oo}}{\partial \theta_\mathrm{s}} - \sum_{\mathrm{i}=1}^{\mathrm{n}}\sum_{\mathrm{j}=1}^{\mathrm{n}} \Big(\frac{\partial \mathrm{k}_\mathrm{oj}}{\partial \theta_\mathrm{s}}\mathrm{d}_\mathrm{ji}\mathrm{k}_\mathrm{oi} + \mathrm{k}_\mathrm{oj}\frac{\partial \mathrm{d}_\mathrm{ji}}{\partial \theta_\mathrm{s}}\mathrm{k}_\mathrm{oi} - \mathrm{k}_\mathrm{oj}\mathrm{d}_\mathrm{ji}\frac{\partial \mathrm{k}_\mathrm{oi}}{\partial \theta_\mathrm{s}}\Big), \tag{7.29}$$

where $\mathrm{o} = 1, \cdots, \mathrm{m}$ denotes the o-th output, d_ji is the j-th row and i-th column entry of $\mathbf{D}_\mathrm{A}^{-1} - \mathbf{D}_\mathrm{A}^{-1}\mathbf{E}_\mathrm{A}\mathbf{D}_\mathrm{A}^{-1}$, k_oj and k_oi are the o-th row, j-th and i-th entries of matrix $\mathbf{K}_*$, respectively. When the kernel function is determined, Equations (7.26)–(7.29) can be used for GPs uncertainty quantification.

7.3.4 Impacts of Noise Level and Hyperparameters on ELBO and UBML

The minimisation of $\mathrm{KL}(\mathrm{q}(\mathbf{f}, \mathbf{u}) \| \mathrm{p}(\mathbf{f}, \mathbf{u}|\mathbf{y}))$ is equivalent to maximise the ELBO [220, 226] as shown in

$$\mathcal{L}_\mathrm{lower} = -\frac{1}{2}\mathbf{y}^\mathrm{T}\mathbf{G}_\mathrm{n}^{-1}\mathbf{y} - \frac{1}{2}\log|\mathbf{G}_\mathrm{n}| - \frac{\mathrm{N}}{2}\log(2\pi) - \frac{\mathrm{t}}{2\sigma_\mathrm{n}^2}, \tag{7.30}$$

where $\mathbf{G}_\mathrm{n} = \mathbf{G}_{\mathbf{xx}} + \sigma_\mathrm{n}^2\mathbf{I}$, and $\mathrm{t} = \mathrm{Tr}(\mathbf{K}_{\mathbf{xx}} - \mathbf{G}_{\mathbf{xx}})$. Combining it with UBML, as shown in Equation (7.31), an interval can be given to quantify the uncertainty in marginal likelihood.

$$\mathcal{L}_\mathrm{upper} = \frac{1}{2}\mathbf{y}^\mathrm{T}\Big(\mathbf{G}_\mathrm{n} + \mathrm{t}\mathbf{I}\Big)^{-1}\mathbf{y} - \frac{1}{2}\log|\mathbf{G}_\mathrm{n}| - \frac{\mathrm{N}}{2}\log(2\pi). \tag{7.31}$$

This paper, however, focuses on investigating how ELBO and UBML change according to σ_n^2 only. Because the investigation of how ELBO and UBML change with respect to kernel hyperparameters involves multiple Neumann series approximations, which makes

the analysis less convincing. We shall leave it as an open problem for future study. The derivatives of Equations (7.30) and (7.31) with respect to σ_{n}^2 are as follows,

$$\frac{\partial \mathcal{L}_{\mathrm{lower}}}{\partial \sigma_{\mathrm{n}}^2} = \frac{1}{2}\Big[\sum_{\mathrm{i}=1}^{\mathrm{n}}(\lambda_{\mathrm{i}}+\sigma_{\mathrm{n}}^2)^{-2}(\sum_{\mathrm{j}=1}^{\mathrm{n}}\mathrm{y_j v_{ji}})^2 - \sum_{\mathrm{i}=1}^{\mathrm{n}}\frac{1}{\lambda_{\mathrm{i}}+\sigma_{\mathrm{n}}^2} + \frac{\mathrm{t}}{\sigma_{\mathrm{n}}^4}\Big], \tag{7.32}$$

$$\frac{\partial \mathcal{L}_{\mathrm{upper}}}{\partial \sigma_{\mathrm{n}}^2} = -\frac{1}{2}\Big[\sum_{\mathrm{i}=1}^{\mathrm{n}}(\lambda_{\mathrm{i}}+\sigma_{\mathrm{n}}^2+\mathrm{t})^{-2}(\sum_{\mathrm{j}=1}^{\mathrm{n}}\mathrm{y_j v_{ji}})^2 + \sum_{\mathrm{i}=1}^{\mathrm{n}}\frac{1}{\lambda_{\mathrm{i}}+\sigma_{\mathrm{n}}^2}\Big]. \tag{7.33}$$

Figure 7.1 shows how σ_{n}^2 affects ELBO and UBML. We set σ_{n}^2 to increase from 0.1 to 200.0 with a step of 0.01. Both ELBO and UBML are recorded step by step. From the figure, we can see that when σ_{n}^2 is small ($\sigma_{\mathrm{n}}^2 \in [0.1, 1.5]$), ELBO increases with different speeds, however, UBML fluctuates as the derivative of UBML jumps between positive and negative. When σ_{n}^2 is in [1.5, 3.0], ELBO still increases, but the speeds slow down significantly. In comparison, UBML keeps decreasing with reducing speeds. The decrements of UBML mean that when σ_{n}^2 increases, though ELBO could be increased still, but the maximum (which is the UBML) can decrease. When $\sigma_{\mathrm{n}}^2 \in [3.0, 20.0]$, ELBO starts to decrease when $\sigma_{\mathrm{n}}^2 \approx 3.2$, while UBML keeps decreasing. This means that as σ_{n}^2 increases, both ELBO and UBML decrease, which indicates that the model becomes less and less effective to explain the data. When σ_{n}^2 keeps increasing ($\sigma_{\mathrm{n}}^2 \in [20.0, 200.0]$), the decreasing speeds of ELBO and UBML becomes similar and approaches zero. This means that UBML and ELBO both converge and together define an interval for the marginal likelihood, which however, can result in non-optimal hyperparameters. Our conclusion is that when σ_{n}^2 increases, UBML tends to decrease, which decreases the maximum that ELBO can reach. ELBO, on the other hand, is robust to the change of σ_{n}^2 (as it keeps increasing when σ_{n}^2 is below $\sim$3.2). However, when σ_{n}^2 exceeds a certain threshold, ELBO turns to decrease, indicating that the GPs model becomes less and less reliable. However, both ELBO and UBML converge, even when σ_{n}^2 becomes very significant, though we can no longer trust the model.

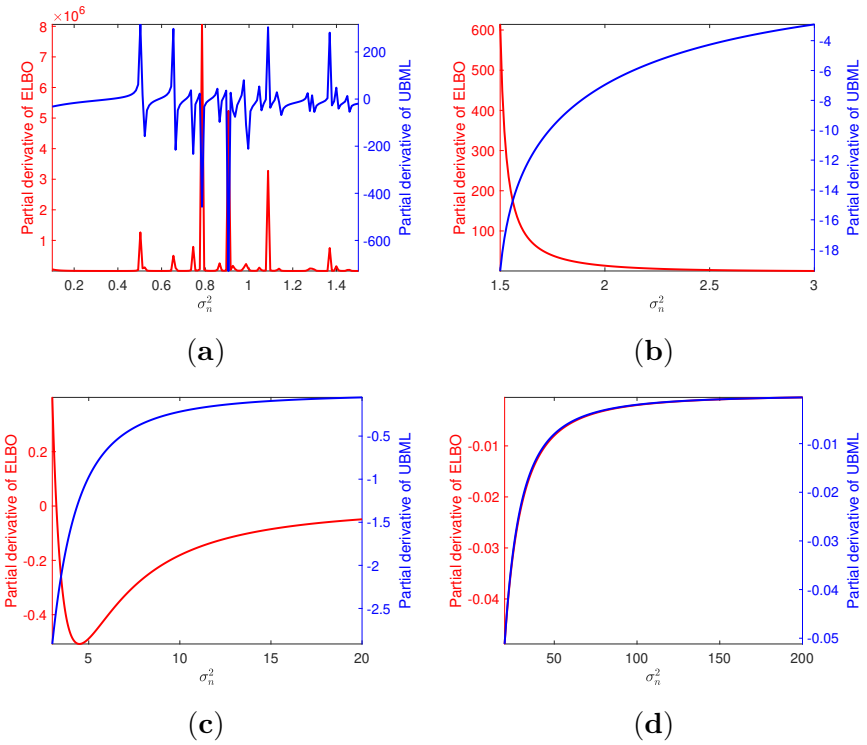

FIGURE 7.1: Impacts of σ_n^2 on ELBO and UBML: (**a**) $\sigma_n^2 \in [0.1, 1.5]$, (**b**) $\sigma_n^2 \in [1.5, 3.0]$, (**c**) $\sigma_n^2 \in [3.0, 20.0]$, (**d**) $\sigma_n^2 \in [20.0, 200.0]$.

7.4 Experiments and Analysis

To verify that the proposed solution can help to identify the impacts of σ_n^2 and θ on the predition accuracy and uncertainty of GPs model and its sparse variants such as the fully independent training conditional (FITC) [227] and variational free energy (VFE) [226] models, we conduct various experiments to process air quality data collected from Sheffield, UK, and Pershawar, Pakistan, during the time period of 24 June 2019–14 July 2019 for three weeks, which will be denoted as W1, W2, and W3 hereafter. The data were collected with digital sensors called AQMesh pod with a 15 min time interval. Though the sensor itself is able to measure the concentrations of quite a few atmospheric pollutants, here we only analyse the concentrations of NO, NO_2, SO_2, and $PM_{2.5}$. Figure 7.2 shows the raw data. We can see directly that the air quality of Sheffield is much better than Pershawar on average. Especially during daytime, concentrations of NO_2 and $PM_{2.5}$ in Pershawar exceed the WHO criteria. Meanwhile, those in Sheffield are much lower than the criteria. Being a postindustrial city itself, Sheffield has improved air quality significantly. The experience can be spread to help cities like Pershwar to improve air quality.

7.4.1 Air Quality Prediction

Figures 7.3 and 7.4 show Sheffield and Pershawar forecasting results of GPs, FITC, and VFE, with 3σ confidence intervals (denoted as Conf in the figures) indicated by the shaded area. We can see that the GPs model reports the best results in general, in terms of absolute error between predicts and measurements (denoted as Meas in the figures). However,

the performance of all the models varies from pollutant types to cities. This is actually one of the reasons why the investigation of how measurement noise level and hyperparameters affect prediction accuracy and uncertainty is necessary. To make the results more convincing, we normalise the data from both cities for uncertainty quantification studies.

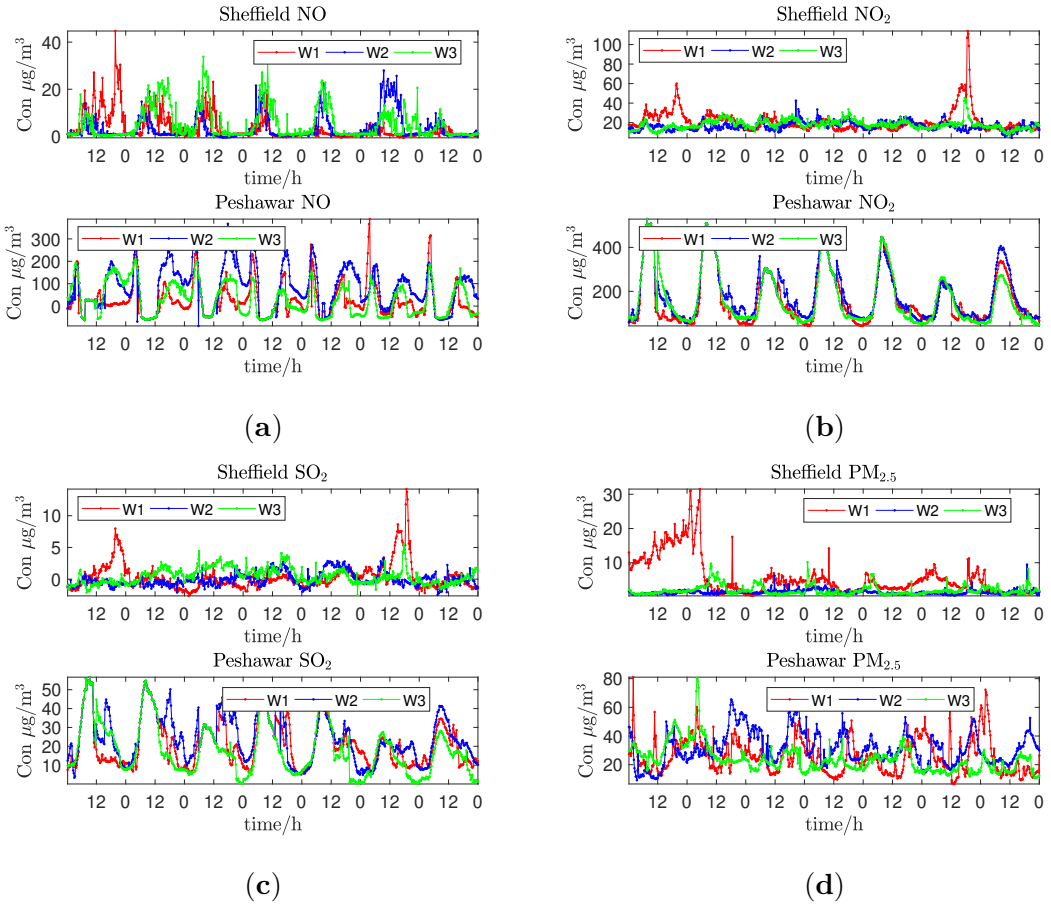

FIGURE 7.2: Concentration of pollutants recorded at the same time period in both Sheffield and Peshawar: (**a**) NO concentration in Sheffield and Peshawar in week W1, W2, and W3, (**b**) NO_2 concentration in Sheffield and Peshawar in week W1, W2, and W3, (**c**) SO_2 concentration in Sheffield and Peshawar in week W1, W2, and W3, (**d**) $PM_{2.5}$ concentration in Sheffield and Peshawar in week W1, W2, and W3.

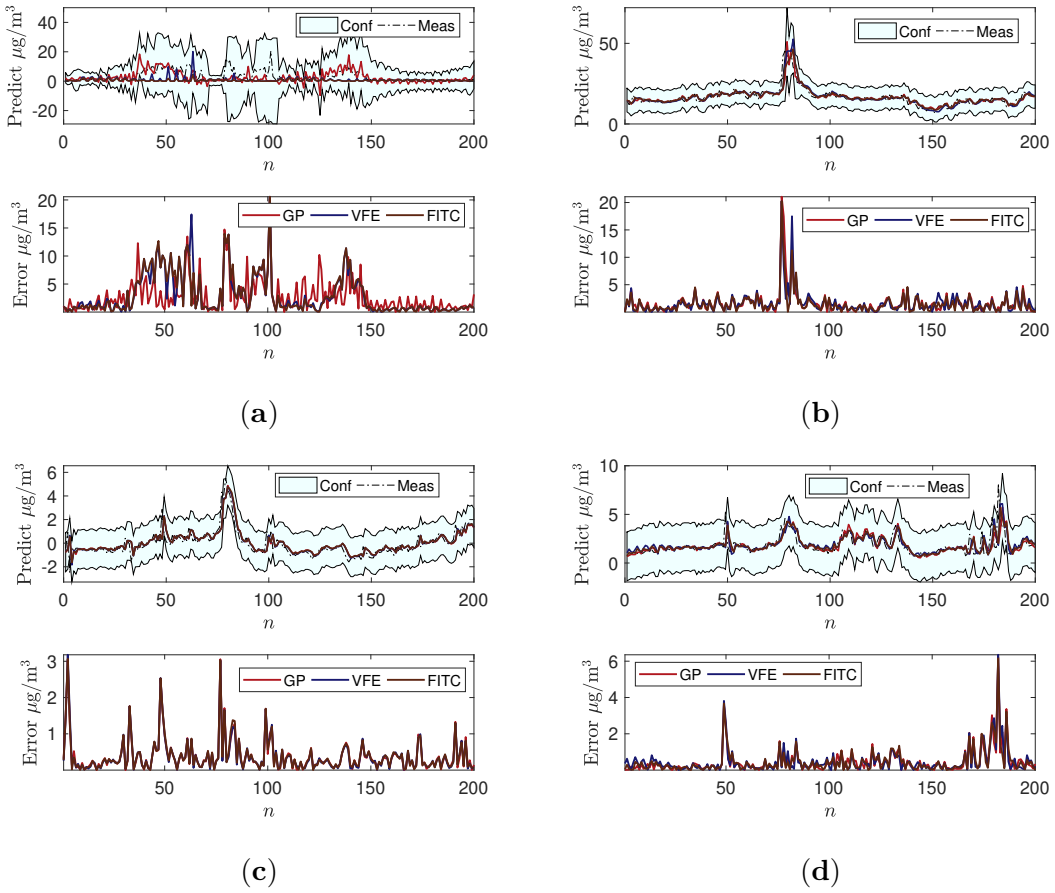

FIGURE 7.3: Prediction and absolute error of pollutants in Sheffield: (**a**) NO, (**b**) NO_2, (**c**) SO_2, (**d**) $PM_{2.5}$.

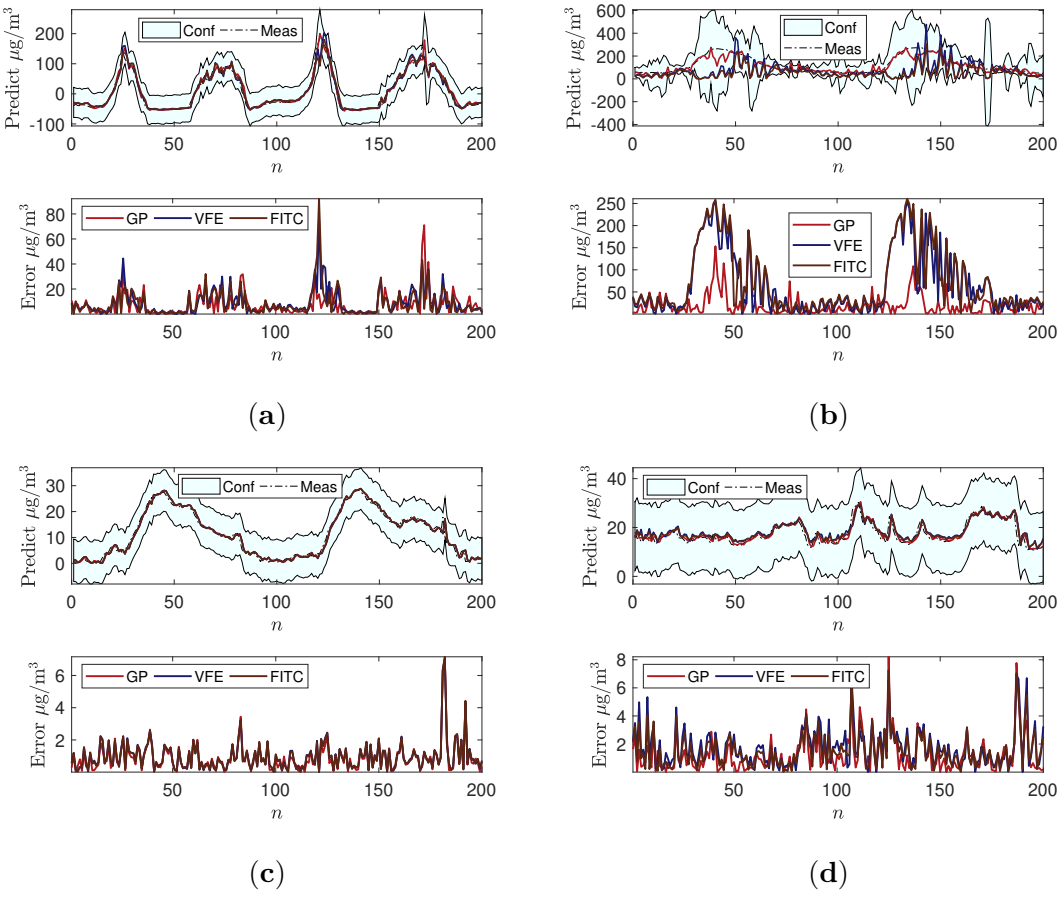

FIGURE 7.4: Prediction and absolute error of pollutants in Peshawar: (**a**) NO, (**b**) NO_2, (**c**) SO_2, (**d**) $PM_{2.5}$.

7.4.2 Impacts of Measurement Noise Level and Hyperparameters

To demonstrate how noise level σ_n^2 and hyperparameters affect prediction accuracy and uncertainty, three sets of experiments are conducted. This paper adopts the squared exponential (SE) kernel, with hyperparameters s_f and l. The analytical derivation can be found in Appendix C. The prediction accuracy is identified by the root mean square error (RMSE), as shown in Equation (8.37), while the uncertainty is identified by $\frac{1}{2}\sigma$ confidence bound. Configurations of the experiments are as follows.

Experiment 1: Impacts of σ_n^2 on prediction accuracy and uncertainty. Both s_f and l are fixed to be the optimised values. σ_n^2 varies from 0.1 through to 20.0. NO, NO_2, SO_2, and $PM_{2.5}$ data from both cities are processed. Six inducing points are applied to both FITC and VFE.

Experiment 2: Impacts of s_f on prediction accuracy and uncertainty. l is set to the optimised value. s_f varies from 0.1 through to 30.0. σ_n^2 is set to 0.5 and 1.5, respectively. NO data from both cities are processed. Six inducing points are applied to both FITC and VFE.

Experiment 3: Impacts of l on prediction accuracy and uncertainty. s_f is set to the optimised value. l varies from 0.1 through to 30.0. σ_n^2 is set to 0.5 and 1.5, respectively.

NO data from both cities are processed. Six inducing points are applied to both FITC and VFE.

$$\text{RMSE} = \sqrt{\frac{\sum_{\text{i}=1}^{\text{Num}}(\text{y}_\text{i} - \widehat{\text{y}}_\text{i})^2}{\text{Num}}}, \tag{7.34}$$

where y_i is the ground truth value and $\widehat{\text{y}}_\text{i}$ represents predicted meant. Num is the sample number in testing set.

Figures 7.5 and 7.6 show the results from **Experiment 1**. To make the results more distinguishable, the horizontal axes of the figures are set to $\log(\sigma_\text{n}^2)$. We can see from Figure 7.5 that when σ_n^2 is small, GPs perform the best in general, while the performance of FITC and VFE varies. We can also observe that as σ_n^2 keeps increasing, the RMSE becomes very significant for all methods/pollutants. Similar results can be observed from Figure 7.6 as well. Both comply with our theoretical conclusions, despite the fact that the Neumann series is used to approximate the matrix inverse. We also notice that σ_n^2 has a more significant impact on Sheffield data as RMSE increases ealier after $\log(\sigma_\text{n}^2)$ reaches zero. From Figure 7.6 (b) and (c), we also see that the uncertainty bounds of Sheffield data are greater after $\log(\sigma_\text{n}^2)$ reaches zero. We think the reason is that Sheffield data are generally less periodical than Pershawar data (see Figure 7.2), which influences the performance of the models.

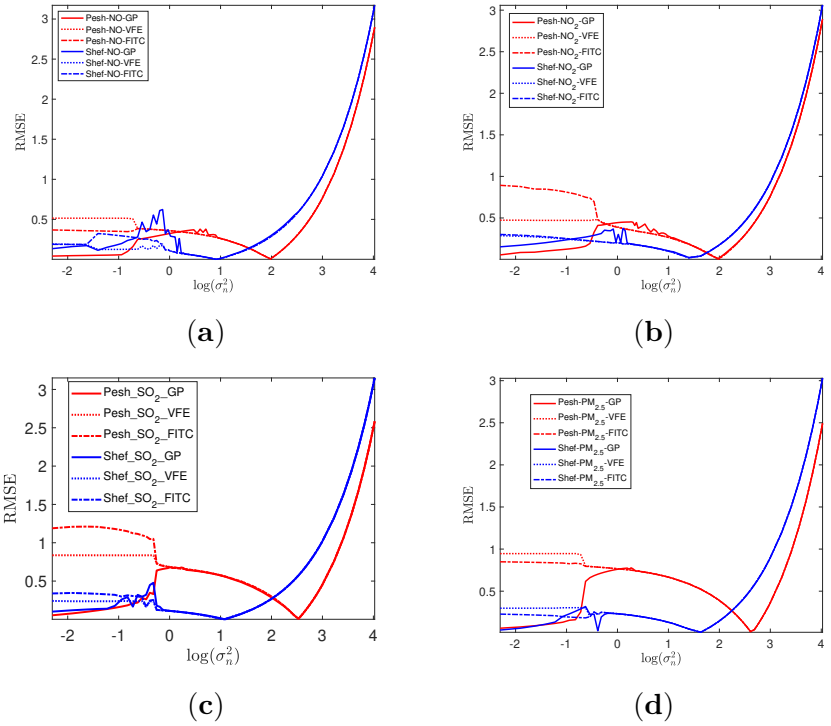

FIGURE 7.5: Relationship of σ_n^2 with four pollutants prediction RMSE: (**a**) NO, (**b**) NO_2, (**c**) SO_2, (**d**) $PM_{2.5}$.

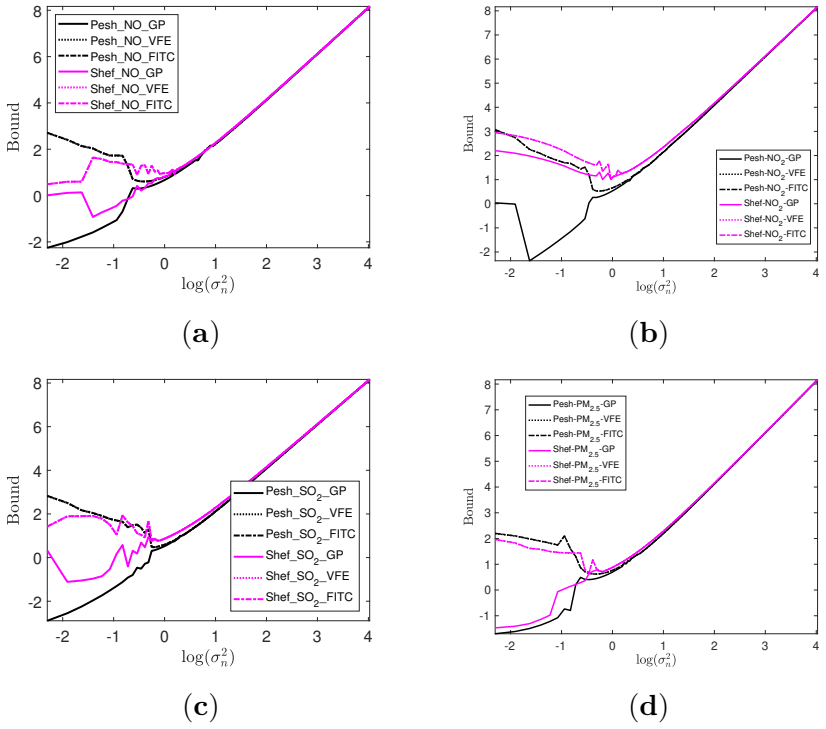

FIGURE 7.6: Relationship of σ_n^2 with pollutants prediction uncertainty bound: (**a**) NO, (**b**) NO_2, (**c**) SO_2, (**d**) $PM_{2.5}$.

7.4.3 Impacts of Noise Level on ELBO and UBML

Figure 7.7 shows the results from **Experiment 2**. According to our theoretical results, the impact of s_f on the uncertainty should become greater as s_f increases. This is verified by the results shown in Figure 7.7 (b) and (d). Our theoretical results also suggest that the variation of s_f would not affect the prediction accuracy. We can see from Figure 7.7 (a) and (c) that when s_f is smaller, it does affect the prediction accuracy, but when it exceeds a certain value, the impacts become negligible. Considering the Neumann series approximation, we would say that the experimental results comply with the theoretical conclusion.

The results of **Experiment 3** are shown in Figure 7.8. We can see that when l is smaller, both RMSE and the uncertainty bounds change rapidly. While after it exceeds certain values, both converge. This again complies with our theoretical conclusions and simulation results. We should also notice from Figures 7.7 and 7.8 that the increment of s_f tends to increase the uncertainty, whereas the increment of l tends to decrease the uncertainty. Taking both into consideration, an optimised uncertainty bound can be obtained.

We also conduct an experiment to demonstrate how the noise level σ_n^2 affects the ELBO and UBML. In our experiment, we set σ_n^2 to vary from 0.5 to 4.5. The results are shown in Figure 7.9. To make the results distinguishable, we set the vertical axes to log(–ELBO/UBML). To make the logrithm work, we reverse the signs of both ELBO and UBML. This is the reason why ELBO is 'greater' than UBML in Figure 7.9. The full GPs model is trained by setting σ_n^2 to $\{1, 7, 13, 19, 25, 31, 37, 43, 49\}$ to obtain 9 sets of hyperparameters. For each set of them, we then set σ_n^2 to vary from 0.5 to 4.5. The

darker the colour in Figure 7.9, the smaller σ_{n}^2 is for model training. We can see that generally, greater σ_{n}^2 can slow down the convergence speed of both ELBO and UBML, while training a model. When the model is trained, the increment of σ_{n}^2 can lower down UBML, which is the maximum that ELBO can reach. This implies that the increment of σ_{n}^2 can cause the failure of a sparse GPs model, as ELBO is deeply related to determine a sparse GPs model. Nevertheless, the experimental results again comply with our theoretical conclusions.

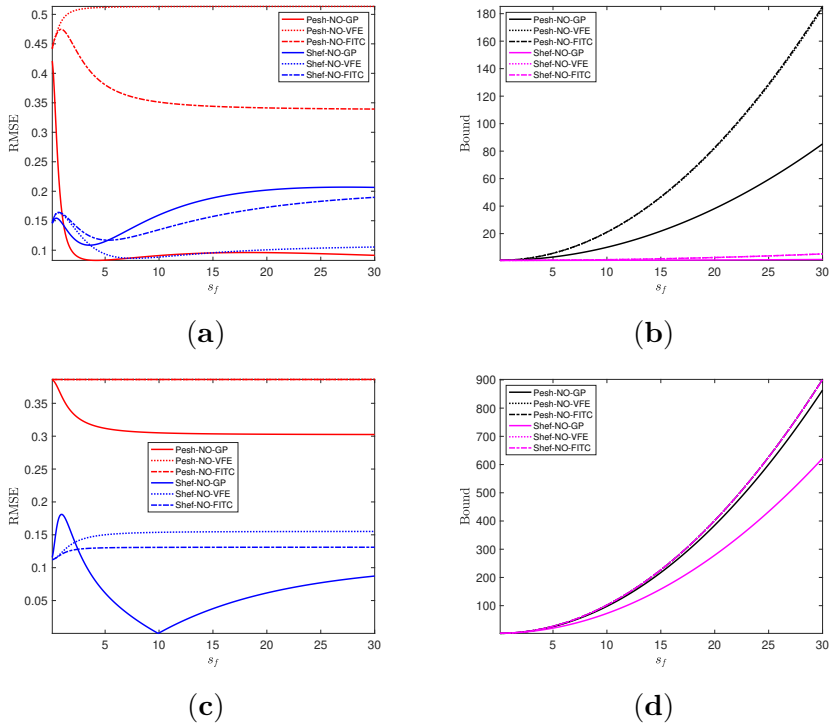

FIGURE 7.7: Relationship of $\mathrm{s_f}$ on NO prediction RMSE and uncertainty bound: (**a**) $\sigma_{\mathrm{n}}^2 = 0.5$, (**b**) $\sigma_{\mathrm{n}}^2 = 0.5$, (**c**) $\sigma_{\mathrm{n}}^2 = 1.5$, (**d**) $\sigma_{\mathrm{n}}^2 = 1.5$.

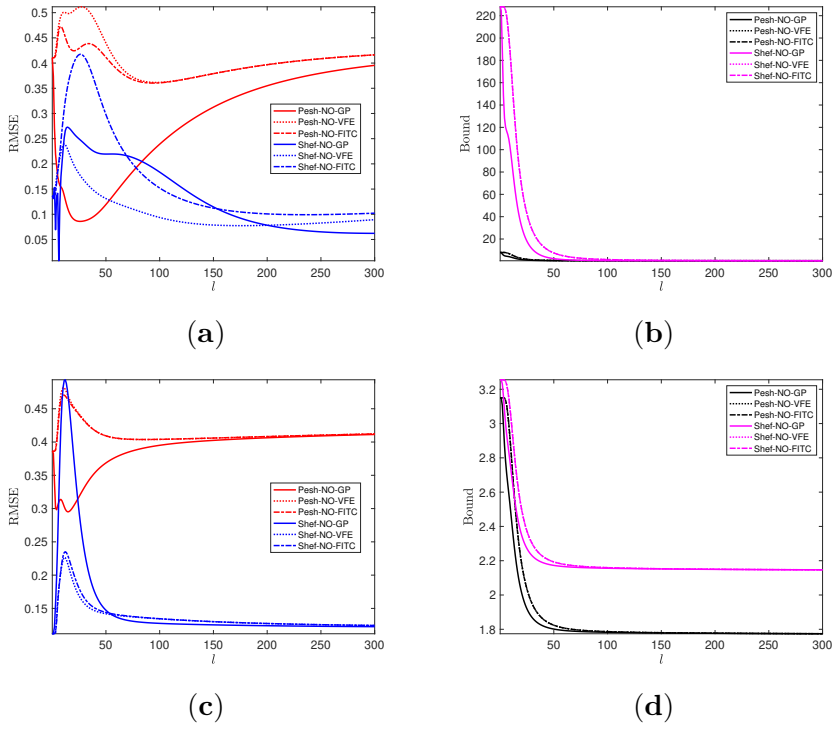

FIGURE 7.8: Relationship of l on NO prediction RMSE and uncertainty bound: (**a**) $\sigma_{\mathrm{n}}^2 = 0.5$, (**b**) $\sigma_{\mathrm{n}}^2 = 0.5$, (**c**) $\sigma_{\mathrm{n}}^2 = 1.5$, (**d**) $\sigma_{\mathrm{n}}^2 = 1.5$.

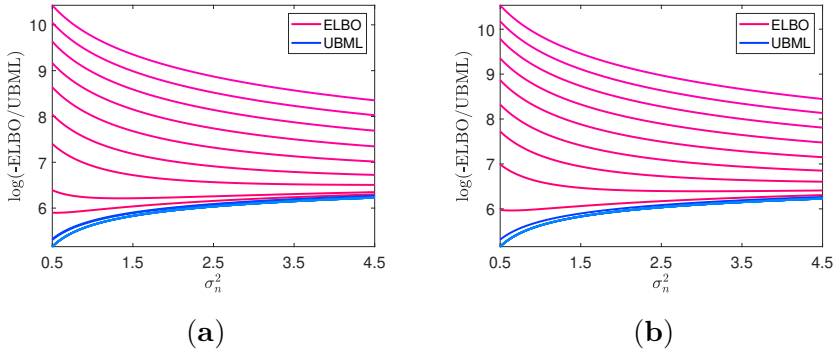

FIGURE 7.9: Effects of σ_{n}^2 on ELBO and UBML: (**a**) NO in Sheffield, (**b**) NO in Peshawar.

7.5 Conclusions

This paper proposes a general method to investigate how the performance variation of a Gaussian process model can be attributed to hyperparameters and measurement noises, etc. The method is demonstrated by applying it to process particulate matter (e.g., $PM_{2.5}$) and gaseous pollutants (e.g., NO, NO_2, and SO_2) from both Sheffield, UK, and Peshawar, Pakistan. Experimental results show that the proposed method provides insights on how measurement noises and hyperparameters, etc. affect the prediction performance of a Gaussian process. The results align with the analytical derivations, which is enabled by adopting Neuman series to approximate matrix inversions in Gaussian process models. The theoretical findings and experimental results combined demonstrate that the proposed

method can generate air quality forecasting results. In the meantime, it provides a way to link uncertainties in measurements and hyperparameters, etc. with the forecasting results. This will help with forecasting performance analysis when measurement noise level or model hyperparameters vary, making the method more general.

7.6 Contribution

R.C. (Rohit Chakraborty):

- **Conceptualization:** I actively participated in the conceptualization of the study, collaborating closely with P.W., L.M., M.M., S.M., K.A., and M.F.K. to define the research's direction and objectives.
- **Sensor Deployment and Calibration:** I played an instrumental role in deploying the sensors used in the study. This involved not only ensuring optimal positioning for accurate data capture but also calibrating the sensors for maximum reliability and precision.
- **Software and Python Programming:** I contributed to the software components of the study, particularly by using Python programming to develop tools and scripts that aided in data processing, analysis, and visualization.
- **Data Curation:** I played a crucial role in curating the data for the study, ensuring its accuracy, relevance, and readiness for analysis. This involved collaborating with S.M., K.A., and M.F.K. to gather, clean, and organize the data sets effectively.
- **Writing – Original Draft Preparation:** I contributed significantly to the preparation of the original manuscript. Collaborating with P.W., L.M., S.M., K.A., and M.F.K., I ensured that the research findings were clearly and effectively communicated.
- **Visualization:** I partnered with P.W. to spearhead the data visualization efforts. My contribution involved translating complex data sets into comprehensible and insightful graphical representations, emphasizing key findings and patterns.
- **Review and Editing:** While my main contributions were in drafting the original manuscript, I actively participated in discussions and provided feedback during the review and editing processes, ensuring the paper's clarity and coherence.
- **Collaboration and Coordination:** Throughout the research process, I collaborated closely with various team members, ensuring that all contributions were harmoniously integrated into the final manuscript.

In addition to the above, I actively engaged in all stages of the research process, from initial discussions to manuscript finalization. My commitment and expertise significantly influenced the paper's direction and quality, ensuring that the research objectives were met effectively.

Chapter 8

A Computationally Efficient Symmetric Diagonally Dominant Matrix Projection-based Gaussian Process Approach

abstract

Although kernel approximation methods have been widely applied to mitigate the $\mathcal{O}(n^3)$ cost of the $n \times n$ kernel matrix inverse in Gaussian process methods, they still face computational challenges. The 'residual' matrix between the covariance and the approximating component is often discarded as it prevents the computational cost reduction. In this paper, we propose a computationally efficient Gaussian process approach that achieves better computational efficiency, $\mathcal{O}(mn^2)$, compared with standard Gaussian process methods, when using $m \ll n$ data. The proposed approach incorporates the 'residual' matrix in its symmetric diagonally dominant form which can be further approximated by the Neumann series. We have validated and compared the approach with full Gaussian process approaches and kernel approximation based Gaussian process variants, both on synthetic and real air quality data.

8.1 Introduction

Gaussian process (GP) methods are renowned for providing Bayesian non-linear and non-parametric solutions to regression and classification tasks [227, 228]. However, they have cubic computational complexity $\mathcal{O}(n^3)$ for the inversion of the kernel matrix of size $n \times n$ and its determinant [221]. This cubic computational cost has effectively limited applications of GPs to data with thousands of samples [229, 230]. This led to intensive studies of the scalability of GPs during the last decades [221], with particular interests in adapting

GPs for various data processing and maintaining their capacity, ideally at the same level of full GPs.

The extensive review of Liu et al. [221] on GPs classifies scalable GPs into local approximations and global approximations. Local approximations follow the *divide-and-conquer* idea to first divide the whole dataset into sub-datasets, each with m samples. A 'local' GP model is next trained on each sub-dataset. These 'local' GP models are aggregated with each GP model responds to inputs that come from a certain 'local' area at the prediction stage. The computational cost is in the order of $\mathcal{O}(\mathrm{m}^2\mathrm{n})$ [221]. In the global GP algorithms, all data is available but sparsity is usually introduced by appropriately selected inducing points or by sub-sampling of the data. Thus for efficiency improvement, a lot of global approximation-based works [222, 229, 231] are dedicated to approximating the kernel matrix $\mathbf{K}_{\mathrm{nn}}$ and can be further categorised into 1) the Subset of Data (SoD) method uses m out of n training samples, resulting in a smaller kernel matrix $\mathbf{K}_{\mathrm{mm}}$; 2) the sparse kernel method sets to zero all entries smaller than a criterion value and hence leads to a sparse kernel matrix $\widetilde{\mathbf{K}}_{\mathrm{nn}}$ [221]; 3) the low-rank method, also known as sparse approximation method, approximates $\mathbf{K}_{\mathrm{nn}}$ with the eigendecompostion or the Nyström method [232] by a low-rank matrix $\mathbf{L}_{\mathrm{nn}}$. We also notice that Zhu et al. [233] apply the nonnegative matrix factorisation in the kernel matrix approximation, which obtains online performance with application in image processing. The SoD and low-rank approximations reduce the computational complexity to $\mathcal{O}(\mathrm{m}^2\mathrm{n})$ if we do not count the computation caused by eigendecomposition. The sparse kernel method reduces the cost to $\mathcal{O}(\alpha\mathrm{n}^3)$, with α being a coefficient in the range $0 < \alpha < 1$.

The third solution is the most popular among all these three global approximations. Especially, the Nyström method [232] has achieved a balance between accuracy and efficiency and several variants have been proposed [227, 229]. We notice that these methods replace the kernel matrix $\mathbf{K}_{\mathrm{nn}}$ with a low rank matrix $\mathbf{L}_{\mathrm{nn}}$, which can be further factorised as $\mathbf{L}_{\mathrm{nn}} = \mathbf{B}_{\mathrm{nm}}\mathbf{B}_{\mathrm{nm}}^{\mathrm{T}}$ [234]. The 'residual' matrix $\widetilde{\mathbf{A}} = \mathbf{K}_{\mathrm{nn}} - \mathbf{L}_{\mathrm{nn}}$ is usually discarded. This approach aligns with the intuition provided by the Sherman-Morrison-Woodbury formula, as detailed in equation (2.7.12) of Chapter 2 [235].

$$\mathbf{K}_{\mathrm{nn}}^{-1} = \widetilde{\mathbf{A}}^{-1} - \widetilde{\mathbf{A}}^{-1}\mathbf{B}_{\mathrm{nm}}(\mathbf{I}_{\mathrm{m}} + \mathbf{B}_{\mathrm{nm}}^{\mathrm{T}}\widetilde{\mathbf{A}}^{-1}\mathbf{B}_{\mathrm{nm}})^{-1}\mathbf{B}_{\mathrm{nm}}^{\mathrm{T}}\widetilde{\mathbf{A}}^{-1}. \tag{8.1}$$

We can see that the computational cost of $\mathbf{K}_{\mathrm{nn}}^{-1}$ remains at $\mathcal{O}(\mathrm{n}^3)$ despite $(\mathbf{I}_{\mathrm{m}}+\mathbf{B}_{\mathrm{nm}}^{\mathrm{T}}\widetilde{\mathbf{A}}^{-1}\mathbf{B}_{\mathrm{nm}})^{-1}$ holds the promise of reducing the overall computational cost of (8.1) such as when $\widetilde{\mathbf{A}}$ is diagonal. The consequence is that two questions remain unanswered: 1) Can we take the 'residual' matrix $\widetilde{\mathbf{A}}$ into consideration? 2) If we consider the 'residual' matrix, can we achieve comparable results with full GP models with a lower computational cost?

This paper aims to provide answers to these two questions. We show that by projecting $\widetilde{\mathbf{A}}$ to be a Symmetric Diagonally Dominant (SDD) matrix $\mathbf{A}$, we obtain an approximation of the kernel matrix $\mathbf{K}_{\mathrm{nn}} \approx \mathbf{L}_{\mathrm{nn}} + \mathbf{A}$ accurately and efficiently. The SDD matrix $\mathbf{A}$ shows appealing characteristics such as symmetry and diagonally dominant, but the challenge in (8.1) remains. However, the SDD matrix characteristics perfectly match the conditions of approximating its inverse matrix with Neumann series, hence avoiding calculating $\widetilde{\mathbf{A}}^{-1}$ directly. We therefore approximate $\widetilde{\mathbf{A}}^{-1}$ with Neumann series and cut the computational cost from $\mathcal{O}(\mathrm{n}^3)$ down to $\mathcal{O}(\mathrm{n}^2)$ [223, 225]. By doing so, we provide a way of computing $\mathbf{K}_{\mathrm{nn}}^{-1}$ and derive a new efficient GP implementation. To summarise, the main contributions of this paper are threefold:
1) The 'residual' matrix between the original kernel matrix and its approximation matrix

is taken into account to approach full GPs performance;
2) The SDD projection and Neumann series are applied to reduce covariance matrix inversion computational complexity;
3) Comparisons of the proposed approach with various GP variants with different kernel settings on both synthetic data and air quality data are given, providing a reference for its potential applications in various fields.

The remaining part of this paper is organised as follows. Section 8.2 reviews some of the related works. Section 8.3 introduces the GP method and how traditional kernel approximation methods work. Section 8.4 details the proposed approach. Performance validation results and analysis are given in Section 8.5, and the paper is concluded in Section 8.6, with a brief discussion of future work.

8.2 Related Work

In literature, there are mainly three categories of low-rank approximations, i.e. the prior approximation, the posterior approximation, and the structured sparse approximation [221, 232, 236]. We are particularly interested in the prior approximation in this paper.

There are two main ways to approximate the prior kernel matrix. The first one is as we mentioned earlier, by applying an eigendecomposition or the Nyström method to reconstruct the kernel matrix with a low rank [237–239]. The second way is by applying variational inference to optimise the Kullback-Leibler divergence between the exact prior and a cluster of distributions that are easy to implement, such as Gaussian distributions [229, 240]. While the Nyström method can reduce the computational complexity, it faces the problem of how to determine the low-rank space such that the reconstructed kernel matrix would provide accurate results. This has stimulated research in two aspects: 1) low-rank approximation error analysis or finding the error bounds [220, 237, 238]; 2) methods that can further improve the approximation accuracy such as greedy approaches and randomised algorithms [241, 242]. Particularly, Stein [239] reports that when neighboring observations are strongly correlated, the performance of the low-rank approximation becomes poor even if the sum of the m largest eigenvalues is much greater than the sum of the remaining eigenvalues. Ding et al. [243] find that bad performance would happen when the length scale of the kernel is small if we only focus on the high eigenvalue part of the spectrum of the kernel matrix. A multi-resolution kernel approximation approach is thus proposed which represents the entire kernel matrix, not just its eigenvectors with the greatest eigenvalues. This approach is capable of calculating the inverse matrix directly and has improved performance compared with other GP kernel approximations considered in [243]. They claim their method is considerably more flexible than existing hierarchical matrix decomposition or approximation [244] methods. Yao et al. propose the kernel-band-projection algorithm for anomaly detection in hyperspectral imagery. They take bands as mapping subjects, and by mapping bands into the kernel space, they construct a projection matrix. When the Gaussian kernel function is used, their method avoids the inversion calculation of the projection matrix, making the method efficient [245]. Burt et al. [220] adopt the Kullback-Leibler divergence to investigate how the number of inducing points m that could change along with the change of the dataset size n, to ensure a certain approximation accuracy. However, this work falls into the posterior approximation category [226].

While the approximation methods and approximation accuracy analysis have been extensively researched, there is little work on how to retain the 'residual' matrix $\widetilde{\mathbf{A}}$ in kernel methods. Particularly, methods that take the 'residual' matrix into account and achieve a balance between efficiency and accuracy, ideally at the same level of full GPs or even better, would make a good complementary to the GP community. Fig. 8.1 demonstrates how the covariance matrix is approximated.

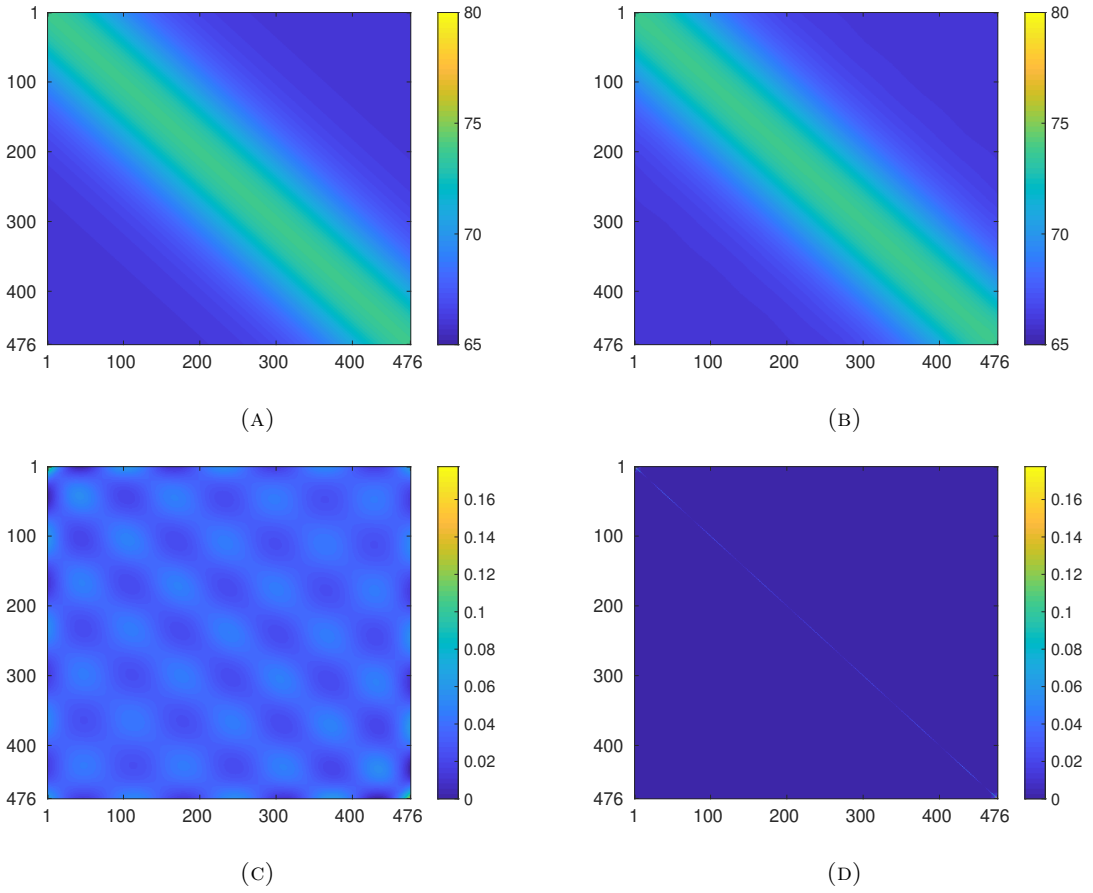

FIGURE 8.1: Matrices involved in the covariance matrix approximation: (a) $\mathbf{K}_{\mathrm{nn}}$, (b) $\mathbf{L}_{\mathrm{nn}}$, (c) the 'residual' matrix $\tilde{\mathbf{A}}$, (d) $\mathbf{A}$. The $\mathbf{L}_{\mathrm{nn}}$ is usually used for approximating $\mathbf{K}_{\mathrm{nn}}$, with $\tilde{\mathbf{A}} = \mathbf{K}_{\mathrm{nn}} - \mathbf{L}_{\mathrm{nn}}$ discarded. The $\mathbf{A}$ is the SDD projection matrix of $\tilde{\mathbf{A}}$, and we use $\mathbf{L}_{\mathrm{nn}} + \mathbf{A}$ to approximate $\mathbf{K}_{\mathrm{nn}}$. The figures are generated from Synthetic dataset 2 with $\mathrm{n} = 476$ for demonstration.

8.3 The Gaussian Process Method and Kernel Approximations

8.3.1 Background Knowledge

Given a set of *training data* $\mathcal{D} = \{(\mathbf{x}_{\mathrm{i}}, \mathrm{y}_{\mathrm{i}}), \mathrm{i} = 1, \cdots, \mathrm{n}\}$ where $\mathbf{x}_{\mathrm{i}} \in \mathcal{X}$ is the input and $\mathrm{y}_{\mathrm{i}} \in \mathbb{R}$ is the observation, we can determine a GP model $\mathrm{f}(\cdot)$ to predict y_* for a new input

$\mathbf{x}_*$. For instance, when the output is one dimensional, the GP model is formulated as

$$\mathrm{f} \sim \mathcal{GP}(\bar{\mathrm{f}}(\mathbf{x}), \mathrm{k}(\mathbf{x}, \mathbf{x}')), \quad \mathrm{y} = \mathrm{f}(\mathbf{x}) + \varepsilon, \quad \varepsilon \sim \mathcal{N}(0, \sigma^2), \tag{8.2}$$

where $\bar{\mathrm{f}} : \mathcal{X} \to \mathbb{R}$ is the *mean function* defined as

$$\bar{\mathrm{f}}(\mathbf{x}) = \mathbb{E}[\mathrm{f}(\mathbf{x})], \tag{8.3}$$

and $\mathrm{k} : \mathcal{X} \times \mathcal{X} \to \mathbb{R}$ is the *kernel function* [220] defined as

$$\mathrm{k}(\mathbf{x}, \mathbf{x}') = \mathbb{E}[(\mathrm{f}(\mathbf{x}) - \bar{\mathrm{f}}(\mathbf{x}))(\mathrm{f}(\mathbf{x}') - \bar{\mathrm{f}}(\mathbf{x}'))], \tag{8.4}$$

where ε is the additive independent identically distributed Gaussian measurement noise with variance $\sigma^2 \neq 0$, and $\mathbb{E}[\cdot]$ denotes the expectation of a random variable.

Given $\mathbf{x}_\mathrm{i}$ a $\mathrm{D} \times 1$ vector, the n inputs can be aggregated into a matrix $\mathbf{X}_{\mathrm{D}\times\mathrm{n}}$, or briefly $\mathbf{X}$ with the corresponding output vector $\mathbf{y}_{\mathrm{n}\times 1}$, or $\mathbf{y}$. Similarly, the function values at the test inputs $\mathbf{X}_*$ with dimensions of $\mathrm{D} \times \mathrm{N}$ can be denoted as $\mathbf{f}_*$, and we next write the joint distribution of $\mathbf{y}$ and $\mathbf{f}_*$ as

$$\begin{bmatrix} \mathbf{y} \\ \mathbf{f}_* \end{bmatrix} \sim \mathcal{N}\left(\mathbf{0}, \begin{bmatrix} \mathbf{K}_{\mathrm{nn}} + \sigma^2\mathbf{I} & \mathbf{K}_{\mathrm{nN}} \\ \mathbf{K}_{\mathrm{Nn}} & \mathbf{K}_{\mathrm{NN}} \end{bmatrix}\right), \tag{8.5}$$

where $\mathbf{I}$ represents the identity matrix. $\mathbf{K}_{\mathrm{nn}} + \sigma^2\mathbf{I}$ is the $\mathrm{n} \times \mathrm{n}$ prior covariance matrix of $\mathbf{y}$ with entry $\mathbf{K}_{\mathrm{ij}} = \mathrm{k}(\mathbf{x}_\mathrm{i}, \mathbf{x}_\mathrm{j}) + \sigma^2\delta_{\mathrm{ij}}$, where δ_{ij} is one iff $\mathrm{i} = \mathrm{j}$ and zero otherwise, and $\mathbf{x}_\mathrm{i}$ and $\mathbf{x}_\mathrm{j}$ are column vectors from $\mathbf{X}$. The matrix $\mathbf{K}_{\mathrm{NN}}$ denotes the $\mathrm{N} \times \mathrm{N}$ prior covariance matrix of $\mathbf{f}_*$ with entry $\mathbf{K}_{\mathrm{ij}} = \mathrm{k}(\mathbf{x}_\mathrm{i}, \mathbf{x}_\mathrm{j})$, where $\mathbf{x}_\mathrm{i}$ and $\mathbf{x}_\mathrm{j}$ are column vectors from $\mathbf{X}_*$. The matrices $\mathbf{K}_{\mathrm{Nn}}$ and $\mathbf{K}_{\mathrm{nN}}$ satisfy $\mathbf{K}_{\mathrm{Nn}} = \mathbf{K}_{\mathrm{nN}}^{\mathrm{T}}$, and the entry of the $\mathrm{N} \times \mathrm{n}$ prior covariance matrix of $\mathbf{f}_*$ and $\mathbf{y}$ is $\mathbf{K}_{\mathrm{ij}} = \mathrm{k}(\mathbf{x}_\mathrm{i}, \mathbf{x}_\mathrm{j})$, where $\mathbf{x}_\mathrm{i}$ is a column vector from $\mathbf{X}_*$ and $\mathbf{x}_\mathrm{j}$ is a column vector from $\mathbf{X}$.

By deriving the conditional distribution of $\mathbf{f}_*$ from (8.5), where the prior mean is set to be zero for simplicity [222], we have the predictive posterior (also given in equation (2.22), Chapter 2 of [222]) at new inputs $\mathbf{X}_*$ as

$$\mathbf{f}_* | \mathbf{X}, \mathbf{y}, \mathbf{X}_* \sim \mathcal{N}(\bar{\mathbf{f}}_*, \mathrm{cov}(\mathbf{f}_*)), \tag{8.6}$$

where

$$\bar{\mathbf{f}}_* \triangleq \mathbb{E}[\mathbf{f}_* | \mathbf{X}, \mathbf{y}, \mathbf{X}_*] = \mathbf{K}_{\mathrm{Nn}}[\mathbf{K}_{\mathrm{nn}} + \sigma^2\mathbf{I}]^{-1}\mathbf{y}, \tag{8.7}$$

is the prediction at $\mathbf{X}_*$, and

$$\mathrm{cov}(\mathbf{f}_*) = \mathbf{K}_{\mathrm{NN}} - \mathbf{K}_{\mathrm{Nn}}[\mathbf{K}_{\mathrm{nn}} + \sigma^2\mathbf{I}]^{-1}\mathbf{K}_{\mathrm{Nn}}^{\mathrm{T}}, \tag{8.8}$$

denotes the covariance of $\mathbf{f}_*$.

The hyperparameter θ incorporated in the mean and covariance functions underpin the predictive performance of GP models, and they are usually estimated by maximising the

logarithm of the marginal likelihood

$$\log \mathrm{p}(\mathbf{y}|\mathbf{X}) = -\frac{1}{2}\mathbf{y}^{\mathrm{T}}(\mathbf{K}_{\mathrm{nn}} + \sigma^2\mathbf{I})^{-1}\mathbf{y} - \frac{1}{2}\log|\mathbf{K}_{\mathrm{nn}} + \sigma^2\mathbf{I}| - \frac{\mathrm{n}}{2}\log 2\pi. \tag{8.9}$$

8.3.2 Kernel Approximations

Scalable GPs have been extensively studied recently, which aims at alleviating the computational complexity while retaining the favourable prediction quality of GPs [221]. One of the most popular methods for kernel matrix approximation utilises a low-rank matrix to approximate $\mathbf{K}_{\mathrm{nn}}$, hence decreasing the computational complexity from $\mathcal{O}(\mathrm{n}^3)$ to $\mathcal{O}(\mathrm{m}^2\mathrm{n})$ with $\mathrm{m} \ll \mathrm{n}$, as introduced in [232]. For instance, in the eigendecomposition paradigm, the $\mathbf{K}_{\mathrm{nn}}$ is presented as

$$\mathbf{K}_{\mathrm{nn}} = \mathbf{U}_{\mathrm{nn}}\mathbf{\Lambda}_{\mathrm{nn}}\mathbf{U}_{\mathrm{nn}}^{\mathrm{T}}, \tag{8.10}$$

where $\mathbf{U}_{\mathrm{nn}}$ comprises all the eigenvectors and is orthonormal, and $\mathbf{\Lambda}_{\mathrm{nn}} = \mathrm{diag}(\lambda_{\mathrm{i}})$, $\lambda_1 \geqslant \lambda_2 \geqslant \cdots \geqslant 0$ is a diagonal matrix with eigenvalues being the diagonal entries. If we choose eigenvectors corresponding to the $\mathrm{m} < \mathrm{n}$ largest eigenvalues and build $\mathbf{U}_{\mathrm{nm}} \in \mathbb{R}^{\mathrm{n}\times\mathrm{m}}$ and let $\mathbf{\Lambda}_{\mathrm{mm}} = \mathrm{diag}(\lambda_1, \cdots, \lambda_{\mathrm{m}})$, we then have the approximation

$$\begin{aligned}(\mathbf{K}_{\mathrm{nn}} + \sigma^2\mathbf{I})^{-1} &\approx (\mathbf{U}_{\mathrm{nm}}\mathbf{\Lambda}_{\mathrm{mm}}\mathbf{U}_{\mathrm{nm}}^{\mathrm{T}} + \sigma^2\mathbf{I})^{-1} \\ &= \sigma^{-2}\mathbf{I}_{\mathrm{n}} - \sigma^{-2}\mathbf{U}_{\mathrm{nm}}(\sigma^2\mathbf{\Lambda}_{\mathrm{mm}}^{-1} + \mathbf{U}_{\mathrm{nm}}^{\mathrm{T}}\mathbf{U}_{\mathrm{nm}})^{-1}\mathbf{U}_{\mathrm{nm}}^{\mathrm{T}}\end{aligned} \tag{8.11}$$

following the Sherman-Morrison-Woodbury formula. Clearly, with the existence of eigendecomposition, this approximation significantly reduces the computational complexity. However, the computational cost of the eigendecomposition is $\mathcal{O}(\mathrm{n}^3)$, which makes the method less favourable.

The Nyström method [232] was then proposed to replace the eigendecomposition to approximate the covariance matrix

$$\mathbf{K}_{\mathrm{nn}} \approx \mathbf{K}_{\mathrm{nm}}\mathbf{K}_{\mathrm{mm}}^{-1}\mathbf{K}_{\mathrm{nm}}^{\mathrm{T}}, \tag{8.12}$$

where $\mathbf{K}_{\mathrm{nm}}$ is obtained by randomly choosing m rows or columns of $\mathbf{K}_{\mathrm{nn}}$ without replacement. Williams et al. [232] observe that even when $\mathrm{m} \ll \mathrm{n}$, there is no significant accuracy reduction when using (8.12) in the GP approach. With the Nyström method and the Sherman-Morrison-Woodbury formula, one can see from

$$(\mathbf{K}_{\mathrm{nm}}\mathbf{K}_{\mathrm{mm}}^{-1}\mathbf{K}_{\mathrm{nm}}^{\mathrm{T}} + \sigma^2\mathbf{I}_{\mathrm{n}})^{-1} = \sigma^{-2}\mathbf{I}_{\mathrm{n}} - \sigma^{-2}\mathbf{K}_{\mathrm{nm}}(\sigma^2\mathbf{K}_{\mathrm{mm}} + \mathbf{K}_{\mathrm{nm}}^{\mathrm{T}}\mathbf{K}_{\mathrm{nm}})^{-1}\mathbf{K}_{\mathrm{nm}}^{\mathrm{T}} \tag{8.13}$$

that the computational complexity is reduced from $\mathcal{O}(\mathrm{n}^3)$ to $\mathcal{O}(\mathrm{mn}^2)$.

8.4 Symmetric Diagonally Dominant Projection-based Gaussian Process

8.4.1 Symmetric Diagonally Dominant Projection

As discussed in Section 8.2 and shown in Fig. 8.1, most kernel approximation methods can be formulated as

$$\mathbf{K}_{\mathrm{nn}} \approx \mathbf{L}_{\mathrm{nn}}, \quad \text{with} \quad \mathbf{K}_{\mathrm{nn}} = \mathbf{L}_{\mathrm{nn}} + \tilde{\mathbf{A}}, \tag{8.14}$$

where $\mathrm{rank}(\mathbf{L}_{\mathrm{nn}}) = \mathrm{K} \ll \mathrm{n}$, and $\tilde{\mathbf{A}}$ is the 'residual' matrix. The $\mathbf{L}_{\mathrm{nn}}$ matrix is calculated by different methods [222], but the $\tilde{\mathbf{A}}$ matrix is typically discarded. Intuitively, full GPs should perform better than the kernel-based approximations in spite of the heavy computational loads. However, in some classification tasks, the latter seems to outperform the full GPs [232]. This is believed to be caused by the high correlations of observations of the latent variables. Therefore, how the number of latent variables is determined would influence the performance of GPs variants, and leads to the phenomenon that full GPs sometimes perform poorer than kernel approximations. In this paper, we show that taking the 'residual' matrix $\tilde{\mathbf{A}}$ into consideration can mitigate the full GP challenges, which is performed by introducing the SDD projection into (8.14).

The SDD projection problem aims at finding an approximation of $\mathbf{K}_{\mathrm{nn}}$ in the form

$$\mathbf{K}_{\mathrm{nn}} \approx \mathbf{L}_{\mathrm{nn}} + \mathbf{A}, \tag{8.15}$$

where $\mathbf{L}_{\mathrm{nn}} = \sum_{\mathrm{k}=1}^{\mathrm{K}} \lambda_{\mathrm{k}} \xi_{\mathrm{k}} \xi_{\mathrm{k}}^{\mathrm{T}}$ with $\mathrm{K} = \mathrm{rank}(\mathbf{L}_{\mathrm{nn}}) \ll \mathrm{n}$, and $\mathbf{A}$ is a symmetric c-diagonally dominant matrix defined as

$$\begin{aligned} &\mathcal{SDD}_{\mathrm{c}}^{+} \\ &= \Big\{ \mathbf{A} = (\mathrm{a_{ij}})_{\mathrm{n}\times\mathrm{n}} : \mathbf{A} = \mathbf{A}^{\mathrm{T}}, \mathrm{a_{jj}} \geqslant \mathrm{c} \textstyle\sum_{\mathrm{i:i}\neq\mathrm{j}} |\mathrm{a_{ji}}| \quad \text{for all} \quad 1 \leqslant \mathrm{j} \leqslant \mathrm{n} \Big\}, \end{aligned} \tag{8.16}$$

with $\mathrm{c} \in \mathbb{R}^{+}$ [246], when $\mathrm{c} = 1$, we omit the subscript and denote (8.16) as $\mathcal{SDD}^{+}$. Ke et al. [246] also describe the problem of finding $\mathbf{A}$ as

$$\min_{(\mathbf{L}_{\mathrm{nn}}, \mathbf{A})} \|\mathbf{K}_{\mathrm{nn}} - \mathbf{L}_{\mathrm{nn}} - \mathbf{A}\|_{\mathrm{F}}, \tag{8.17}$$

where $\|\cdot\|_{\mathrm{F}}$ is the matrix Frobenius norm. They also provide a nonconvex solution to (8.17), which can be achieved at the cost of $\mathcal{O}(\mathrm{n}^2 \max\{\log(\mathrm{n}), \mathrm{K}\})$.

In this paper, algorithm 1 is used to find $\mathbf{A} \in \mathcal{SDD}_{\mathrm{c}}^{+}$, i.e. satisfying (8.16), which is next added to the low rank matrix $\mathbf{L}_{\mathrm{nn}}$ to approximate $\mathbf{K}_{\mathrm{nn}}$, as shown in (8.15). Please note that $\mathcal{P}_{\mathcal{DD}_{\mathrm{c}}^{+}}(\cdot)$ in Algorithm 1 denotes the projection of an arbitrary matrix to a c-diagonally dominant cone indicated by $\mathcal{DD}_{\mathrm{c}}^{+}$. When $\mathrm{c} = 1$, we denote it as $\mathcal{DD}^{+}$ for brevity. Here we provide a three-dimensional example to help understanding Step 6, which is also known as Mendoza-Raydan-Tarazaga projection [247].

Algorithm 1: The Iterative SDD Projection

Input: The covariance matrix $\mathbf{K}_{\mathrm{nn}}$ and a tolerance criterion (TOL) and TOL decreasing step η.

Output: $\mathbf{A} \in \mathcal{SDD}_{\mathrm{c}}^{+}$.

Let $\mathbf{A}^{(0)} = \mathbf{K}_{\mathrm{nn}} - \mathbf{L}_{\mathrm{nn}}$, where $\mathbf{L}_{\mathrm{nn}} = \mathbf{U}_{\mathrm{nm}}\Lambda_{\mathrm{mm}}\mathbf{U}_{\mathrm{nm}}^{\mathrm{T}}$, with $\mathrm{m} \leqslant \mathrm{n}$ and $\Lambda_{\mathrm{mm}} = \mathrm{diag}\{\lambda_1, \cdots, \lambda_{\mathrm{m}}\}$, $\hat{\mathbf{A}}^{(0)} = \mathbf{A}^{(0)}$ and $\mathbf{J}^{(0)} = \mathbf{0}_{\mathrm{nn}}$.
for $\mathrm{t} = 1, 2, \cdots$ **do**
  $\hat{\mathbf{A}}^{(\mathrm{t})} = \mathcal{P}_{\mathcal{DD}_{\mathrm{c}}^{+}}(\mathbf{A}^{(\mathrm{t}-1)} - \mathbf{J}^{(\mathrm{t}-1)})$. ← − Diagonally Dominant Projection
  $\mathbf{A}^{(\mathrm{t})} = \left(\hat{\mathbf{A}}^{(\mathrm{t}-1)} + (\hat{\mathbf{A}}^{(\mathrm{t}-1)})^{\mathrm{T}}\right)/2$. ← − Symmetric Projection
  $\mathbf{J}^{(\mathrm{t})} = \mathbf{J}^{(\mathrm{t}-1)} + (\hat{\mathbf{A}}^{(\mathrm{t})} - \mathbf{A}^{(\mathrm{t}-1)})$.
  if $\|\mathbf{J}^{(\mathrm{t})} - \mathbf{J}^{(\mathrm{t}-1)}\|_{\mathrm{F}} \leqslant$ TOL **then**
    $\mathbf{A} = \mathbf{A}^{(\mathrm{t})}$.
    if (8.32) is satisfied **then**
      stop.
    else
      TOL = TOL - η, continue.
    end if
  else
    continue.
  end if
end for

Example 1: Given a 3×3 matrix

$$\mathbf{G} = \begin{bmatrix} \mathrm{g}_{11} & \mathrm{g}_{12} & \mathrm{g}_{13} \\ \mathrm{g}_{21} & \mathrm{g}_{22} & \mathrm{g}_{23} \\ \mathrm{g}_{31} & \mathrm{g}_{32} & \mathrm{g}_{33} \end{bmatrix}, \tag{8.18}$$

we can regard each row as a vector and they are depicted in Fig. 8.2. Without loss of generality, let's assume that $\mathbf{G}$ is entry-wisely positive and take $\mathbf{g}_3 = [\mathrm{g}_{31}, \mathrm{g}_{32}, \mathrm{g}_{33}]$ an example. For some tasks such as dimension reduction, we need to project $\mathbf{g}_3$ to obtain $\tilde{\mathbf{g}}_3 = [0, \mathrm{g}_{32}, \mathrm{g}_{33}]$ as the best approximation of $\mathbf{g}_3$ in terms of the minimum Euclidean distance $\|\mathbf{g}_3 - \tilde{\mathbf{g}}_3\|_2$. Obviously, if $\mathrm{g}_{32} \geqslant \mathrm{g}_{33}$, we cannot guarantee that a diagonally dominant approximation of $\mathbf{G}$ can be obtained through this type of projection. In this paper, we follow the process introduced in [247] to guarantee that $\hat{\mathbf{G}} \in \mathcal{DD}^{+}$ is valid for approximating $\mathbf{G}$. To be specific, for the i-th row of a $\mathrm{h} \times \mathrm{h}$ matrix $\mathbf{G}$ ($\mathrm{i} = 3$ and $\mathrm{h} = 3$ in our case), we first do

- $\mathrm{d}_{\mathrm{k}} = \sum_{\mathrm{k}=\mathrm{j}}^{\mathrm{h}} \mathrm{g}_{\mathrm{ik}} - \mathrm{g}_{\mathrm{ii}}$, where $\mathrm{k} \neq \mathrm{i}$ and $1 \leqslant \mathrm{k} \leqslant \mathrm{h}$;
- $\mathrm{c}_{\mathrm{k}} = \mathrm{h} - \mathrm{k} + 1$ for $\mathrm{k} < \mathrm{i}$, and $\mathrm{c}_{\mathrm{k}} = \mathrm{h} - \mathrm{k} + 2$ for $\mathrm{k} > \mathrm{i}$;
- $\bar{\mathrm{d}}_{\mathrm{k}} = \mathrm{d}_{\mathrm{k}}/\mathrm{c}_{\mathrm{k}}$.

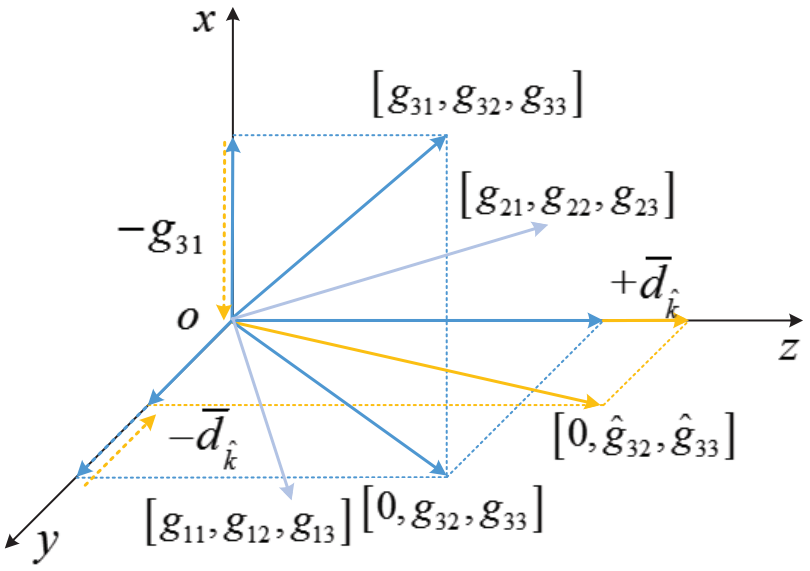

FIGURE 8.2: Illustration of Mendoza-Raydan-Tarazaga projection [247].

Next, we find $\hat{k}$ such that $g_{i\hat{k}} > 0$ and $\bar{d}_{\hat{k}} \leqslant g_{i\hat{k}}$, and finally the approximation matrix $\hat{\mathbf{G}}$ is generated as follows:

$$\hat{g}_{ik} = \begin{cases} g_{ik} + \bar{d}_{\hat{k}}, & k = i, \\ g_{ik} - g_{ik}, & 1 \leqslant k \leqslant \hat{k} - 1 \text{ and } k \neq i, \\ g_{ik} - \bar{d}_{\hat{k}}, & \hat{k} \leqslant k \leqslant h \text{ and } k \neq i. \end{cases} \tag{8.19}$$

Fig. 8.2 shows a geometrical example of how $\hat{\mathbf{g}}_3 = [0, \hat{g}_{32}, \hat{g}_{33}]$ is generated. In this case, we assume that $\hat{k} = 2$. Therefore, $\hat{g}_{31} = g_{31} - g_{31} = 0$, $\hat{g}_{32} = g_{32} - \bar{d}_{\hat{k}}$, and $\hat{g}_{33} = g_{33} + \bar{d}_{\hat{k}}$. By comparing $\tilde{\mathbf{g}}_3$ with $\hat{\mathbf{g}}_3$, one sees that they are both approximations of $\mathbf{g}_3$. However, $\hat{\mathbf{g}}_3$ is generated in a way to ensure that $\hat{g}_{33} \geqslant \hat{g}_{32}$ stands, such that $\hat{\mathbf{G}}$ obtained is diagonally dominant. Similarly to the uniqueness of $\tilde{\mathbf{g}}_3$, $\hat{\mathbf{g}}_3$ is proved to be unique as well [247]. This ensures that if $\mathbf{G}$ has a diagonally dominant counterpart, it would be unique. We are interested in the latter as it leads to a diagonally dominant matrix $\hat{\mathbf{G}}$ that is usually positive definite, which helps us solving the matrix inverse problem in GPs.

8.4.2 Neumann Series for Diagonally Dominant Matrix Inversion Approximation

After solving (8.17) with Algorithm 1, we can next approximate $(\mathbf{K}_{nn} + \sigma^2\mathbf{I})^{-1}$ with

$$(\mathbf{K}_{nn} + \sigma^2\mathbf{I})^{-1} \approx (\mathbf{L}_{nn} + \mathbf{A} + \sigma^2\mathbf{I})^{-1} = (\mathbf{L}_{nn} + \mathbf{M})^{-1}, \tag{8.20}$$

where $\mathbf{M} = \mathbf{A} + \sigma^2\mathbf{I}$. Although the SDD matrix $\mathbf{A}$ ensures that $\mathbf{M} \in \mathcal{SDD}_c^+$, the computational cost of $\mathbf{M}^{-1}$ is still at $\mathcal{O}(n^3)$. This is not favourable. Therefore, we introduce the Neumann series to approximate $\mathbf{M}^{-1}$.

Given a matrix $\mathbf{M}$, the inverse $\mathbf{M}^{-1}$ of which can be expanded as the following Neumann series [223]

$$\mathbf{M}^{-1} = \sum_{\mathrm{i}=0}^{\infty} (\mathbf{X}^{-1}(\mathbf{X} - \mathbf{M}))^{\mathrm{i}}\mathbf{X}^{-1}, \tag{8.21}$$

which holds if $\lim_{\mathrm{i}\to\infty} (\mathbf{I} - \mathbf{X}^{-1}\mathbf{M})^{\mathrm{i}} = \mathbf{0}$ is satisfied. In general, we can use (8.21) to approximate the inverse of any matrix. However, approximation with quick convergence requires $\mathbf{M}$ to be diagonally dominant [223, 225]. In our case, suppose

$$\mathbf{M} = \mathbf{A} + \sigma^2\mathbf{I} \triangleq \mathbf{D}_{\mathrm{M}} + \mathbf{E}_{\mathrm{M}}, \tag{8.22}$$

where $\mathbf{D}_{\mathrm{M}}$ is the main diagonal of $\mathbf{M}$ and $\mathbf{E}_{\mathrm{M}}$ is the hollow. If we substitute $\mathbf{X}$ in equation (8.21) by $\mathbf{D}_{\mathrm{M}}$, we get

$$\mathbf{M}^{-1} = \sum_{\mathrm{i}=0}^{\infty} (-\mathbf{D}_{\mathrm{M}}^{-1}\mathbf{E}_{\mathrm{M}})^{\mathrm{i}}\mathbf{D}_{\mathrm{M}}^{-1}, \tag{8.23}$$

which is guaranteed to converge when $\lim_{\mathrm{i}\to\infty} (-\mathbf{D}_{\mathrm{M}}^{-1}\mathbf{E}_{\mathrm{M}})^{\mathrm{i}} = \mathbf{0}$. When Neumann series given in (8.23) converges, we can then approximate $\mathbf{M}^{-1}$ with only the first L terms. The L-term approximation is computed as follows:

$$\widetilde{\mathbf{M}}_{\mathrm{L}} = \sum_{\mathrm{i}=0}^{\mathrm{L}-1} (-\mathbf{D}_{\mathrm{M}}^{-1}\mathbf{E}_{\mathrm{M}})^{\mathrm{i}}\mathbf{D}_{\mathrm{M}}^{-1}, \tag{8.24}$$

For instance, when $\mathrm{L} = 1, 2, 3$, we have the approximations

$$\widetilde{\mathbf{M}}_{\mathrm{L}} = \begin{cases} \mathbf{D}_{\mathrm{M}}^{-1}, & \mathrm{L} = 1 \\ \mathbf{D}_{\mathrm{M}}^{-1} - \mathbf{D}_{\mathrm{M}}^{-1}\mathbf{E}_{\mathrm{M}}\mathbf{D}_{\mathrm{M}}^{-1}, & \mathrm{L} = 2 \\ \mathbf{D}_{\mathrm{M}}^{-1} - \mathbf{D}_{\mathrm{M}}^{-1}\mathbf{E}_{\mathrm{M}}\mathbf{D}_{\mathrm{M}}^{-1} + \mathbf{D}_{\mathrm{M}}^{-1}\mathbf{E}_{\mathrm{M}}\mathbf{D}_{\mathrm{M}}^{-1}\mathbf{E}_{\mathrm{M}}\mathbf{D}_{\mathrm{M}}^{-1}. & \mathrm{L} = 3 \end{cases} \tag{8.25}$$

From equations (8.24) and (8.25), we see that Neumann series approximation reduces the cost of $\mathbf{M}^{-1}$ from $\mathcal{O}(\mathrm{n}^3)$ to $\mathcal{O}(\mathrm{n}^2)$ when $\mathrm{L} \leq 2$, which is of particular favour when n becomes large. Wu et al. also mention that the calculation of the Neumann series can be accelerated by proper adjustment of the terms [223]. As mentioned earlier, when $\mathbf{M}$ is diagonally dominant [223, 225], the approximation would be both quick and accurate, this would help to improve the GPs performance.

8.4.3 Symmetric Diagonally Dominant Projection-based Gaussian Processes

By transforming the 'residual' matrix $\tilde{\mathbf{A}}$ into a diagonally dominant matrix $\mathbf{A}$, and approximating $\mathbf{M}^{-1}$ with (8.24), we know the inverse matrix involved in GPs can be approximated

Algorithm 2: The SDD projection-based GPs

Input: $\mathbf{X}$ the inputs, $\mathbf{y}$ the outputs, k the kernel function, σ^2 the observation noise level, TOL a tolerance criterion, and the test inputs $\mathbf{X}_*$

Output: $\bar{\mathbf{f}}_*$ and $\text{cov}(\mathbf{f}_*)$

1: $\mathbf{K}_{\text{nn}} \approx \mathbf{K}_{\text{nm}}\mathbf{K}_{\text{mm}}^{-1}\mathbf{K}_{\text{nm}}^{\text{T}} + \mathbf{A}$, with $\mathbf{A}$ diagonally dominant $\leftarrow-$ Solving (8.17)
2: L-term Neumann Series Approximation: $\widetilde{\mathbf{M}}_{\text{L}} \approx \mathbf{M}^{-1}$, with $\mathbf{M} = \mathbf{A} + \sigma^2\mathbf{I}$
3: Cholesky factorisation: $\mathbf{C} := \text{cholesky}(\mathbf{K}_{\text{mm}} + \mathbf{K}_{\text{nm}}^{\text{T}}\widetilde{\mathbf{M}}_{\text{L}}\mathbf{K}_{\text{nm}})$
4: $(\mathbf{K}_{\text{nn}} + \sigma^2\mathbf{I})^{-1} \approx \widetilde{\mathbf{M}}_{\text{L}} - \mathbf{V}^{\text{T}}\mathbf{V}$, with $\mathbf{V} = \mathbf{C} \setminus \mathbf{Y}_{\text{mn}}$ and $\mathbf{Y}_{\text{mn}} = \mathbf{K}_{\text{nm}}^{\text{T}}\widetilde{\mathbf{M}}_{\text{L}}$.
5: Mean: $\bar{\mathbf{f}}_* = \mathbf{K}_{\text{Nn}}\mathbf{Q}\mathbf{y}$, with $\mathbf{Q} = \widetilde{\mathbf{M}}_{\text{L}} - \mathbf{V}^{\text{T}}\mathbf{V}$
6: Covariance: $\text{cov}(\mathbf{f}_*) = \mathbf{K}_{\text{NN}} - \mathbf{K}_{\text{Nn}}\mathbf{Q}\mathbf{K}_{\text{Nn}}^{\text{T}}$, with $\mathbf{Q} = \widetilde{\mathbf{M}}_{\text{L}} - \mathbf{V}^{\text{T}}\mathbf{V}$

through

$$\begin{aligned}(\mathbf{K}_{\text{nn}} + \sigma^2\mathbf{I})^{-1} &\approx (\mathbf{L}_{\text{nn}} + \mathbf{A} + \sigma^2\mathbf{I})^{-1} \\ &= (\mathbf{K}_{\text{nm}}\mathbf{K}_{\text{mm}}^{-1}\mathbf{K}_{\text{nm}}^{\text{T}} + \mathbf{M})^{-1} \\ &= \mathbf{M}^{-1} - \mathbf{M}^{-1}\mathbf{K}_{\text{nm}}(\mathbf{K}_{\text{mm}} + \mathbf{K}_{\text{nm}}^{\text{T}}\mathbf{M}^{-1}\mathbf{K}_{\text{nm}})^{-1}\mathbf{K}_{\text{nm}}^{\text{T}}\mathbf{M}^{-1}.\end{aligned} \tag{8.26}$$

The overall SDD projection-based GP (SDD GP) is described in Algorithm 2. For brevity, we denote the approximation of $\mathbf{K}_{\text{nn}}$ as $\mathbf{K}_{\text{nm}}\mathbf{K}_{\text{mm}}^{-1}\mathbf{K}_{\text{nm}}^{\text{T}}$. One can observe from Algorithm 2 that with the proposed SDD GP, the computational cost is reduced overall from $\mathcal{O}(\text{n}^3)$ to $\mathcal{O}(\text{mn}^2)$, and we are still able to retain the 'residual' matrix.

8.4.4 Theoretical Performance Analysis

By comparing the proposed approach with a full GP model, one can see that the major difference is demonstrated by

$$\begin{aligned}(\mathbf{K}_{\text{nn}} + \sigma^2\mathbf{I})^{-1} &= (\mathbf{L}_{\text{nn}} + \tilde{\mathbf{A}} + \sigma^2\mathbf{I})^{-1} \leftarrow \text{GP} \\ &\approx (\mathbf{L}_{\text{nn}} + \mathbf{A} + \sigma^2\mathbf{I})^{-1} \leftarrow \text{SDD GP}.\end{aligned} \tag{8.27}$$

Since $\mathcal{SDD}_{\text{c}}^{+}$ and Neumann series approximations are key in the proposed approach, we present a theoretical analysis of their impact on the algorithm performance as follows.

Lemma 1: Given $\mathbf{A}$ as the $\mathcal{SDD}^{+}$ approximation of $\tilde{\mathbf{A}}$, one can then take $\mathbf{M}$ as an $\mathcal{SDD}_{\text{c}}^{+}$ approximation of $\tilde{\mathbf{A}} + \sigma^2\mathbf{I}$, i.e. $\mathbf{M} \in \mathcal{SDD}_{\text{c}}^{+}$ with $\text{c} > 1$ satisfied.

Proof: According to the definition of $\mathbf{M}$, we know that the diagonal entries of $\mathbf{M}$ are $\text{m}_{\text{jj}} = \text{a}_{\text{jj}} + \sigma^2$, $\text{j} = 1, \cdots, \text{n}$, where a_{jj} are the diagonal entries of $\mathbf{A}$. The off-diagonal

entries of $\mathbf{M}$ and $\mathbf{A}$ are identical. Therefore, we have

$$\begin{cases} \mathrm{m}_{11} \geqslant \mathrm{c}_1 \sum_{\mathrm{i}:\mathrm{i}\neq 1} |\mathrm{a}_{1\mathrm{i}}|, \\ \vdots \\ \mathrm{m}_{\mathrm{jj}} \geqslant \mathrm{c}_{\mathrm{j}} \sum_{\mathrm{i}:\mathrm{i}\neq \mathrm{j}} |\mathrm{a}_{\mathrm{ji}}|, \\ \vdots \\ \mathrm{m}_{\mathrm{nn}} \geqslant \mathrm{c}_{\mathrm{n}} \sum_{\mathrm{i}:\mathrm{i}\neq \mathrm{n}} |\mathrm{a}_{\mathrm{ni}}|, \end{cases} \tag{8.28}$$

where $\mathrm{c}_{\mathrm{j}} > 1$, $\mathrm{j} = 1, \cdots, \mathrm{n}$ hold for $\sigma^2 > 0$, which is normally the case as there is no point to consider a zero mean zero variance Gaussian noise. It is straightforward that by setting $\mathrm{c} = \min\{\mathrm{c}_1, \mathrm{c}_2, \cdots, \mathrm{c}_{\mathrm{n}}\}$, **Lemma 1** stands. According to [246], $\mathbf{M}^{-1}$ can be bounded by

$$||\mathbf{M}^{-1}||_{\mathrm{F}} \leqslant \frac{\mathrm{c}}{\mathrm{c}-1} |||[\mathrm{diag}(\mathbf{M})]^{-1}||_{\mathrm{F}}, \tag{8.29}$$

which is the condition of making $(\mathbf{L}_{\mathrm{nn}} + \mathbf{A} + \sigma^2\mathbf{I})^{-1}$ a good estimator of $(\mathbf{K}_{\mathrm{nn}} + \sigma^2\mathbf{I})^{-1}$. More details can be found on the right half of Page 2 in [246].

Furthermore, because $\mathbf{M}^{-1}$ is approximated in the paper by the L-term Neumann series given in (8.24), we then investigate the error between (8.23) and (8.24) to demonstrate the approximation performance. Suppose the error is denoted by

$$\begin{aligned} \Delta_{\mathrm{M|L}} &= \sum_{\mathrm{i}=\mathrm{L}}^{\infty} (-\mathbf{D}_{\mathrm{M}}^{-1}\mathbf{E}_{\mathrm{M}})^{\mathrm{i}}\mathbf{D}_{\mathrm{M}}^{-1} \\ &= (-\mathbf{D}^{-1}\mathbf{E}_{\mathrm{M}})^{\mathrm{L}} \sum_{\mathrm{i}=0}^{\infty} (-\mathbf{D}_{\mathrm{M}}^{-1}\mathbf{E}_{\mathrm{M}})^{\mathrm{i}}\mathbf{D}_{\mathrm{M}}^{-1} \\ &= (-\mathbf{D}_{\mathrm{M}}^{-1}\mathbf{E}_{\mathrm{M}})^{\mathrm{L}}\mathbf{M}^{-1}. \end{aligned} \tag{8.30}$$

Let's assume that there exists a column vector $\mathbf{h}_{\mathrm{M}}$, such that the l_2 norm of $||\mathbf{M}^{-1}\mathbf{h}_{\mathrm{M}}||_2 \leq \infty$. Then according to [223] (Subsection B in Section III), the l_2-norm of $\Delta_{\mathrm{M|L}}\mathbf{h}_{\mathrm{M}}$ satisfies

$$\begin{aligned} ||\Delta_{\mathrm{M|L}}\mathbf{h}_{\mathrm{M}}||_2 &= ||(-\mathbf{D}_{\mathrm{M}}^{-1}\mathbf{E}_{\mathrm{M}})^{\mathrm{L}}\mathbf{M}^{-1}\mathbf{h}_{\mathrm{M}}||_2 \\ &\leqslant ||(-\mathbf{D}_{\mathrm{M}}^{-1}\mathbf{E}_{\mathrm{M}})^{\mathrm{L}}||_{\mathrm{F}} ||\mathbf{M}^{-1}\mathbf{h}_{\mathrm{M}}||_2 \\ &\leqslant ||\mathbf{D}_{\mathrm{M}}^{-1}\mathbf{E}_{\mathrm{M}}||_{\mathrm{F}}^{\mathrm{L}} ||\mathbf{M}^{-1}\mathbf{h}_{\mathrm{M}}||_2. \end{aligned} \tag{8.31}$$

We can see that if

$$||\mathbf{D}_{\mathrm{M}}^{-1}\mathbf{E}_{\mathrm{M}}||_{\mathrm{F}} < 1 \tag{8.32}$$

holds, then the approximation error approaches zero as L increases [223], implying that the approximation of (8.23) by (8.24) is becoming better. It is also demonstrated in [225] that the approximation accuracy of $\mathbf{M}^{-1}$ using (8.24) is fairly high when $\mathbf{M}$ is diagonally dominant, which is case in our paper.

By increasing L, the approximation performance of Neumann series can be improved. In addition, we can use the SDD projection to enhance the approximation performance. One can see that the matrices $\mathbf{A}$, $\mathbf{D}_{\mathrm{M}}$, and $\mathbf{E}_{\mathrm{M}}$ are linked through (8.22), which shows that $\mathbf{D}_{\mathrm{M}}$

and $\mathbf{E}_{\mathrm{M}}$ change along with $\mathbf{A}$. When $\mathbf{A}$ is updated by Algorithm 1, a new set of $\mathbf{D}_{\mathrm{M}}$ and $\mathbf{E}_{\mathrm{M}}$ are generated according to (8.22) subsequently and condition (8.32) is checked. When the condition is satisfied, one can see from (8.31) that the performance of approximating (8.23) by (8.24) can be further improved.

8.5 Performance Validation

8.5.1 Datasets and Baselines

To validate the proposed approach, we design two sets of experiments. In the first set, two synthetic datasets and the Mauna Loa CO_2 [1] data are processed. The synthetic datasets are generated by two deterministic functions that are perturbed by Gaussian noises, as shown in

$$\mathrm{y} = \sin(\mathrm{x}) + \mathrm{v}_1, \tag{8.33}$$

with $\mathrm{v}_1 \sim \mathcal{N}(0, 0.15)$ and $\mathrm{x} \in [-5.0, 5.0]$, and

$$\mathrm{y} = 5\mathrm{x}^2 * \sin(12\mathrm{x}) + (\mathrm{x}^3 - 0.5) * \sin(3\mathrm{x} - 0.5) + 4 * \cos(2\mathrm{x}) + \mathrm{v}_2, \tag{8.34}$$

with $\mathrm{v}_2 \sim \mathcal{N}(0, 0.45)$ and $\mathrm{x} \in [-0.2, 1.2]$. We adopt models (8.33) and (8.34) because 1) they are substantially nonlinear functions with function values known at any given inputs, and this comparison of the proposed approach with other approaches can demonstrate well their performance. 2) The impact of different noises on the solutions can be easily demonstrated. This helps to generate datasets with various noise levels, including outliers, to test the robustness of the proposed approach. 3) The number of samples can be easily controlled to test the proposed approach on datasets of different sizes.

In the second set, we separately process temperature and NO_2 concentration data from Sheffield, the United Kingdom, and from Peshawar, Pakistan. For the data in the second set, we converted the original time stamp (year-day-hour-minute) into decimal form first, then both the time and the observation are standardised for all the GP models. In our case, the data were collected every 15 minutes in both cities from June 22, 2019 to July 14, 2019. Therefore, four samples can be collected in each hour and 96 samples are accumulated per day. This information enables us to convert the year-day-hour-minute time stamps into decimal numbers through

$$\mathrm{t}_{\mathrm{dec}} = \mathrm{t}_{\mathrm{year}} + (\mathrm{t}_{\mathrm{day}} - 1) + (\mathrm{t}_{\mathrm{hour}} * 4 + \mathrm{t}_{\mathrm{minute}}/60 * 4)/96, \tag{8.35}$$

where $\mathrm{t}_{\mathrm{dec}}$ is the decimal number, $\mathrm{t}_{\mathrm{year}}$ is the year, $\mathrm{t}_{\mathrm{day}}$ denotes the day, for example, the 173-th day of the year is June 22, 2019, $\mathrm{t}_{\mathrm{hour}}$ is the hour, and $\mathrm{t}_{\mathrm{minute}}$ is the minute. Note that since the data were collected every 15 minutes, $\mathrm{t}_{\mathrm{minute}}$ can only be 0, 15, 30, and 45 and this is part of the current validation.

Since the proposed approach belongs to the group with prior approximation, we hence compare it with full GP variants with different kernels [222] and a sparse GP model, i.e. the Fully Independent Training Conditional (FITC) [227, 229] GP. We also compare the

[1] https://iridl.ldeo.columbia.edu/SOURCES/.KEELING/.MAUNA_LOA/

developed approach with the variants where the 'residual' $\tilde{\mathbf{A}}$ are discarded. We denote the model as SDD^{-} GP for short.

8.5.2 Performance Metrics

In order to assess the overall performance of different GP variants, we employ the Mean Absolute Error (MAE) and Root Mean Squared Error (RMSE) to evaluate the prediction performance. These two metrics are defined as:

$$\text{MAE} = \frac{1}{\text{N}_\text{s}} \sum_{\text{i}=1}^{\text{N}_\text{s}} |\text{y}_\text{i} - \hat{\text{y}}_\text{i}|, \tag{8.36}$$

$$\text{RMSE} = \sqrt{\frac{1}{\text{N}_\text{s}} \sum_{\text{i}=1}^{\text{N}_\text{s}} (\text{y}_\text{i} - \hat{\text{y}}_\text{i})^2}, \tag{8.37}$$

where y_i and $\hat{\text{y}}_\text{i}$ indicate the i-th true value and prediction, respectively, N_s is the number of samples in the testing set.

Note for Sheffield and Peshawar NO_2 and temperature datasets, and the Mauna Loa CO_2 dataset, we do not have 'exact' function values. To evaluate the performance, we compare observations with predictions of different GP models.

8.5.3 Implementation Details

We have implemented the SDD GP and the SDD^{-} GP with Python based on GPy [2], and adjusted the full GP and the sparse GP from GPy to process our data for comparison.

For each dataset, we take N_t samples, which is 75% the number of samples as training data and the left as testing data, with size N_s. To be specific, for the two sets of synthetic data and the Mauna Loa CO_2 dataset, there are 635 samples for each. For the Sheffield and Peshawar temperature and air quality data, we use 2016 samples. This makes $\text{N}_\text{t} = 477$ for the Mauna Loa CO_2 and the synthetic datasets, and $\text{N}_\text{t} = 1512$ for the Sheffield and Peshawar temperature and air quality datasets. For sparse GP, we set the number of inducing points to roughly 1.5% the number of samples. For the SDD GP and SDD^{-} GP, we take m eigenvectors for covariance matrix approximation to achieve good performance. We increase m from 5 up to half of the number of samples and record the corresponding RMSE and MAE, to investigate the impact of m on the performance. The iteration index t in Algorithm 1 is set to 15 for results generation. To study the algorithms' performance, we use various kernels as listed in Table 8.1 to design composition kernels to capture different data patterns. The Squared Exponential Automatic Relevance Determination (SE-ARD) kernel is also applied to each dataset for comparison. The kernel settings are given in Table 8.2. The hyperparameters are estimated by maximising the logarithm marginal likelihood as shown in (8.9). We use 'GP-ARD' for brevity hereafter to indicate that the SE-ARD kernel is used.

[2] https://sheffieldml.github.io/GPy/

TABLE 8.1: Covariance kernels used in this paper.

Kernel Name	Covariance Function
Squared Exponential	$\mathrm{k_{SE}}(\mathrm{x},\mathrm{x}') = \sigma_{\mathrm{s}}^2 \exp\left(-\frac{(\mathrm{x}-\mathrm{x}')^2}{2\ell_{\mathrm{s}}^2}\right)$
Rational Quadratic	$\mathrm{k_{RQ}}(\mathrm{x},\mathrm{x}') = \sigma_{\mathrm{r}}^2\left(1+\frac{(\mathrm{x}-\mathrm{x}')^2}{2\alpha\ell_{\mathrm{r}}^2}\right)^{-\alpha}$
Periodic	$\mathrm{k_{Per}}(\mathrm{x},\mathrm{x}') = \sigma_{\mathrm{p}}^2 \exp\left(-\frac{2\sin^2(\pi\lvert\mathrm{x}-\mathrm{x}'\rvert/\mathrm{p})}{\ell_{\mathrm{p}}^2}\right)$
White	$\mathrm{k_W}(\mathrm{x},\mathrm{x}') = \sigma_{\mathrm{noise}}^2$ if $\mathrm{x}=\mathrm{x}'$, else $\mathrm{k_W}(\mathrm{x},\mathrm{x}')=0$
Squared Exponential ARD	$\mathrm{k_{SE\text{-}ARD}}(\mathrm{x},\mathrm{x}') = \sigma_{\mathrm{se}}^2 \exp\left(-\sum_{\mathrm{i}=1}^{\mathrm{N}}\frac{(\mathrm{x_i}-\mathrm{x_i}')^2}{2\ell_{\mathrm{i}}^2}\right)$

TABLE 8.2: Kernel settings for performance evaluation.

Datasets	Kernel Setting 1	Kernel Setting 2
Synthetic 1	$\mathrm{k_{SE}} + \mathrm{k_{Per}}$	$\mathrm{k_{SE\text{-}ARD}}$
Synthetic 2	$\mathrm{k_{SE}} + \mathrm{k_{Per}}$	$\mathrm{k_{SE\text{-}ARD}}$
Mauna CO_2	$\mathrm{k_{SE}} + \mathrm{k_{Per}} * \mathrm{k_{SE}} + \mathrm{k_{RQ}} + \mathrm{k_W}$	$\mathrm{k_{SE\text{-}ARD}}$
Sheffield/Peshawar Temp	$\mathrm{k_{SE}} + \mathrm{k_{Per}} * \mathrm{k_{SE}} + \mathrm{k_{RQ}}$	$\mathrm{k_{SE\text{-}ARD}}$
Sheffield/Peshawar NO_2	$\mathrm{k_{SE}} + \mathrm{k_{Per}} * \mathrm{k_{SE}} + \mathrm{k_{RQ}}$	$\mathrm{k_{SE\text{-}ARD}}$

8.5.4 Performance and Analysis

Fig. 8.3 shows the logarithm RMSE of different GP implementations on the synthetic dataset 1, synthetic dataset 2, and the Mauna Loa CO_2 dataset. We can see that the performance of the proposed SDD GP converges to that of the full GP, for both kernel setting 1 and 2. We also notice that kernels would affect the performance of GP variants as well as the proposed approach. For instance, Figs. 8.3a and 8.3c show that GP variants with the SE-ARD kernel (kernel setting 2) outperform their counterparts with kernel setting 1, whereas Fig. 8.3b shows that GP variants with kernel setting 1 perform better in terms of RMSE. To further generalise the results, we change the variances for both (8.33) and (8.34) and show how they affect the proposed approach in terms of RMSE. The results are given in Fig. 8.4, where Figs. 8.4a and 8.4b are the results generated with kernel setting 1, and Figs. 8.4c and 8.4d are generated with kernel setting 2. One can see that as the noise variances become big, the prediction RMSE of the proposed approach shows an increasing trend for both functions, for both kernel settings 1 and 2. This is intuitive as the proposed approach is essentially a regression model, whose performance could be degraded by noises.

Fig. 8.5 shows the RMSE of GP variants with different kernels on Sheffield and Peshawar NO_2 and temperature datasets, respectively. One can see from these figures that the SDD GP generally outperforms the SDD$^-$ GP and the sparse GP. We can also see that as m increases, the SDD GP outperforms or is comparable with the full GP when kernel setting 1 is used. When the SE-ARD kernel is used, we can see that the performance of SDD GP-ARD approaches the full GP-ARD as m increases till converge.

(A) Synthetic dataset 1

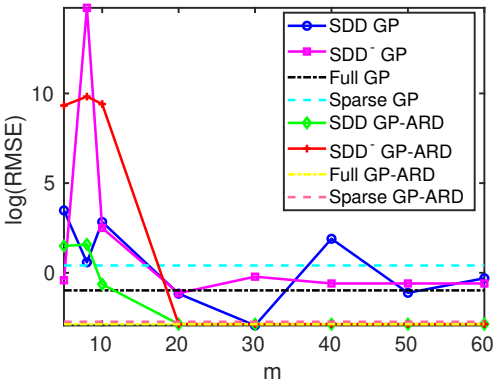

(B) Synthetic dataset 2

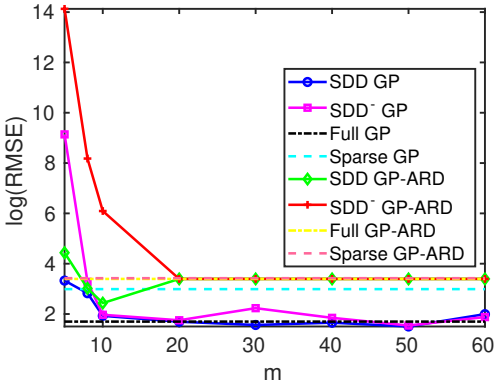

(C) Mauna Loa dataset

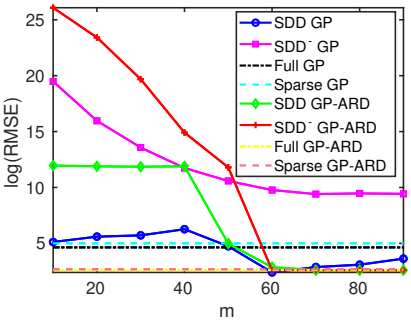

FIGURE 8.3: Logarithm RMSE of different methods on the Synthetic and the Mauna Loa datasets.

When focusing on the performance of the proposed approach with different kernels, i.e. SDD GP and SDD GP-ARD, we see that when m increases, their performance in terms of RMSE drops and then tends to converge. The same rule applies to the SDD$^-$ GP and SDD$^-$ GP-ARD. However, the latter does not always show the convergence trends. Particularly, the performance of the SDD$^-$ GP changes dramatically along with m as given in Fig. 8.5c and 8.5d. This is because when the 'residual' matrix $\tilde{\mathbf{A}}$ is considered, a better approximation of the covariance matrix is achieved, hence leading to better performance of the SDD GP compared with the SDD$^-$ GP. When m keeps increasing, the 'residual' matrix can be neglected, and the performance of SDD GP and SDD$^-$ GP becomes similar. Similar trends can be observed for SDD GP-ARD and SDD$^-$ GP-ARD. It is worth mentioning that when the SE-ARD kernel is used, the RMSEs change less dramatically compared with the results generated by using the kernel setting 1.

To further demonstrate that taking the 'residual' matrix $\tilde{\mathbf{A}}$ into account would improve the performance, we have compared the RMSE and MAE of 1) SDD GP with the SDD$^-$ GP; 2) SDD GP-ARD with the SDD$^-$ GP-ARD on each dataset. Table 8.3 shows the percentage when the SDD GP (SDD GP-ARD) outperforms the SDD$^-$ GP (SDD$^-$ GP-ARD) in terms of RMSE and MAE, respectively. We see that the percentage of the SDD GP (SDD GP-ARD) outperforms the SDD$^-$ GP (SDD$^-$ GP-ARD) is all equal to or bigger than 50%. This again demonstrates considering $\tilde{\mathbf{A}}$ would help to improve the proposed GP model's performance.

We also list the minimum and median RMSE and MAE of the GP variants on each dataset. The median RMSE and MAE are considered as they demonstrate the resilience

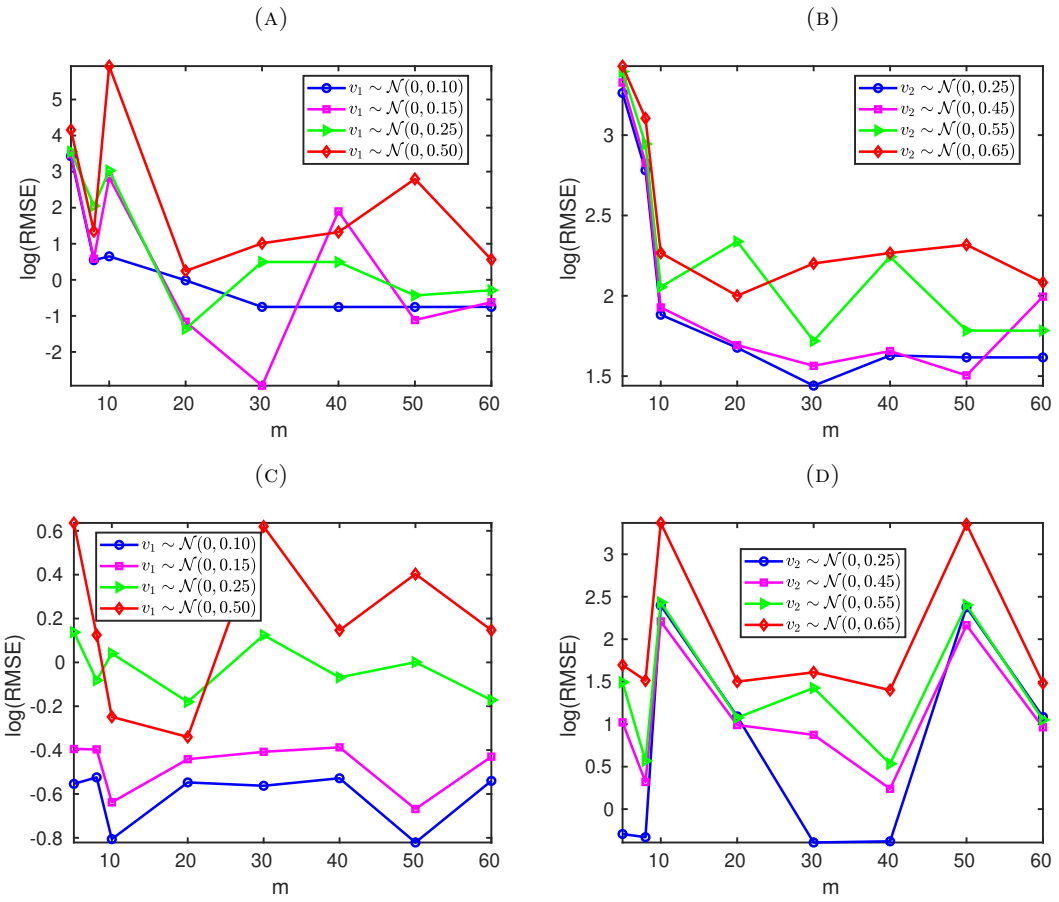

FIGURE 8.4: The impact of noise on the performance of the proposed approach: (a) Synthetic dataset 1 with kernel setting 1; (b) Synthetic dataset 2 with kernel setting 1; (c) Synthetic dataset 1 with kernel setting 2; (d) Synthetic dataset 2 with kernel setting 2.

TABLE 8.3: The percentage of results with RMSE and MAE of the SDD GP smaller than the SDD$^-$ GP: ONE indicates kernel setting 1 in Table 8.2 is used; TWO indicates kernel setting 2 in Table 8.2 is used.

	Syn. 1	Syn. 2	M. L. CO_2	S. Temp	P. Temp	S. NO_2	P. NO_2
MAE ONE	50%	75%	100%	59%	59%	53%	69%
RMSE ONE	50%	88%	100%	59%	53%	53%	69%
MAE TWO	100%	100%	78%	94%	65%	74%	94%
RMSE TWO	100%	100%	78%	94%	65%	79%	100%

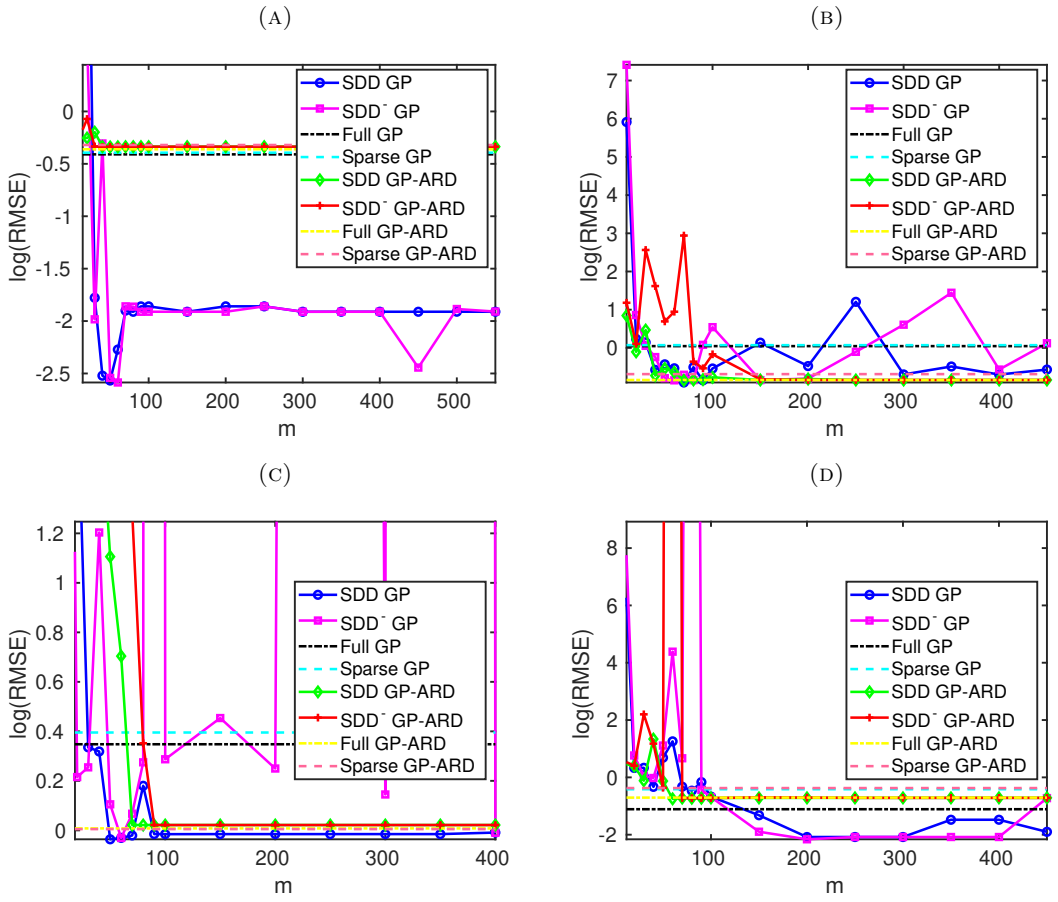

FIGURE 8.5: Logarithm RMSE of different methods on Peshawar and Sheffield NO_2 and temperature: (a) Peshawar NO_2; (b) Sheffield NO_2; (c) Peshawar temperature; (d) Sheffield temperature.

of the proposed approach. To be specific, the minimum and median RMSEs and MAEs of the GP variants on synthetic dataset 1, synthetic dataset 2, and the Mauna Loa CO_2 dataset are given in Table 8.4 and 8.5, respectively. One can see from Table 8.4 that the SDD GP achieves the minimum RMSE on all three datasets, and the minimum MAE on synthetic dataset 2 and the Mauna Loa CO_2 dataset. When it comes to the median RMSE and MAE as shown in Table 8.5, we see that the full GP variants show better performance except on synthetic dataset 1, where the SDD GP-ARD achieves the best performance.

TABLE 8.4: The performance comparison among different methods and kernels on the synthetic and public datasets. We take the minimum RMSE and MAE for the SDD GP (SDD GP-ARD) and SDD$^-$ GP (SDD$^-$ GP-ARD).

	Syn. 1		Syn. 2		M. L. CO_2	
——	RMSE	MAE	RMSE	MAE	RMSE	MAE
SDD GP	**0.053**	0.187	**4.502**	**1.832**	**11.054**	**2.735**
SDD$^-$ GP	0.321	0.433	4.681	1.933	1.219e+04	99.151
Full GP	0.079	0.203	5.466	2.013	103.459	8.298
Sparse GP	0.579	0.641	19.876	3.718	148.698	11.168
SDD GP-ARD	0.057	0.194	11.410	2.932	13.444	3.049
SDD$^-$ GP-ARD	0.057	0.194	29.806	4.520	13.447	3.051
Full GP-ARD	0.195	**0.052**	29.805	4.520	13.563	3.063
Sparse GP-ARD	0.211	0.065	30.684	4.926	14.540	3.173

TABLE 8.5: The performance comparison among different methods and kernels on the synthetic and public datasets. We take the median RMSE and MAE for the SDD GP (SDD GP-ARD) and SDD$^-$ GP (SDD$^-$ GP-ARD).

	Syn. 1		Syn. 2		M. L. CO_2	
——	RMSE	MAE	RMSE	MAE	RMSE	MAE
SDD GP	1.267	0.871	6.155	2.049	114.708	8.362
SDD$^-$ GP	0.606	0.648	6.858	2.205	3.948e+04	184.845
Full GP	0.079	0.203	**5.466**	**2.013**	103.459	8.298
Sparse GP	0.579	0.641	19.876	3.718	148.698	11.168
SDD GP-ARD	**0.057**	**0.194**	29.806	4.520	144.676	10.577
SDD$^-$ GP-ARD	0.057	0.194	29.806	4.520	1.325e+05	348.360
Full GP-ARD	0.057	0.195	29.805	4.520	**13.563**	**3.063**
Sparse GP-ARD	0.065	0.211	30.684	4.926	14.540	3.173

The corresponding results on Sheffield and Peshawar NO_2 and temperature datasets are separately given in Table 8.6 and 8.7. One can see that the SDD-GP performs the best in general on the Peshwar temperature and Sheffield NO_2 datasets. It also achieves the smallest MAE on the Sheffield temperature dataset. Otherwise, the SDD$^-$ GP slightly performs better than the SDD GP. When it comes to the median RMSE and MAE, the SDD GP outperforms the full GP variants except on the Sheffield temperature and NO_2 datasets.

TABLE 8.6: The performance comparison among different methods and kernels on Sheffield and Peshawar datasets. We take the minimum RMSE and MAE for the SDD GP (SDD GP-ARD) and SDD$^-$ GP (SDD$^-$ GP-ARD).

	S. Temp (°C)		P. Temp (°C)		S. NO_2 ($^-$g/m^3)		P. NO_2 ($^-$g/m^3)	
——	RMSE	MAE	RMSE	MAE	RMSE	MAE	RMSE	MAE
SDD GP	0.125	**0.270**	**0.965**	**0.819**	**0.404**	**0.394**	0.077	0.212
SDD$^-$ GP	**0.115**	0.270	0.970	0.827	0.413	0.395	**0.075**	**0.209**
Full GP	0.329	0.482	1.416	1.005	1.0472	0.779	0.664	0.578
Sparse GP	0.661	0.695	1.485	1.025	1.074	0.762	0.675	0.652
SDD GP-ARD	0.473	0.586	1.021	0.880	0.427	0.436	0.712	0.722
SDD$^-$ GP-ARD	0.484	0.599	1.022	0.881	0.431	0.446	0.713	0.721
Full GP-ARD	0.494	0.604	1.008	0.870	0.431	0.446	0.697	0.731
Sparse GP-ARD	0.689	0.701	1.005	0.868	0.503	0.519	0.726	0.755

TABLE 8.7: The performance comparison among different methods and kernels on Sheffield and Peshawar datasets. We take the median RMSE and MAE for the SDD GP (SDD GP-ARD) and SDD$^-$ GP (SDD$^-$ GP-ARD).

	S. Temp (°C)		P. Temp (°C)		S. NO_2 ($^-$g/m^3)		P. NO_2 ($^-$g/m^3)	
——	RMSE	MAE	RMSE	MAE	RMSE	MAE	RMSE	MAE
SDD GP	0.629	0.664	**0.985**	**0.839**	0.603	0.532	**0.148**	**0.314**
SDD$^-$ GP	0.647	0.694	1.303	0.963	0.902	0.634	0.148	0.314
Full GP	**0.329**	**0.482**	1.416	1.005	1.047	0.779	0.664	0.578
Sparse GP	0.661	0.695	1.485	1.025	1.074	0.762	0.675	0.652
SDD GP-ARD	0.489	0.602	1.022	0.880	0.435	0.450	0.715	0.724
SDD$^-$ GP-ARD	0.490	0.603	1.022	0.880	0.697	0.548	0.715	0.724
Full GP-ARD	0.494	0.604	1.008	0.870	**0.431**	**0.446**	0.697	0.731
Sparse GP-ARD	0.689	0.701	1.005	0.868	0.503	0.519	0.726	0.755

In general, as m increases, the performance of the developed approach reaches the performance of a full GP variant with the same kernel. When we adopt the minimum and median RMSE and MAE as metrics, we have shown that the performance of the proposed SDD GP (SDD GP-ARD) and the full GP (full GP-ARD) alternates. Fig. 8.3 and 8.5 also show that when m is small, the full GP variants outperform the proposed approach

with the same kernels in general. This is because when m is too small, entries of the 'residual' matrix $\tilde{\mathbf{A}}$ are still significantly big, forcing it to be SDD would not improve the approximation accuracy of the covariance matrix.

In addition to the aforementioned validation results, we also test the proposed approach with kernel setting 1 and 2 on data with outliers, in comparison with the corresponding full GP variants. The results are shown in Figs. 8.6 and 8.7, respectively. The outliers are generated by adding noises with prominent variances to both (8.33) and (8.34). To be specific, we set the variance of v_1 to 0.5 and the variance of v_2 to 1.65, which generates noise of comparable scales with the real value of (8.33) and (8.34).

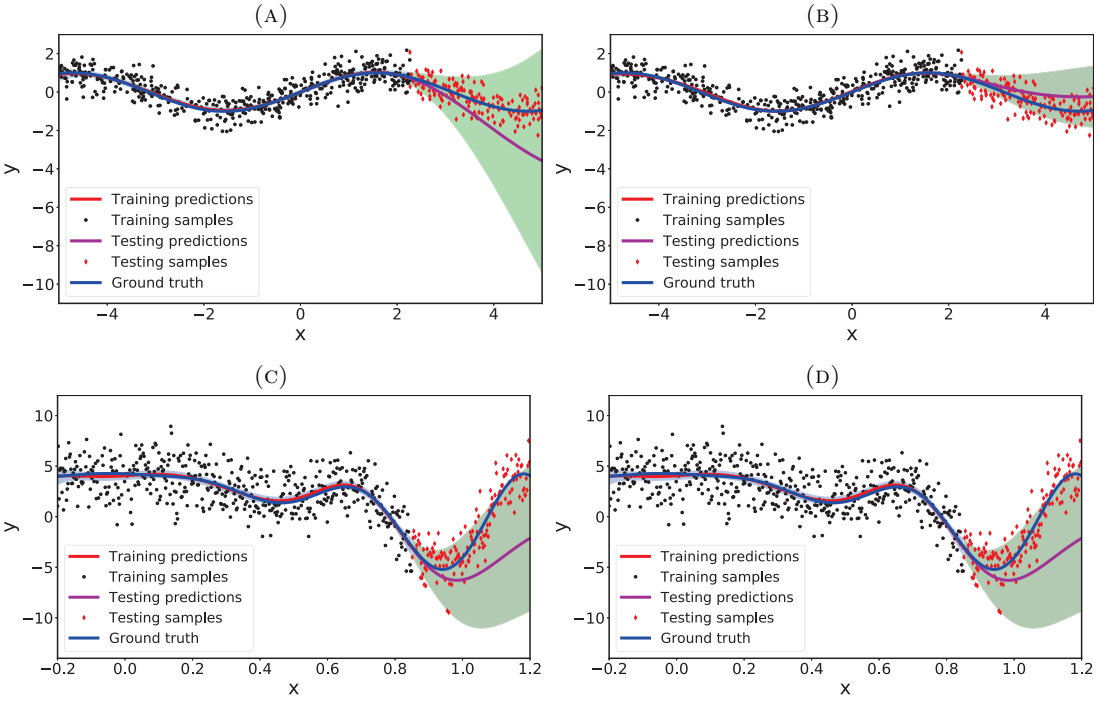

FIGURE 8.6: Impacts of outliers on (8.33) and (8.34), with kernel setting 1 in Table 8.2: (a) Full GP with $\mathrm{v}_1 \sim \mathcal{N}(0, 0.50)$; (b) SDD with $\mathrm{v}_1 \sim \mathcal{N}(0, 0.50)$; (c) Full GP with $\mathrm{v}_2 \sim \mathcal{N}(0, 1.65)$; (d) SDD with $\mathrm{v}_2 \sim \mathcal{N}(0, 1.65)$. The shaded areas indicate the 95% confidence interval.

We can see from Figs. 8.6 and 8.7 that the proposed approach is still able to produce comparable results as full GP variants with the same kernel despite the impact of outliers. It is worth mentioning that just like noises, kernels could affect the performance of GP models as well. This can be observed from the difference between Fig. 8.6a and Fig. 8.7a, as well as from the difference between Fig. 8.6d and Fig. 8.7d.

We then increase the number of samples and test the proposed approach over larger scale datasets compared with aforementioned settings. To be precise, we set the number of samples to 6,000 and 12,000 respectively for both (8.33) and (8.34). The proposed approach with kernel setting 1 and 2 are applied to process the data separately and the results are given in Fig. 8.8 and Fig. 8.9, respectively. Figs. 8.8a and 8.8b are the results from SDD GP with 6,000 and 12,000 samples from (8.33). Fig. 8.8c and 8.8d separately show the results of SDD GP with 6,000 and 12,000 samples from (8.34). The corresponding results obtained by using the SDD GP-ARD to process data from (8.33) are given in Figs. 8.9a and 8.9b, whereas Figs. 8.9c and 8.9c show the results achieved

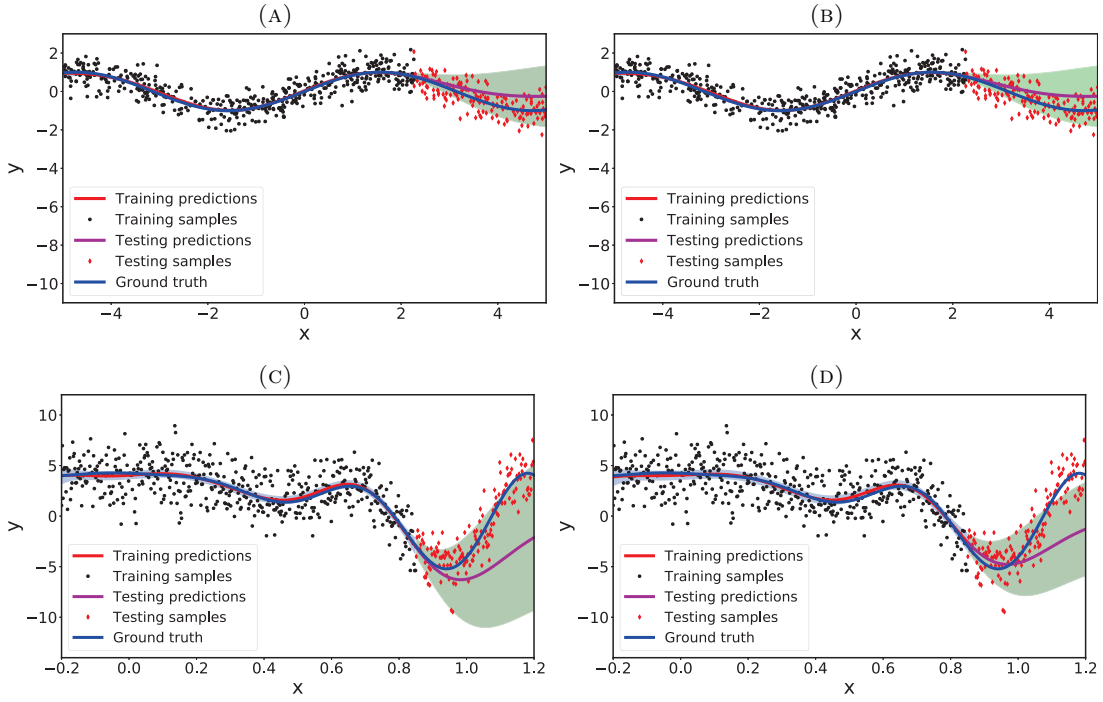

FIGURE 8.7: Impacts of outliers on (8.33) and (8.34), with kernel setting 2 in Table 8.2: (a) Full GP-ARD with $v_1 \sim \mathcal{N}(0, 0.50)$; (b) SDD GP-ARD with $v_1 \sim \mathcal{N}(0, 0.50)$; (c) Full GP-ARD with $v_2 \sim \mathcal{N}(0, 1.65)$; (d) SDD GP-ARD with $v_2 \sim \mathcal{N}(0, 1.65)$. The shaded areas indicate the 95% confidence interval.

by using SDD GP-ARD to process data from (8.34). As the number of samples increases, the full GP variants become slow for the new datasets, while the proposed approach still achieves comparable results more efficiently than the full GP variants as shown in Table 8.8. It is worth mentioning that GP variants using the kernel setting 2 are generally more efficient than those using kernel setting 1.

TABLE 8.8: Efficiency comparison of SDD GP (SDD GP-ARD) and full GP (full GP-ARD) with different kernel settings

	Syn. 1			Syn. 2		
Sample Number	635	6,000	12,000	635	6,000	12,000
SDD GP Time (s)	2.3	50.6	673.8	3.2	60.6	590.4
Full GP Time (s)	5.1	123.6	1566.2	6.5	126.0	1476.4
SDD GP-ARD Time (s)	1.6	38.9	200.2	1.5	52.2	239.2
Full GP-ARD Time (s)	3.4	83.2	454.5	3.5	108.6	509.5

8.6 Conclusion

In this paper, we propose a new kernel matrix approximation approach that considers the residual matrix and compares it with traditional kernel approximation methods. The key novelty of the paper stems from considering the residual matrix in covariance matrix approximation. The residual matrix is approximated by a symmetric diagonally dominant matrix whose inverse can be easily approached by the Neumann series. A new Gaussian process variant denoted as SDD GP is hence built upon the proposed approximation

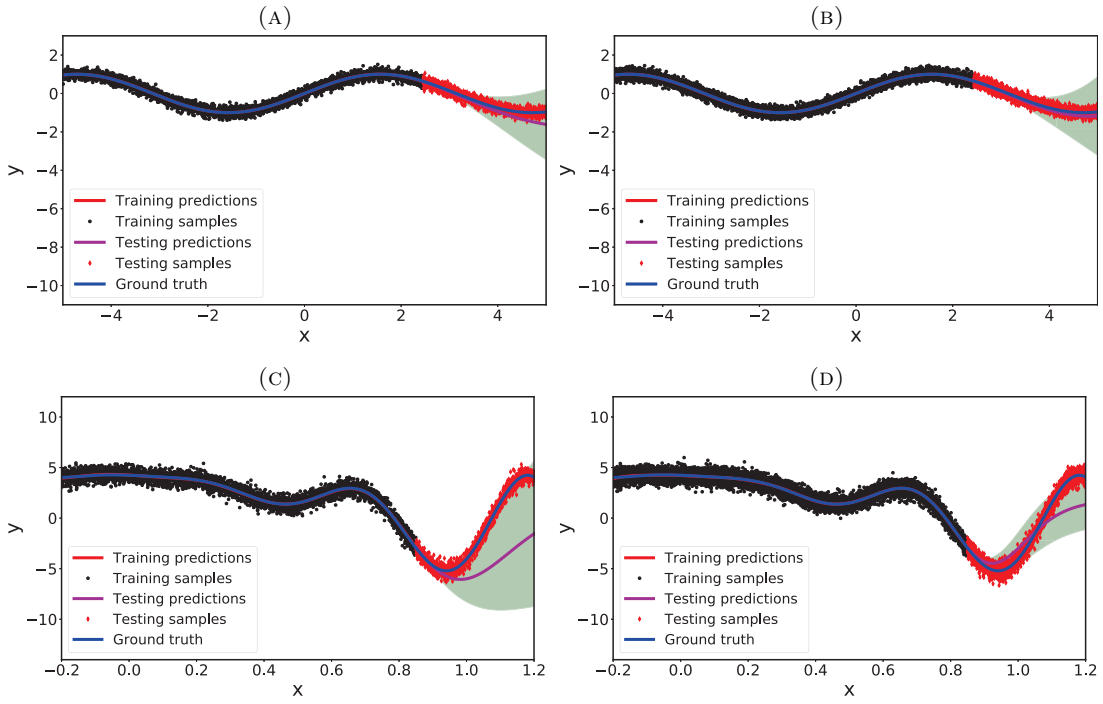

FIGURE 8.8: Performance of the proposed approach on large scale datasets, with kernel setting 1 in Table 8.2 used: (a) SDD GP with 6,000 samples from (8.33); (b) SDD GP with 12,000 samples from (8.33); (c) SDD GP with 6,000 samples from (8.34); (d) SDD GP with 12,000 samples from (8.34). $v_1 \sim \mathcal{N}(0, 0.15)$, $v_2 \sim \mathcal{N}(0, 0.45)$. The shaded areas indicate the 95% confidence interval.

method, which achieves comparable or better performance compared with full GP on both synthetic datasets and real air quality datasets, with lower computational complexity. Furthermore, the SE-ARD kernel is applied in addition to the composition kernels, to demonstrate the generality of the proposed approach.

We have applied the Mendoza-Raydan-Tarazaga projection to help us achieve a symmetric diagonally dominant projection of the residual matrix. We observed that the projection algorithm can affect the efficiency of the proposed approach, despite good prediction performance. Hence, we shall continue with the efficiency improvement of the proposed approach in the future.

8.7 Contribution

R.C. (Rohit Chakraborty):

- **Writing – Drafting:** I played a significant role in drafting the original manuscript. My contributions ensured that the research findings and methodologies were clearly articulated, providing a solid foundation for the paper.
- **Writing – Review and Editing:** Beyond the initial draft, I actively participated in the review and editing processes, refining the content for clarity, coherence, and academic rigor. I collaborated with other authors to ensure the manuscript effectively conveyed our research findings.

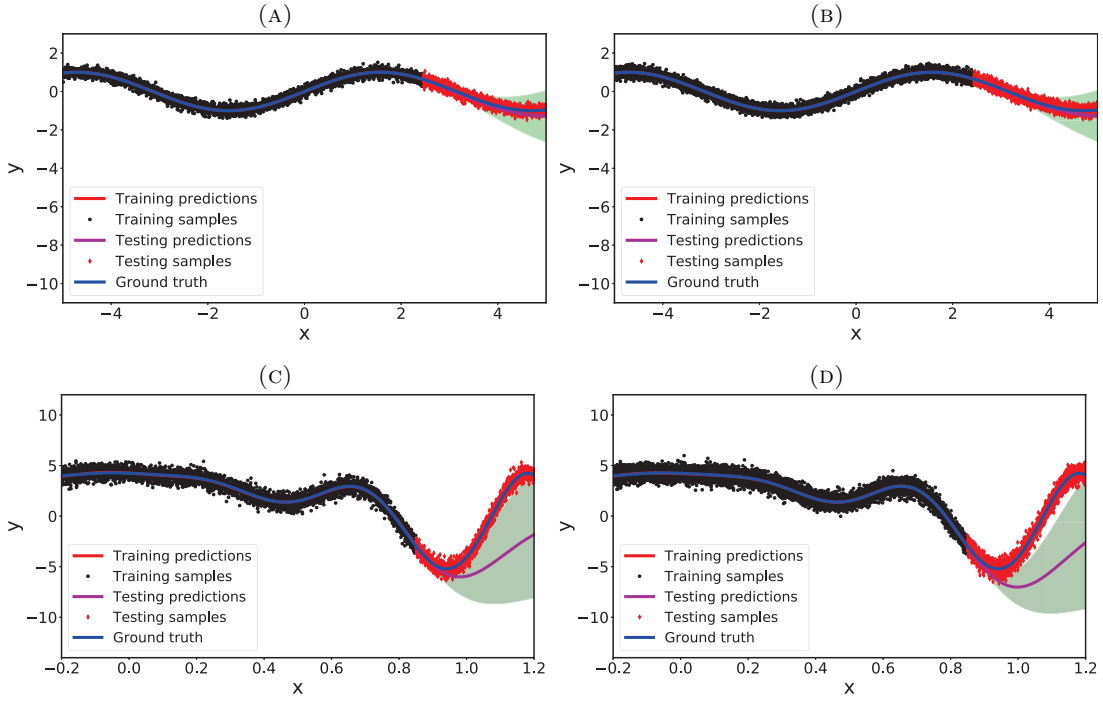

FIGURE 8.9: Performance of the proposed approach on large scale datasets, with kernel setting 2 in Table 8.2 used: (a) SDD GP-ARD with 6,000 samples from (8.33); (b) SDD GP-ARD with 12,000 samples from (8.33); (c) SDD GP-ARD with 6,000 samples from (8.34); (d) SDD GP-ARD with 12,000 samples from (8.34). $v_1 \sim \mathcal{N}(0, 0.15)$, $v_2 \sim \mathcal{N}(0, 0.45)$. The shaded areas indicate the 95% confidence interval.

- **Software Development:** I contributed to the software components of the study, developing and utilizing tools that facilitated data processing and analysis. My expertise in software ensured that the research was supported by robust and reliable technological solutions.
- **Methodology:** I played a pivotal role in designing the research methodology, ensuring that our approaches and techniques were sound, rigorous, and appropriate for the study's objectives.
- **Data Curation:** I was actively involved in curating the data for the study, ensuring its accuracy, relevance, and readiness for analysis. This involved gathering, cleaning, and organizing data sets, making them suitable for subsequent analysis and interpretation.

Throughout the research process, I collaborated closely with various team members, ensuring that my contributions complemented and enhanced the overall research effort. My commitment, combined with my expertise in software, methodology, and writing, had a substantial impact on the paper's direction and quality.

Chapter 9

Can Portable Air Quality Monitors Protect Children from Air Pollution on the School Run? An Exploratory Study

Abstract

With air quality issues in urban areas garnering increasing media attention, concerned citizens are beginning to engage with air monitoring technology as a means of identifying and responding to the environmental risks posed. However, while much has been written about the accuracy of this sensing equipment, little research has been conducted into the effect it has on users. As such, this research deploys coping theory to explore the specific ways in which portable air quality sensors influence user behaviour. This is done using a qualitative exploratory design, targeting parents and carers of children on the school run. Drawing from survey and interview responses, the article illustrates the decision-making pathways underpinning engagement with monitors and the ways in which they influence beliefs and behaviours around air pollution. The study demonstrates that personal environmental monitors can play a role in protecting children from air pollution on the school run. They can raise awareness about air pollution and disrupt misconceptions about where it does and does not occur. They can also encourage the public to change their behaviour in an attempt to mitigate and manage risks. However, the findings additionally reveal that sensor technology does not generate a simple binary response among users, of behavioural change or not. When attempts at behavioural change fail to reduce risk, resulting negative feelings can lead to inaction. Hence, the relationship between the technology and the individual is entwined with various social circumstances often beyond a parent or carer's control. Thus, top-down support aimed at tackling air pollution at source is essential if this bottom-up technology is to fulfil its full potential.

9.1 Introduction and Background

Urban air pollution is one of the most pressing concerns for governments world- wide, with the United Nations calling on national and subnational governments to commit to achieving air quality safe for citizens by 2030 [248]. Linked to around 40,000 premature deaths each year in the UK alone [249], air pollution poses several other risks to human health. Both long- and short-term, high- and low-level exposures are associated with adverse effects ([250], particularly when considering that for two of the main components in polluted air – particulate matter and ozone – there exist no 'safe' levels [251]. Ambient, or outdoor, air pollution is associated with increased rates of lung cancer, emphysema, bronchitis and other respiratory infections, with traffic-related air pollutants being suspected of initiating 'diverse lethal diseases to considerably reduce life expectancy' [252, 253]. A 'significant association' has been found between particulate matter 2.5 (PM 2.5) exposure and stroke, dementia, alzheimer's disease, autism spectrum disorder and Parkinson's disease [62]. As highlighted by a global review into the human health conse- quences of air pollution, lungs and airways notwithstanding, air pollution also damages 'most other organ systems in the body' [63] The risks to children are particularly pronounced because they tend to be exposed to higher concentrations than adults. Not only are their immature and developing immune systems and lungs implicated, along with their relatively high inhalation rate [254, 255], but they spend more time outside, and often walk or are pushed in buggies, usually at the height of exhaust emissions [256].Cognitive development among primary school children is also negatively affected, particularly working memory and attentiveness [257], with air pollution also being linked to the onset of neurological disorders. This includes autism and attention deficit/hyperactivity disorder [258], and is associated with decreases in the protein important to cognition and the white matter involved in learning and brain function [259]; see also [260]. Such effects continue across the life course; The evidence to date is coherent in that exposure to a range of largely traffic-related pollutants has been associated with quantifiable impairment of brain development in the young and cognitive decline in the elderly' [250].

In the UK, these risks have long been recognised by the government. However, since 2011, its efforts at reducing air pollution have been repeatedly deemed inadequate by the courts. In the latest decision, the High Court described government countermeasures as "unlawful" ([2018] EWHC 315 (Admin) Case No: CO/ 4922/2017, para 118), while a cross-party inquiry concluded that "[t]he Government cannot continue to put public health at risk" by continuing to pursue ineffective countermeasures (The Environment, Food and Rural Affairs Committee 2018). The degree of inaction taking place gains prominence when recognising that outdoor air pollution exceeds World Health Organisation (2016) limits for 90% of the UK's population. It is a situation that caused the UN Special Rapporteur on the human rights implications of hazardous substances, Baskut Tuncak (UN Human Rights Council 2017: 9), to express alarm that despite repeated judicial instruction, and recommendations by the UN Committee on the Rights of the Child, the government "continues to flout its duty to ensure adequate air quality and protect the rights to life and health of its citizens".

As a consequence of this dormancy, citizens have to rely on small networks of official monitors that are often unable to capture the complexity of urban air pollution [261].

In response to this situation, individuals and community groups are increasingly making use of an emerging technology – relatively low-cost personal air quality monitors – to evaluate environmental risks and respond accordingly (Marsh, 2017). As Oltra et al

(2017: 296) note, the number of citizen-led, participatory sensing projects has 'increased significantly in recent years', with much being written about the accuracy of the equipment in terms of its ability to contribute to official monitoring programmes. Indeed, several companies have brought such technology to market, including the Plume Labs 'Flow', the CleanSpace Tag, and Atmotube Pro, to name a few. However, as a recent systematic review of the literature concluded, '[c]urrently, there are very few studies that evaluate [its] social or economic implications' (Hubbell et al, 2018: 887). It is directly in this gap that the present research is situated.

The studies that do exist are insightful, providing preliminary conclusions to suggest that personal exposure information can challenge existing ideas and inform people's responses to air pollution. In relation to perceptions and emotions, the reported effects of monitor use range from an increased awareness of air pollution and intense emotional reactions (Oltra et al, 2017), through to enjoyment and surprise (Bales et al, 2019; Wong-Pardi et al, 2018; Bales et al, 2012). In relation to behaviour, Wong-Pardi et al (2018) and Zappi et al (2012) found minor behaviour changes to occur, which includes actions like closing windows and ceasing to burn incense indoors, while Oltra et al (2017) did not witness any alteration – intentional or real – as a result of monitor use.

Table 9.1: Existing Studies on Behavioural Responses to Personal Air Quality Data

Study	**Focus**	**Duration**	**Size**	**Sample**
Zappi et al. [35]	Human responses on the commute	2-4 weeks	16	On-campus workers
Bales et al. [262]	Human responses on the commute	4 weeks	16	On-campus workers
Oltra et al. [33]	Comparison with traditional sources	7 days	12	Selected by demographics
WongParodi et al. [263]	Indoor air pollution responses	3 weeks	4[a]	Library users[b]
Bales et al. [264]	Human responses on the commute	4 weeks	29	Group 1 and Group 2 workers
Heydon and Chakraborty (2020)	Adult responses on the school run	2 weeks	45	Parents and carers

[a] 26 participants were surveyed, but only 4 agreed to be interviewed.
[b] Selected from those who borrowed an indoor pollution monitor.

While insightful, these studies collectively exhibit several limitations. First, little attention is given to the specific mechanics of the transformative process. It is therefore not understood how the data intersects with individual beliefs and thought processes on the way to generating a given response. Second, they are overwhelmingly atheoretical, meaning analyses are not informed by a sufficiently detailed understanding of how human beings react to stressful encounters, such as that elicited by exposure to high levels of air pollution. Third, none of the existing studies are sensitive to context, neglecting to account for any external factors which may influence the possibilities for change and lead to a one-dimensional account of how monitors may affect behaviour. Finally, there are a myriad of shared shortcomings pertaining to the methodologies deployed; the majority of existing studies draw on relatively small and homogenous samples, while Zappi et al [35] and Bales et al. [262, 264] all use figures from the same study conducted almost a decade ago, although the latest iteration is augmented with more recent data.

In light of these limitations, the purpose of this article is three-fold. First, it explores the extent to which perceptions and behaviours around air pollution on the school run are altered by personal exposure information. Second, it deploys Lazarus and Folkman's (1984) coping theory [265] to draw out the specific decision-making processes by which this transformation does or does not occur. Almost forty years on from its publication, this theory 'remains the cornerstone of psychological stress and coping research across multiple fields and disciplines' [266]. Third, by providing parents and carers on the school run with personal monitoring technology its use is situated in the real-world. This allows for the intersections between structure and agency to be observed and enables individual coping processes to be understood in context. Taken together, this exploratory study aims to provide further information on the transformative potential of this emerging technology in a context of heightened environmental risk. In doing so, it seeks to illustrate some of the opportunities and barriers that relate to personal environment monitors and draw out the extent to which they can be used to protect some of the most-vulnerable populations in society from the harms of air pollution.

9.2 Theoretical Lens

Given the lack of theory guiding existent research on the social implications of personal air quality monitor use, direction can be taken from research into the adjacent area of wearable healthcare devices. Much of this literature is concerned with determining the 'infusion' of this technology into a person's life and the various barriers to that (see [267, 268]). For instance, concerns around health and privacy risks have been found to inhibit use ([269, 270]). However, similar to the research on personal environment monitors, little detailed information exists on the specifics of this encounter. To address this limitation, Marakhimov and Joo [271] applied coping theory to wearable healthcare devices in order to ascertain the specific ways in which people respond to the concerns presented by the technology. In much the same manner, but using an exploratory qualitative orientation, this study uses coping theory to understand how adults respond to personal air quality data on the school run.

Originally developed by Lazarus and Folkman [272], the process-based model of coping explains how a person evaluates and responds to stressful encounters. It is 'process-based' because coping is not conceived as a personality trait, referring instead to an unfolding and iterative relationship between person and environment. As such, 'coping' refers to the 'thoughts and behaviours used to manage the internal and external demands of situations that are appraised as stressful' ([273]). Internal demands are conceived of as personal factors, encompassing commitments and beliefs, while external demands pertain to the more contextual properties of events themselves. Importantly, the 'extent to which any event is stressful is determined by a confluence of person and situation factors in a specific transaction' ([272]).

The theory posits that a chosen coping behaviour is based on an initial two-part appraisal of a given encounter with environmental stimuli. During a 'primary appraisal', a person evaluates the impact of the event on his/her personal well-being, with the transaction being deemed positive, irrelevant or stressful ([266]). It is here where the meaning attached to what is at stake holds importance as it influences how stress appraisals are categorised. Explaining this further, Lazarus and Folkman [272] note that such stress may be regarded as a form of 'harm/loss', where some damage to the person has already been sustained, as

a 'threat', which involves harms or losses that have not yet taken place but are anticipated, or a 'challenge', which is relatively positive and focuses on the potential for gain or growth. Also implicated at this stage is the 'secondary appraisal', where a person evaluates the extent of their control over the stressor to determine what can be done to manage it or mitigate its consequences. These two forms of appraisal are not sequential, but work upon one another to produce a perception of the situation:

When that which is at stake is meaningful and coping resources are judged less than adequate for managing the demands of the situation, psychological stress is experienced. The greater the imbalance, the greater the stress.

(Folkman [273])

Taken together, this initial bifold stage of 'cognitive appraisal' is important because 'an individual's appraisal of the situation greatly influences their resultant emotions, coping strategies, and subsequent outcomes' (Biggs et al [266]). Indeed, it is only following this stage, where an individual encounters a given stimuli, conceptualises it as stressful or not, and decides what can be done to manage it that actual mental and behavioural responses are engaged.

A myriad of coping responses can result from this antecedent stage, but they can be grouped into two distinct but related categories; problem-focused and emotion-focused coping ([272, 274, 275]). Problem-focused outcomes refer to individual attempts at managing or mitigating the source of the stress. Emphasising proactive attempts at altering the situation, this includes efforts at reducing or removing obstacles, attaining new knowledge or skills, planning, taking action and seeking assistance ([272]). By contrast, emotion-focused responses regulate emotions, referring to internal attempts at mitigating the emotional distress brought on by the stressful event (ibid). Writing just before his death, Lazarus [274] bemoaned the rigidity of these categories, noting that 'it would be desirable to abandon the idea' of their independence from one another. Instead, research should acknowledge that in reality they 'operate together as a coherent unit and to separate them and set them up as competitive is to distort the way coping actually works' (ibid: 23).

Following this process of cognitive appraisal and coping response, individuals may initiate a 'reappraisal' in order to ascertain whether a given problem- or emotion-focused coping effort was effective at mitigating the stress experienced. It refers to a new process of appraisal following an earlier one but, in essence, 'appraisal and reappraisal do not differ' [272]. 'Reappraisal' therefore converts what appears to be a linear process into a circular one, acknowledging that an initial coping response can alter a subsequent appraisal of the situation.

To conceive of individual responses to environmental stimuli in this way, as a process through which meaning is attributed to a given situation and then acted upon or not, draws attention to the specific cognitive and behavioural stages involved and the relationships between them. In doing so, coping theory provides a more nuanced and informed framework for analysis when compared to the atheoretical approach adopted by all existing scholarship on personal environmental monitor use. Taking this as the point of departure, the article now turns to the application of this framework to personal air quality monitors, with the aim of understanding how adults on the school run respond to the data encountered.

9.3 Method

Research Design

The design of this study is exploratory and qualitative. The data was collected from surveys and interviews, with a sample of parents and carers drawn from 15 primary schools across Sheffield, England. With the primary aim of exploring the extent to which perceptions and behaviours of air pollution are altered by personal exposure information, the surveys were administered prior to receipt of the portable sensors. Participants were then asked to use the monitors for two weeks on the school run before being interviewed about changes in their experiences and behaviours during this time. The fieldwork was conducted between April and July 2019.

Sample

The sample consisted of forty-five participants, the average age of which was 42. Thirty-eight of these were female and seven male, reflecting the gendered nature of the school run journey more broadly [276]. Participation was limited to parents and carers that make the school run journey at least three days a week to a primary or infant school. Owed to the consumerist nature of the monitoring technology in question, participation was based on self-selection. As understanding real-world engagement with the technology was of priority, and those most concerned about air pollution are also most likely to purchase the monitors, this approach was deemed consistent with the purpose of the study. Indeed, 84% (n=38) of participants responded with 'strongly agree' or 'agree' when surveyed about the extent of their agreement with the statement 'air quality is a problem on my school run'. Participants were recruited through school newsletters and social media.

Procedure

Following the initial expression of interest, participants were sent an electronic copy of the survey to complete. Qualtrics was used for this purpose. Arrangements were then made to hand over the monitor. Upon meeting, one of the research team would link the participant's mobile phone to the specific monitor, explain and demonstrate how it and the accompanying app work, and address any questions. They were then instructed to use the monitor on the school run for two weeks and to check the monitor and app during this time. Interviews were conducted at the conclusion of this period, with questions centring on participant psychological and behavioural experiences over this time. To facilitate reflection on aspects of change within this experience, specific survey responses given by each participant were also recalled during the interview; those reflecting the degree with which participants considered air pollution to be a problem on the school run, their level of concern about the issue, knowledge of pollutants, and their origins and health effects. Interviews were conducted by an experienced social researcher.

The measurements were taken with a Plume Labs 'Flow' air quality monitor, which senses $PM_{2.5}$, PM_{10}, NOx and VOCs. The unit weighs 70g and the charge lasts approximately 24 hours. The monitor displays four colours depending on the quality of air being measured. Using guidelines established by the World Health Organisation and U.S. Environment Protection Agency, these include green for "low" air pollution, yellow for "moderate", red for "high" and purple for "very high". The app itself provides more details, displaying the real-time air quality index figures to which the colours correspond. This particular unit is also linked to a mobile phone, using its Global Position System capability to plot these colours on a map according to where the user travelled. No restrictions on use

were introduced, only a minimum requirement to use the monitor on the school run over 2 weeks. No substantive changes were made to the monitoring unit or graphical user interface over this time.

Analysis

The interview transcripts were thematically analysed according to the framework established by Braun and Clarke [277]. This was conducted alongside the data collection stage, allowing participant recruitment to continue until no new or deviating data was being added to the categories of analysis. This is a standard akin to theoretical saturation, but without the framework of grounded theory (see Saunders et al [278]). The analysis allowed for both inductive and deductive codes to be generated, although those pertaining to the key stages of coping theory formed primary focus. The qualitative analysis was conducted using NVivo, while the quantitative survey data was exported from Qualtrics and analysed using SPSS.

Limitations

44 of the 45 participants lived within three miles of the school. This may be a feature of primary schools which have catchment areas. The results may be different with parents of those at secondary schools. Similarly, the results may be different for groups with less constraints on their time (not parents).

9.4 Findings and Analysis

The data gathered illustrates that a large proportion of participants engaged in problem-solving efforts, attempting to change their behaviour as a means of mitigating the perceived 'threat' of air pollution. This was followed by a reappraisal to see if said changes were effective. A second, smaller group of participants followed a different process, pursuing efforts affiliated with emotion-focused coping without first attempting behavioural alteration. Changes in general and specific beliefs about air pollution were also reported, which were common across the sample and did not depend on the specific coping efforts deployed. Each of these aspects are taken in turn, following the structure of coping theory.

9.4.1 Primary and Secondary Appraisal: Threat and Agency

Primary appraisal ascribes meaning to a specific transaction, determining the significance of that to an individual's well-being [272]. The transaction may be deemed positive, irrelevant or stressful. For the majority of participants (n=40), the monitors heightened or confirmed pre-existing perceptions of air pollution as a problem on the school run. For 40% (n=18), air pollution was seen to be more of a problem than originally thought, prior to use of the monitor, whereas the others reported having their preconceptions confirmed. 4 people no longer thought air pollution was a problem on their school run and 1 remained uncertain. Following this recognition, the majority (n=41) of participants defined their encounter with air pollution readings negatively and in terms of anticipated harm. This conforms to Lazarus and Folkman's [272] concept of 'threat', which refers to an expected loss. All those whose primary appraisal was defined by 'threat' anticipated loss in terms of the health of children, and not only their own:

When the kids were involved it's definitely a lot more emotional. And I'm more angry, because I'm like 'for fucks sake, this is no good. I don't want this going into my kids' lungs'. You see people pushing babies around and stuff like that and, you know, it's like 'oh god'. When our kids were in buggies and prams and they're right down there, they're right at the front, at the crossing lights and things like that. And you do get a bit of guilt, thinking 'crikey, what have I done?'. (Participant 9)

I worry about the long-term effects on me and my kids, my wife and everyone... and the fact that the schools are there, so all the kids...And there's no barriers – at the junior's or the infant's – between them and the road, so it' just goes straight in. (Participant 20)

I'm worried. I've got school kids, obviously, but I've also got 20 month and 9-month-old children and I'm pushing them along at exhaust level... and while the pavement is quite wide often there's traffic blocking the roads and it's queuing at their level. (Participant 41)

As can be seen, throughout the interviews air pollution was primarily interpreted as a threat to the health of children; an unsurprising characteristic given that participants were selected on the basis of their school run journey. Yet, this is relevant because the meaning attached to a given encounter has an influence on the secondary appraisal; what individuals think they can do to manage the stressor and its associated distress [279]. Of the 41 that defined air pollution as a 'threat', 63% (n=26) believed they had the capacity to make behavioural adjustments sufficient to mitigate it. For these, this balance between primary and secondary appraisal led to various attempts at problem-focused coping.

9.4.2 Problem-focused Coping

When a situation is deemed to be stressful, requiring efforts to manage or resolve it, coping actions are enacted [265] In this regard, 26 participants altered their behaviour as a result of the monitor data. The main change attempted was to try alternate routes, away from the main roads; 16 attempted this. 6 participants also used their car less, while 4 reported asking people to turn off their engines if seen idling outside school:

I think that's one thing that's come out of using the sensor. Almost every day I've had to ask someone to turn off their engine. The thing that's really... I've never been the sort of person to ask a stranger to do something because I feel like it's a bit presumptuous and I don't like being... I just don't like telling people what to do, I'm not a very confrontational person. But I feel like if I don't, I don't know how long they're going to sit there idling their car and I'm looking at the monitor and thinking 'it's getting red, it's red!', and we're breathing in all the particles... so since having the monitor it's made me that little bit... it's given me the courage to ask people to turn their engines off. (Participant 7)

I am trying to use the car less. I probably would have driven probably four times a week to school... but we're trying not to drive at all now. We maybe drive once a week. It has changed quite drastically for us, so that we leave the car at home. (Participant 14)

Me and one of my friends have consciously not walked along [the main road] as much to get to school and back, so we'll go right round the back streets a bit more. (Participant 34)

Upon enacting these changes, participants believed that improvements in the quality of air would be visible, thereby easing their stress. It is here where, for the 26 who attempted problem-solving strategies, early engagement with the monitor is characterised by a very specific secondary appraisal; one reliant on the assumption that individuals can alter their situation and minimise the 'threat' envisaged.

Air pollution in urban areas is, however, complicated, entailing dynamic and complex interactions between natural and anthropogenic environmental parameters. 20 of the 26 that attempted problem-focused coping experienced this complexity, with the monitoring data recording minimal changes to their exposure despite the behavioural changes adopted:

It just felt like every route was bad or good depending on the day. I didn't feel like there was a solution. And we literally only have two routes, so there's not really many options. (Participant 6)

Me changing my route at this specific time might work this week, but next week I might get different readings. It might be a bit of a, not a waste of your time, but a waste of your mental capacity trying to actively dodge things... One thing that these apps show you is that it might not matter where you are. (Participant 12)

I hoped it would change because the routes are pretty bad, and if there were clear differences – if one was green, one was yellow and one was red – then I would definitely take one over the other, but they've been alternating. So you get ones higher on some days and others higher on other days. It's hard to know, really. (Participant 22)

The 15 participants who perceived air pollution as a 'threat' but did not act moved straight onto coping efforts associated with emotion-focused coping (see below), but those who attempted behavioural changes moved back into the stage of 'cognitive reappraisal'. Here, the effect of any changes made were re-evaluated to see if they had addressed the initial stressful 'threat' perception.

9.4.3 Cognitive Reappraisal: Powerlessness and Heightened Threat

Participants who had changed their behaviour entered the reappraisal stage of coping expecting to see a difference in the levels of air pollution encountered. While most continued with their new pattern of behaviour for the duration of the study, the expected improvements tended not to be reflected in the monitoring data. As such, when participants reappraised the situation following their behaviour changes, the over-riding feeling was very different to that felt during the initial appraisal. They now started to feel powerless:

I felt really, really, really rubbish. Verging on depressed. Questioning my life choices. Really sad and powerless because we're not in a position where we can move house or just buy an electric car. We're just not in that financial position. So, powerless, upset and ignorant as well. 'How come I didn't know this before?'. 'Why is it not on the weather forecast every day?'. (Participant 4)

Something that's become quite apparent is that you can't actually avoid the pollution. And that's it. You can't free my or the children that live in my community from the air pollution. They live too close to dirty roads. It's a bit depressing really. (Participant 17)

I was just thinking 'I want to move' actually. I was seeing the readings outside the house and you think 'well, I still have to take the kids to school'. You feel like there's no escape from it. (Participant 26)

I suppose it's a powerlessness. I know that [the road to school] is awful and that's where I walk my children to twice a day and that's where they go to school, and on a hot day they have their windows open and it's all just going in. From my point of view it's been pretty bad because it's confirmed that 'oh no, it's really bad and I knew it was really bad, and now I know it's definitely bad'. So yeah, a powerlessness on the day to day level. (Participant 29)

At the point of reappraisal, the same formula holds as for an initial appraisal; the difference between 'primary' and 'secondary' appraisal influences the degree of 'threat' felt. As such, at this point the monitors had not only served to reveal how poor the air quality on the school run was, thereby increasing awareness about the already-present concern for their children's health, but also demonstrated that their ability to avoid it – either through behavioural changes or seeking refuge in perceived 'sanctuary spaces' (see below) – was constrained by factors beyond individual agency. As a result, the definition of their encounter with air pollution data did not change from the 'threat' designation, but heightened it:

I wouldn't say it's kept me up at night, but there were times when I'd wake up at night and I'd be thinking about it... it's kind of taking over. I'm really thinking about this all the time. (Participant 1)

I think it's even worse than I thought it was, which is really scary. Really scary. (Participant 18)

I think I'm more concerned now, if I'm honest. I would say very concerned. It's pretty bad at times. (Participant 22)

This response was common across the sample of participants. After using the monitors, 44 of the 45 participants reported concern with the levels of air pollution on the school run, with just over 70% (n=32) being either 'extremely concerned' or 'very concerned'. 40% (n=18) of participants thought it was more concerning than originally thought, while 18% (n=8) experienced a decrease but still retained some degree of concern. The 4 participants who thought air pollution was 'no longer a problem' are not all mirrored in numbers for the 'unconcerned' category because 3 noted that, while they now saw their school run as pollution-free, they were still concerned about other children on other routes.

9.4.4 Emotion-focused Coping: Resignation

As the feelings of powerlessness became increasingly embedded with each cycle of attempted behavioural change, the appraisal-reappraisal feedback loop tended to result in feelings of resignation. This did not appear to supplant problem-focused efforts, where they were attempted, but were instead experienced alongside them, according with Lazarus' [274] call for the two to be viewed together. Other expressions thematically related to this category were reported, including sadness, helplessness and acceptance, but the over-riding form of emotion-focused coping communicated at the conclusion of the study was this notion of resignation:

I was comparing it to somebody to Brexit, where you might have been really passionate at the start of Brexit, but by now you're just like 'I don't care anymore'. With this, it's kind of like 'well, I really want to make some good choices but, actually, everything is bad; there's nothing I can do'. So, that's been a bit of a shame (Participant 3)

I think initially I was more frustrated and scared but as it goes on you get used to what's going on and you're not surprised by what's happening, so I guess the feelings dissipate a little bit. That's probably what happened. 'Oh, there it is again. Yeah, that's what I expected'. (Participant 11)

> *You get this data, you go 'okay', then it just makes you feel a bit worse.* (Participant 12)

I became resigned. I am only one ant in the grand scheme of things and, really, what can I do to change anything? (Participant 18)

I felt sad and a bit helpless because at the beginning we were getting some green readings and I thought it would maybe never turn green on this road. And there was a couple of school runs that we did, earlier, that were green, and I felt a little glimmer of hope like 'oh, this isn't as bad as I thought it was'. But then, actually quite quickly it turned to where I can't actually remember the last time I saw a green reading for it. (Participant 21)

Such expressions of resignation were not limited to those pursuing behavioural adjustments, but were also reported by many of those that did not make changes. Here, a dovetailing of the various coping efforts can be witnessed, where use of personal air quality monitors eventually resulted in resignation irrespective of whether problem-focused efforts had been made at some point or not. This occurred for two reasons.

1. First, as noted above, avoiding air pollution in densely populated urban areas, particularly at peak times of travel, is complicated. Distance-decay gradients differ depending on wind direction [280, 281]; upwind, particulate concentrations can fall to near background levels within 200m, but downwind, concentrations do not reach background levels until 300-500m. In some studies, this was extended to 800m for ultrafine particles [282] and 1500m for NO_2 [281]. This is further complicated by the basis of these figures on patterns of motorway pollution; they do not account for settings where other sources of emissions are in close proximity, which is the reality of urban areas.

2. Second, the context in which the technology was used had a bearing on the options available for behaviour change. 75% (n=34) of participants described their feelings of resignation in relation to real-world circumstances that served to inhibit their ability to alter behaviour in ways they thought would be of benefit. The two primary constraints mentioned pertained to time, as manifest through responsibilities to school, work or family, and space, including a lack of route alternatives or availability or safe, efficient and affordable transport options. For those who did not make behavioural changes, these constraints exerted an absolute constraint, whereas for those who did, they served to limit the range of options available:

   I've tried... but there is only a couple of routes we can take to school so you can't do too much. I looked at getting the bus and walking to work and back but I've got

such a small time period to get back from work, pick the kids up, I just can't do it. There aren't enough hours in the day for me to do it all. (Participant 10)

Some days because I have two – one is in nursery not far from [city ward] *– I can't physically get one and then the other one and walk, so I have to drive. And what I've done is drive halfway to school and then we'll walk through the woods and we'll walk back through the woods, get in the car and then drive to the other one.* (Participant 11)

Cycling, I really enjoy it but I'm also a bit scared of it as well because it's not very well set up for it. We have seats for the little ones that we use on holiday... but I would never take them on a road in one. I would admit... if the cycle lanes were segregated it would be so much better. We would cycle loads more. I wish I could cycle more than I do, but I don't feel like it's a safe option necessarily. It's too dangerous, it's really dangerous. (Participant 13)

There's no way... whichever way we go there's a busy road. And there's no route that can go down the side streets or anything. To get to a side road you have to go down an even busier road. It's tricky. (Participant 15)

As can be seen, at this point the more structural constraints of the social environment are coming to bear on participants. Resulting in the emotion-focused response of resignation among both major groups - those who attempted behavioural changes and those who did not – this brings into sharp focus the limits of individual agency within a socio-structural context unconducive to change.

9.4.5 General Beliefs: Uncomfortable Awareness and Understanding

Although resignation is a negative response, it is important to note that participants also described the use of the monitors in positive – albeit qualified – terms. This was because of the effect exerted on their general and specific beliefs about air pollution. Participants widely noted becoming more sensitive to sources of air pollution in the immediate vicinity of the school run, and aware that air pollution in a given locale can originate from much further afield. Many also reported being more sensitive to news stories on the topic and of air pollution being an issue elsewhere, such as in cities or on journeys unrelated to the school run. Taken together, this amounted to an increasing awareness of air pollution both narrowly and more generally; a response deemed positive for two main reasons. The first was intrinsic, with participants appreciating the data for no other reason than to know. Here, positivity was derived from the way in which the monitors revealed an issue previously hidden from immediate view. The second was extrinsic, with many seeing the data as being able to imbue their claims with credibility should they approach others about pursuing remedial measures, such as school managers and local politicians. However, while deemed positive, this awareness was also perceived as simultaneously uncomfortable, especially when coupled with the realisation that structural and environmental factors largely beyond individual control were inhibiting their ability to respond effectively to the 'threat' of air pollution:

My experience was positive and negative; a bit of both. So, positive in my own head, but also negative in my own head as well because it makes you aware of something that isn't very nice and something that you don't have much control over. Positive because I feel like there are some things I can do about it. Feeling positive if I cycle and negative if I go in the car, feeling guilty. Feeling more cross with other people but then recognising that I

don't know why people are in their cars; there could be multiple different reasons. Being cross with the council or the government, but knowing that actually the council can't do much about it because they haven't got any money. So positives and negatives on all levels, really. (Participant 17)

It was positive because it's always positive to learn something. And it was negative in that it was worse than I was expecting. But it was positive that you're more aware and that you're thinking about it more. Ignorance is bliss isn't it; you can pretend it's not happening when you don't know about it. (Participant 20)

It's positive in the sense that it's given me a better awareness of air quality and made me think I should think in different ways. Negative, just in the sense of like I say, it makes you aware that there is bad air around school and it's just a bit sad. It would have been really positive if it had been really green there and we could have thought 'oh, this is good', but it wasn't. (Participant 34)

Much like that described by [33], there is an important distinction to be made between awareness and understanding. While awareness denotes an increasing sensitivity to air pollution issues and its association with certain sources, understanding refers to specific knowledge of air pollutants, origins and their impact on human health. The monitors proved to be highly effective at increasing the former, but less effective at improving the latter. As Participant 18 noted, 'it has made me more aware, but I also now know how little I know'; a distinction echoed by Participant 37 who, using slightly different language, explained that 'I'm more aware but not educated'. This difference was present throughout the sample. Compared to responses prior to using the monitor, over half (n=24) reported 'no change' in understanding, 44% (n=20) a minor increase and 1 a decrease as they became aware of the complexity of the issue. Taken together, at the conclusion of the study 80% (n=36) of participants categorised their understanding of air pollution as either 'none' or 'slight'. As such, the monitors were effective at raising awareness and sensitising participants to air pollution being an issue, but not so effective at providing detail on air pollution in relation to its make-up, origins and effects on human health.

9.4.6 Specific Beliefs: The Disruption of Perceived Sanctuary

While the monitors exerted a more general influence on participant awareness of air pollution as an issue, they also affected more specific beliefs. The two mainly spoken of by participants pertained to the notion of sanctuary; one relating to indoor space and the other to outdoor. Taking the first as a point of departure, almost half of the sample (n=19) experienced a form of surprise when the monitors reported poor air quality in the home. This belief lay dormant and unacknowledged until revealed and then disrupted by the data. Echoing the 'home-as-haven' concept, where 'private' and 'public' space tend to be positioned along the respective lines of security and insecurity [283], air pollution is here believed to be a phenomenon existing outside of residential space:

I just keep looking in the house and I was going 'oh my god, this is in our own house! What am I doing to everybody?'. That alarmed me. (Participant 5)

It's definitely changed the way I view my house as a safe environment. I think as a parent you think 'okay, we're home, we're safe, it's all fine'. Well I don't think I can believe that anymore. (Participant 9)

There was this moment where it was really high in the sitting room, and I've got the windows open and I'm checking it and it's high and I'm thinking 'what's going on here?' (Participant 13)

I would consider getting an air purifier in my house because I didn't realise how bad it was. That shocked me. (Participant 14)

Many encountered high levels when cooking meals either side of the school run, or around the time family members were getting ready in the morning. This is because indoor NO_2 and particulate matter tend to originate from domestic appliances which burn carbon containing fuels, such as boilers, heaters, fires, stoves and ovens, with VOCs emanating from cleaning and personal care products, building materials and household consumer goods, such as carpets, laminate furniture, air fresheners and cleaning products (Public Health England, 2018). However, this was largely unknown to participants; a feature reported elsewhere, with one survey of 2,000 adults noting that 46% could not detail any causes of indoor air pollution and only 36% were aware of its effects on health ([284**?**]). The reasons for this are not clear, but it may be because research on indoor air pollution is overshadowed by its outdoor counterpart. Indeed, this situation caused the Royal College of Paediatrics and Child Health (2018: 1; 2019) to label indoor air pollution a 'Cinderella subject', by virtue of its marginalisation, and initiate a wide-ranging study on its intersection with child health. This could have subsequent consequences for media coverage on indoor air pollution, which is also seen to eschew information on its human health effects (see Mayer, 2012). Whatever the reason, the 'home-as-haven' idea rests on this absence of knowledge, which is why the monitoring data served to destabilise it, precipitating a surprise response and a subsequent change in individual beliefs.

This bears similarity to the second belief demonstrated, where almost half of the participants (n=22) reported surprise at the levels of air pollution encountered in green spaces. Exposing an important caveat to the 'home-as-haven' concept, where not all outdoor spaces are perceived as equally threatening (see [285]), this 'green-is-clean' assumption nevertheless suggests a belief that trees and plants can remove air pollution at a rate able to mitigate levels harmful to human health. Again, it is only in the presence of the monitoring data that this belief becomes perceptible and, in much the same way as the 'home-as-haven' idea, undermined:

I was really surprised when we went down to the park. I was expecting that to be fine... it's all surrounded by trees and it was still pretty high. I was thinking 'oh gosh, we can't escape this!' (Participant 2)

We always walk through the woods. It's safer for the children and it's more interesting, but also there's that idea that there's a bit of a green barrier. But we would be in the middle of the woods and it would still be quite high. I think I was expecting to find areas of sanctuary from it, but I realised that actually on some days there isn't, you know? It's everywhere. So that was surprising to me. (Participant 13)

Because our school is set back from the road, it's amongst a lot of greenery and you think you know the school run is bad but you think that once you're amongst that greenery that somehow that helps but, I mean, honestly... We've been campaigning for a green wall at [school name]. They've put in what we could afford. Is it good though? Because now we're thinking 'oh my goodness, is that going to make any difference whatsoever?'. (Participant 21)

It was quite concerning because I didn't think it would be so bad. Around here it's quite leafy and green, isn't it? Even with the main road I thought 'well, there's trees all along it we'll probably be alright'. But it was worse than I expected. (Participant 38)

Considering that people who live in areas with more and/or larger street trees report better health perception [286], and Sheffield boasts more trees per person than any other city in Europe (Styles, 2011), the presence of this belief is somewhat understandable. Buttressed by national news stories noting the mitigating effect of tree planting on climate change (see [287, 288]), these beliefs are reflected in a growing body of research demonstrating a relationship between positive experiences and time spent in greener environments. For instance, it is associated with the prevention and mitigation of stress, anxiety and depression for both adults and children ([289–292]), particularly in urban areas ([293–295]). There are also case-specific features to account for. Sheffield has, for almost half a decade now, been a site of well-publicised tension over the city council's felling of street trees. Without recounting the situation in detail (see Heydon, forthcoming), the media coverage following the initial 'dawn raid' by police on elderly protestors, and subsequent high-profile advocacy campaigns by community groups, does mean Sheffield citizens have been exposed to a disproportionate level of information relating to the benefits of street trees. Many of the participants mentioned this ongoing situation.

Whatever the specific origin of this 'green-is-clean' belief, the monitors both reveal its presence and subsequently undermine it, again bringing the complexities of air pollution to bear on participant assumptions. Trees can remove gaseous air pollution through uptake ([296, 297], and act as a barrier by retaining particles on the plant surface [298], but they can also have an adverse effect on air quality. Not only can certain species emit volatile organic compounds [299], but vegetation is of little benefit for reducing nitrogen dioxide in urban areas, can exacerbate the build-up of pollution in street canyons by reducing air flow, and is better at redistributing air pollution than removing it (National Institute for Health and Care Excellence [65, 300]). The monitors served to alert participants to the 'green-is-clean' belief before disrupting it, making them attentive to this more complicated reality and contributing to their increased awareness of the air pollution issue at hand.

9.5 Discussion

There are several ways in which personal air quality monitors influence individual thought and action around environmental risk. The technology works to alter the behaviour of users by making a previously imperceptible risk visible. On becoming visible, preconceptions about the "threat" it poses to what is "meaningful", which in this case is the health of children, are confirmed. This intersects with the idea that individual action can manage such a "threat", providing the initial impetus to consider undertaking changes aimed at minimising the exposure of children to air pollution on the school run. To a large extent, this confirms the findings of existing studies, where individual attempts at avoiding or mitigating air pollution have also been witnessed in users of similar technology (Bales et al. 2019; Wong-Parodi et al. 2018; Zappi et al. 2012). Where the findings diverge is in relation to the factors implicated in, and the influences acting upon, the decision-making pathways underpinning this decision-making process, a divergence that adds to existing understandings in three key respects.

First, the findings show that sensor technology does not generate a simple binary response among users—behavioural change [34, 264] or not [33]—but instead shows it to be capable of producing both in the same user over the same period. Over time, as attempted behavioural changes fail to produce the improvements in exposure expected, and the range of options available for pursuing effective change starts to narrow, negative feelings can colour users' increased awareness of air pollution with discomfort and risk eliciting an eventual inclination towards inaction. That said, it is not difficult to see how this relationship could also move the other way, with users settling on emotion-focused coping at the outset but pursuing more problem-focused efforts as their circumstances change (e.g. if air pollution in a region is less pervasive, they move to another house, or their children progress to more senior schools that are further away).

Second, monitor use is capable of altering beliefs about air pollution independent of behavioural change. This was seen in relation to the ability of monitors to reveal and subsequently disrupt misconceptions about indoor and outdoor "sanctuary spaces". Further, alerting users to the pervasiveness of air pollution both generally and specifically, this exerted influence at the point of reappraisals by introducing a perception of inescapability into user beliefs; a reaction intrinsically linked to the reported feelings of powerlessness. This holds relevance because existing literature has given disproportionate priority to the influence of monitors on behavioural change. Yet, their ability to alter beliefs is at least as important because such cognitive configurations are heavily implicated in behaviour change. As Lazarus and Folkman [272] take care to note, beliefs are "pre-existing notions about reality which serve as a perceptual lens... determining what is fact, that is, "how things are" in the environment, and they shape the understanding of its meaning". With perceptions acting as a filter through which external reality is experienced, further exploring the effect of personal monitors on this aspect of cognition is a key to understanding their influence on human behaviour.

Third, existing studies conceptualise monitor use in terms of a simple dualistic relationship between technology and individual. However, as can be seen here, it is more accurate to conceive of the relationship as tripartite: between monitor, individual and socio-structural context. Indeed, the extent to which behaviour change continues over time is largely determined not by the agency of individuals, but by the various socio-structural circumstances with which they are entwined. As noted above, the main difference between the two broad groups of participants—those who pursued change from the outset and those who did not—was the point at which these circumstances converged to produce strategy asphyxiation during secondary appraisal. The associated feelings of powerlessness and resignation cannot therefore be said to originate in the monitoring technology itself, but in the social structure that limits what users can do with the information provided by it. Existing literature has highlighted the limits personal efforts have on either the degree of exposure or level of emissions present in a given area, largely because of their complications and partial efficacy when compared with measures targeting emissions at source [301], but these are different to the temporal and spatial constraints reported by participants here. As such, this study draws attention to the importance of external social factors when determining internal human responses to monitoring data. Indeed, it is for this reason that, when considering the influence of personal monitoring technology on decision-making, socio-structural context cannot be seen as peripheral to the process, but integral to it.

9.6 Conclusion

Taken together, the study has demonstrated that personal environment monitors can play a role in protecting children from air pollution on the school run. They are effective at raising awareness about air pollution, disrupting misconceptions about where it does and does not occur, and encouraging users to change their behaviour in an attempt to mitigate and manage the risks. However, their ability to produce lasting and effective behaviour change is stymied by socio-structural constraints. As such, it is only with top-down support aimed at tackling air pollution at source that this bottom-up technology will attain its full potential.

This has several implications for advancing personal environment monitors and for future research on their social consequences, three of which will be emphasised here. With regard to the former, the social dimension of the technology itself requires further development. Currently, the monitors mistakenly represent public issues as private problems. The more this technology can encourage cooperation between interested individuals then the likelihood for effective collective action—that is, a social response to social-structural constraints—is magnified. Similarly, the data collected could be integrated with projects aimed at collating this data and making it publicly available, an approach already underway at the Urban Flows Observatory at the University of Sheffield (2018). The technology also needs to improve its educational dimension, in terms of the accessibility, in order to capitalise on its effective awareness-raising role. With regard to the latter, further research is needed into the long-term effects of this technology not only on beliefs and behaviours, but also on how decision-making patterns differ between populations embedded in a range of socio-structural circumstances. Only then can a full appreciation of the transformative potential of this technology for a variety of user groups be fully understood.

9.7 Contribution

R.C. (Rohit Chakraborty):

- **Conceptualization:** I played a foundational role in conceptualizing the research, framing the key research questions, and determining the study's overarching direction and objectives.
- **Sensor Deployment:** I was directly involved in the deployment of air quality sensors, ensuring their calibration for accurate data capture. My involvement ensured the reliability and precision of the data collected.
- **Writing – Drafting and Editing:** I was a co-contributor to both the drafting and editing of the manuscript. My efforts ensured the clear articulation of our research findings through the sensor driven along with the surveys and interview data, methodologies, and conclusions, maintaining academic rigor and coherence throughout the paper.
- **Data Analysis:** I took charge of the data analysis, applying rigorous methods to interpret the collected data both qualitative (in the paper) and quantitative. My expertise ensured that patterns were deduced accurately, insights were extracted, and the results were presented in a meaningful manner.

- **Discussions and Interpretation:** I was actively involved in discussions around the data, its implications, and the broader context of air quality and citizen engagement. My insights and expertise played a pivotal role in shaping the study's conclusions and recommendations.
- **Methodology:** I contributed significantly to designing the research methodology, ensuring our approaches were robust, appropriate, and tailored to address our research objectives effectively.
- **Collaboration and Coordination:** As one of the two co-authors, I collaborated closely with my counterpart, ensuring our combined expertise and efforts were harmoniously integrated into the final manuscript. Our joint efforts ensured the paper's quality and impact.

Given the paper's focus on exploring the influence of portable air quality sensors on user behavior, my involvement was comprehensive, spanning from the initial stages of conceptualization to the final stages of manuscript preparation and review. My dedication and expertise were instrumental in realizing the research objectives and ensuring the study's success.

Chapter 10

Wood Burning Stoves, Participatory Sensing and 'Cold Stark Data'

Abstract

This study explores whether participatory sensing technology, namely air quality monitors, influences the perceptions and behaviours of wood burning stove users when they are made aware of their exposure to indoor emissions. Situated in the literature on participatory sensing, which is an approach to citizen science where lay persons use monitoring equipment to analyse various issues, and that on public understandings of air pollution, this study uses coping theory to explore the cognitive and behavioural implications of engagement with indoor air quality data. Drawing on interview data from stove users equipped with air quality monitors, the results suggest that quantitative representations of air pollution data, such as air quality indexes, can be difficult to interpret by lay persons. The absence of meaning inherent to these forms of display encourage a search for meaning elsewhere. In these situations, participatory sensing technologies act to pull wider preconceptions of indoor air pollution into the process by which monitoring data is interpreted. As these preconceptions hold stoves in a positive light, while concurrently painting other sources of air pollution as harmless, the perceived risks posed by indoor stove emissions are minimised. This renders air pollution data less persuasive and, in turn, less successful at changing the perceptions and behaviours of wood burning stove users. On this basis, it is recommended that future research into air pollution monitoring and participatory sensing prioritise the roles of data presentation and wider social constructions of risk in influencing perceptions and behaviour change.

10.1 Introduction

One of the most harmful components of air pollution is particulate matter (PM). Particles with an aerodynamic diameter equal to 2.5 µm or less ($PM_{2.5}$) can move into every organ in the body, being linked with seven million deaths per year globally [17]. It heightens the risk of developing a host of illnesses ranging respiratory infections through to dementia, strokes, and Parkinson's disease [62]. Much of the research into PM emissions focuses on those generated by industry and traffic [302, 303]. However, in the United Kingdom (UK) the primary source for $PM_{2.5}$ is the domestic burning of wood and coal for heating. Residential stoves are responsible for 38% of ambient $PM_{2.5}$ pollution nationally, being generated by just 8% of the population [304]. As such, the popularity of wood burning residential stoves is a pressing issue, particularly for those in urban areas.

While the outdoor emissions generated by these stoves have been well-documented, studies also show that they contribute to indoor air pollution irrespective of design. PM originates from older stoves [305–307], which are without emissions control features and lack approval by national environment regulators. They are also produced by newer stoves, which are equipped with such features or carry a marker of regulatory approval [56, 308, 309]. Even locations that see older stoves replaced by newer models confirm the continued presence of indoor emissions [310, 311]. Such pollutants have been found to result from leakages [312], but a larger body of evidence associates indoor PM with the opening of the stove door during lighting or periodic refuelling [308, 310, 311, 313]. Chakraborty et al. [56] refer to this as 'flooding', where plumes of PM enter the room when the stove door is opened and linger for at least the period in which the stove is in use. The present study sought to understand the ways in which people interpret and act upon air quality information revealing this reality, thus providing insight into how new sensing technologies may provide opportunities for stove users to manage their exposure to PM emissions in the home.

Attempts at making the levels and risks of outdoor air pollution visible have been ongoing for fifty years. Much of the early work in the UK focused on the operation of smoke control areas, with several studies in the 1970s using surveys to investigate public responses to air pollution on a broad scale [314–317]. According to Bickerstaff and Walker [316], this, along with its associated literature on public responses to environmental risk, was based overwhelmingly on a 'deficit model' of public understandings of scientific information. Under this approach, the divergence between scientifically defined and publicly understood environmental risk is framed in terms of ignorance and irrationality on behalf of the latter [318, 319]. By contrast, the turn of the century saw a more sociological literature emerge that emphasised the ways in which the public actively negotiate scientific information; through a social process of reflexive interpretation and critical evaluation, instead of passive assimilation restricted to the level of the individual [320–324]. As Cupples et al. [325] explain, compared to professional scientists,

> the public, which is the target of this information, processes it in a more random and imprecise way, drawing also on lay knowledges and embodied experiences... cultural circumstances are not external to scientific knowledges but are, in fact, the sites on which scientific knowledges circulate...

In accordance with this, sociological research has increasingly highlighted a range of psychological, social, geographic, and cultural influences on public perceptions of and reactions to air quality information. Direct experience provides much of the basis for these understandings [321], emphasizing the primary role undertaken by the senses in risk perception [326, 327]. However, this is mediated by social constructions of place, where sense perception is tied up with socio-cultural commitments to location and community memory [318, 328, 329]. For instance, a 'halo effect' has been found to exist at the level of homes [330], neighbourhoods [320, 331] and public parks [332]. This is where positively perceived spaces are seen to provide 'sanctuary' from air pollution relative to other, more negatively perceived areas and irrespective of actual levels of air pollution. Also implicated is the trustworthiness of the institutions responsible for regulating air quality [333], gender, where women with children have been found to be more aware of air pollution than men [334], and the cultural meanings attached to air polluting activities [335].

Much of the literature on public understandings of air pollution focuses on outdoor emissions and the technology through which air quality information is provided, such as Ceefax, weather information, and documentaries [319, 320, 334]. Similarly, it has only recently focused attention on technologies associated with participatory research [336]. At least two decades old, participatory research is a form of citizen science that involves non-scientific actors in scientific study [337]. Boso et al. [336] describe 'participatory sensing' as a 'new stage' in this approach, based on the idea that technology now permits members of the public to 'objectively record, analyze, and discover a variety of patterns concerning important issues in their lives, such as health, environmental quality, and traffic'. According to Goldman et al. [338], this facilitates a new collective ability where people can participate in examining aspects of their every day that 'before were invisible'. Much of this literature focuses on technological efficacy, or what the sensors can reveal about hitherto unseen aspects of the environment [56], but few studies have evaluated its cognitive and behavioural implications [339]. Those that do exist illustrate how engagement with air pollution sensors can elicit enjoyment and surprise in users [263, 340], increased awareness [336], intense emotional reactions [334], and resignation [332]. Sensor use has also been found to encourage various behavioural changes depending on the situation in which they are used, ranging from inaction on behaviours contributing to outdoor emissions [334, 336], the closure of windows and alteration of stove management practices relating to residential stove use [263, 341], and alteration of the school run route in response to traffic emission data [332].

This study addresses several gaps in knowledge left untouched by these literatures. First, accounts of sensor data provoking a given response are largely atheoretical. Studies tend to focus on the outcome of data engagement – behaviour change or not – as opposed to the personal, situational and contextual factors acting upon the encounter to produce said outcome. By contrast, this research draws upon Lazarus and Folkman's [272] coping theory to draw out the decision-making process implicated in these responses, thereby offering a fuller understanding of how people engage with participatory sensing technologies. Second, there is a lack of existing literature on whether perceptions of air pollution data mirror actual levels of indoor exposure [330]. Following Boso et al. [336], this will address the question of whether the 'home halo' effect accurately reflects indoor air pollution levels. Finally, the literature on public understandings of air pollution and that on participatory sensing have only recently started to speak to one another [336]. This study aims to further bridge this gap, establishing the processes by which wider social constructs exert influence on individual perceptions of sensor data.

In addressing these gaps, the study contributes to knowledge on the transformative potential of participatory sensing in the context of indoor air pollution. It illustrates that the predominant focus on behavioural responses to monitoring technology comes at the expense of cognitive processes acting to mediate behaviour. By challenging this approach, the study demonstrates how features of data presentation, including quantification and numeric threshold limits, are experienced by users as unrelatable and ambiguous. This encourages a search for meaning elsewhere, pulling wider social constructions of air polluting behaviours into the cognitive space and allowing them to influence interpretations of the sensor data. To attend to these complexities, the study shows how research on cognitive appraisal, public responses to air pollution data and participatory sensing can draw more deeply from one another and, in doing so, explore these intersections. Such an agenda is critical if the potential for participatory sensing technologies to inform and encourage behaviour change is to be realised in future.

10.1.1 Theoreticial Lens

The process-based model of coping explains how a person evaluates and responds to potentially stressful encounters. Developed by Lazarus and Folkman [272], it is 'process-based' because instead of coping being conceived as a personality trait it is understood to result from a recursive relationship between person and environment. Under this approach, 'coping' refers to the 'thoughts and behaviours used to manage the internal and external demands of situations that are appraised as stressful' [342]. The model defines 'internal' demands as stemming from beliefs and commitments, and 'external' demands as relating to the features of the circumstances in question. Following this, the extent to which a given event is defined as 'stressful' is determined by a combination of factors relating to the person and the situation [272].

Proceeding from the need to understand cognitive processes underpinning participatory sensing, this study uses coping theory to understand how adults respond to monitoring data on indoor emissions from residential stoves. Almost four decades since its publication, coping theory remains key to understanding responses to environmental stimuli across multiple disciplines [266]. Originally taking cue from the literature on wearable healthcare devices, much of which is concerned with the 'infusion' of technology into a person's life [271, 343], this study replicates the use of coping theory in other participatory sensing studies [332]. Doing so addresses Irwin et al.'s [318] early call for a 'contextual approach [to engagement with air quality information] which is sensitive to the processes through which people make sense of their immediate environment'. By drawing attention to the cognitive process triggered by an environmental encounter, coping theory sensitises analyses to internal and external influences upon people on the way to a given behavioural outcome. In doing so, the study provides a more nuanced account of those engaged in participatory sensing when compared to the largely atheoretical approach adopted by existing scholarship. Furthermore, replicating the approach undertaken in prior studies allows for comparisons to be made between different user groups, furthering knowledge on variable responses to sensor use. In this way, the study directly responds to Hubbell et al.'s [339] request for future research into how different groups interpret, communicate and respond to air pollution data. According to the theory, coping behaviour results from an initial two-part appraisal of a person's encounter with environmental stimuli. A 'primary appraisal' occurs when a situation is first evaluated as exerting an influence on someone's well-being, with the outcome being considered positive, irrelevant or stressful [266]. Here,

what is deemed to be at stake influences which of these categories the encounter falls into. Stress may result from the interpretation of the situation as 'harmful', where some damage or loss to the person has already occurred, or as a 'threat', which involves anticipated harms or losses [272]. Also implicated at this point is a 'secondary appraisal', which entails a person's evaluation of their control over the stressor to determine their ability to manage or alleviate its consequences. Despite having the labels 'primary' and 'secondary' these forms of appraisal are not sequential. As Folkman [265] clarifies:

> When that which is at stake is meaningful and coping resources are judged less than adequate for managing the demands of the situation, psychological stress is experienced. The greater the imbalance, the greater the stress.

It is the outcome of this two-part appraisal that influences subsequent emotions, coping strategies and outcomes [266]. Put another way, this initial stage of 'cognitive appraisal', where an individual encounters a given stimuli, interprets it as stressful or not and decides whether it can be managed, acts as the precursor to subsequent mental and behavioural adaptations to the situation. The coping efforts triggered by this prior stage of appraisal can take many forms, but they are associated with two different but related categories: problem-focused and emotion-focused coping efforts. The former of these outcomes refers to attempts at managing or mitigating the source of stress. Speaking to proactive efforts at altering the situation, this includes – among others – attempts at removing or reducing obstacles, attaining new skills, seeking assistance or planning for action towards these efforts [272]. By contrast, emotion-focused coping refers to internal attempts at mitigating the mental and emotional distress elicited by a stressful encounter, including redefinitions of the situation, denials or acceptance (ibid). Although different, these categories are not wholly independent from one another and to 'set them up as competitive is to distort the way coping actually works' [344].

Following these two stages of cognitive appraisal followed by coping effort, people may then 'reappraise' the situation to determine whether their problem- or emotion- focused coping responses worked to mitigate the stress experienced. This third stage refers to a new process of appraisal following earlier iterations, converting what has up until now appeared to be a linear process into a circular one[272]. In essence, this acknowledges that an initial coping effort may work to alter the outcome of a subsequent appraisal. Taking this as the point of departure, the article now applies this model to those using air pollution sensors to detect indoor emissions from residential stoves.

10.2 Materials and methods

10.2.1 Research Design

The design of this study is exploratory and primarily qualitative, with most of the data being collected from three instruments administered in sequence: surveys, research diaries and interviews. Quantitative sensor data on the indoor emissions from residential stoves was collected for the purposes of a sister study [56], some of which is also presented here. With the primary aim of exploring the influence of personal exposure information on

perceptions of and behaviour towards indoor air pollution, the surveys were administered prior to receipt of the sensor technology. Participants were then asked to complete a research diary entry each time they used the stove over a four-week period. Each participant was then interviewed about their experiences, perceptions and behaviours at the conclusion of this period. The fieldwork was conducted between January and April 2020. The study was granted ethical approval by the Research Ethics Sub-Committee at the University of Nottingham. The Reference Number evidencing this approval is 1920-059-STAFF. Free, prior and informed consent was received by all participants prior to conducting the study.

10.2.2 Sample and Procedure

The sample consisted of thirty participants drawn from across the city of Sheffield in the north of England. The majority of participants were homeowners (n=28) and lived with one other adult (n=25). Two thirds of participants lived in the same household (n=20). Participation was limited to adults in households with a DEFRA-approved stove (n=19) or an open fire that was used according to DEFRA guidelines (n=1). A minority of households used a stove as the primary heat source (n=2). Participants were recruited through local community social media pages. Following the initial expression of interest, participants were sent an electronic copy of the survey to complete. Jisc Surveys was used for this purpose. Arrangements were then made to install the indoor and outdoor monitors. At the point of installation, participants were also given a tablet computer and instructed on how to access the sensor data. Information on the thresholds and colour coded data display was also provided. They were then asked to check the sensor data and complete the research diary each time the stove was used. Interviews were conducted after four weeks, with questions centring on participant mental and behavioural experiences over this time. Consistent with Heydon and Chakraborty [332], to facilitate reflection on aspects of change within this experience, specific survey responses given by each participant were also recalled during interviews. Interviews were conducted by an experienced social researcher. Methodological details relating to the sensor data are outlined in Chakraborty et al. [56].

10.2.3 Analysis

The qualitative data gathered from the surveys, research diaries and interviews were thematically analysed according to the approach outlined by Braun and Clark [345]. This was conducted on a rolling basis and justified on the grounds of theoretical saturation, where participant recruitment continues until no new or deviating data was being added to the categories of analysis [346]. This was disrupted somewhat by introduction of the Covid-19 lockdown across the UK on March 23rd 2020, but lockdown also coincided with the end of the UK stove season. As such, participant recruitment was already ceasing. The analysis allowed for both inductive and deductive codes to be generated, although those pertaining to the tenets of coping theory formed primary focus. Analysis of the qualitative data was conducted using NVivo, while the quantitative data was analysed using Microsoft Excel.

10.2.4 Limitations

The study exhibits several limitations. First, it draws its data from stove users within a relatively narrow geographic area, the majority of which use stoves as a secondary heat source. As such, the findings may not be generalisable to those using stoves under different circumstances, such as in rural areas or in situations where stoves are relied on as the primary heating source. Second, the study focuses on perspectives relating to indoor emissions, meaning different conclusions may be reached if perspectives on outdoor stove emissions were under investigation. Third and finally, several limitations are associated with the quantitative sensor data relating to variability in the research setting, due to it exploratory design and focus on real-world use [56].

10.3 Results

10.3.1 Two Appraisal Pathways, One Outcome: No Perceived Threat

As illustrated in Fig 10.1, two main appraisal pathways were undertaken by participants when engaging with the sensor data. Those in Pathway A, which comprised just under half of the participants (n=13), understood the sensor data as indicating a 'threat', to use the language of coping theory. They then made conscious behavioural adjustments to try and mitigate the perceived risk. By contrast, those in Pathway B, which comprised of just over half of the participants (n=17), did not perceive the indoor air quality data as indicating a threat and, as such, made no conscious behavioural adjustments following engagement. Each pathway will be examined in turn.

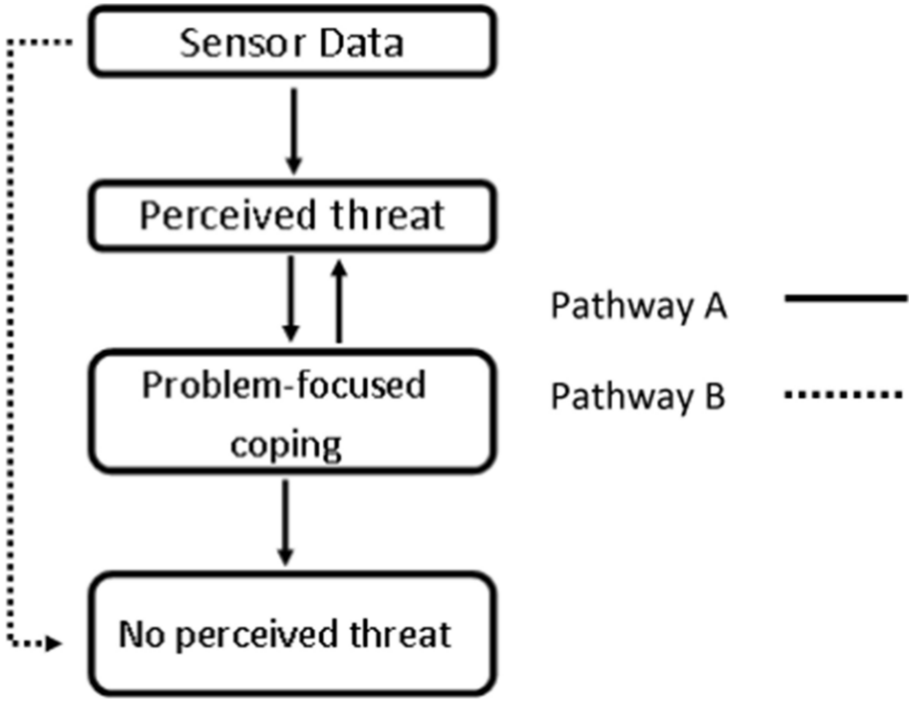

FIGURE 10.1: Two Main Cognitive Appraisal Pathways.

When an encounter is conceived as stressful, coping actions aimed at managing or mitigating it are enacted [272]. Those in Pathway A (n=13) altered their behaviour because of the emission peaks witnessed on the monitors at the point of stove lighting [56]. A variety of coping efforts were attempted by this group, most of which focused on stove management actions. These included opening the stove door less wide and less frequently (n=4), closing stove air vents (n=4), minimising refuelling (n=4), improving ventilation through opening doors and windows or purchasing an air purifier (n=3), avoiding stoking the fire (n=1), putting logs on more slowly (n=1) and striking the match inside the stove (n=1). Some made multiple changes at once in an attempt to reduce their exposure to the peaks. All were low-cost adjustments similar to those reported by sensor users in Boso et al. [336].

The coping efforts made by users in Pathway A led to reappraisal and, ultimately, served to assuage their concerns about the PM levels seen on the monitors. Compared to pre-sensor use, all but one saw their levels of concern stay the same or decrease through engagement with the data. Of the 13 in Pathway A, 5 finished the study 'not at all concerned', 5 'slightly concerned', 2 'very concerned' and 1 'concerned'. Only 1 of the 'very concerned' respondents experienced an increase in concern. This is why the cognitive appraisal process for those in Pathway A ends with no threat being perceived; the coping efforts are considered effective at reducing the peaks in indoor PM detailed on the monitors, requiring no reappraisal or further action:

> . . . if you're lighting it and it's not properly lit and it's all smouldering and you open the door, and opening the door creates a puff of air out. . . that's where you need to be careful. We saw it spike up a bit and come down. Having the sensors there, I was able to tune the time I had that open and get that better. I think it took me three days to get it right.

(Participant 1, interview)

> The more particulates were visible on lighting and then the first, maybe, half hour after that. Then once we were able to get the fire hot, really hot, it started to die down. Once it was started, the levels in particular didn't really concern me. It was just the initial stage.

(Participant 26, interview)

This absence of concern was more immediate for those following Pathway B (n=17), where participants perceived the same peaks as those in Pathway A but did not interpret them as a stressor. As a result, these sensor users did not pursue problem-focused coping efforts. As Participant 30 noted, "the readings went high when we first lit the fire but then they were very low. I actually feel much better about using it because of how low they are". Similarly:

> There was a spike in all particle readings just after lighting. All levels declining since lighting. Results don't seem too severe and enjoyment of the log burner is more important to me.
>
> (Participant 5, research diary)

> On the monitor you could tell when we opened and lit the stove, and there was an initial rise, but it was still within the sort of safe limits. Then, after, they gradually decreased again... so we began to feel confident that the stove is generally pretty safe for us.
>
> (Participant 7, interview)

Comparing reported levels pre- and post- monitor use, all 17 in Pathway B experienced the same or decreased feelings of concern about their stove following engagement with the data. Of the 17, 10 finished the four weeks 'not at all concerned' about the effects of their stove on indoor air quality, while the remaining 7 were only 'slightly concerned'. Combined with the results from Pathway A, the prevailing effect of sensor use across both pathways was to decrease concern about the indoor emissions from their residential stoves (see Fig 10.2). Engagement with sensor data therefore generated a combination of 'irrelevant' and 'benign-positive' appraisals, eliciting either an indifference towards or positive perception of stoves. As Lazarus and Folkman [272] note, such a combination is not unexpected; 'appraisals can be complex and mixed, depending on person factors and situational context'. As can be seen below, the intersection of these two spheres is heavily implicated in the decreasing concern reported.

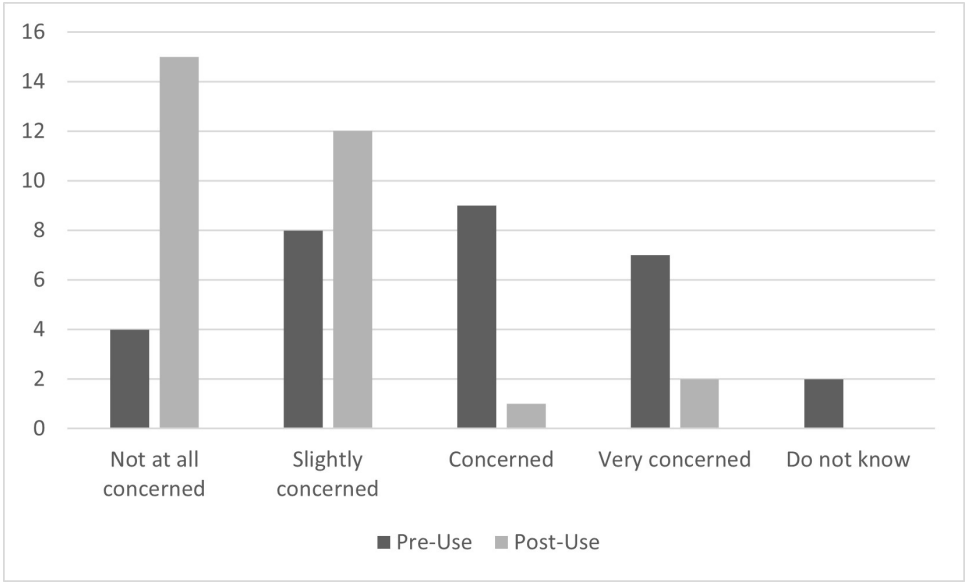

FIGURE 10.2: **Reported Concern about Indoor Air Pollution from Stoves Pre- and Post- Sensor Use.**

10.3.2 No Perceived Threat: Interpretation vs. Reality

For participants across both pathways, the perceived absence of threat does not accord with the levels of exposure recorded by the sensors. Fig 10.3 illustrates that for most stoves the median indoor $PM_{2.5}$ emitted over the average 4 hours in which they were lit sits between 10 and 20 $\mu g/m^3$. However, there is widespread variability around this exposure level, as illustrated by the upper quartiles and the maximum values across the stoves. While Fig 10.3 does not show the high intensity 'peaks' of indoor pollution experienced by participants, these events varied between a maximum peak average of 47.60 $\mu g/m^3$ for $PM_{2.5}$ and 36.15 $\mu g/m^3$ for PM_1, with some users being exposed to maximum values of up to 160 $\mu g/m^3$ $PM_{2.5}$ in a single sitting [56]. In light of this, and contrary to participant perceptions, the sensor data indicates that real-world stove operation is not harmless and instead involves frequent though variable exposure to intense levels of $PM_{2.5}$ inside the home. This addresses a gap in the participatory sensing literature, answering the question of whether the 'home halo effect' accords with actual exposure [330]; across the households under study here, it does not. This echoes the findings of Boso et al. [336], adding weight to the idea that people overestimate the quality of air in their homes. These findings also echo the sociological literature on the divergences seen between official air quality measurements and personal assessments of risk, which arise largely because of the mediating role of interpretation [321, 334].

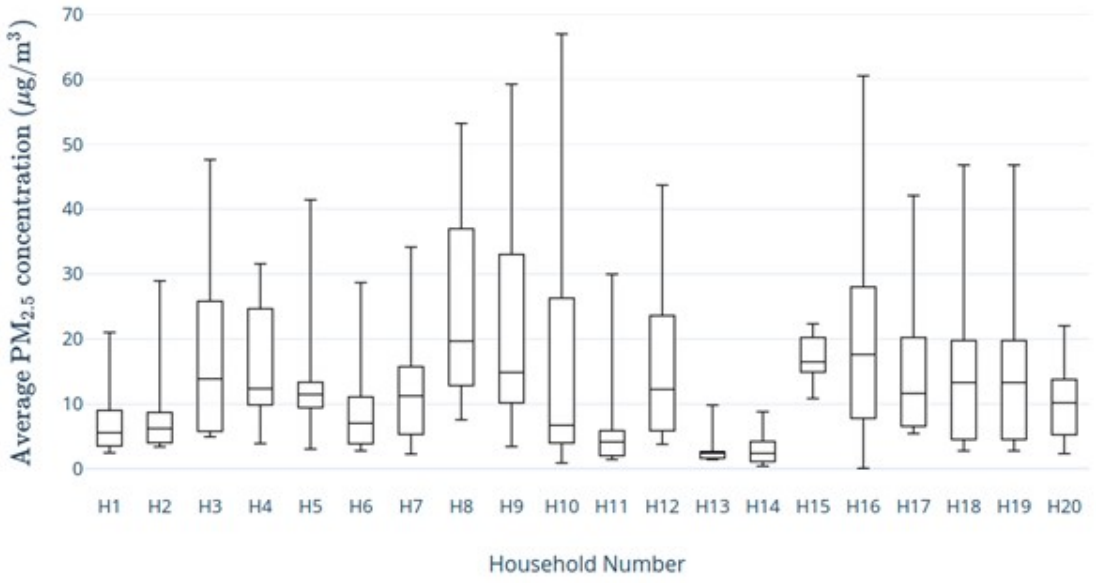

FIGURE 10.3: Average $PM_{2.5}$ Exposure per Stove.

As Fig 10.3 shows, households 1, 2, 11, 13 and 14 experienced much lower indoor emissions relative to other households in the study. The qualitative evidence for those in this group concurs with the quantitative data from the sister study, where indoor emissions are seen to result from the opening of the stove door. As such, efforts aimed at minimising the time and frequency of this action appeared to reduce exposure [56]:

> We've tried to minimise the amount we're opening the door, whereas me particularly I used to make a very small fire and gradually just keep adding stuff... I now just really stack it up inside with progressively thicker stuff and light it and leave it shut. Then by the time you have to put more stuff on it's already hotter so the draw is much greater, so there's it's far less likely to come into your room.
>
> (Participant 2, Household 1)

> I was more careful with the kindling and more careful with the initial three logs, and then the next two logs and the next two logs, and I was careful with the amount of time I opened the door... I just pulled it half an inch, then slowly opened it, then I put the logs on as fast as possible...I started putting the match box inside the stove and just doing a forward strike and then lighting it and closing the door quick.
>
> (Participant 16, Household 11)

Despite such efforts, peaks still occurred and maximum average values still exceeded thresholds in three of these five households. This echoes the variability of exposure to indoor emissions, reduction of which is highly dependent on the user's ability to consistently limit the frequency and duration in which the stove door is opened. Some reported this to be challenging during high winds (Participant 16, Household 11), if there was too little ash in the stove bed (Participant 1, Household 1), or the user was having an 'off day' (Participant 23, Household 13). Taken together, this speaks to residential stoves being embedded in a dynamic system, with various system inputs and external factors acting to produce undesirable emissions, often without any optimal control or stability [347]. This is particularly salient when looking at outdoor emissions, as stove emission factors vary depending on their type, manufacturer, model, design [348], fuel moisture content [349], house ventilation, chimney insulation [350], flue height and diameter [306], distance between roof ridge and outlet [351], ambient weather, outdoor air quality, and surrounding topography. Add into this already-dynamic system a human being, whose inconsistent behaviour intersects with many of these elements [352], then production of consistently minimal emissions both indoors and outdoors is always going to be difficult to attain under real-world conditions.

10.3.2.1 Situation Factors Influencing Interpretation: The Role of Data Presentation.

As can be seen, exposure to intense peaks and average increases occurred for the majority but were not perceived as particularly harmful. Even those that perceived the peaks as

'threatening' considered risk to be almost completely negated through minimal behaviour changes. This divergent interpretation arose for those in both coping pathways for reasons relating to data presentation format and preconceptions about stoves. This mirrors coping theory in that the 'extent to which any event is stressful is determined by a confluence of person and situation factors in a specific transaction [272]. Taking the situation factor of data presentation as the point of departure, while 6 participants were relatively satisfied with the data presentation format, the remaining 24 described it as decontextualised and lacking relatability. As noted by participant 12, '[a]lthough I've learnt what stuff means, as in I've learnt what PM_1 is, I can't actually relate that to anything'. Similarly:

> You can see what the figure is but it's not telling you what the impact is. There's no comparison with anything else. It's not contextualised in any way... it's not bound to anything, is it? It's cold, stark data.

(Participant 15, interview)

> I think this actually speaks... to the lack of information that the numbers give us. Like, while they do give us lots of information they also don't tell us a lot about the actual [health effects]... that sort of meaning, you know?

(Participant 18, interview)

The quantification spoken of here is visible in Fig 10.4. The data was presented using a set of dials with real-time PM_1, $PM_{2.5}$ and PM_{10} exposure data displayed at the top of the screen, and with longitudinal graphics illustrating exposure over a 24-hour period. There is no known safe limit for PM_1, but the 'traffic-light' system used for the other fractions are colour-coded according to the WHO's 24-hour exposure thresholds. This approach is common in the air quality sensor industry, where this colour scheme and threshold combination are widely used to inform data displays. However, the only non-quantified meaning being communicated is via the traffic-light system and, even then, each colour only depicts a quantity of PM $\mu g/m^3$. A level of risk is communicated by this colour coding, but what that translates to in terms of health effects or equivalent risks is not detailed.

FIGURE 10.4: Data Display for Air Quality Sensor.

A second feature implicated in the interpretation of data relates to the suitability of the presentation format for the indoor emission pattern produced by stoves. As Chakraborty et al. [56] demonstrate, indoor exposure takes the form of intense 'peaks' and average increases of PM over the time in which stoves are lit. The real-time dials are effective at displaying this information in the moment, but it is only short-lived. By contrast, the longitudinal graphs display this data over time, allowing users to view their exposure over a longer period. However, these graphs actually obscure the significance of such 'peaks' because they are based on the WHO 24-hour average threshold. Even when the peaks are of a very high intensity or occur repeatedly before returning to lower levels, their significance is lost in a graphical interface that presents more information on the period in which stoves are not lit than when they are (see Fig 10.4). The absence of meaning inherent to these presentation characteristics had consequences. It served to generate a space in which participants searched for indicators of meaning elsewhere. For many, these 'signs' came in the form of other emissions picked up by the air quality sensors, including those from cooking, lighting candles and cleaning, amongst other things. Comparing stove emissions to these more 'everyday' activities served as a benchmark by which the figures relating to stoves could be better understood. However, as the quantification and 24-hour average thresholds inherent to the presentation format remained unchanged, participants drew from their already-existing understandings of these other activities as harmless when reading the data. This is visible in their interpretations, which further diluted the perception of indoor stove emissions as harmful:

> [T]oast gives massive spikes. . . joss sticks and candles, they give off loads. So that made me think, well, you need to judge pollution against other things that are happening. So, I guess I went from, to begin with, thinking 'oh my god, this stove is leaking, it's giving us spikes', to then thinking, 'actually, in the context of other things that seem quite normal, maybe it's not so bad'.

(Participant 10, interview)

> After I saw the readings of the first couple of times of having it on I thought 'oh jeez, we're all in there', you know, especially having a child. . . But I was worried at first and now I'm not particularly, so obviously the effects haven't lasted. We got some really big peaks when we were cooking, which everybody does, and you can't really get away from that so how bad can it be, really?

(Participant 25, interview)

[0]Participants had the option of displaying the data on the tablet computer in a landscape or portrait orientation. In portrait, fewer data fields appear on screen at once.

It is at this precise point where the data presented by the individual monitors encounter more personal understandings of indoor air pollution. Much like the 'clues' sought by participants in [318] study, the ambiguity communicated by the sensor data encouraged users to seek a relatable explanation elsewhere. Here, already-existing understandings of air pollution from other indoor activities came to occupy the interpretive space created. At the point of encounter, the sensor data was not exerting influence on a neutral position of understanding, but came to contend with already-existing terrains of knowing and unknowing with which it vied for influence. Ultimately, the ambiguous presentation format generated the space for other influences to enter the appraisal process, appearing to minimise the threat perceived and affecting the coping efforts undertaken thereafter.

10.3.2.2 Person Factors Influencing Interpretation: The Role of Preconception.

While coping theory emphasises the situational encounter in explaining how people respond to environmental circumstances, it also acknowledges that such responses do not occur in a vacuum and that person factors also influence how somebody responds to a situation. This is particularly so when the situational information required for an appraisal is unclear or insufficient. As Folkman and Lazarus [265] make clear, such ambiguity causes the person to:

> [i]nfer meanings based on personal dispositions, beliefs or experiences. The greater the ambiguity, the more influence person factors have in determining the meaning of the environmental configuration... whenever there is ambiguity, person factors shape the understanding of the situation, thereby making the interpretation of the situation more a function of the person than of the objective stimulus...

As illustrated throughout **Introduction** section, the sociological literature is replete with examples of people interpreting air pollution data through internal mediation processes. These draw upon already-existing experiences, understandings and social constructs to influence how sensor information is interpreted and subsequently acted upon. As can be seen in subsection **Situation Factors Influencing Interpretation: The Role of Data Presentation**, interpretations of the sensor data relating to other indoor sources were based on pre-existing understandings of whether emissions from these activities were harmful. However, the research design also allows for some of the more general preconceptions to be viewed, demonstrating that the sensor data is not only failing to convince because of an unrelatable data presentation format, but also because it is entering a cognitive process already coloured by a predisposition to view residential stoves in a positive light. Compared to knowledge of their detrimental effects on outdoor air quality, user knowledge of indoor stove emissions was far less certain (see Fig 10.5)). Those answering 'neither agree nor disagree' recognised that indoor emissions resulted from stove use but considered it to be insignificant. This ambiguity about indoor stove emissions specifically may be related to the lack of knowledge about indoor air pollution more generally. For instance, one survey of 2,000 adults found that 46% could not name a

source of indoor air pollution and only 36% were aware of its effects on health [353, 354]. This may be associated with the status of indoor air pollution research being historically overshadowed by its outdoor counterpart [302, 355]. Indeed, research on indoor emissions from DEFRA-approved stoves is a relatively recent undertaking[56], meaning there is little wider social commentary supported by credible evidence about the indoor air pollution produced by these forms of heating.

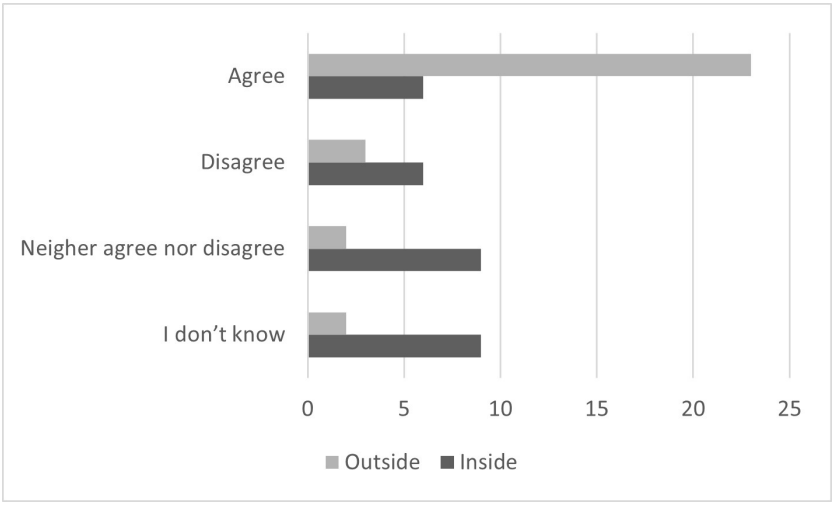

FIGURE 10.5: 'My stove reduces the quality of air outside my house' vs. 'My stove reduces the quality of air inside my house' Pre-sensor use.

The second and third preconceptions were more positive in orientation and built on this ambiguity, with the former concerning the justification for stove use and the latter how 'environmentally friendly' users considered their stoves to be. The dominant reasons given for stove use included warmth (n=24) and 'cosiness' (n=21), often being presented together (n=18). This mirrors a recent DEFRA (2020: 86) survey of almost 1,000 UK stove users, which found the primary reason for lighting a fire was 'to create a homely feel'. A similar result is reflected in the national Domestic Wood Survey [356], where 27% of respondents burned wood for 'aesthetic value'.Emden and Murphy [357] also associate the continued demand for stoves with this aesthetic component. As such, wider visual imaginaries around wood burning are here exerting influence within the cognitive appraisal process to affect interpretations of sensor data.

The third characteristic added to this positive preconception, with the majority of participants (n=18) considering their stove to be 'environmentally friendly'. For most, this perception drew its credibility from several sources; the DEFRA stove certification, use of seasoned wood instead of wet wood, and comparisons with the CO_2 produced by gas-fired central heating systems. As participant 20 noted, 'I don't know if it's environmentally friendly, but the blurb says DEFRA approved, so...'. Similarly:

> The stove is DEFRA approved for smoke control areas and refers to environmental credentials in sales literature. I burn fully seasoned, waste wood and burn far less gas as a result.
>
> (Participant 12, pre-use survey)

> Yes, it is environmentally friendly. It's DEFRA-exempt, we burn only well-seasoned dry logs, is CO_2 neutral and we use locally sourced fuel.
>
> (Participant 19, pre-use survey)

> It's DEFRA-rated, we burn a waste wood-based briquette product and seasoned logs, carefully monitoring burning conditions. It's likely better in terms of carbon neutrality than the gas central heating.
>
> (Participant 28, pre-use survey)

Amounting to a position that holds stoves in a positive regard aesthetically and environmentally, these preconceptions are reflected in wider research on public knowledge of residential stove pollution. A recent survey of 2,000 UK stove users found half to be unaware that stoves can have a negative impact on health, a third associated stove use with positive aesthetics, and one fifth considered wood burners and coal fires to be the most environmentally friendly ways of heating homes [358]. This is further supported by research into 16,000 members of the public from across seven European countries, which found that people consistently underestimate air pollution from residential stoves compared to other sources [359].

Taken together, the absence of knowledge about indoor emissions linked with the 'cosiness' aesthetic and 'environmentally friendly' moniker to create a relatively positive baseline perspective on stoves. The preconceptions underpinning this position were not passive and, instead, were pulled into the cognitive appraisal process by the ambiguity created by the sensor data. As Lazarus and Folkman [272] note, '[e]ven in situations where there are cues signalling harm or danger, ambiguity can be used to reduce threat by allowing alternative – perhaps reassuring – interpretations of the meaning of the situation'. The quantitative data, presented using WHO 24-hour average thresholds and colour coded real-time displays, was not relatable enough to stand alone as a persuasive source of information about the risks posed by the indoor emissions being produced. Instead, the data presentation format encouraged a search for meaning in preconceptions, minimised the perceived threat and did little to alter the positive perception of stoves already established in the minds of users.

10.4 Discussion

The findings show that households experienced high but variable 'peaks' of indoor PM from their residential stoves [56]. Perceptions of this exposure as a 'stressor' varied, with participants falling into one of two groups; those that did not conceive of the 'peaks' as harmful and those that did. The former group did not change their behaviour, as no threat was perceived, while the latter pursued problem-focused coping efforts to reduce exposure. These concentrated on changing stove management practices, mirroring existing

studies where similarly individualised attempts at avoiding or mitigating air pollution were also triggered by sensor technology [263, 332, 336, 340, 341]. Over the four-week period in which air quality sensors were installed, users in this group reported a reduction in concern to such an extent that it was not perceived at the conclusion of the study. As such, while both groups followed different coping pathways, sensor use resulted in similar responses to the data; a perception that indoor emissions produced by stoves are not harmful. Implicated in this was the way in which data presentation format triggered a search for meaning elsewhere, in more relatable activities, importing pre-conceptions about these activities into the cognitive appraisal process and influencing how the data was interpreted. This has several consequences for the participatory sensing literature.

First, echoing recent work by [336], the home-halo effect does not correspond with actual levels of indoor air pollution [330, 332, 333]. Despite concern decreasing amongst users following engagement with the sensors, households experienced high but variable 'peaks' of indoor PM from their residential stoves which served to increase their average exposure over the duration in which the stoves were lit [56].

Second, the way in which sensor data is presented has a substantive bearing on user perceptions. Echoing existing research on public interpretations of air pollution data [319, 333], widely used WHO thresholds, display formats based on 24hr averages, and PM exposure expressed in the units of $\mu g/m^3$ are experienced as overly quantified and unrelatable. This is compounded by the effect of 24-hour averages obfuscating the significance of peaks-orientated patterns of indoor stove emissions [56, 308]. When coupled with its almost wholly quantified format, the 'threat' associated with exposure to high intensities of PM over shorter periods of time is not made explicit by such approaches [360, 361]. This adds an additional dimension to the participatory sensing literature, where the focus tends to be on the outcome of sensor engagement instead of the process by which that outcome is produced [263, 334, 340]. Future research should prioritise the ways in which air quality data is presented within participatory sensing projects, addressing questions of suitability to situation and relatability to person as a matter of priority. Relying on quantified representations alone risks repeating past errors by uncritically transporting the 'deficit model' of public understandings of scientific information into the participatory sensing projects of the future [319]. The danger of doing otherwise, by continuing to rely primarily on quantification alone, risks impeding the potential for this technology to become an effective means of communicating air quality information.

Third, the ambiguity created by an unrelatable data presentation format encourages a search for more relatable markers from which to derive meaning elsewhere. By failing to act as a singular source of information whose relevance to the person is clear, the sensors actively draw wider socio-cultural knowledges of air pollution into the appraisal process, filling the interpretive space. Under this scenario, participatory sensing becomes both a trigger and gateway to existing incomplete or imprecise understandings of air pollution as opposed to a source for new and accurate meanings. While not exhaustive, a cluster of specific preconceptions stepped into the space created by the data ambiguity. For instance, normative understandings of cooking emissions as harmless were used as a comparator by which to judge data on stove emissions, rendering them similarly harmless in the minds of users. However, research has consistently found this not to be the case[362–365], speaking to the influence of wider social constructions of risk – or, more accurately, the absence of these constructions – in the interpretation of sensor data [325, 330].

The absence of accurate understandings of indoor emissions intersects with other preconceptions, mainly around the aesthetic of stoves being 'cosy' and 'environmentally friendly',

to create a cognitive terrain characterised by favourability. Not only do such positions work against the introduction of air quality policies in local areas [366, 367], but they render air pollution data less persuasive. As such, participatory sensing alone cannot be relied upon to change perceptions and behaviour on air pollution. Its effectiveness is contingent on parallel socio-cultural meanings around emissions producing behaviours, which step into the void when the data presentation format is deemed unsuitable or unrelatable by users. Thus, while participatory sensing can be helpful in making people more sensitive to air pollution issues [332, 336], wider air pollution information campaigns may be a more efficient and effective means through which to accurately inform and encourage behaviour change. Put another way, if social constructions of air polluting behaviours are always standing behind participatory sensing initiatives, ready to exert influence at the point in which users attempt to interpret the data, wider air quality campaigns may elicit more impactful results.

10.5 Conclusion

Taken together, this study has illustrated that older social constructivist arguments about scientific-lay understandings being relational [318], and air pollution data passing through mediating processes informed by both normative experience and context during interpretation [325, 333], still apply to the relatively new world of participatory sensing. This echoes claims about sensor-based interventions facing the same challenges as more traditional information campaigns [368]. It also reinforces the idea that context needs to be understood as integral to decision-making informed by sensor use and not peripheral to it [332]. Indeed, while the role of physical socio-structural context is widely recognised as influencing actions taken in response to participatory sensing data, this study also illustrates the role of socio-cultural knowledge within this process [325]. As Bickerstaff and Walker [324] noted almost two decades ago, with regard to public interpretations of more general air pollution data, these processes are embedded in an 'entangled interaction of society-environment-technology'. This study has shown that data derived from participatory sensing is no different. Research must interrogate the spaces between these components, treating the junctures as opportunities for understanding in order to facilitate the transformative potential of participatory sensing initiatives in the future.

10.6 Contribution

R.C. (Rohit Chakraborty):

- **Conceptualization and Continuation:** Leveraging the foundational insights from Chapter 6, I played a central role in conceptualizing and framing Chapter 10's focus on participatory sensing and its impact on wood burning stove users' perceptions. My vision ensured a seamless transition and extension of ideas from the quantitative analysis of Chapter 6 to the more qualitative and perceptual aspects addressed in Chapter 10.

- **Sensor Deployment and Data Collection:** Drawing from the experience in Chapter 6, I was actively involved in deploying air quality monitors for the participatory sensing study, ensuring accurate data capture from stove users. I was also involved in data curation through the surveys and interview transcripts.
- **Writing – Drafting and Editing:** As one of the primary authors, I spearheaded the drafting, refining, and finalization of the manuscript, integrating both quantitative data and qualitative insights to present a comprehensive account of our research.
- **Data Analysis and Interpretation:** Combining the quantitative methodologies from Chapter 6 with the qualitative explorations of Chapter 10, I delved into a multifaceted analysis, ensuring that both numerical and perceptual aspects of our findings were rigorously examined and interpreted.
- **Participatory Sensing and User Engagement:** I played a pivotal role in engaging with wood burning stove users, exploring their interactions with the sensing technology, and understanding the cognitive and behavioral implications of their engagement with indoor air quality data.
- **Collaboration and Coordination:** I collaborated closely with co-author and participants, integrating diverse perspectives and insights to ensure the richness and depth of the research.
- **Project Leadership:** Given my primary authorship in Chapter 6 and extensive involvement in Chapter 10, I provided overarching guidance, ensuring continuity, depth, and rigor across both chapters.

Building on the foundational research from Chapter 6, my extensive involvement in Chapter 10 was instrumental in exploring the nuanced interplay between participatory sensing technology and user perceptions. My comprehensive engagement, from conceptualization to manuscript finalization, significantly influenced the study's direction, quality, and impact.

Chapter 11

Conclusion

In conclusion, the present thesis emphasized the significance of Low-Cost Sensors (LCS) in monitoring air pollution, which remains a persistent global problem with severe consequences for human health, both physically and mentally, as well as its impacts on society. This research highlighted the potential of LCS to gather air quality data accurately, leading to the development of effective policies and interventions to tackle air pollution.

The use of LCS in air pollution monitoring has been established as a cost-effective and efficient solution. LCS provides localized measurements with high resolution and enables the collection of long-term data, which would be challenging or even impossible to gather with traditional monitoring methods. This leads to the identification of hotspots of high pollution, tracking changes in air quality over time, and supporting the development of targeted interventions and policies aimed at improving air quality.

The role of LCS in air pollution monitoring has been given increased attention in recent years due to their low cost and portability, making them accessible to a wider range of users, including individuals, communities, and policy-makers. LCS can be successfully used to monitor $PM_{2.5}$ levels.

LCS also offers the opportunity to collect real-time data in higher resolution, and used in conjuction with spatiotemporal predictive model to "fill in the gaps" such as Conv-LSTM model tested in this thesis, which can be useful in making informed decisions related to air quality. This information can be used to support policy-making processes by providing relevant data to decision-makers, including data on air pollution levels, spatial and temporal patterns, and trends. With the increasing availability of LCS, there is a need for standardization of measurement methods to ensure that the data collected is consistent and comparable across different sensors.

In addition to its role in monitoring air pollution, LCS also provides opportunities for community engagement and empowerment. By involving communities in air quality monitoring, LCS can increase public awareness about the issues of air pollution and encourage individuals to take action to improve air quality. This can also lead to the development of community-led initiatives to address air pollution and promote sustainable development.

In conclusion, LCS has demonstrated its potential as a valuable tool in the fight against air pollution. Its ability to provide accurate, localized and real-time data at a low cost, along

with its potential for community engagement and empowerment, highlights the significance of LCS in air pollution monitoring and policy-making. The continued development and improvement of LCS has the potential to drive significant progress towards the goal of clean air for all.

The essence of this thesis lies in the exploration and validation of Low-Cost Sensors (LCS) in the domain of air pollution monitoring. This chapter consolidates the key findings and contributions made throughout the research while also highlighting the roadmap for potential future work.

Summary of Achievements

The overarching objective of this research was to elucidate the capabilities and significance of LCS in capturing air quality data, especially when juxtaposed against the backdrop of traditional monitoring methodologies.

The research underscored the agility of LCS in offering localized, high-resolution measurements that can persistently track changes, thereby facilitating the identification of pollution hotspots and aiding policy formulation.

The merit of LCS doesn't merely reside in its cost-effectiveness or portability but also in its capacity to democratize air quality monitoring. This democratization extends to diverse stakeholders, encompassing individuals, community bodies, and policy architects.

A pivotal finding was the efficacy of LCS in monitoring PM levels. When integrated with advanced spatiotemporal predictive models, like the Conv-LSTM tested herein, LCS can pave the way for real-time, high-fidelity data acquisition.

The research also unveiled the socio-environmental dimensions of LCS deployment. Notably, it was discerned that LCS can serve as catalysts for community mobilization, fostering increased public cognizance regarding air pollution and galvanizing collective action towards sustainable practices.

An essential facet of the thesis was the juxtaposition of LCS data with other ancillary datasets, unraveling intricate interplays between air quality, meteorological conditions and traffic patterns. This helped to fill in the gaps where there are no sensor data available.

Contributions to Knowledge

The contributions to knowledge from this research are manifold.

Validation of LCS: The thesis methodically validated the precision and utility of LCS in monitoring air pollution, bridging a significant gap in literature and offering empirical evidence to substantiate LCS's capabilities.

Integration with Predictive Models: This research introduced a novel paradigm by integrating LCS data with advanced spatiotemporal predictive models, demonstrating the potential of such synergies in advancing the granularity and accuracy of air quality predictions.

Socio-Environmental Implications: A nuanced understanding of the socio-environmental ramifications of LCS deployment was presented, emphasizing the role of community engagement and the transformational potential of grassroots initiatives.

Quality Control of Data

A systematic approach was adopted for quality control of the data. Rigorous outlier detection mechanisms were instituted, ensuring the robustness of the data. Imputation techniques were employed to address any gaps or anomalies in the dataset, ensuring the integrity and reliability of the research findings.

11.1 Future Work

Future work in this field should focus on improving the accuracy and reliability of LCS in measuring air pollution - this is more important in case of monitoring NO_2. This could include the development of new sensors, advances in data processing and analysis techniques, and the integration of stakeholder engagement and policy making to ensure that the results of LCS monitoring are effectively translated into action. In doign so, more research is needed to understand the potential of LCS in shaping policymaking.

In addition to the points already mentioned, there are several other areas of future work that could be pursued to further advance the use of LCS in monitoring air pollution.

1. One area that could be explored is the integration of LCS with other air quality monitoring technologies. For example, LCS could be used in conjunction with satellite imagery or remote sensing to provide a more comprehensive understanding of air pollution at a regional or global scale.

2. Second area of future work could be the integration of LCS with other forms of data (as shown in the thesis) such as meteorological data, traffic data, or land-use data in official reporting. This could help to identify the sources of air pollution and the factors that contribute to it. Additionally, the integration of LCS with other forms of data could also enable the development of more accurate and sophisticated air quality models.

3. Third important area of future work is the development of new sensors for LCS. Currently, most LCS systems use electrochemical or optical sensors, but there are other types of sensors that are currently being developed but yet to be used in LCS, such as NanoPlasmonic Sensing (NPS) developed by Insplorion Ltd. These sensors could provide more accurate and detailed measurements of air pollutants, which would be particularly useful for monitoring pollutants that are difficult to detect, such as specific volatile organic compounds like formaldehyde or Nitrogen Dioxide (NO_2).

4. Fourth, another area of future work is the development of new data processing and analysis techniques. With processing power becoming less of an issue, the use of machine learning algorithms, such as neural networks or decision trees on the fly for

calibration and reporting data, could enable the development of more sophisticated data analysis methods.

5. Furthermore, more research is needed to understand the potential of LCS in shaping policy-making. There are many ways in which LCS data can be used to inform policy-making, but it is important to understand the most effective ways of using this data. For example, LCS data could be used to identify areas of high pollution and to target interventions and policies to these areas. Additionally, LCS data could be used to evaluate the effectiveness of existing policies and to identify areas where policies need to be strengthened or changed.

Overall, the use of LCS in monitoring air pollution is a promising approach that has the potential to make a significant contribution to addressing this pressing public health issue. By pursuing these areas of future work, it is possible to further advance the use of LCS in monitoring air pollution and to improve the well-being of communities around the world.

References

[1] World Health Organisation, https://www.who.int/mediacentre/news/releases/2014/air-pollution/en//, 2014.

[2] Bert Brunekreef and Stephen T Holgate. Epidemiology of air pollution and health. *The Lancet*, 360(9326):1233–1242, 2002.

[3] C Arden Pope and Douglas W Dockery. Health effects of fine particulate air pollution: lines that connect. *Journal of the Air & Waste Management Association*, 56 (6):709–742, 2006.

[4] Robert W Pinder. Air quality modeling: history, status, and future directions. *Atmospheric environment*, 41(36):7836–7851, 2007.

[5] L Katherine Emmons, Peter G Hess, and Steven Walters. Air quality modeling for policy applications. *Annual review of physical chemistry*, 61:441–462, 2010.

[6] Jos Lelieveld, Jason S Evans, Muhammad Fnais, Dalia Giannadaki, and Andrea Pozzer. Global air pollution crossroads over the mediterranean. *Nature*, 525(7567): 367, 2015.

[7] Jintai Lin and Yuhang Wang. The transport and fate of pollutants in the atmosphere. *Annual review of earth and planetary sciences*, 44:385–410, 2016.

[8] Jintai Chang, Yuhang Wang, Jintai Lin, and Yuhang Wang. Air quality modeling: recent developments, challenges, and future directions. *Environmental science & technology*, 50(9):4529–4538, 2016.

[9] N. Christina Hsu, Arlene M Fiore, Larry W Horowitz, and Jean-François Lamarque. Chemical transport models: past, present, and future. *Atmospheric environment*, 166:1–20, 2017.

[10] Y. Chen, Q. Zhang, D. Tong, T. Wang, Y. Chen, Q. Zhang, D. Tong, and T. Wang. Statistical models for air quality: recent developments and future directions. *Environmental science & technology*, 52(17):9875–9887, 2018.

[11] G. Janssens-Maenhout, F. Dentener, I. Bey, W. Lefebvre, F. Raes, R. Van Dingenen, F. Dentener, I. Bey, W. Lefebvre, F. Raes, and R. Van Dingenen. Spatiotemporal forecasting of air pollution: a review. *Environmental science & technology*, 51(17): 9875–9887, 2017.

[12] C. Gan, J. Li, Y. Wang, C. Gan, J. Li, and Y. Wang. A review of air quality forecasting techniques and evaluation metrics. *Environmental science & technology*, 52(24):14229–14241, 2018.

[13] Haizhu Lin and Chunhui Deng. Development of Hf4+-immobilized polydopamine-coated magnetic graphene for highly selective enrichment of phosphopeptides. *Talanta*, 149:91–97, 2016. ISSN 00399140. doi: 10.1016/j.talanta.2015.11.037. URL http://dx.doi.org/10.1016/j.talanta.2015.11.037.

[14] M.L. Bell, K. Ebisu, B. Ostro, S. Green, R. Broadwin, S. Green, and R. Broadwin. Health impact assessment of air pollution. *Environmental health perspectives*, 115 (2):192–197, 2007.

[15] D. Kang, J. Huang, J. Li, Y. Wang, D. Kang, J. Huang, J. Li, and Y. Wang. Data assimilation in air quality modeling: a review. *Environmental science & technology*, 53(16):9307–9317, 2019.

[16] Y. Zhang, J. Li, and Y. Wang. High-performance computing in air quality modeling: current status and future directions. *Environmental science & technology*, 52(24): 14242–14250, 2018.

[17] World Health Organization. *9 out of 10 people worldwide breathe polluted air, but more countries are taking action.* WHO, 2018. Available from: https://rb.gy/5xqhg.

[18] H Ritchie and M Roser. Emissions of air pollutants — ourworldindata.org. https://ourworldindata.org/grapher/emissions-of-air-pollutants?time=1970..2016&country=~GBR, 2021. [Accessed 23-Jan-2023].

[19] Aaron J Cohen, Michael Brauer, Richard Burnett, H Ross Anderson, Joseph Frostad, Kara Estep, Kalpana Balakrishnan, Bert Brunekreef, Lalit Dandona, Rakhi Dandona, Valery Feigin, Greg Freedman, Bryan Hubbell, Amelia Jobling, Haidong Kan, Luke Knibbs, Yang Liu, Randall Martin, Lidia Morawska, C Arden Pope, 3rd, Hwashin Shin, Kurt Straif, Gavin Shaddick, Matthew Thomas, Rita van Dingenen, Aaron van Donkelaar, Theo Vos, Christopher J L Murray, and Mohammad H Forouzanfar. Estimates and 25-year trends of the global burden of disease attributable to ambient air pollution: an analysis of data from the global burden of diseases study 2015. *Lancet*, 389(10082):1907–1918, May 2017.

[20] Greenpeace UK. Air pollution and child health: prescribing clean air. https://www.greenpeace.org.uk/challenges/air-pollution/, 2020. (Accessed on 01/29/2023).

[21] Xu-Qin Jiang, Xiao-Dong Mei, and Di Feng. Air pollution and chronic airway diseases: what should people know and do? *J. Thorac. Dis.*, 8(1):E31–40, January 2016.

[22] J Evelyn. Fumifugium, or, The inconveniencie of the aer and smoak of London dissipated together with some remedies humbly proposed / by J.E. esq. to His Sacred Majestie, and to the Parliament now assembled. — name.umdl.umich.edu. http://name.umdl.umich.edu/A38788.0001.001, 1661. [Accessed 29-Jan-2023].

[23] Battersea Borough Council. The Great Smog of 1952 — metoffice.gov.uk. https://www.metoffice.gov.uk/weather/learn-about/weather/case-studies/great-smog, 1952. [Accessed 29-Jan-2023].

[24] Y Pang NR Passant, TP Murrells. Uk informative inventory report (1980 to 2012). *DEFRA*, 2012.

[25] HM Government. Environmental protection act, 1990. Available from: https://www.legislation.gov.uk/ukpga/1990/43/contents.

[26] Department of the Environment. Automatic Urban and Rural Network, 1973.

[27] F. Karagulian, Maurizio Barbiere, A. Kotsev, L. Spinelle, M. Gerboles, F. Lagler, N. Redon, S. Crunaire, and A. Borowiak. Review of the performance of low-cost sensors for air quality monitoring. *Atmosphere*, 2019. doi: 10.3390/atmos10090506.

[28] Katie R Smith, P. Edwards, P. Ivatt, James D. Lee, F. Squires, Chengliang Dai, R. Peltier, M. J. Evans, Yele Sun, and A. Lewis. An improved low-power measurement of ambient NO_2 and o3 combining electrochemical sensor clusters and machine learning. *Atmospheric Measurement Techniques*, 2019. doi: 10.5194/AMT-12-1325-2019.

[29] Emily G. Snyder, Timothy H. Watkins, Paul A. Solomon, Eben D. Thoma, Ronald W. Williams, Gayle S. W. Hagler, David Shelow, David A. Hindin, Vasu J. Kilaru, and Peter W. Preuss. The changing paradigm of air pollution monitoring. *Environmental Science & Technology*, 47(20):11369–11377, oct 2013. doi: 10.1021/es4022602. URL https://doi.org/10.1021%2Fes4022602.

[30] Federico Karagulian, Maurizio Barbiere, Alexander Kotsev, Laurent Spinelle, Michel Gerboles, Friedrich Lagler, Nathalie Redon, Sabine Crunaire, and Annette Borowiak. Review of the performance of low-cost sensors for air quality monitoring. *Atmosphere*, 10:506, aug 2019. doi: 10.3390/atmos10090506. URL https://doi.org/10.3390%2Fatmos10090506.

[31] R Subramanian and Rebecca Garland. Editorial: The powerful potential of low-cost sensors for air quality research in africa. *Clean Air Journal*, 31(1), jun 2021. doi: 10.17159/caj/2021/31/1.11274. URL https://doi.org/10.17159%2Fcaj%2F2021%2F31%2F1.11274.

[32] Gerboles, Spinelle M., Borowiak L, and A. Measuring air pollution with low-cost sensors — publications.jrc.ec.europa.eu. https://publications.jrc.ec.europa.eu/repository/handle/JRC107461, 2017. [Accessed 30-Jan-2023].

[33] C. Oltra, R. Sala, A. Boso, and S. Asensio. Public engagement on urban air pollution: an exploratory study of two interventions. *Environmental Monitoring and Assessment*, 189, 2017. doi: 10.1007/s10661-017-6011-6. URL https://doi.org/10.1007/s10661-017-6011-6.

[34] G. Wong-Parodi, B. Dias, and M. Taylor. Effect of using an indoor air quality sensor on perceptions of and behaviors toward air pollution (pittsburgh empowerment library study): online survey and interviews. *JMIR mHealth and uHealth*, 6, 2018. doi: 10.2196/mhealth.8273. URL https://doi.org/10.2196/mhealth.8273.

[35] Zappi, P., Bales, E., Park, J., Griswold, W, and Rosing, T. The citisense air quality monitoring mobile sensor node, available at: https://seelab.ucsd.edu/papers/zappi_ipsn12.pdf., 2012. URL https://seelab.ucsd.edu/papers/Zappi_IPSN12.pdf.

[36] Heydon, j. (2020). procedural environmental injustice in 'europe's greenest city': a case study into the felling of sheffield's street trees. social science. (in

press.) http://apps.who.int/iris/bitstream/handle/10665/250141/9789241511353-eng.pdf?sequence=1, 2020. URL http://apps.who.int/iris/bitstream/handle/10665/250141/9789241511353-eng.pdf?sequence=1.

[37] Ning Qiao, Qiang Li, Lu Wang, Zhiqiang Li, Xia Li, and Hong Wang. Design and implementation of a low-cost open-source air quality monitoring system. *IEEE Sensors Journal*, 16(16):6637–6644, 2016.

[38] Jie Chen, Weijie Liu, Dongdong Zhang, Zhen Chen, Jie Cai, Zhigang Li, and Yulan Li. Open-source low-cost air quality monitoring system for pm2.5 and pm10: design and evaluation. *Sensors*, 19(2):294, 2019.

[39] Frank de Leeuw, Christina van der Meijden, Theo Korten, Peter Gijsbers, Martijn van der Laan, and Ed van der Meijden. Assessment of low-cost sensors for particulate matter monitoring. *Environmental Science & Technology*, 49(24):14189–14197, 2015.

[40] Ning Li, Hong Wang, Hong Guo, Hong Yang, Lu Wang, and Qiang Li. Evaluation of low-cost sensors for particulate matter monitoring in indoor and outdoor environments. *Environmental Science: Processes & Impacts*, 20(7):939–947, 2018.

[41] G. MacKerron and S. Mourato. Life satisfaction and air quality in london. *Ecological Economics*, 68:1441–1453, 2009. doi: 10.1016/J.ECOLECON.2008.10.004.

[42] ClientEarth. Top court confirms uk has broken air pollution law, 2021. URL https://www.clientearth.org/latest/press-office/press/top-court-confirms-uk-has-broken-air-pollution-law/. Accessed: July 19, 2023.

[43] Transport for London (TfL). Ultra low emission zone, 2023. URL https://tfl.gov.uk/modes/driving/ultra-low-emission-zone. Accessed: July 20, 2023.

[44] Sheffield City Council. Clean air zone sheffield, 2023. URL https://www.sheffield.gov.uk/clean-air-zone-sheffield. Introduced: February 2023; Accessed: Aug. 10, 2023.

[45] European Parliament and Council. Regulation (eu) 2023/851 of the european parliament and of the council of 19 april 2023 amending regulation (eu) 2019/631 as regards strengthening the CO_2 emission performance standards for new passenger cars and new light commercial vehicles in line with the union's increased climate ambition (text with eea relevance), 2023. URL https://eur-lex.europa.eu/eli/reg/2023/851/oj. Document 32023R0851; Accessed: Aug. 10, 2023.

[46] UK Government. The road to zero: Next steps towards cleaner road transport and delivering our industrial strategy, July 2018. URL https://assets.publishing.service.gov.uk/government/uploads/system/uploads/attachment_data/file/739460/road-to-zero.pdf.

[47] M. A. Zaidan, Naser Hossein Motlagh, P. Fung, David Lu, H. Timonen, J. Kuula, J. Niemi, S. Tarkoma, T. Petäjä, M. Kulmala, and T. Hussein. Intelligent calibration and virtual sensing for integrated low-cost air quality sensors. *IEEE Sensors Journal*, 20:13638–13652, 2020. doi: 10.1109/JSEN.2020.3010316.

[48] N. Castell, F. Dauge, P. Schneider, M. Vogt, U. Lerner, B. Fishbain, D. Broday, and A. Bartoňová. Can commercial low-cost sensor platforms contribute to air quality monitoring and exposure estimates? *Environment international*, 99:293–302, 2017. doi: 10.1016/j.envint.2016.12.007.

[49] S. Munir, M. Mayfield, D. Coca, Stephen A. Jubb, and O. Osammor. Analysing the performance of low-cost air quality sensors, their drivers, relative benefits and calibration in cities—a case study in sheffield. *Environmental Monitoring and Assessment*, 191, 2019. doi: 10.1007/s10661-019-7231-8.

[50] L. Crilley, M. Shaw, Ryan J. Pound, L. Kramer, Robin Price, S. Young, A. Lewis, and F. Pope. Evaluation of a low-cost optical particle counter (alphasense opc-n2) for ambient air monitoring. *Atmospheric Measurement Techniques*, 11:709–720, 2017. doi: 10.5194/AMT-11-709-2018.

[51] Nuria Castell, Mike Kobernus, Hai-Ying Liu, Philipp Schneider, William Lahoz, Arne J Berre, and Josef Noll. Mobile technologies and services for environmental monitoring: The citi-sense-mob approach. *Urban climate*, 14:370–382, 2015.

[52] M. Mueller, Jonas Meyer, and C. Hueglin. Design of an ozone and nitrogen dioxide sensor unit and its long-term operation within a sensor network in the city of zurich. *Atmospheric Measurement Techniques*, 10:3783–3799, 2017. doi: 10.5194/AMT-10-3783-2017.

[53] J. Kuula, T. Mäkelä, M. Aurela, K. Teinilä, Samu Varjonen, Óscar González, and H. Timonen. Laboratory evaluation of particle-size selectivity of optical low-cost particulate matter sensors. *Atmospheric Measurement Techniques*, 13:2413–2423, 2020. doi: 10.5194/AMT-13-2413-2020.

[54] OpenStreetMap contributors. Openstreetmap, 2021. URL https://www.openstreetmap.org. Data retrieved in Jan 2022.

[55] Marina Zusman, Cooper S. Schumacher, Amanda J. Gassett, Elizabeth W. Spalt, Elena Austin, Timothy V. Larson, Graeme Carvlin, Edmund Seto, Joel D. Kaufman, and Lianne Sheppard. Calibration of low-cost particulate matter sensors: Model development for a multi-city epidemiological study. *Environment International*, 134:105329, January 2020. doi: 10.1016/j.envint.2019.105329. URL https://doi.org/10.1016/j.envint.2019.105329.

[56] R. Chakraborty, J. Heydon, M. Mayfield, and L. Mihaylova. Indoor air pollution from residential stoves: Examining the flooding of particulate matter into homes during real-world use'. *Atmosphere*, 11, 2021.

[57] X Cao and F Tay. Time series forecasting using support vector regression. *IEEE Transactions on Neural Networks*, 14(3):622–631, 2003.

[58] H Kim. Support vector regression for time series prediction. *Neurocomputing*, 50: 321–337, 2003.

[59] Haotian Xu Stéphane Guerrier, Roberto Molinari and Yuming Zhang. Applied Time Series Analysis with R — smac-group.github.io. https://smac-group.github.io/ts/. [Accessed 24-Jan-2023].

[60] Xingjian Shi, Zhourong Chen, Hao Wang, Dit-Yan Yeung, Wai-kin Wong, and Wang-chun Woo. Convolutional lstm network: A machine learning approach for precipitation nowcasting, 2015. URL https://arxiv.org/abs/1506.04214.

[61] Nuno R. Martins and Guilherme Carrilho da Graça. Impact of PM2.5 in indoor urban environments: A review. *Sustain. Cities Soc.*, 42(May):259–275, 2018. ISSN 22106707. doi: 10.1016/j.scs.2018.07.011.

[62] P. Fu, X. Guo, F. Cheung, and K. Yung. The association between pm2.5 exposure and neurological disorders: a systematic review and meta-analysis. *Science of the Total Environment*, 10, 2019. doi: 10.1016/j.scitotenv.2018.11.218. URL https://doi.org/10.1016/j.scitotenv.2018.11.218.

[63] D. Schraufnagel, J. Balmes, C. Cowl, S. Matteis, S. Jung, K. Mortimer, R. Perez-Padilla, M. Rice, H. Riojas-Rodriguez, A. Sood, G. Thurston, T. To, A. Vanker, and D. Wuebbles. Air pollution and non-communicable diseases. *CHEST*, 155, 2019. doi: 10.1016/j.chest.2018.10.041. URL https://doi.org/10.1016/j.chest.2018.10.041.

[64] DEFRA. :home/cip18rc/Downloads/cited articles put in here/DEFRA 2019.pdf:pdf. *Clean Air Strategy*, 1(10):9, 2019. ISSN 0301018X.

[65] Department for Energy and Climate Change. Summary results of the domestic wood use survey, 2016.

[66] Anna Font and Gary Fuller. Airborne particles from wood burning in UK cities. *Defra Rep.*, pages 1–52, 2017.

[67] Air Quality Expert Group. The Potential Air Quality Impacts from Biomass Combustion, 2017. URL https://uk-air.defra.gov.uk/assets/documents/reports/cat11/1708081027{_}170807{_}AQEG{_}Biomass{_}report.pdf.

[68] Anselm Eisentraut, Brown Adam, and IEA International Energy Agency. Heating without global warming. *Featur. Insight*, page 92, 2014.

[69] Amelie Bertrand, Giulia Stefenelli, Emily A. Bruns, Simone M. Pieber, Brice Temime-Roussel, Jay G. Slowik, André S.H. Prévôt, Henri Wortham, Imad El Haddad, and Nicolas Marchand. Primary emissions and secondary aerosol production potential from woodstoves for residential heating: Influence of the stove technology and combustion efficiency. *Atmos. Environ.*, 169:65–79, 2017. ISSN 18732844. doi: 10.1016/j.atmosenv.2017.09.005.

[70] Ekbordin Winijkul and Tami C. Bond. Emissions from residential combustion considering end-uses and spatial constraints: Part II, emission reduction scenarios. *Atmos. Environ.*, 124:1–11, 2016. ISSN 18732844. doi: 10.1016/j.atmosenv.2015.10.011. URL http://dx.doi.org/10.1016/j.atmosenv.2015.10.011.

[71] Robin Nyström, Robert Lindgren, Rozanna Avagyan, Roger Westerholm, Staffan Lundstedt, and Christoffer Boman. Influence of Wood Species and Burning Conditions on Particle Emission Characteristics in a Residential Wood Stove. *Energy & Fuels*, 31(5):5514–5524, may 2017. ISSN 0887-0624. doi: 10.1021/acs.energyfuels.6b02751. URL https://pubs.acs.org/doi/10.1021/acs.energyfuels.6b02751.

[72] Rozanna Avagyan, Robin Nyström, Robert Lindgren, Christoffer Boman, and Roger Westerholm. Particulate hydroxy-PAH emissions from a residential wood log stove using different fuels and burning conditions. *Atmos. Environ.*, 140:1–9, 2016. ISSN 18732844. doi: 10.1016/j.atmosenv.2016.05.041. URL http://dx.doi.org/10.1016/j.atmosenv.2016.05.041.

[73] Kaung Myat Win and Tomas Persson. Emissions from residential wood pellet boilers and stove characterized into start-up, steady operation, and stop emissions. *Energy and Fuels*, 28(4):2496–2505, 2014. ISSN 15205029. doi: 10.1021/ef4016894.

[74] Gregory W. Traynor, Michael G. Apte, Andrew R. Carruthers, James F. Dillworth, David T. Grimsrud, and Lara A. Gundel. Indoor air pollution due to emissions from wood-burning stoves. *Environ. Sci. Technol.*, 21(7):691–697, jul 1987. ISSN 0013-936X. doi: 10.1021/es00161a010. URL https://pubs.acs.org/doi/abs/10.1021/es00161a010.

[75] Nuno Canha, Susana Marta Almeida, Maria do Carmo Freitas, Hubert Th Wolterbeek, João Cardoso, Casimiro Pio, and Alexandre Caseiro. Impact of wood burning on indoor PM2.5 in a primary school in rural Portugal. *Atmos. Environ.*, 94: 663–670, sep 2014. ISSN 13522310. doi: 10.1016/j.atmosenv.2014.05.080. URL https://linkinghub.elsevier.com/retrieve/pii/S1352231014004464.

[76] Erin O. Semmens, Curtis W. Noonan, Ryan W. Allen, Emily C. Weiler, and Tony J. Ward. Indoor particulate matter in rural, wood stove heated homes. *Environ. Res.*, 138:93–100, 2015. ISSN 10960953. doi: 10.1016/j.envres.2015.02.005. URL http://dx.doi.org/10.1016/j.envres.2015.02.005.

[77] M. T. Piccardo, M. Cipolla, A. Stella, M. Ceppi, M. Bruzzone, A. Izzotti, and F. Valerio. Indoor pollution and burning practices in wood stove management. *J. Air Waste Manag. Assoc.*, 64(11):1309–1316, 2014. ISSN 21622906. doi: 10.1080/10962247.2014.943353. URL http://dx.doi.org/10.1080/10962247.2014.943353.

[78] Dongbin Wang, Qing Li, Guofeng Shen, Jianguo Deng, Wei Zhou, Jiming Hao, and Jingkun Jiang. Significant ultrafine particle emissions from residential solid fuel combustion. *Sci. Total Environ.*, 715:1–7, 2020. ISSN 18791026. doi: 10.1016/j.scitotenv.2020.136992.

[79] E. D. Vicente, A. M. Vicente, M. Evtyugina, F. I. Oduber, F. Amato, X. Querol, and C. Alves. Impact of wood combustion on indoor air quality. *Sci. Total Environ.*, 705:135769, 2020. ISSN 18791026. doi: 10.1016/j.scitotenv.2019.135769. URL https://doi.org/10.1016/j.scitotenv.2019.135769.

[80] Ryan W. Allen, Sara Leckie, Gail Millar, and Michael Brauer. The impact of wood stove technology upgrades on indoor residential air quality. *Atmos. Environ.*, 43 (37):5908–5915, 2009. ISSN 13522310. doi: 10.1016/j.atmosenv.2009.08.016. URL http://dx.doi.org/10.1016/j.atmosenv.2009.08.016.

[81] C. W. Noonan, W. Navidi, L. Sheppard, C. P. Palmer, M. Bergauff, K. Hooper, and T. J. Ward. Residential indoor PM 2.5 in wood stove homes: Follow-up of the Libby changeout program. *Indoor Air*, 22(6):492–500, 2012. ISSN 09056947. doi: 10.1111/j.1600-0668.2012.00789.x.

[82] Chen Chen, Huichu Li, Yue Niu, Cong Liu, Zhijing Lin, Jing Cai, Weihua Li, Wenzhen Ge, Renjie Chen, and Haidong Kan. Impact of short-term exposure to fine particulate matter air pollution on urinary metabolome: A randomized, double-blind, crossover trial. *Environ. Int.*, 130(January):104878, 2019. ISSN 18736750. doi: 10.1016/j.envint.2019.05.072. URL https://doi.org/10.1016/j.envint.2019.05.072.

[83] Christian Madsen, Pal Rosland, Dominic Anthony Hoff, Wenche Nystad, Per Nafstad, and Øyvind Erik Næss. The short-term effect of 24-h average and peak air pollution on mortality in Oslo Norway. *Eur. J. Epidemiol.*, 27(9):717–727, 2012. ISSN 03932990. doi: 10.1007/s10654-012-9719-1.

[84] Lyndsey A. Darrow, Mitchel Klein, Jeremy A. Sarnat, James A. Mulholland, Matthew J. Strickland, Stefanie E. Sarnat, Armistead G. Russell, and Paige E. Tolbert. The use of alternative pollutant metrics in time-series studies of ambient air pollution and respiratory emergency department visits. *J. Expo. Sci. Environ. Epidemiol.*, 21(1):10–19, 2011. ISSN 15590631. doi: 10.1038/jes.2009.49.

[85] Krishnan Bhaskaran, Shakoor Hajat, Ben Armstrong, Andy Haines, Emily Herrett, Paul Wilkinson, and Liam Smeeth. The effects of hourly differences in air pollution on the risk of myocardial infarction: Case crossover analysis of the MINAP database. *BMJ*, 343(7824):1–11, 2011. ISSN 09598146. doi: 10.1136/bmj.d5531.

[86] Hualiang Lin, Kendra Ratnapradipa, Xiaojie Wang, Yonghui Zhang, Yanjun Xu, Zhenjiang Yao, Guanghui Dong, Tao Liu, Jessica Clark, Rebecca Dick, Jianpeng Xiao, Weilin Zeng, Xing Li, Zhengmin (Min) Qian, and Wenjun Ma. Hourly peak concentration measuring the PM2.5-mortality association: Results from six cities in the Pearl River Delta study. *Atmos. Environ.*, 161(April):27–33, 2017. ISSN 18732844. doi: 10.1016/j.atmosenv.2017.04.015. URL http://dx.doi.org/10.1016/j.atmosenv.2017.04.015.

[87] Pablo Orellano, Julieta Reynoso, Nancy Quaranta, Ariel Bardach, and Agustin Ciapponi. Short-term exposure to particulate matter (PM10 and PM2.5), nitrogen dioxide (NO_2), and ozone (O3) and all-cause and cause-specific mortality: Systematic review and meta-analysis. *Environ. Int.*, 142(December 2019): 105876, 2020. ISSN 18736750. doi: 10.1016/j.envint.2020.105876. URL https://doi.org/10.1016/j.envint.2020.105876.

[88] E. J.S. Mitchell, A. R. Lea-Langton, J. M. Jones, A. Williams, P. Layden, and R. Johnson. The impact of fuel properties on the emissions from the combustion of biomass and other solid fuels in a fixed bed domestic stove. *Fuel Process. Technol.*, 142:115–123, 2016. ISSN 03783820. doi: 10.1016/j.fuproc.2015.09.031. URL http://dx.doi.org/10.1016/j.fuproc.2015.09.031.

[89] E. D. Vicente, M. A. Duarte, A. I. Calvo, T. F. Nunes, L. Tarelho, and C. A. Alves. Emission of carbon monoxide, total hydrocarbons and particulate matter during wood combustion in a stove operating under distinct conditions. *Fuel Process. Technol.*, 131:182–192, 2015. ISSN 03783820. doi: 10.1016/j.fuproc.2014.11.021. URL http://dx.doi.org/10.1016/j.fuproc.2014.11.021.

[90] M. Mcnamara, J. Thornburg, E. Semmens, T. Ward, and C. Noonan. Coarse particulate matter and airborne endotoxin within wood stove homes. *Indoor Air*, 23 (6):498–505, 2013. ISSN 09056947. doi: 10.1111/ina.12043.

[91] Alma Lorelei de Jesus, Md Mahmudur Rahman, Mandana Mazaheri, Helen Thompson, Luke D. Knibbs, Cheol Jeong, Greg Evans, Wei Nei, Aijun Ding, Liping Qiao, Li Li, Harri Portin, Jarkko V. Niemi, Hilkka Timonen, Krista Luoma, Tuukka Petäjä, Markku Kulmala, Michal Kowalski, Annette Peters, Josef Cyrys, Luca Ferrero, Maurizio Manigrasso, Pasquale Avino, Giorgio Buonano, Cristina Reche, Xavier Querol, David Beddows, Roy M. Harrison, Mohammad H. Sowlat, Constantinos Sioutas, and Lidia Morawska. Ultrafine particles and PM2.5 in the air of cities around the world: Are they representative of each other? *Environ. Int.*, 129:118–135, aug 2019. ISSN 18736750. doi: 10.1016/j.envint.2019.05.021. URL https://doi.org/10.1016/j.envint.2019.05.021.

[92] P. Penttinen, K. L. Timonen, P. Tiittanen, A. Mirme, J. Ruuskanen, and J. Pekkanen. Ultrafine particles in urban air and respiratory health among adult asthmatics. *Eur. Respir. J.*, 17(3):428–435, 2001. ISSN 09031936. doi: 10.1183/09031936.01.17304280.

[93] Testing of solid fuel stoves, https://www.bsria.com/uk/news/article/testing-of-solid-fuel-stoves, 2020. URL https://www.bsria.com/uk/news/article/testing-of-solid-fuel-stoves.

[94] Tunga Salthammer, Tobias Schripp, Sebastian Wientzek, and Michael Wensing. Impact of operating wood-burning fireplace ovens on indoor air quality. *Chemosphere*, 103:205–211, 2014. ISSN 18791298. doi: 10.1016/j.chemosphere.2013.11.067. URL http://dx.doi.org/10.1016/j.chemosphere.2013.11.067.

[95] Sheffield The, For Leeds, Population Census, The Ons, The Ons, and The Population Census. 2011 Census First Results : Population Estimates, 2015.

[96] The City Council Sheffield. Air Quality : Action Plan, 2015.

[97] Urban Flows Observatory, https://urbanflows.ac.uk/, 2018. URL https://urbanflows.ac.uk/.

[98] Rohan Jayaratne, Xiaoting Liu, Phong Thai, Matthew Dunbabin, and Lidia Morawska. The influence of humidity on the performance of a low-cost air particle mass sensor and the effect of atmospheric fog. *Atmos. Meas. Tech.*, 11(8):4883–4890, 2018. ISSN 18678548. doi: 10.5194/amt-11-4883-2018.

[99] Florentin M.J. Bulot, Steven J. Johnston, Philip J. Basford, Natasha H.C. Easton, Mihaela Apetroaie-Cristea, Gavin L. Foster, Andrew K.R. Morris, Simon J. Cox, and Matthew Loxham. Long-term field comparison of multiple low-cost particulate matter sensors in an outdoor urban environment. *Sci. Rep.*, 9(1):1–13, 2019. ISSN 20452322. doi: 10.1038/s41598-019-43716-3. URL http://dx.doi.org/10.1038/s41598-019-43716-3.

[100] Gottfried Hänel. The properties of atmospheric aerosol particles as functions of the relative humidity at thermodynamic equilibrium with the surrounding moist air. *Adv. Geophys.*, 19(C):73–188, 1976. ISSN 00652687. doi: 10.1016/S0065-2687(08)60142-9.

[101] Norbert Streibl. Influence of Humidity on the Accuracy of Low-Cost Particulate Matter Sensors, 2017.

[102] Hilding Köhler. The nucleus in and the growth of hygroscopic droplets. *Trans. Faraday Soc.*, 32(1152):1152–1161, 1936. ISSN 00147672. doi: 10.1039/TF9363201152.

[103] M. D. Petters and S. M. Kreidenweis. A single parameter representation of hygroscopic growth and cloud condensation nucleus activity-Part 3: Including surfactant partitioning. *Atmos. Chem. Phys.*, 13(2):1081–1091, 2013. ISSN 16807316. doi: 10.5194/acp-13-1081-2013.

[104] B. Svenningsson, J. Rissler, E. Swietlicki, M. Mircea, M. Bilde, M. C. Facchini, S. Decesari, S. Fuzzi, J. Zhou, J. Mønster, and T. Rosenørn. Hygroscopic growth and critical supersaturations for mixed aerosol particles of inorganic and organic compounds of atmospheric relevance. *Atmos. Chem. Phys.*, 6(7):1937–1952, 2006. ISSN 16807324. doi: 10.5194/acp-6-1937-2006.

[105] South Coast Air Quality Management District (SCAQMD). Field Evaluation of SainSmart Background. http://www.aqmd.gov/aq-spec/evaluations/field, 2017.

[106] A I R Quality and Expert Group. Fine Particulate Matter (PM 2 . 5) in the United Kingdom, 2012. URL https://uk-air.defra.gov.uk/assets/documents/reports/cat11/1212141150{_}AQEG{_}Fine{_}Particulate{_}Matter{_}in{_}the{_}UK.pdf.

[107] Greg Ridgeway. Generalized Boosted Models: A guide to the gbm package. *Compute*, 1(4):1–12, 2007. ISSN 14679752. doi: 10.1111/j.1467-9752.1996.tb00390.x. URL http://cran.r-project.org/web/packages/gbm/vignettes/gbm.pdf.

[108] David C. Carslaw and Paul J. Taylor. Analysis of air pollution data at a mixed source location using boosted regression trees. *Atmos. Environ.*, 43(22-23):3563–3570, 2009. ISSN 13522310. doi: 10.1016/j.atmosenv.2009.04.001. URL http://dx.doi.org/10.1016/j.atmosenv.2009.04.001.

[109] Joo Chuan Tong. Cross-Validation. *Encycl. Syst. Biol.*, pages 508–508, 2013. doi: 10.1007/978-1-4419-9863-7_941.

[110] The Natural Environment Research Council, https://bit.ly/3kjWfn8, 2020. URL https://nerc.ukri.org/research/funded/programmes/clean-air/news/outcome-uk-clean-air-networks.

[111] Majid Ezzati and Daniel M. Kammen. The health impacts of exposure to indoor air pollution from solid fuels in developing countries: Knowledge, gaps, and data needs. *Environ. Health Perspect.*, 110(11):1057–1068, 2002. ISSN 00916765. doi: 10.1289/ehp.021101057.

[112] Ralph J. Delfino, Robert S. Zeiger, James M. Seltzer, Donald H. Street, and Christine E. McLaren. Association of asthma symptoms with peak particulate air pollution and effect modification by anti-inflammatory medication use. *Environ. Health Perspect.*, 110(10):607–617, 2002. ISSN 00916765. doi: 10.1289/ehp.021100607.

[113] A. Castro, A. I. Calvo, C. Blanco-Alegre, F. Oduber, C. Alves, E. Coz, F. Amato, X. Querol, and R. Fraile. Impact of the wood combustion in an open fireplace on the air quality of a living room: Estimation of the respirable fraction. *Sci. Total Environ.*, 628-629:169–176, 2018. ISSN 18791026. doi: 10.1016/j.scitotenv.2018.02.001. URL https://doi.org/10.1016/j.scitotenv.2018.02.001.

[114] World Health Organisation. *Air Pollution and Child Health: Prescribing Clean Air Summary*. World Health Organisation, Geneva, Switzerland, 2018. URL https://www.who.int/publications/i/item/9789241510781.

[115] L. Calder'on-Garcidue nas, R. Engle, A. Mora-Tiscare no, M. Styner, G. G'omez-Garza, H. Zhu, V. Jewells, R. Torres-Jard'on, L. Romero, M.E. Monroy-Acosta, et al. Exposure to severe urban air pollution influences cognitive outcomes, brain volume and systemic inflammation in clinically healthy children. *Brain Cogn*, 77: 345–355, 2011. URL https://www.ncbi.nlm.nih.gov/pubmed/21647768.

[116] C. Freire, R. Ramos, R. Puertas, M.J. Lopez Espinosa, J. Julvez, I. Aguilera, F. Cruz, M.F. Fernandez, J. Sunyer, and N. Olea. Association of traffic-related air pollution with cognitive development in children. *J Epidemiol Community Health*, 64:223–228, 2010. URL https://www.ncbi.nlm.nih.gov/pubmed/19949794.

[117] S. Roberts, L. Arseneault, B. Barratt, S. Beevers, A. Danese, C.L. Odgers, T.E. Moffitt, A. Reuben, F.J. Kelly, and H.L. Fisher. Exploration of NO_2 and pm2.5 air pollution and mental health problems using high-resolution data in london-based children from a uk longitudinal cohort study. *Psychiatry Res*, 272:8–17, 2019. URL https://www.ncbi.nlm.nih.gov/pubmed/30737466.

[118] F. An, J. Liu, W. Lu, and D. Jareemit. A review of the effect of traffic-related air pollution around schools on student health and its mitigation. *J Transp Health*, 23:101249, 2021. URL https://www.sciencedirect.com/science/article/pii/S2214140520303957.

[119] R. Brugha and J. Grigg. Urban air pollution and respiratory infections. *Paediatr Respir Rev*, 15:194–199, 2014. URL https://www.ncbi.nlm.nih.gov/pubmed/24793794.

[120] D. C. Payne-Sturges, M. A. Marty, F. Perera, M. D. Miller, M. Swanson, K. Ellickson, D. A. Cory-Slechta, B. Ritz, J. Balmes, L. Anderko, et al. Healthy air, healthy brains: Advancing air pollution policy to protect children's health. *Am. J. Public Health*, pages 550–554, 2019. doi: 10.2105/AJPH.2018.304902.

[121] D. Sofia, F. Gioiella, N. Lotrecchiano, and A. Giuliano. Mitigation strategies for reducing air pollution. *Environ. Sci. Pollut. Res.*, 27:19226–19235, 2020. doi: 10.1007/s11356-020-08647-x.

[122] M. Amann, G. Kiesewetter, W. Schöpp, Z. Klimont, W. Winiwarter, J. Cofala, P. Rafaj, L. Höglund-Isaksson, A. Gomez-Sabriana, and C. Heyes. Reducing global air pollution: The scope for further policy interventions: Achieving clean air worldwide. *Philos. Trans. R. Soc. A*, 378:1–27, 2020. doi: 10.1098/rsta.2019.0331.

[123] European Commission. *Green Infrastructure (GI) — Enhancing Europe's Natural Capital*. Brussels, 2013.

[124] M. del C. Redondo Bermúdez. *Plants, Ambient Air Quality, and Human Health*, pages 1–12. Springer, Cham, 2020. ISBN 9783319696270.

[125] R. Baldauf. *Air pollution mitigation through vegetation barriers and green space*, pages 437–453. Elsevier Inc., 2020. ISBN 9780128181225.

[126] P. Deshmukh, V. Isakov, A. Venkatram, B. Yang, K.M. Zhang, R. Logan, and R. Baldauf. The effects of roadside vegetation characteristics on local, near-road air quality. *Air Qual. Atmos. Heal.*, 12:259–270, 2019. doi: 10.1007/s11869-018-0651-8.

[127] R. Grote, R. Samson, R. Alonso, J.H. Amorim, P. Cariñanos, G. Churkina, S. Fares, D. Le Thiec, Ü. Niinemets, and T.N. Mikkelsen. Functional traits of urban trees: air pollution mitigation potential. *Front. Ecol. Environ.*, 14:543–550, 2016. doi: 10.1002/fee.1426.

[128] US EPA. Best practices for reducing near-road pollution exposure at schools, 2015.

[129] Landscape & urban design, 2019.

[130] Groundwork. *Air Quality Green Infrastructure: A Toolkit for Schools.* London, 2019.

[131] Bbc newsround air pollution: How a school in manchester is fighting back against air pollution, 2021.

[132] T. Barrett. 'life-saving' scheme to tackle air pollution at manchester schools. *airqualitynews.com*, 2019.

[133] Mayor of London Press Office. Mayor's green fund helps schools fight toxic air, 2019.

[134] K. V. Abhijith, V. Kukadia, and P. Kumar. Investigation of air pollution mitigation measures, ventilation, and indoor air quality at three schools in london. *Atmos. Environ.*, 289, 2022. doi: 10.1016/j.atmosenv.2022.119303.

[135] A.N. Al-dabbous and P. Kumar. The influence of roadside vegetation barriers on airborne nanoparticles and pedestrians exposure under varying wind conditions. *Atmos. Environ.*, 90:113–124, 2014. doi: 10.1016/j.atmosenv.2014.03.040.

[136] W.R. Chang. Effect of porous hedge on cross ventilation of a residential building. *Build. Environ.*, 41:549–556, 2006. doi: 10.1016/j.buildenv.2005.02.032.

[137] Y. Xing and P. Brimblecombe. Role of vegetation in deposition and dispersion of air pollution in urban parks. *Atmos. Environ.*, 201:73–83, 2019. doi: 10.1016/j.atmosenv.2018.12.027.

[138] V.M. Jayasooriya, A.W.M. Ng, S. Muthukumaran, and B.J.C. Perera. Green infrastructure practices for improvement of urban air quality. *Urban For. Urban Green.*, 21:34–47, 2017. doi: 10.1016/j.ufug.2016.11.007.

[139] A.P.R. Jeanjean, J. Gallagher, P.S. Monks, and R.J. Leigh. Ranking current and prospective NO_2 pollution mitigation strategies: An environmental and economic modelling investigation in oxford street, london. *Environ. Pollut.*, 225:587–597, 2017. doi: 10.1016/j.envpol.2017.03.027.

[140] T.A.M. Pugh, A.R. MacKenzie, J.D. Whyatt, and C.N. Hewitt. Effectiveness of green infrastructure for improvement of air quality in urban street canyons. *Environ. Sci. Technol.*, 46:7692–7699, 2012. doi: 10.1021/es300826w.

[141] T.E. Morakinyo and Y.F. Lam. Simulation study of dispersion and removal of particulate matter from traffic by road-side vegetation barrier. *Environ. Sci. Pollut. Res.*, 23:6709–6722, 2016. doi: 10.1007/s11356-015-5839-y.

[142] B.A. Maher, T. Gonet, V. V. Karloukovski, H. Wang, and T.J. Bannan. Protecting playgrounds: local-scale reduction of airborne particulate matter concentrations through particulate deposition on roadside 'tredges' (green infrastructure). *Sci. Rep.*, 12:1–11, 2022. doi: 10.1038/s41598-022-18509-w.

[143] Uk department for transport road traffic statistics - local authority sheffield. https://roadtraffic.dft.gov.uk/local-authorities/159, 2021. Accessed on Jul 20, 2022.

[144] Institute for Government. Timeline of uk government coronavirus lockdowns and restrictions, 2021. Available online: https://www.instituteforgovernment.org.uk/charts/uk-government-coronavirus-lockdowns (accessed on Apr 4, 2022).

[145] P.F. Ortiz. Urban flows observatory portal, 2019. Available online: https://sheffield-portal.urbanflows.ac.uk/uflobin/ufportal/ (accessed on Oct 30, 2021).

[146] M. del C. Redondo-Bermúdez, A. Jorgensen, R.W. Cameron, and M. Val Martin. Green infrastructure for air quality plus (gi4aq+): defining critical dimensions for implementation in schools and the meaning of 'plus' in a uk context. *Nature-Based Solut.*, 2:2–13, 2022. doi: 10.1016/j.nbsj.2022.100017.

[147] M del C Redondo-Berm'udez, IT Gulenc, RW Cameron, and BJ Inkson. 'green barriers' for air pollutant capture: Leaf micromorphology as a mechanism to explain plants capacity to capture particulate matter. *Environmental Pollution*, 288:1–12, 2021. doi: 10.1016/j.envpol.2021.117809.

[148] R Chakraborty, J Heydon, M Mayfield, and L Mihaylova. Indoor air pollution from residential stoves: Examining the flooding of particulate matter into homes during real-world use. *Atmosphere*, 11(12):1–25, 2020. doi: 10.3390/atmos11121326.

[149] S Munir, M Mayfield, D Coca, and SA Jubb. Structuring an integrated air quality monitoring network in large urban areas – discussing the purpose, criteria and deployment strategy. *Atmospheric Environment X*, 2:1–8, 2019. doi: 10.1016/j.aeaoa.2019.100027.

[150] Global co-location comparison trials, 2020. URL https://www.aqmesh.com/performance/co-location-comparison-trials/.

[151] Breathe London. Breathe london technical report. pilot phase (2018-2020), 2021.

[152] W. Mohammed, N. Shantz, L. Neil, T. Townend, A. Adamescu, and H. A. Al-Abadleh. Air quality measurements in kitchener, ontario, canada using multisensor mini monitoring stations. *Atmosphere (Basel)*, 2022. doi: 10.3390/atmos13010083.

[153] Sheffield City Council. Air quality in sheffield, 2021. URL https://www.sheffield.gov.uk/home/pollution-nuisance/air-quality. Accessed on Nov 19, 2021.

[154] DEFRA. Diffusion tubes overview, 2022. URL https://laqm.defra.gov.uk/air-quality/air-quality-assessment/diffusion-tubes-overview/. Accessed on Mar 10, 2022.

[155] N. Castell, P. Schneider, S. Grossberndt, M. F. Fredriksen, G. Sousa-Santos, M. Vogt, and A. Bartonova. Localized real-time information on outdoor air quality at kindergartens in oslo, norway using low-cost sensor nodes. *Environ. Res*, pages 410–419, 2018. doi: 10.1016/j.envres.2017.10.019.

[156] Environmental Instruments Ltd. Aq mesh an air quality monitoring system available online: (accessed on nov 18, 2021. URL https://www.aqmesh.com/products/aqmesh/.

[157] DEFRA. Information resource site information for sheffield devonshire green (uka00575) available online: (accessed on nov 19, 2021. URL https://uk-air.defra.gov.uk/networks/site-info?uka_id=UKA00575.

[158] A. Loader. NO_2 diffusion tubes for laqm: Guidance note for local authorities, 2006.

[159] Sheffield City Council. Map of diffusion tubes, 2022. URL https://www.sheffield.gov.uk/home/pollution-nuisance/air-quality. Accessed on Feb 2, 2022.

[160] O. Oguntoke, F.O. Emoruwa, and M.A. Taiwo. Assessment of air pollution and health hazard associated with sawmill and municipal waste burning in abeokuta metropolis, nigeria. *Environ. Sci. Pollut. Res.*, 26:32708–32722, 2019. doi: 10.1007/s11356-019-04310-2.

[161] A. Embiale, F. Zewge, B. S. Chandravanshi, and E. Sahle-Demessie. Commuter exposure to particulate matters and total volatile organic compounds at roadsides in addis ababa, ethiopia. *Int. J. Environ. Sci. Technol*, pages 4761–4774, 2019. doi: 10.1007/s13762-018-2116-x.

[162] P. Apparicio, J. Gelb, M. Carrier, M.È. Mathieu, and S. Kingham. Exposure to noise and air pollution by mode of transportation during rush hours in montreal. *J. Transp. Geogr*, pages 182–192, 2018. doi: 10.1016/j.jtrangeo.2018.06.007.

[163] A. N. Al-Dabbous and P. Kumar. The influence of roadside vegetation barriers on airborne nanoparticles and pedestrians exposure under varying wind conditions. *Atmos. Environ*, pages 113–124, 2014. doi: 10.1016/j.atmosenv.2014.03.040.

[164] Urban Flows Observatory. The MOBIUS project, 2021. URL https://urbanflows.ac.uk/mobius/. Accessed on Nov 18, 2021.

[165] R. Bao and A. Zhang. Does lockdown reduce air pollution? evidence from 44 cities in northern china. *Sci. Total Environ.*, 731:1–12, 2020. doi: 10.1016/j.scitotenv.2020.139052.

[166] L. Menut, B. Bessagnet, G. Siour, S. Mailler, R. Pennel, and A. Cholakian. Impact of lockdown measures to combat covid-19 on air quality over western europe. *Sci. Total Environ.*, 741:1–9, 2020. doi: 10.1016/j.scitotenv.2020.140426.

[167] K. Ropkins and J.E. Tate. Early observations on the impact of the covid-19 lockdown on air quality trends across the uk. *Sci. Total Environ.*, 754:142374, 2021. doi: 10.1016/j.scitotenv.2020.142374.

[168] N. Mohajeri, A. Walch, A. Gudmundsson, C. Heaviside, S. Askari, P. Wilkinson, and M. Davies. Covid-19 mobility restrictions: impacts on urban air quality and health. *Build. Cities*, 2:759–788, 2021. doi: 10.5334/bc.124.

[169] D.C. Carslaw. Deweather—an R package to remove meteorological variation from air quality data, 2021. URL https://github.com/davidcarslaw/deweather. Accessed on Dec 10, 2021.

[170] G. Ridgeway. gbm—generalized boosted models. R package, 2022. URL https://cran.r-project.org/package=gbm. Accessed on Jan 3, 2022.

[171] D.C. Carslaw. Worldmet—R package for accessing noaa integrated surface database (isd) meteorological observations, 2010.

[172] D.C. Carslaw and K. Ropkins. openair—an R package for air quality data analysis. *Environ. Model. Softw.*, 27-28:52–61, 2012.

[173] S. Munir, M. Mayfield, D. Coca, L.S. Mihaylova, and O. Osammor. Analysis of air pollution in urban areas with airviro dispersion model-a case study in the city of sheffield, united kingdom. *Atmosphere (Basel)*, 11:1–27, 2020. doi: 10.3390/atmos11030285.

[174] Greater London Authority. Using green infrastructure to protect people from air pollution, 2019.

[175] K. V Abhijith, P. Kumar, J. Gallagher, A. Mcnabola, R. Baldauf, F. Pilla, B. Broderick, S. Di Sabatino, and B. Pulvirenti. Air pollution abatement performances of green infrastructure in open road and built-up street canyon environments - a review. *Atmos. Environ.*, 162:71–86, 2017. doi: 10.1016/j.atmosenv.2017.05.014.

[176] P. Kumar, J.C. Zavala-Reyes, M. Tomson, and G. Kalaiarasan. Understanding the effects of roadside hedges on the horizontal and vertical distributions of air pollutants in street canyons. *Environ. Int.*, 158:1–15, 2022. doi: 10.1016/j.envint.2021.106883.

[177] K. V Abhijith, P. Kumar, J. Gallagher, A. Mcnabola, R. Baldauf, F. Pilla, B. Broderick, S. Di Sabatino, and B. Pulvirenti. Air pollution abatement performances of green infrastructure in open road and built-up street canyon environments - a review. *Atmos. Environ.*, 162:71–86, 2017. doi: 10.1016/j.atmosenv.2017.05.014.

[178] R. Baldauf. Roadside vegetation design characteristics that can improve local, near-road air quality. *Transp. Res. Part D*, 52:354–361, 2017. doi: 10.1016/j.trd.2017.03.013.

[179] H. Pearce, J.G. Levine, X. Cai, and A. Rob Mackenzie. Introducing the green infrastructure for roadside air quality (gi4raq) platform: Estimating site-specific changes in the dispersion of vehicular pollution close to source. *Forests*, 12, 2021. doi: 10.3390/f12060769.

[180] I. Neft, M. Scungio, N. Culver, and S. Singh. Simulations of aerosol filtration by vegetation: Validation of existing models with available lab data and application to near-roadway scenario. *Aerosol Sci. Technol*, pages 937–946, 2016. doi: 10.1080/02786826.2016.1206653.

[181] T.E. Morakinyo, Y.F. Lam, and S. Hao. Evaluating the role of green infrastructures on near-road pollutant dispersion and removal: Modelling and measurement. *J. Environ. Manage.*, 182:595–605, 2016. doi: 10.1016/j.jenvman.2016.07.077.

[182] A. Tiwari, P. Kumar, R. Baldauf, K.M. Zhang, F. Pilla, S. Di Sabatino, E. Brattich, and B. Pulvirenti. Considerations for evaluating green infrastructure impacts in microscale and macroscale air pollution dispersion models. *Sci. Total Environ.*, 672:410–426, 2019.

[183] H. Pearce, J.G. Levine, X. Cai, and A.R. MacKenzie. Introducing the green infrastructure for roadside air quality (gi4raq) platform: Estimating site-specific changes in the dispersion of vehicular pollution close to source. *Forests*, 12:1–29, 2021. doi: 10.3390/f12060769.

[184] M. Tomson, P. Kumar, Y. Barwise, P. Perez, H. Forehead, K. French, L. Morawska, and J.F. Watts. Green infrastructure for air quality improvement in street canyons. *Environ. Int.*, 146:106288, 2021. doi: 10.1016/j.envint.2020.106288.

[185] X.B. Li, Q.C. Lu, S.J. Lu, H. Di He, Z.R. Peng, Y. Gao, and Z.Y. Wang. The impacts of roadside vegetation barriers on the dispersion of gaseous traffic pollution in urban street canyons. *Urban Forestry & Urban Greening*, 17:80–91, 2016. doi: 10.1016/j.ufug.2016.03.006.

[186] A.H. Temper and D.C. Green. The impact of a green screen on concentrations of nitrogen dioxide at bowes primary school , enfield prepared for the london borough of enfield, 2018.

[187] Emissions of air pollutants in the uk – particulate matter (pm10 and pm2.5). https://www.gov.uk/government/statistics/emissions-of-air-pollutants/emissions-of-air-pollutants-in-the-uk-particulate-matter-pm10-and-pm2.5#major-emission-sources-for-pm10-and-pm25-in-the-uk, 2022. accessed on Apr 10, 2022.

[188] F. Amato, I. Rivas, M. Viana, T. Moreno, L. Bouso, C. Reche, M. Àlvarez Pedrerol, A. Alastuey, J. Sunyer, and X. Querol. Sources of indoor and outdoor pm2.5 concentrations in primary schools. *Sci. Total Environ.*, 490:757–765, 2014. doi: 10.1016/j.scitotenv.2014.05.051.

[189] B. Zeb, K. Alam, A. Sorooshian, T. Blaschke, I. Ahmad, and I. Shahid. On the morphology and composition of particulate matter in an urban environment. *Aerosol Air Qual. Res.*, 18:1431–1447, 2018. doi: 10.4209/aaqr.2017.09.0340.

[190] T. Pachauri, V. Singla, A. Satsangi, A. Lakhani, and K. Maharaj Kumari. Sem-edx characterization of individual coarse particles in agra, india. *Aerosol Air Qual. Res.*, 13:523–536, 2013. doi: 10.4209/aaqr.2012.04.0095.

[191] Z.H. Zhang, A. Khlystov, L.K. Norford, Z.K. Tan, and R. Balasubramanian. Characterization of traffic-related ambient fine particulate matter (pm2.5) in an asian city: Environmental and health implications. *Atmos. Environ.*, 161:132–143, 2017. doi: 10.1016/j.atmosenv.2017.04.040.

[192] P. Pant and R.M. Harrison. Estimation of the contribution of road traffic emissions to particulate matter concentrations from field measurements: A review. *Atmos. Environ.*, 77:78–97, 2013. doi: 10.1016/j.atmosenv.2013.04.028.

[193] T. Gonet, B. A. Maher, and J. Kukutschová. Source apportionment of magnetite particles in roadside airborne particulate matter. *Sci. Total Environ*, 2021. doi: 10.1016/j.scitotenv.2020.141828.

[194] C.L.S. Wiseman and F. Zereini. Airborne particulate matter, platinum group elements and human health: A review of recent evidence. *Sci. Total Environ.*, 407: 2493–2500, 2009. doi: 10.1016/j.scitotenv.2008.12.057.

[195] K. Ravindra, L. Bencs, and R. Van Grieken. Platinum group elements in the environment and their health risk. *Sci. Total Environ.*, 318:1–43, 2004. doi: 10.1016/S0048-9697(03)00372-3.

[196] U. Weerakkody, J.W. Dover, P. Mitchell, and K. Reiling. Particulate matter pollution capture by leaves of seventeen living wall species with special reference to rail-traffic at a metropolitan station. *Urban For. Urban Green.*, 27:173–186, 2017. doi: 10.1016/j.ufug.2017.07.005.

[197] K. V. Abhijith and P. Kumar. Quantifying particulate matter reduction and their deposition on the leaves of green infrastructure. *Environ. Pollut.*, 265:114884, 2020. doi: 10.1016/j.envpol.2020.114884.

[198] A. Diener and P. Mudu. How can vegetation protect us from air pollution? a critical review on green spaces' mitigation abilities for air-borne particles from a public health perspective - with implications for urban planning. *Sci. Total Environ.*, 796: 1–18, 2021. doi: 10.1016/j.scitotenv.2021.148605.

[199] Y. Barwise and P. Kumar. Designing vegetation barriers for urban air pollution abatement: a practical review for appropriate plant species selection. *Clim. Atmos. Sci.*, 3:1–19, 2020. doi: 10.1038/s41612-020-0115-3.

[200] DEFRA. Emissions of air pollutants in the uk – nitrogen oxides (nox), 2020. URL https://www.gov.uk/government/statistics/emissions-of-air-pollutants/emissions-of-air-pollutants-in-the-uk-nitrogen-oxides-nox. Accessed on May 17, 2022.

[201] C.N. Hewitt, K. Ashworth, and A.R. Mackenzie. Using green infrastructure to improve urban air quality (gi4aq). *Ambio*, 2020. doi: 10.1007/s13280-019-01164-3.

[202] London lockdown sees spike in outdoor fires — london-fire.gov.uk. https://www.london-fire.gov.uk/news/2020-news/april/london-lockdown-sees-spike-in-outdoor-fires/, 2020. [Accessed 29-Jan-2023].

[203] S. Munir, G. Coskuner, M.S. Jassim, Y.A. Aina, A. Ali, and M. Mayfield. Changes in air quality associated with mobility trends and meteorological conditions during covid-19 lockdown in northern england, uk. *Atmosphere (Basel)*, 12:1–27, 2021. doi: 10.3390/atmos12040504.

[204] World Health Organization. WHO global ambient air quality database (update 2018). *World Health Organization, Geneva, Switzerland*, 2018.

[205] Philip J Landrigan. Air pollution and health. *The Lancet Public Health*, 2(1):e4–e5, 2017.

[206] World Health Organization. Health effects of particulate matter: Policy implications for countries in Eastern Europe, Caucasus and central Asia (2013). *World Health Organization Regional Office for Europe, Copenhagen*, 2013.

[207] Hong Chen, Jeffrey C Kwong, Ray Copes, Karen Tu, Paul J Villeneuve, Aaron Van Donkelaar, Perry Hystad, Randall V Martin, Brian J Murray, Barry Jessiman, et al. Living near major roads and the incidence of dementia, parkinson's disease, and multiple sclerosis: a population-based cohort study. *The Lancet*, 389(10070): 718–726, 2017.

[208] Haneen Khreis, Kees de Hoogh, and Mark J Nieuwenhuijsen. Full-chain health impact assessment of traffic-related air pollution and childhood asthma. *Environment international*, 114:365–375, 2018.

[209] DEFRA. Improving air quality: national plan for tackling nitrogen dioxide in our towns and cities - Defra - Citizen Space — consult.defra.gov.uk. https://consult.defra.gov.uk/airquality/air-quality-plan-for-tackling-nitrogen-dioxide/, 2015. [Accessed 29-Jan-2023].

[210] Aakash C Rai, Prashant Kumar, Francesco Pilla, Andreas N Skouloudis, Silvana Di Sabatino, Carlo Ratti, Ansar Yasar, and David Rickerby. End-user perspective of low-cost sensors for outdoor air pollution monitoring. *Science of The Total Environment*, 607:691–705, 2017.

[211] Tongshu Zheng, Michael H Bergin, Ronak Sutaria, Sachchida N Tripathi, Robert Caldow, and David E Carlson. Gaussian process regression model for dynamically calibrating and surveilling a wireless low-cost particulate matter sensor network in delhi. *Atmospheric Measurement Techniques*, 12(9):5161–5181, 2019.

[212] Jiaming Shen. $PM_{2.5}$ concentration prediction using times series based data mining. *City*, 2013:2014–2020, 2012.

[213] Camillo Silibello, Alessio D'Allura, Sandro Finardi, Andrea Bolignano, and Roberto Sozzi. Application of bias adjustment techniques to improve air quality forecasts. *Atmospheric Pollution Research*, 6(6):928–938, 2015.

[214] Donald F Specht. A general regression neural network. *IEEE Transactions on Neural Networks*, 2(6):568–576, 1991.

[215] David E Rumelhart, Geoffrey E Hinton, and Ronald J Williams. Learning representations by back-propagating errors. *Nature*, 323(6088):533–536, 1986.

[216] KuoPing Lin, PingFeng Pai, and ShunLing Yang. Forecasting concentrations of air pollutants by logarithm support vector regression with immune algorithms. *Applied Mathematics and Computation*, 217(12):5318–5327, 2011.

[217] Yushun Mao and Shiejue Lee. Deep convolutional neural network for air quality prediction. In *Journal of Physics: Conference Series*, volume 1302, pages 1–6. IOP Publishing, 2019.

[218] Adrià Garriga-Alonso, Carl Edward Rasmussen, and Laurence Aitchison. Deep convolutional networks as shallow gaussian processes. *arXiv preprint arXiv:1808.05587*, 2018.

[219] Peng Wang, Lyudmila Mihaylova, Said Munir, Rohit Chakraborty, Jikai Wang, Martin Mayfield, Khan Alam, Muhammad Fahim Khokhar, and Daniel Coca. A computationally efficient symmetric diagonally dominant matrix projection-based gaussian process approach. *Signal Processing*, 183:108034, 2021.

[220] David R Burt, Carl E Rasmussen, and Mark Van Der Wilk. Rates of convergence for sparse variational Gaussian process regression. *arXiv preprint arXiv:1903.03571*, 2019.

[221] Haitao Liu, Yew-Soon Ong, Xiaobo Shen, and Jianfei Cai. When gaussian process meets big data: A review of scalable gps. *IEEE transactions on neural networks and learning systems*, 31(11):4405–4423, 2020.

[222] Christopher KI Williams and Carl Edward Rasmussen. *Gaussian processes for machine learning*. MIT press Cambridge, MA, 2006.

[223] Michael Wu, Bei Yin, Guohui Wang, Chris Dick, Joseph R Cavallaro, and Christoph Studer. Large-scale mimo detection for 3gpp lte: Algorithms and fpga implementations. *IEEE Journal of Selected Topics in Signal Processing*, 8(5):916–929, 2014.

[224] Zexun Chen and Bo Wang. How priors of initial hyperparameters affect Gaussian process regression models. *Neurocomputing*, 275:1702–1710, 2018.

[225] Dengkui Zhu, Boyu Li, and Ping Liang. On the matrix inversion approximation based on neumann series in massive mimo systems. In *2015 IEEE international conference on communications (ICC)*, pages 1763–1769. IEEE, 2015.

[226] Michalis Titsias. Variational learning of inducing variables in sparse Gaussian processes. In *Proceedings of Artificial Intelligence and Statistics*, pages 567–574, 2009.

[227] Edward Snelson and Zoubin Ghahramani. Sparse Gaussian processes using pseudo-inputs. In *Proceedings of Advances in neural information processing systems*, pages 1257–1264, 2006.

[228] Clément Magnant, Audrey Giremus, Eric Grivel, Laurent Ratton, and Bernard Joseph. Bayesian non-parametric methods for dynamic state-noise covariance matrix estimation: Application to target tracking. *Signal Processing*, 127:135–150, 2016.

[229] Joaquin Quiñonero-Candela and Carl Edward Rasmussen. A unifying view of sparse approximate Gaussian process regression. *Journal of Machine Learning Research*, 6(12):1939–1959, 2005.

[230] Peng Wang, Youngjoo Kim, Lubos Vaci, Haoze Yang, and Lyudmila Mihaylova. Short-term traffic prediction with vicinity Gaussian process in the presence of missing data. In *2018 Sensor Data Fusion: Trends, Solutions, Applications (SDF)*, pages 1–6. IEEE, 2018.

[231] Haijun Wang, Xinbo Gao, Kaibing Zhang, and Jie Li. Fast single image super-resolution using sparse Gaussian process regression. *Signal Processing*, 134:52–62, 2017.

[232] Christopher KI Williams and Matthias Seeger. Using the Nyström method to speed up kernel machines. In *Proc. from Advances in Neural Information Processing Systems*, pages 682–688, 2001.

[233] Fei Zhu and Paul Honeine. Online kernel nonnegative matrix factorization. *Signal Processing*, 131:143–153, 2017.

[234] R Ben Abdallah, Arnaud Breloy, Mohammed Nabil El Korso, and David Lautru. Bayesian signal subspace estimation with compound gaussian sources. *Signal Processing*, 167:107310, 2020.

[235] William H Press, Saul A Teukolsky, William T Vetterling, and Brian P Flannery. *Numerical Recipes in C*. Cambridge University Press, Cambridge, 1988.

[236] Sivaram Ambikasaran, Daniel Foreman-Mackey, Leslie Greengard, David W Hogg, and Michael O'Neil. Fast direct methods for Gaussian processes. *IEEE Transactions on Pattern Analysis and Machine Intelligence*, 38(2):252–265, 2015.

[237] Kai Zhang, Ivor W Tsang, and James T Kwok. Improved nyström low-rank approximation and error analysis. In *Proceedings of the 25th international conference on Machine learning*, pages 1232–1239, 2008.

[238] Li He, Nilanjan Ray, and Hong Zhang. Error bound of nyström-approximated ncut eigenvectors and its application to training size selection. *Neurocomputing*, 239: 130–142, 2017.

[239] Michael L Stein. Limitations on low rank approximations for covariance matrices of spatial data. *Spatial Statistics*, 8:1–19, 2014.

[240] David M Blei, Alp Kucukelbir, and Jon D McAuliffe. Variational inference: A review for statisticians. *Journal of the American Statistical Association*, 112(518): 859–877, 2017.

[241] Marie Ouimet and Yoshua Bengio. Greedy spectral embedding. In *Proceedings of the 10th International Workshop on Artificial Intelligence and Statistics*, pages 253–260, 2005.

[242] Cameron Musco and Christopher Musco. Recursive sampling for the nyström method. In *Advances in Neural Information Processing Systems*, pages 3833–3845, 2017.

[243] Yi Ding, Risi Kondor, and Jonathan Eskreis-Winkler. Multiresolution kernel approximation for Gaussian process regression. In *Advances in Neural Information Processing Systems*, pages 3740–3748, 2017.

[244] Jichuan Li and Arye Nehorai. Gaussian mixture learning via adaptive hierarchical clustering. *Signal Processing*, 150:116–121, 2018.

[245] Xifeng Yao and Chunhui Zhao. Kernel-band-projection algorithm for anomaly detection in hyperspectral imagery. In *Proceedings of the 14th IEEE International Conference on Signal Processing (ICSP)*, pages 300–303. IEEE, 2018.

[246] Zheng Tracy Ke, Lingzhou Xue, and Fan Yang. Diagonally-dominant principal component analysis. *Journal of Computational and Graphical Statistics*, pages 1–16, 2020. accepted.

[247] María Mendoza, Marcos Raydan, and Pablo Tarazaga. Computing the nearest diagonally dominant matrix. *Numerical linear algebra with applications*, 5(6):461–474, 1998.

[248] United Nations. United nations announces 2019 climate action summit 'clean air initiative', calls on governments at all levels to join., 2019. URL https://www.un.org/sustainabledevelopment/blog/2019/07/clean-air-initiative-calls-climate-action/.

[249] Royal College of Paediatrics and Child Health. Every breath we take: the lifelong impact of air pollution, available at: https://www.rcplondon.ac.uk/projects/outputs/every-breath-we-take-lifelong-impact-air-pollution., 2016. URL https://www.rcplondon.ac.uk/projects/outputs/every-breath-we-take-lifelong-impact-air-pollution.

[250] A. Clifford, L. Lang, R. Chen, K. J. Anstey, and A. Seaton. Exposure to air pollution and cognitive functioning across the life course–a systematic literature review. *Environmental Research*, 147, 2016. doi: 10.1016/j.envres.2016.01.018. URL https://doi.org/10.1016/j.envres.2016.01.018.

[251] M. S. Qian, M. S. Yan Wang, A. Zanobetti, Y. Wang, P. Koutrakis, C. Choirat, F. Dominici, and J. Schwartz. Air pollution and mortality in the medicare population. *The New England Journal of Medicine*, 376, 2017. doi: 10.1056/NEJMoa1702747. URL https://doi.org/10.1056/NEJMoa1702747.

[252] K. Kim, P. Kumar, J. Szulejko, A. Adelodun, M. Junaid, M. Uchimiya, and S. Chambers. Toward a better understanding of the impact of mass transit air pollutants on human health. *Chemosphere.*, 174, 2017. doi: 10.1016/j.chemosphere.2017.01.113. URL https://doi.org/10.1016/j.chemosphere.2017.01.113.

[253] F. Kelly and J. Fussell. Air pollution and public health: emerging hazards and improved understanding of risk. *Environmental Geochemistry and Health*, 37, 2015. doi: 10.1007/s10653-015-9720-1. URL https://doi.org/10.1007/s10653-015-9720-1.

[254] Gehring, U., et al. Air pollution exposure and lung function in children: the escrape project. environmental health perspectives., 2013.

[255] J. J. Kim. Ambient air pollution: health hazards to children. *Pediatrics*, 114, 2004. doi: 10.1542/peds.2004-1001. URL https://doi.org/10.1542/peds.2004-1001.

[256] H. S. Kenagy, C. Lin, H. Wu, and M. R. Heal. Greater nitrogen dioxide concentrations at child versus adult breathing heights close to urban main road kerbside. *Air Quality, Atmosphere and Health*, 9, 2016. doi: 10.1007/s11869-015-0370-3. URL https://doi.org/10.1007/s11869-015-0370-3.

[257] J. Forns, P. Dadvand, M. Esnaola, M. Alvarez-Pedrerol, M. López-Vicente, R. Garcia-Esteban, M. Cirach, X. Basagaña, M. Guxens, and J. Sunyer. Longitudinal association between air pollution exposure at school and cognitive development in school children over a period of 3.5 years. *Environmental Research*, 159, 2017. doi: 10.1016/j.envres.2017.08.031. URL https://doi.org/10.1016/j.envres.2017.08.031.

[258] O. Myhre, M. Låg, G. Villanger, B. Oftedal, J. Øvrevik, J. Holme, H. Aase, R. Paulsen, A. Bal-Price, and H. Dirven. Early life exposure to air pollution particulate matter (pm) as risk factor for attention deficit/ hyperactivity disorder (adhd): need for novel strategies for mechanisms and causalities. *Toxicology and Applied Pharmacology*, 1, 2018. doi: 10.1016/j.taap.2018.03.015. URL https://doi.org/10.1016/j.taap.2018.03.015.

[259] R. J. Sram, M. Veleminksy, and J. Stejskalova. The impact of air pollution to central nervous system in children and adults. *Neuro Endocrinology Letters*, 38, 2017.

[260] A. Bandyopadhyay. Neurological disorders from ambient (urban) air pollution emphasizing ufpm and pm2.5. *Current Pollution Reports*, 2, 2016. doi: 10.1007/s40726-016-0039-z. URL https://doi.org/10.1007/s40726-016-0039-z.

[261] Paulos, E., Honicky, R. J., & Hooker, B. Citizen science: enabling participatory urbanism. in m. foth (ed.), handbook on research on urban infomatics: the practice and promise of the real-time city (pp. 414–436). hershey: Goldman et al. 2009: 3., 2009.

[262] Bales, E., Nikzad, N., Quick, N., Ziftci, C., Patrick, K. & Griswold, W. Citisense: mobile air quality sensing for individuals and communities. design and deployment of the citisense mobile air-quality system. proceedings of the 6th international conference on pervasive computing technologies for healthcare. 3-6. https://doi.org/10.1145/2384716.2384728, 2012.

[263] G. Wong-Parodi, M. B. Dias, and M. Taylor. Effect of using an indoor air quality sensor on perceptions of and behaviors toward air pollution (pittsburgh empowerment library study): online survey and interviews'. *JMIR mHealth and uHealth*, 6: 3, 2018.

[264] Bales, E., Nikzad, N., Quick, N., Ziftci, C., Patrick, K., & Griswold, W. Personal pollution monitoring: mobile real-time air quality in daily life. personal and ubiquitous computing, 23(2), 309–328., 2019.

[265] S. Folkman. *An approach to the measurement of coping'*. Journal of Organisational Behaviour;, 1982.

[266] Amanda Biggs, Paula Brough, and Suzie Drummond. Lazarus and folkman's psychological stress and coping theory. In *The Handbook of Stress and Health*, pages 349–364. John Wiley & Sons, Ltd, February 2017. doi: 10.1002/9781118993811.ch21. URL https://doi.org/10.1002/9781118993811.ch21.

[267] Casselman, J., Onopa, N., & Khansa, L. Wearable healthcare: lessons from the past and a peek into the future. telematics and informatics., 2017.

[268] K. R. Evenson, M. Goto, and R. Furberg. Systematic review of the validity and reliability of consumer-wearable activity trackers. *International journal of behavioural nutrition and physical activity*, 12, 2015. doi: 10.1186/s12966-015-0314-1. URL https://doi.org/10.1186/s12966-015-0314-1.

[269] L. Piwek, D. Ellis, S. Andrews, and A. Johnson. The rise of consumer health wearables: promises and barriers. *PLoS Medicine*, 13, 2016. doi: 10.1371/journal.pmed.1001953. URL https://doi.org/10.1371/journal.pmed.1001953.

[270] A. Mills, R. Watson, L. Pitt, and J. Kietzmann. Wearing safe: physical and informational security in the age of the wearable device. *Business Horizons*, 59, 2016. doi: 10.1016/j.bushor.2016.08.003. URL https://doi.org/10.1016/j.bushor.2016.08.003.

[271] A. Marakhimov and Joo J. Consumer adaptation and. *and infusion of wearable devices for healthcare'*. Computers in Human Behaviour;, 2017.

[272] Richard S Lazarus and Susan Folkman. *Stress, appraisal, and coping*. Springer Publishing company, New York, 1984.

[273] S. Folkman. An approach to the measurement of coping. *Journal of Organisational Behaviour*, 3, 1982. doi: 10.1002/job.4030030108. URL https://doi.org/10.1002/job.4030030108.

[274] R. Lazarus. Emotions and interpersonal relationships: toward a person-centred conceptualization of emotions and coping. *J Pers*, 74, 2006. doi: 10.1111/j.1467-6494.2005.00368.x. URL https://doi.org/10.1111/j.1467-6494.2005.00368.x.

[275] S. Folkman and J. Moskowitz. Coping: pitfalls and promise. *Annual Review of Psychology*, 55, 2004. doi: 10.1146/annurev.psych.55.090902.141456. URL https://doi.org/10.1146/annurev.psych.55.090902.141456.

[276] J. Jain, T. Line, and G. Lyons. A troublesome transport challenge? working round the school run. *Journal of Transport Geography*, 19, 2011. doi: 10.1016/j.jtrangeo.2011.04.007. URL https://doi.org/10.1016/j.jtrangeo.2011.04.007.

[277] C. Braun and C. Clarke. Using thematic analysis in psychology. *Qualitative Research in Psychology*, 3, 2006. doi: 10.1191/1478088706qp063oa. URL https://doi.org/10.1191/1478088706qp063oa.

[278] B. Saunders, J. Sim, T. Kingstone, S. Baker, J. Waterfield, B. Bartlam, H. Burrows, and C. Jinks. Saturation in qualitative research: exploring its conceptualisation and operationalization. *Quantity and Quality*, 52, 2017. doi: 10.1007/s11135-017-0574-8. URL https://doi.org/10.1007/s11135-017-0574-8.

[279] Dewe, P. & C.L. Cooper. 'coping research and measurement in the context of work related stress' in g.p. hodgkinson and j. kevin ford (eds) international review of industrial and organizational psychology 22, pp.141–191., 2007.

[280] R. McConnell, K. Berhane, L. Yao, F. Lurmann, E. Avol, and J. Peters. Predicting residential ozone deficits from nearby traffic. *Science of the Total Environment*, 363, 2005.

[281] N. Gilbert, S. Woodhouse, D. Stieb, and J. Brook. Ambient nitrogen dioxide and distance from a major highway. *Science of the Total Environment*, 312, 2003. doi: 10.1016/S0048-9697(03)00228-6. URL https://doi.org/10.1016/S0048-9697(03)00228-6.

[282] T. Reponen, S. Grinshpun, S. Trakumas, D. Martuzevicius, Z. Wang, G. LeMasters, J. Lockey, and P. Biswas. Concentration gradient patterns of aerosol particles near interstate highways in the greater cincinnati airshed. *Journal of Environmental Monitoring*, 5, 2003. doi: 10.1039/b303557c. URL https://doi.org/10.1039/b303557c.

[283] Graham, L., Gosling, S., & Travis, C. The psychology of home environments. perspectives on psychological science, 10(3), 346–356., 2015.

[284] Niphadkar, P., Rangnekar, K., Tulaskar, P., Deo, S., Mahadik, S., & Kakade, A. Poor awareness and knowledge about indoor air pollution in the urban population of mumbai, india. journal of the association of physicians of india, 57., 2009.

[285] S. Mallett. Understanding home: a critical review of the literature. *The Sociological Review*, 52, 2004. doi: 10.1111/j.1467-954X.2004.00442.x. URL https://doi.org/10.1111/j.1467-954X.2004.00442.x.

[286] O. Kardan, P. Gozdyra, M. Bratislav, F. Moola, L. Palmer, P. Tomas, and M. Berman. Neighbourhood greenspace and health in a large urban centre. *Scientific Reports*, 5, 2015. doi: 10.1038/srep11610. URL https://doi.org/10.1038/srep11610.

[287] D. Carrington. Tree-planting 'has mind-blowing potential' to tackle climate crisis, 2019. Guardian. Available from: https://rb.gy/zlif8.

[288] England, R. Climate change: tree planting rise 'needs to happen quickly, bbc news, available at: https://www.bbc.co.uk/news/uk-england-47541491, 2019.

[289] J. Sefcik, M. Kondo, H. Klusaritz, E. Sarantschin, S. Solomon, A. Roepke, E. South, and S. Jacoby. Perceptions of nature and access to green space in four urban neighbourhoods. *International Journal of Environmental Research and Public Health*, 16, 2019. doi: 10.3390/ijerph16132313. URL https://doi.org/10.3390/ijerph16132313.

[290] K. M. Beyer, A. Kaltenbach, A. Szabo, S. Bogar, F. J. Nieto, and K. M. Malecki. Exposure to neighborhood green space and mental health: evidence from the survey of the health of wisconsin. *International Journal of Environmental Research and Public Health*, 11, 2014. doi: 10.3390/ijerph110303453. URL https://doi.org/10.3390/ijerph110303453.

[291] J. Maas, R. A. Verheij, S. Vries, P. Spreeuwenberg, F. G. Schellevis, and P. P. Groenewegen. Morbidity is related to a green living environment. *Journal of Epidemiology and Community Health*, 63, 2009. doi: 10.1136/jech.2008.079038. URL https://doi.org/10.1136/jech.2008.079038.

[292] M. Berman, J. Jonides, and S. Kaplan. The cognitive benefits of interacting with nature. *Psychological Science*, 19, 2008. doi: 10.1111/j.1467-9280.2008.02225.x. URL https://doi.org/10.1111/j.1467-9280.2008.02225.x.

[293] N. Razani, S. Morshed, M. A. Kohn, N. M. Wells, D. Thompson, M. Alqassari, A. Agodi, and G. W. Rutherford. Effect of park prescriptions with and without group visits to parks on stress reduction in low-income parents: Shine randomized trial. *PLoS One*, 13, 2018. doi: 10.1371/journal.pone.0192921. URL https://doi.org/10.1371/journal.pone.0192921.

[294] M. L. Fair, A. T. Kaczynski, S. M. Hughey, G. M. Besenyi, and A. R. Powers. An initiative to facilitate park usage, discovery, and physical activity among children and adolescents in greenville county, south carolina, 2014. *Preventing Chronic Disease*, 14, 2017. doi: 10.5888/pcd14.160043. URL https://doi.org/10.5888/pcd14.160043.

[295] W. Thompson, C. Roe, P. Aspinall, R. Mitchell, A. Clow, and D. Miller. More green space is linked to less stress in deprived communities: evidence from salivary cortisol patterns. *Landscape and Urban Planning*, 105, 2012. doi: 10.1016/j.landurbplan.2011.12.015. URL https://doi.org/10.1016/j.landurbplan.2011.12.015.

[296] H. Setälä, V. Viippola, A. Rantalainen, A. Pennanen, and V. Yli-Pelkonen. Does urban vegetation mitigate air pollution in northern conditions? *Environmental Pollution*, 183, 2013. doi: 10.1016/j.envpol.2012.11.010. URL https://doi.org/10.1016/j.envpol.2012.11.010.

[297] D. Nowack, D. Crane, and J. Stevens. Air pollution removal by urban trees and shrubs in the united states. *Urban Forestry and Urban Greening*, 4, 2006. doi: 10.1016/j.ufug.2006.01.007. URL https://doi.org/10.1016/j.ufug.2006.01.007.

[298] Z. Tong, R. Baldauf, V. Isakov, P. Deshmukh, and M. Zhang. Roadside vegetation barrier designs to mitigate near-road air pollution impacts. *Science of the Total Environment*, 541, 2016. doi: 10.1016/j.scitotenv.2015.09.067. URL https://doi.org/10.1016/j.scitotenv.2015.09.067.

[299] G. Vivaldo, E. Masi, C. Taiti, G. Calderelli, and S. Mancuso. The network of plants volatile organic compounds. *Scientific Reports*, 7, 2017. doi: 10.1038/s41598-017-10975-x. URL https://doi.org/10.1038/s41598-017-10975-x.

[300] Air Quality Expert Group. Impacts of vegetation on urban air pollution, 2018. URL https://uk-air.defra.gov.uk/assets/documents/reports/cat09/1807251306_180509_Effects_of_vegetation_on_urban_air_pollution_v12_final.pdf.

[301] R. Laumbach, Q. Meng, and H. Kipen. What can individuals do to reduce personal health risks from air pollution? *Journal of Thoracic Disease*, 7, 2015.

[302] R. C. Paediatrics and C. Health. *Effects of indoor air quality on children and young people's health: systematic review scope.* , url = https://pubs.rsc.org/en/content/chapter/9781839160431-00151/978-1-83916-043-1, 2018.

[303] Pant, P. and Harrison, R. Estimation of the contribution of road traffic emissions to particulate matter concentrations from field measurements: a review'. *Atmospheric Environmentp*, pages 78–79, 2013.

[304] DEFRA. Emissions of air pollutants, 2021. URL https://www.gov.uk/government/statistics/emissions-of-air-pollutants.

[305] E. Semmens, C. Noonan, R. Allen, E. Weiler, and T. Ward. *Indoor particulate matter in rural.* wood stove heated homes', Environmental Research, Vol;, 2015.

[306] M. Piccardo, A. Cipolla, M. Stella, M. Ceppi, and A. Bruzzone. Izzotti, et al. *Indoor pollution and burning practices in wood stove management'. Journal of the Air I& Waste Management Association*, 64(11):1309–1316, 2014.

[307] M. Mcnamara, J. Thornburg, E. Semmens, T. Ward, and C. Noonan. *Coarse particulate matter and airborne endotoxin within wood stove homes'.* Indoor Air;, 2013.

[308] E. Vicente, A. Vicente, M. Evtyugina, F. Oduber, F. Amato, and X. Querol. al. *Impact of wood combustion on indoor air quality', Science of the Total Environment*, 705, 2020.

[309] D. Wang, Q. Li, G. Shen, J. Deng, W. Zhou, and J. Hao. *al.* Significant ultrafine particle emissions from residential solid fuel combustion'. Science of the Total Environment, Vol;, 2020.

[310] C. W. Noonan, W. Navidi, L. Sheppard, C. P. Palmer, M. Bergauff, and K. Hooper. al. *Residential indoor PM*, 2:5, 2012.

[311] R. Allen, S. Leckie, G. Millar, and M. Brauer. *The impact of wood stove technology upgrades on indoor residential air quality'.* Atmospheric Environment;, 2009.

[312] A. Castro, A. I. Calvo, C. Blanco-Alegre, F. Oduber, C. Alves, and E. Coz. *al.* Estimation of the respirable fraction'. Science of the Total Environment;, Impact of the wood combustion in an open fireplace on the air quality of a living room, 2018.

[313] T. Salthammer, T. Schripp, S. Wientzek, and M. Wensing. *Impact of operating wood-burning fireplace ovens on indoor air quality'.* Chemosphere, Vol;, 2014.

[314] G. Wall. Public response to air pollution in sheffield, england'. *Environment and Behaviour*, 5:219–248, 1974.

[315] Kirkby AV. Perception of air pollution as a hazard and individual adjustment to it in exeter, sheffield and edinburgh'. In *Paper: Man and Environment Commission Symposium.* Calgary;, 1972.

[316] M. Blacksell. Attitudes toward smoke control in exeter. In *Paper: Man and Environment Commission Symposium.* Calgary;, 1972.

[317] McBoyle GR. The public perception of air pollution in aberdeen'. In *Taylor JA*, pages 173–191. itor. Climatic Resources and Economic Activity; A Symposium. London, David and Charles; p, 1972.

[318] A. Irwin, P. Simmons, Walker G. Faulty Environments, and Risk Reasoning. The local understanding of industrial hazards', environment and planning a. *Economy and Space*, 31(7):1311–1326, 1999.

[319] K. Bickerstaff and G W. Clearing the smog? *Public responses to air quality information'. The International Journal of Justice and Sustainability*, 4(3):279–294, 1999.

[320] J. Bush, S. Moffatt, and C. Dunn. Keeping the public informed? *Public negotiation of air quality information'. Public Understanding of Science*, 10:213–229, 2001.

[321] K. Bickerstaff and G. Walker. Public understandings of air pollution: the localisation of environmental risk'. *Global Environmental Change-human and Policy Dimensions*, 11:133–145, 2001.

[322] D. Howel, S. Moffat, J. Bush, E Dc, and H. Prince. Public views on the links between air pollution and health in northeast england'. *Environmental Research*, 91:163–171, 2003.

[323] J. Bush, S. Moffatt, and Dunn CE. Contextualisation of local and global environmental issues in northeast england: Implications for debates on globalisation and the risk society'. *The International Journal of Justice and Sustainability*, 7(2): 119–133, 2002.

[324] K. Bickerstaff and Walker G. The place(s) of matter. matter out of place – public understandings of air pollution'. *Progress in Human Geography*, 27(1):45–67, 2003.

[325] J. Cupples, V. Guyatt, and J. Pearce. Put on a jacket, you wuss. *: cultural identities, home heating, and air pollution in Christchurch, New Zealand'. Environment and Planning A*, 39(12):2883–2898, 2007.

[326] J. Xu, C. S. Chi, and Zhu K. Concern or Apathy. The attitude of the public toward urban air pollution'. *Journal of Risk Research*, 20(4):482–498, 2017.

[327] Johnson B. Gender and. and race in beliefs about outdoor air pollution'. *Risk Analysis*, 22(4):725–738, 2002.

[328] S. Brody, M. Peck, and W. Highfield. Examining localised patterns of air quality perception in texas: A spatial and statistical analysis'. *Risk Analysis*, 24(6):1561–1574, 2004.

[329] S. Moffatt, J. Bush, C. Dunn, D. Howel, and H. Prince. *Public Awareness of Air Quality and Respiratory Health and the Impact of Health Advice*. Department of Epidemiology and Public Health, University of Newcastle;, Newcastle, 1999.

[330] A. Hofflinger, A. Boso, and C. Oltra. The home halo effect: how air quality perception is influenced by place attachment'. *Human Ecology*, 47:589–600, 2019.

[331] J. Vaske and Kobrin K. Place attachment and. and environmentally responsible behaviour'. *Journal of Environmental Education*, 32(4):16–21, 2001.

[332] J. Heydon and R. Chakraborty. Can portable air quality monitors protect children from air pollution on the school run? *An exploratory study'. Environmental Monitoring and Assessment*, 192(195):1–16, 2020.

[333] Bickerstaff K. Risk perception research. socio-cultural perspectives on the public experience of air pollution'. *Environment International*, 30(6):827–840, 2004.

[334] C. Oltra and R. Sala. Perception of risk from air pollution and reported behaviours: A cross-sectional survey study in four cities'. *Journal of Risk Research*, 21(7):869–884, 2016.

[335] Cupples J. Culture. nature and particulate matter – hybrid reframings in air pollution scholarship'. *Atmospheric Environment*, 43:207–217, 2009.

[336] A. Boso, B. Alvarez, C. Oltra, and J. Garrido. *Mu noz C, Galvez-García G.* a field experiment examining the home halo effect'. Sustainability;, The grass is always greener on my side, 2020.

[337] P. Aoki, A. Woodruff, B. Yellapragada, and Willett W. Environmental protection and. and agency: Motivations, capacity, and goals in participatory sensing'. *HCI and Collective Action*, pages 3138–3150, 2017.

[338] J. Goldman, K. Shilton, J. Burke, D. Estrin, M. Hansen, and N. Ramanathan. *al.* Participatory sensing: a citizen-powered approach to illuminating the patterns that shape our world'; Available from: , 2009. URL https://scholarworks.umass.edu/esence/362/.

[339] B. Hubbell, A. Kaufman, L. Rivers, K. Schulte, G. Hagler, and J. Clougherty. *al.. Understanding social and behaviour drivers and impacts of air quality sensor use.* Science of the Total Environment;, 2018.

[340] E. Bales, N. Nikzad, N. Quick, C. Ziftci, K. Patrick, and Griswold W. Personal pollution monitoring. *mobile real-time air quality in daily life'.* Personal and Ubiquitous Computing;, 2019.

[341] P. Zappi, E. Bales, J. H. Park, and W. Griswold. Šimunić t. the citisense air quality monitoring mobile sensor node. In *Proceedings of the 11th ACM/IEEE conference on information processing in sensor networks*, China;, 2012. Beijing.

[342] S. Folkman and Moskowitz J. Coping: Pitfalls and. Promise. *Coping: pitfalls and promise Annual Review of Psychology*, 55:747–774, 2004.

[343] J. Casselman, N. Onopa, and Khansa L. Wearable healthcare. *lessons from the past and a peek into the future.* Telematics and Informatics;, 2017.

[344] Lazarus R. Emotions and. and interpersonal relationships: toward a person-centred conceptualization of emotions and coping'. *Journal of Personality*, 2006.

[345] C. Braun and C. Clarke. *Using thematic analysis in psychology'.* Qualitative Research in Psychology;, 2006.

[346] B. Saunders, J. Sim, T. Kingstone, S. Baker, J. Waterfield, and B. Bartlam. *al.* exploring its conceptualisation and operationalization', Quantity and Quality;, Saturation in qualitative research, 2017.

[347] S. Butcher and E. A Sorenson. Study of wood stove particulate emissions'. *Journal of the Air Pollution Control Association*, 29(7):724–728, 1979.

[348] E. Mitchell, J. Cottom, D. Phillips, and B. A Dooley. *review of the impact of domestic combustion on UK air quality.* , url = https://www.hetas.co.uk/?ddownload=250495, 2019.

[349] G. Shen, M. Xue, S. Wei, Y. Chen, Q. Zhao, B. Li, et al. Influence of fuel moisture, charge size, feeding rate and air ventilation conditions on the emissions of pm, oc, ec, parent pahs, and their derivatives from residential wood combustion'. *Journal of Environmental Sciences*, 25(9):1808–1816, 2013.

[350] Z. Ai and C. Mak. From street canyon microclimate to indoor environmental quality in naturally ventilated urban buildings: Issues and possibilities for improvement'. *Building and Environment*, 94:489–503, 2015.

[351] British Flue and Chimney Manufacturer's Association. *General guidance on the selection and installation of flues and chimneys for wood burning and multi fuel appliances in residential properties'.* , url = https://www.hetas.co.uk/wp-content/mediauploads/BFCMA-General-Guidance-10-12-12.pdf, 2012.

[352] F. Fachinger, F. Drewnick, R. Gieré, and S. Borrmann. How the user can influence particulate emissions from residential wood and pellet stoves: Emission factors for different fuels and burning conditions. *Atmospheric Environment*, 158:216–226, 2017. doi: {https://doi.org/10.1016/j.atmosenv.2017.03.027}.

[353] K. Whiffen. *Clean air day campaign highlights indoor air quality, available*. Available from: at, url = https://www.opinium.co.uk/clean-air-day-campaign-highlights-indoor-air-quality/, 2018.

[354] P. Niphadkar, K. Rangnekar, P. Tulaskar, S. Deo, S. Mahadik, and Kakade A. Poor awareness and. and knowledge about indoor air pollution in the urban population of mumbai. *India' Journal of the Association of Physicians of India*, 57, 2009.

[355] R. C. Paediatrics and C. Health. *Effects of indoor air quality on children and young people's health.* , url = https://ash.org.uk/wp-content/uploads/2019/04/RCPCH-Indoor-Air-Quality-ASH-and-ASH-Scotland-joint-response.pdf, 2019.

[356] DEFRA. Summary results of the domestic wood use survey, 2016. URL https://www.gov.uk/government/publications/summary-results-of-the-domestic-wood-use-survey.

[357] Emden, J. and Murphy L. Lethal but Legal. *Air Pollution from Domestic Burning.* , url = https://www.ippr.org/files/2018-10/1539184665˙lethal-but-legal-october18.pdf, 2018.

[358] Heating Equipment Testing and Approvals Scheme. Burn better, 2020. URL https://www.hetas.co.uk/burn-better/.

[359] M. Maione, E. Mocca, K. Eisfeld, Y. Kazepov, and S. Fuzzi. *Public perception of air pollution sources across Europe*. Ambio, 2021. doi: {10.1007/s13280-020-01450-5},.

[360] P. Orellano, J. Reynoso, N. Quaranta, A. Bardach, and A. Ciapponi. Short-term exposure to particulate matter (pm10 and pm2.5), nitrogen dioxide (NO_2), and ozone (o3) and all-cause and cause-specific mortality: Systematic review and meta-analysis. *Environ Int*, 142(10587):6, 2020.

[361] C. Chen, H. Li, Y. Niu, C. Liu, Z. Lin, J. Cai, et al. Impact of short-term exposure to fine particulate matter air pollution on urinary metabolome: A randomized, double-blind, crossover trial. *Environ Int*, 130(10487):8, 2019.

[362] M. Torkmahalleh, S. Gorjinezhad, H. Unluevcek, and P. Hopke. Review of factors impacting emission/concentration of cooking generated particulate matter'. *Science of the Total Environment*, 586:1046–1056, 2017.

[363] N. Seltenrich. Take care in the kitchen: Avoiding cooking-related pollutants'. *Environmental Health Perspectives*, 122(6):154–160, 2014.

[364] L. Abdullahi, J. Delgado-Saborit, and R. Harrison. Emissions and indoor concentrations of particulate matter and its specific chemical components from cooking: A review. *Atmospheric Environment*, 71:260–294, 2013.

[365] C. Long, H. Suh, and P. Koutrakis. Characterization of indoor particle sources using continuous mass and size monitors'. *Journal of the Air & Waste Management Association*, 50:7–1236, 2000.

[366] A. Boso, A. Hofflinger, C. Oltra, B. Alvarez, and J. Garrido. Public support for wood smoke mitigation policies in south-central chile'. *Air Quality, Atmosphere and Health*, 11:1109–1119, 2018.

[367] N. Bhullar, D. Hine, A. Marks, C. Davies, J. Scott, and W. Phillips. The affect heuristic and public support for three types of wood smoke mitigation policies'. *Air Quality, Atmosphere and Health*, 7(3):347–56, 2014.

[368] A. Boso, T. Ariztia, and Fonseca F. Usos. resistencias y aceptacion de tecnologias energeticas emergentes en el hogar. *El caso de la politica de recambio de estufas en Tumeco, Chile'. Revista Internacional de Sociologia*, 75:4, 2017.

[369] World Health Organization et al. Who air quality guidelines for particulate matter, ozone, nitrogen dioxide and sulphur dioxide. global update 2005. *World Health Organization. Available from: http://www. euro. who. int/__data/assets/pdf_file/0005/786*, 38:E90038, 2006.

Appendix A

Appendix

A.1 Data Collection

Peshawar (34.015° N, 71.52° E) is a city located in Khyber Pakhtunkhwa, Pakistan, situated at an elevation of 340 m above sea level. Peshawar covers an area of 1257 km^2 and has a population of 1,218,773 making it the biggest city in Khyber Pakhtunkhwa. Peshawar is predominantly hot during summer (May–Mid July) with an average maximum temperature of 40 °C followed by monsoon and cold winter.

Local vehicular emission, fossil fuel energy plants and industrial processes are the significant sources of air pollution in Peshawar. Wind direction and wind speed also play a crucial role to observe transboundary pollution build-up. Furthermore, at this site, the distribution and dispersion of air pollution are further impacted by the nearby buildings, and its proximity to Grand Trunk Road, creating a built-up street canyon environment, generated primarily from nearby, increasing traffic pollution.

The air quality monitoring sensor (AQMS) was installed at the University of Peshawar's Physics Department Building (see Figure A.1) at 6 m height from the ground surface level. It is described as an urban background site.

Sheffield (53°23′ N, 1°28′ W) is a geographically diverse city located in county South Yorkshire, UK, built on several hills thus situated at an elevation of 29–500 m above sea level. Sheffield covers a total area of 367.9 km^2 with a growing population of 582,506. Sheffield is claimed to be the "greenest city" in England by the local city council. Sheffield enjoys a temperate climate with July considered the hottest month, with an average maximum temperature of 20.8 °C.

The air pollution in the city is primarily due to both road transport and industry, and to a lesser extent, fossil fuel-run processes, such as energy supply and commercial or domestic heating systems (for example, wood burners).

The AQMS is installed at 2.5 m height from the elevated ground surface level at the playground of Hunter's Bar Infants School (see Figure A.2), which lies in close proximity to a busy roundabout, and at the intersection of Ecclesall Road, Brocco Bank, Sharrow

Vale Road and Junction Road; thus, traffic is the primary source of pollution. It is also described as an urban background site.

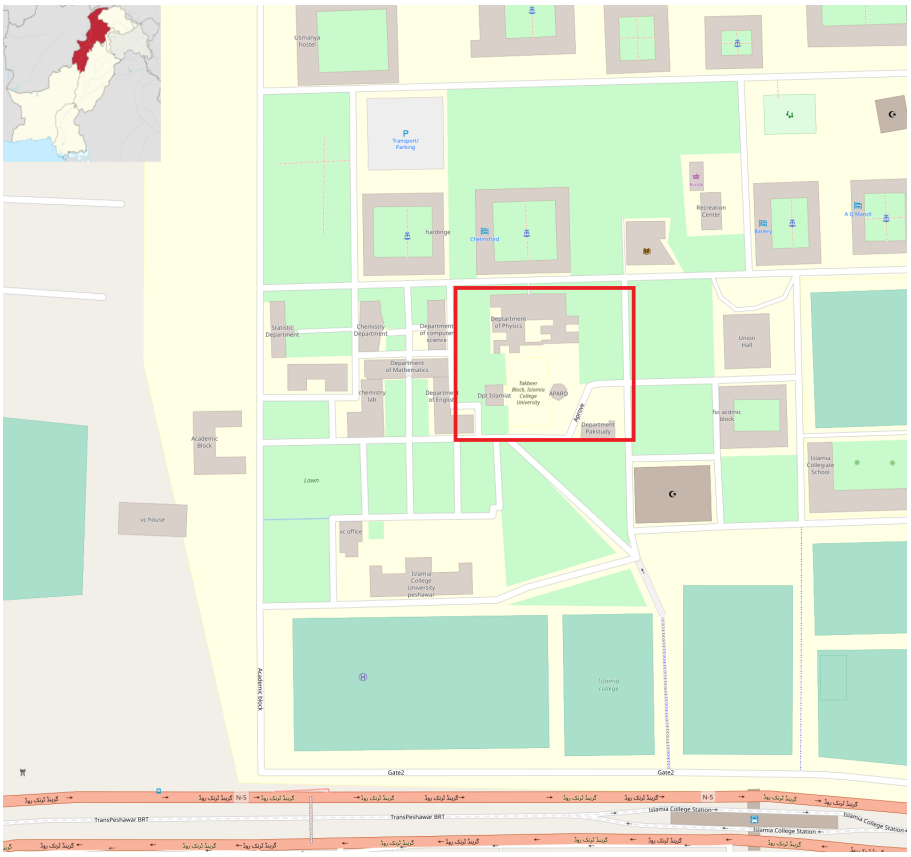

FIGURE A.1: Peshawar study site © OpenStreetMap contributors.

In our case, the AQMSs are commercially low cost sensor nodes AQMesh. They have been deployed at the two sites in Peshawar and Sheffield. A "black box" post calibration is applied to the data by the manufacturer to eliminate the impact of humidity and temperature on the sensor and to eliminate cross sensitivity. The data are aggregated and sampled every 15 min. The data collected from these nodes are transferred to the cloud-based AQMesh database via standard GPRS communication integrated. The data are then accessed through the dedicated API.

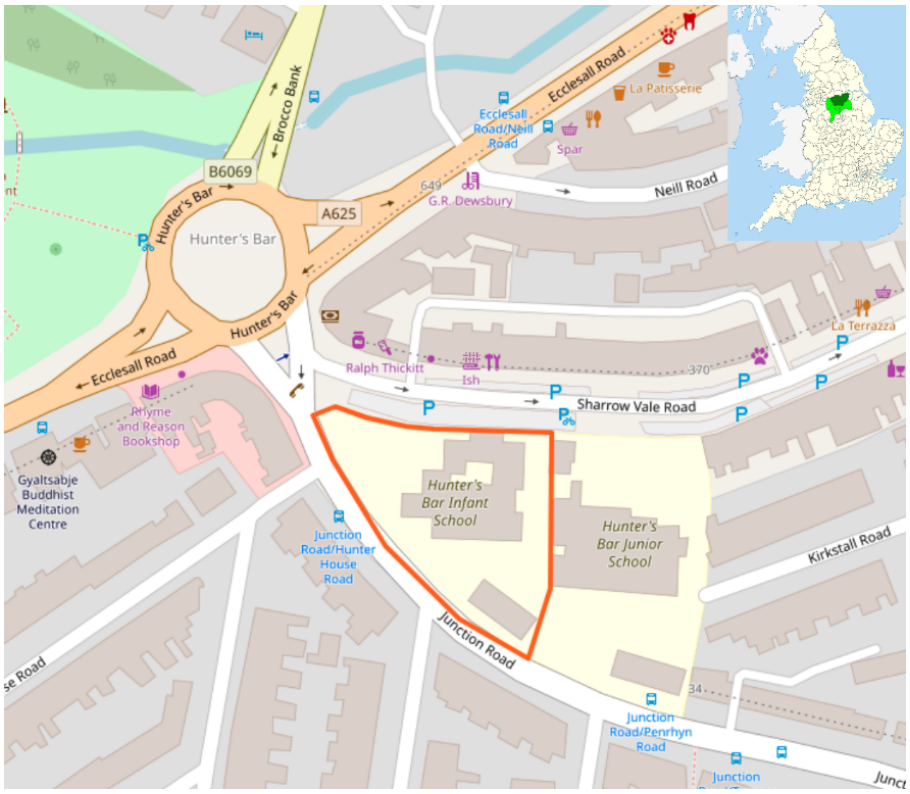

FIGURE A.2: Sheffield study site © OpenStreetMap contributors.

A.2 The WHO Concentration Criteria for Pollutants

All data from 'WHO Air quality guidelines for particulate matter, ozone, nitrogen dioxide and sulfur dioxide [369].

WHO SO_2

TABLE A.1: WHO sulfur dioxide guidelines.

Sulfur Dioxide	24-h Mean	10-min Mean
SO_2	20 $^{-}g/m^3$	500 $^{-}g/m^3$

WHO $PM_{2.5}$ and PM_{10}

TABLE A.2: WHO particulate matter guidelines.

Particulate Matter	Annual Mean	24-h Mean
$PM_{2.5}$	5 $^{-}g/m^3$	15 $^{-}g/m^3$
PM_{10}	20 $^{-}g/m^3$	50 $^{-}g/m^3$

WHO O_3

Table A.3: WHO Ozone guidelines.

Ozone	**8-h Mean**
$\mathbf{O}_3$	100 $^{-}$g/m^3

A.3 Approximated Derivatives of SE Kernel

By specifying a kernel function, we can obtain analytical forms of Equations (7.28) and (7.29) immediately. In this paper, we adopt the widely used SE kernel shown in Equation (A.1) as an example.

$$\mathrm{k_{SE}}(\mathrm{x},\mathrm{x}') = \mathrm{s_f^2}\exp\Big(-\frac{(\mathrm{x}-\mathrm{x}')^2}{2\mathrm{l}^2}\Big). \tag{A.1}$$

There are two hyperparameters, i.e., the signal variance $\mathrm{s_f}$ and length-scale l are involved. Equations (A.2) and (A.3) show the expectation (prediction mean) partial derivative (EPD) and covariance partial derivative (CPD) of $\mathrm{s_f}$,

$$\begin{aligned}
&\Big(\frac{\partial\bar{\mathbf{f}}_*}{\partial\theta_\mathrm{s}}\Big)_\mathrm{o}\Big|_{\theta_\mathrm{s}=\mathrm{s_f}}\\
=&\sum_{\mathrm{i}=1}^{\mathrm{n}}\sum_{\mathrm{j}=1}^{\mathrm{n}}\Big(\mathrm{k_{oj}}\frac{\partial\mathrm{d_{ji}}}{\partial\mathrm{s_f}}+\frac{\partial\mathrm{k_{oj}}}{\partial\mathrm{s_f}}\mathrm{d_{ji}}\Big)\mathrm{y_i}\\
=&\sum_{\mathrm{i}=1}^{\mathrm{n}}\sum_{\mathrm{j}=1}^{\mathrm{n}}\mathrm{y_i}\left\{\begin{array}{ll}0, & \mathrm{j}\neq\mathrm{i}\\ 0, & \mathrm{j}=\mathrm{i}\end{array}\right\},
\end{aligned} \tag{A.2}$$

$$\begin{aligned}
&\Big(\frac{\partial\mathrm{cov}(\mathbf{f}_*)}{\partial\theta_\mathrm{s}}\Big)_\mathrm{oo}\Big|_{\theta_\mathrm{s}=\mathrm{s_f}}\\
=&\frac{\partial\mathbf{K}(\mathbf{X}_*,\mathbf{X}_*)_\mathrm{oo}}{\partial\mathrm{s_f}}-\sum_{\mathrm{i}=1}^{\mathrm{n}}\sum_{\mathrm{j}=1}^{\mathrm{n}}\Big(\frac{\partial\mathrm{k_{oj}}}{\partial\mathrm{s_f}}\mathrm{d_{ji}}\mathrm{k_{oi}}+\mathrm{k_{oj}}\frac{\partial\mathrm{d_{ji}}}{\partial\mathrm{s_f}}\mathrm{k_{oi}}-\mathrm{k_{oj}}\mathrm{d_{ji}}\frac{\partial\mathrm{k_{oi}}}{\partial\mathrm{s_f}}\Big)\\
=&2\mathrm{s_f}-\sum_{\mathrm{i}=1}^{\mathrm{n}}\sum_{\mathrm{j}=1}^{\mathrm{n}}\left\{\begin{array}{ll}2\mathrm{s_f}\exp(-\frac{(\mathrm{x_o}-\mathrm{x_j})^2+(\mathrm{x_j}-\mathrm{x_i})^2+(\mathrm{x_o}-\mathrm{x_i})^2}{2\mathrm{l}^2}), & \mathrm{j}\neq\mathrm{i}\\ -2\mathrm{s_f}\exp(-\frac{(\mathrm{x_o}-\mathrm{x_j})^2+(\mathrm{x_o}-\mathrm{x_i})^2}{2\mathrm{l}^2}), & \mathrm{j}=\mathrm{i}\end{array}\right\}.
\end{aligned} \tag{A.3}$$

While the derivatives of l are given in Equations (A.4) and (A.5),

$$\begin{aligned}
&\Big(\frac{\partial\bar{\mathbf{f}}_*}{\partial\theta_\mathrm{s}}\Big)_\mathrm{o}\Big|_{\theta_\mathrm{s}=\mathrm{l}}\\
=&\sum_{\mathrm{i}=1}^{\mathrm{n}}\sum_{\mathrm{j}=1}^{\mathrm{n}}\Big(\mathrm{k_{oj}}\frac{\partial\mathrm{d_{ji}}}{\partial\mathrm{l}}+\frac{\partial\mathrm{k_{oj}}}{\partial\mathrm{l}}\mathrm{d_{ji}}\Big)\mathrm{y_i}\\
=&\sum_{\mathrm{i}=1}^{\mathrm{n}}\sum_{\mathrm{j}=1}^{\mathrm{n}}\mathrm{y_i}\left\{\begin{array}{ll}-\exp(-\frac{(\mathrm{x_o}-\mathrm{x_j})^2+(\mathrm{x_j}-\mathrm{x_i})^2}{2\mathrm{l}^2})\frac{(\mathrm{x_o}-\mathrm{x_j})^2+(\mathrm{x_j}-\mathrm{x_i})^2}{\mathrm{l}^3}, & \mathrm{j}\neq\mathrm{i}\\ \exp(-\frac{(\mathrm{x_o}-\mathrm{x_j})^2}{2\mathrm{l}^2})\frac{(\mathrm{x_o}-\mathrm{x_j})^2}{\mathrm{l}^3}, & \mathrm{j}=\mathrm{i}\end{array}\right\},
\end{aligned} \tag{A.4}$$

$$
\begin{aligned}
&\Big(\frac{\partial \mathrm{cov}(\mathbf{f}_*)}{\partial \theta_\mathrm{s}}\Big)_{\mathrm{oo}}\Big|_{\theta_\mathrm{s}=\mathrm{l}} \\
=&\frac{\partial \mathbf{K}(\mathbf{X}_*,\mathbf{X}_*)_{\mathrm{oo}}}{\partial \mathrm{l}} - \sum_{\mathrm{i}=1}^{\mathrm{n}}\sum_{\mathrm{j}=1}^{\mathrm{n}}\Big(\frac{\partial \mathrm{k_{oj}}}{\partial \mathrm{l}}\mathrm{d_{ji}}\mathrm{k_{oi}} + \mathrm{k_{oj}}\frac{\partial \mathrm{d_{ji}}}{\partial \mathrm{l}}\mathrm{k_{oi}} - \mathrm{k_{oj}}\mathrm{d_{ji}}\frac{\partial \mathrm{k_{oi}}}{\partial \mathrm{l}}\Big) \\
=&\sum_{\mathrm{i}=1}^{\mathrm{n}}\sum_{\mathrm{j}=1}^{\mathrm{n}}\left\{\begin{array}{ll} \exp(-\dfrac{(\mathrm{x_o}-\mathrm{x_j})^2+(\mathrm{x_j}-\mathrm{x_i})^2+(\mathrm{x_o}-\mathrm{x_i})^2}{2\mathrm{l}^2}) & \\ *\ \dfrac{(\mathrm{x_o}-\mathrm{x_j})^2+(\mathrm{x_j}-\mathrm{x_i})^2-(\mathrm{x_o}-\mathrm{x_i})^2}{\mathrm{l}^3}\mathrm{s_f^2}, & \mathrm{j}\neq\mathrm{i} \\ 0, & \mathrm{j}=\mathrm{i} \end{array}\right\}.
\end{aligned}
\tag{A.5}
$$

Appendix B

Supplementary Material

sustainability

MDPI

Article

A practical green infrastructure intervention to mitigate air pollution in a UK school playground

Supplementary Material

Figure S1 shows the partial dependencies – with Sch-GB site as an example – between $PM_{2.5}$, NO_2, and the weather covariates employed in the de-seasonalisation model. The model's performance was evaluated using tenfold cross-validation, and the resulting model fitting results are also displayed.

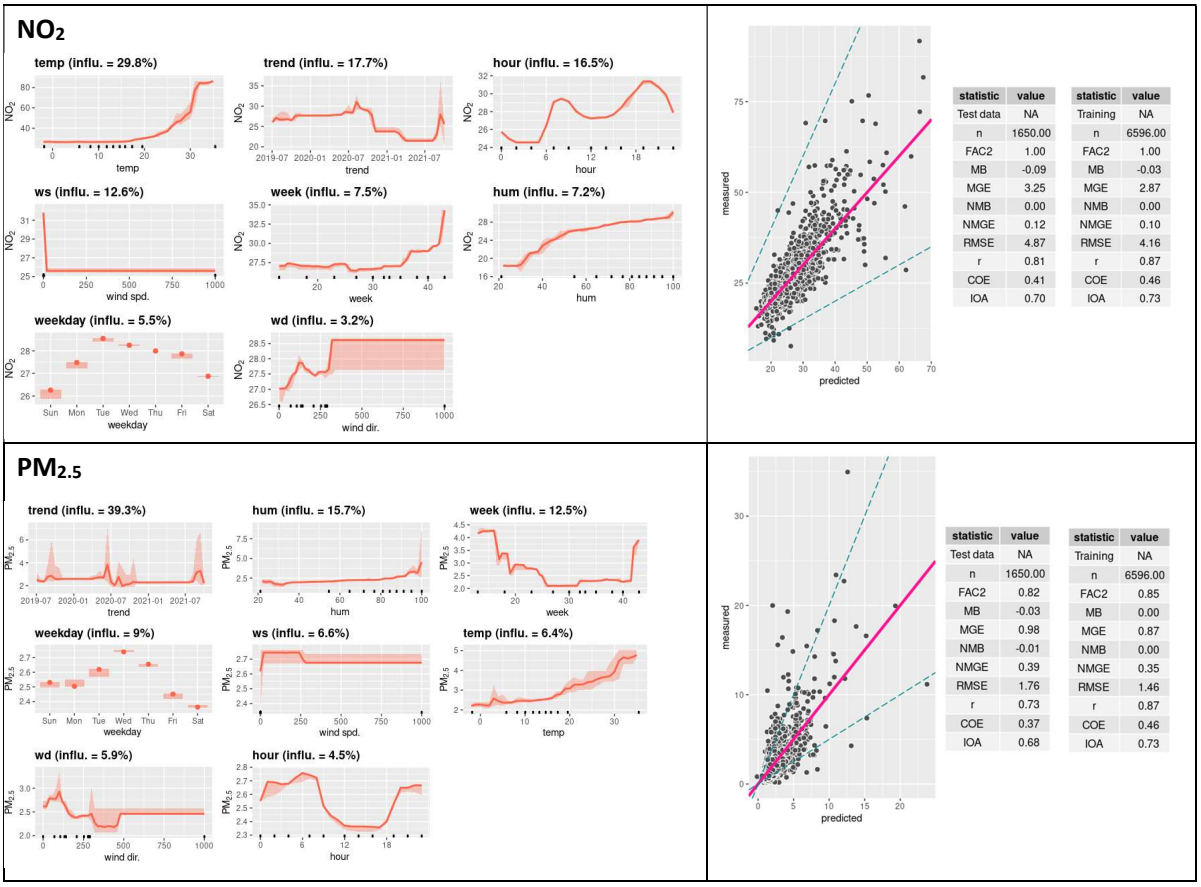

Figure S1. Model results and partial dependency of the covariates on $PM_{2.5}$ and NO_2 concentrations at Sch-GB from 2019 to 2021. Covariates: temp = temperature, hum = humidity, ws = wind speed, wd = wind direction, week = week of the year, hour = hour of the day, weekday, and trend.

A field co-location between low-cost mobile device (Aeroqual series 500) and the reference sensor MOBIUS (MOBIle Urban Sensing vehicle) from the Urban Flows Observatory, The University of Sheffield, was conducted to improve PM2.5 data quality. The co-location lasted 11-hour in total in three separate events, and data were collected with 1-min resolution.

The measurements from the low-cost mobile device were calibrated against a reference-grade PALAS Fidas sensor built in the MOBIUS. A concentration range correction was applied based on the relationship between $PM_{2.5}$ concentration range and sensor performance. Accuracy of the low-cost monitor modelled data is shown in Figure S2.

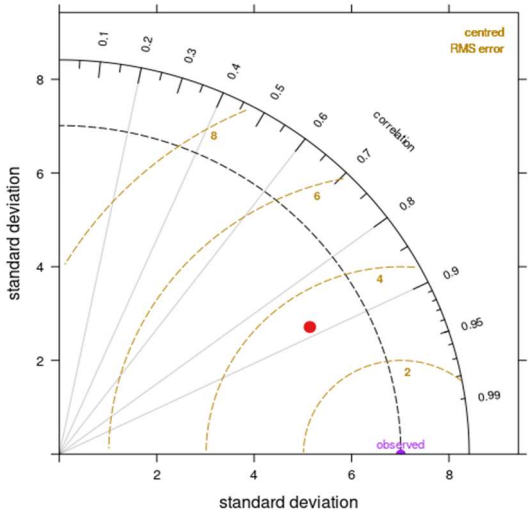

Figure S2. Taylor diagram comparing the modelled data (red dot) which are the corrected low-cost mobile device measurements for the reference data (observed). Correlation (R) - between 0.8-0.9; observed variability between 2-3 μg m^{-3} (through Standard Deviation); centred RMS error <4.

De-seasonalised data visualisations (boxplots) for each study period at all sites are presented below in figures S3 and S4.

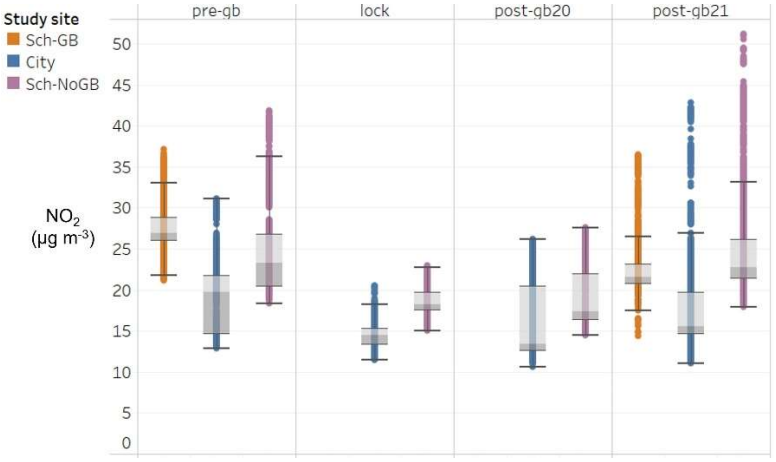

Figure S3. De-seasonalised NO_2 concentrations (µg m^{-3}) for each data collection period and study site. Colour change from light to dark grey within boxes represent the median NO_2 concentration, and whiskers extend to 1.5 the InterQuartile Range (IQR).

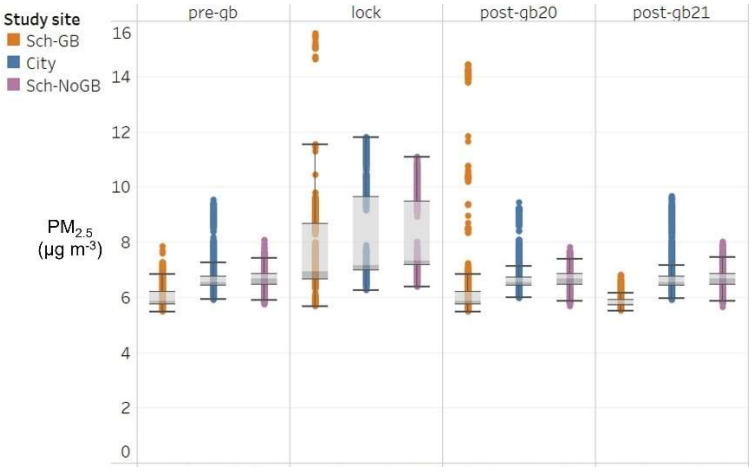

Figure S4. De-seasonalised $PM_{2.5}$ concentrations (µg m^{-3}) for each data collection period and study site. Colour change from light to dark grey within boxes represent the median $PM_{2.5}$ concentration, and whiskers extend to 1.5 the InterQuartile Range (IQR).